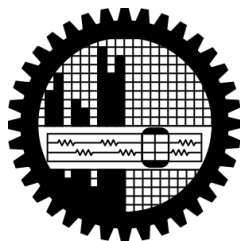


**BEHAVIOUR OF LONG SPAN BOX GIRDER BRIDGES DUE TO
ASYNCHRONOUS INPUT MOTION CONSIDERING DAMPING
PROPERTIES OF BEARINGS**

by

MD. SHAMIM KABIR SARKER

MASTER OF SCIENCE IN CIVIL ENGINEERING (STRUCTURAL)



**DEPARTMENT OF CIVIL ENGINEERING
BANGLADESH UNIVERSITY OF ENGINEERING AND TECHNOLOGY
DHAKA, BANGLADESH**

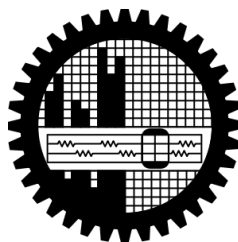
Behaviour of Long Span Box Girder Bridges Due to Asynchronous Input Motion Considering Damping Properties of Bearings

By

Md. Shamim Kabir Sarker

(Roll: 0413042346)

A thesis submitted to the Department of Civil Engineering, Bangladesh University of Engineering and Technology in Partial Fulfilment of the Requirement for the Degree of Masters of Science in Civil Engineering (Structural)



Department of Civil Engineering
Bangladesh University of Engineering and Technology
Dhaka-1000, Bangladesh

March 2019

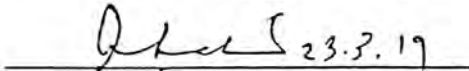
This thesis titled “Behaviour of Long Span Box Girder Bridges Due to Asynchronous Input Motion Considering Damping Properties of Bearings”, submitted by Md. Shamim Kabir Sarker, Roll No. 0413042346, Session: April 2013, has been accepted as satisfactory in partial fulfilment of the requirement for the degree of Master of Science in Civil Engineering (Structural) on March 23, 2019.

Board of Examiners



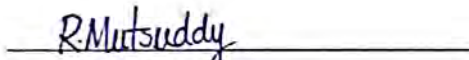
Dr. Raquib Ahsan
Professor
Department of Civil Engineering
BUET, Dhaka

Chairman
(Supervisor)



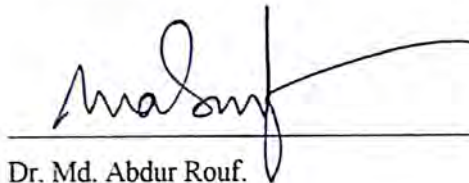
Dr. Ahsanul Kabir
Professor and Head
Department of Civil Engineering
BUET, Dhaka

Member
(Ex-Officio)



Dr. Rupak Mutsuddy.
Assistant Professor.
Department of Civil Engineering
BUET, Dhaka

Member



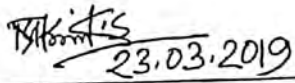
Dr. Md. Abdur Rouf.
Professor
Department of Civil Engineering
Ahsanullah University of Science and Technology (AUST), Dhaka.

Member
(External)

DECLARATION

It is hereby declared that except for the contents where specific references have been made to the work of others, the studies contained in this thesis is the result of investigation carried out by the author. No part of this thesis has been submitted to any other University or other educational establishment for a Degree, Diploma or other qualification (except for publication)

Signature of the Candidate


23.03.2019

Md. Shamim Kabir Sarker

ACKNOWLEDGEMENT

The author wishes to convey his profound gratitude to Almighty Allah for His graciousness, unlimited kindness and for allowing him to complete the thesis.

It is the author's great pleasure and privilege to record his deepest sense of gratitude, indebtedness and thankful acknowledgement to Dr. Raquib Ahsan, Professor, Department of Civil Engineering, Bangladesh University of Engineering and Technology, for his continuous support, invaluable ideas, excellent comments, feedback and most importantly his encouragement to carry out this work. His knowledge, guidance and cooperation have provided the author as the basis and inspiration to complete this work.

The author wishes to express his deep regard and profound love to his parents, family members who always motivated him to go ahead.

ABSTRACT

Asynchronous input motion has been identified to cause unfavorable response for long structures particularly bridges. Based on observed damage patterns from previous earthquakes and many previous analytical studies, it is seen that asynchronous motion may play significant role in these observed damage patterns.

In this study, three bridge FEM models having different span lengths (75m, 100m and 125m) are subjected to different cases of both synchronous and asynchronous motions. Time history analysis for asynchronous motion with time lag of 0.01 s, 0.05 s, 0.1 s, 0.2s, 0.5s and 1.0s have been conducted. The results show that displacement at longitudinal direction, remains constant along the long direction of bridge for all the cases of synchronous and asynchronous motion. In all cases of displacement in vertical direction, asynchronous (0.5s time lag) motion governs for all the bridges. For all the cases of transverse displacement, synchronous motion is found to be maximum. 100m span module is modelled such that it resembles a 7-span module of the Bangabandhu bridge. Damping properties of seismic devices is determined such that suggested maximum displacement is achieved for earthquake load by equivalent static method. For other bridges, stiffness properties are taken proportionally.

El-Centro earthquake have also been used in this study. For this data input, asynchronous motion with 0.01s time lag governs in longitudinal displacement for 75m and 100m span module. For 125m span module synchronous motion governs as usual. For displacement in vertical direction, mostly asynchronous with time lag 1.0s was found to be governing in that case for 100m and 125m bridge. For 75m span module, asynchronous 0.5s time lag governs.

In all the cases of bridges without any seismic isolation, displacement due to asynchronous motion governs and significantly exceeds the allowable displacement. Thus, designing for situations, where seismic isolations malfunction, may not be feasible. As 100m span module is similar to that of a 7-span module of The Bangabandhu multipurpose bridge, it can be seen that present bearings are essential for proper functioning of the bridge during seismic event. If seismic isolation does not properly function during major earthquake, severe structural damage may occur due to asynchronicity of motion. Thus, maintenance of the bearings is critical for the proper seismic performance of The Bangabandhu Multipurpose bridge.

TABLE OF CONTENT

ACKNOWLEDGEMENT	II
ABSTRACT	III
TABLE OF CONTENT	IV
LIST OF ABBREVIATION	VII
NOTATION	VIII
Chapter 1 INTRODUCTION	
1.1 General	1
1.2 Objectives of the Study	2
1.3 Scope of the Study	3
Chapter 2 LITERATURE REVIEW	
2.1 Introduction	4
2.2 Box Girder Bridge	4
2.3 Segmental Construction	8
2.4 Bearings in Bridge	9
2.4.1 Types of Bearings	9
2.4.2 Bearings Used in the Bangabandhu Bridge	12
2.5 Previous Records of Earthquakes	18
2.5.1 Damages to Bridges in Recent Earthquakes	18
2.5.2 Risk of Earthquake in Bangladesh	24
2.6 Design Provision of Box Girder Bridge	25
2.6.1 Structural Design Code	25
2.6.2 Seismic Design	26
2.7 Analysis Method for Box Girder Bridges	26
2.7.1 Finite Element Method	27
2.8 Structural Seismic Analysis	28
2.8.1 Response Spectrum Analysis	28
2.8.2 Time History Analysis	28
2.9 Asynchronous Motion	28
2.10 Previous Studies on Asynchronous Motion	29

Chapter 3 MODELLING OF THE BRIDGE

3.1	General	35
3.2	Modelling Elements	35
3.2.1	Frame Element	35
3.2.2	Shell Element	36
3.2.3	Link Element	36
3.2.4	Tendon Element	37
3.3	Salient Features of Bridges	38
3.4	Basic Features of the Bridge	40
3.4.1	Layout Line	40
3.4.2	Lane	41
3.4.3	Girder Section	42
3.4.4	Abutment and bent	52
3.5	Bearing and Seismic Isolation	54
3.5.1	Stiffness Properties of Seismic Devices	54
3.5.2	Damping properties of Seismic Devices	60
3.5.3	Assignment of Seismic Devices	62
3.6	Prestress	64
3.7	Loads	76
3.7.1	Dead Loads	76
3.7.2	Live Loads	76
3.8	Seismic Motion Data Input	78
3.8.1	Seismic Data from The Bangabandhu Bridge with Scale Factor	78
3.8.2	El Centro Earthquake Data (1940)	80
3.8.3	Seismic Motion Input Assignment	81

Chapter 4 VERIFICATION OF BRIDGE ANALYSIS MODEL

4.1	Introduction	85
4.2	Span to Depth Ratio	85
4.3	Sectional Efficiency (Rodriguez, 2004)	88
4.4	Comparison with Deflection Criteria	92
4.4.1	Deflection Due to Dead Load	92
4.4.2	Deflection Due to Vehicular Load	92
4.4.3	Total Deflection of Dead Load, Live Load and Prestress Force	96

4.5	Flexure and Stress Check	96
4.6	100-meter Bridge Bearing Properties Verification	106
4.7	Verification of 100 Meter Model Based on Design Value	107
4.7.1	Equivalent Static Force Method Verification	107
4.7.2	Verification of Horizontal Displacement	111
4.7.3	Verification of Vertical load in Typical Multidirectional Bearing	113
Chapter 5 RESULTS AND DISCUSSIONS		
5.1	Introduction	117
5.2	100 m Model Results	120
5.2.1	Deck Displacement at Top Mid-Points Due to Load Case 1	120
5.2.2	Horizontal load at point of fixity	124
5.2.3	Deck Displacement Due to Wave Passage Effect for Different Time Lag	125
5.2.4	EI-Centro Earthquake Data Input	149
5.3	Modal Participation Mass Ratios and Time Period	158
5.4	Flexural and Stress Capacity Check for Extreme Event	160
Chapter 6 CONCLUSIONS AND RECOMMENDATIONS		
6.1	Conclusions	170
6.2	Recommendations	171
	References	173
Appendices		

LIST OF ABBREVIATION

SVGEM	Spatially Varying Earthquake Ground Motions
FEM	Finite Element Method
STU	Shock Transmission Unit
MSE	Multiple Support Excitation
RC	Reinforced Concrete
AASHTO	The American Association of State Highway and Transportation Officials
LRFD	Load Resistance Factor Design

NOTATION

ρ	Sectional Efficiency Ratio
y_t	Distance from the Neutral Axis to the Top Fiber
y_b	Distance from the Neutral Axis to the Bottom Fiber
I	Moment of Inertia
A	Cross Sectional Area of Box Girder
L	Span Length
D_s	Depth at Pier
D_M	Depth at centre of mid-span
f'_c	Compressive Strength of Concrete
f_y	Tensile Strength of reinforcement
\overline{V}_{s30}	Wave Velocity to 30 m Depth
ξ	Damping Ratio,
ω	Angular Frequency
f	Predominant Frequency
k	Stiffness
C	Damping Co-efficient

Chapter 1

INTRODUCTION

1.1 General

Bangladesh faces a high risk of moderate to strong earthquakes that may result in widespread damage and loss of thousands of lives according to experts.

Bangladesh also faces the risk of tsunami as four active sources of earthquake in the Bay of Bengal can generate tremors with a magnitude of over 7 on the Richter scale in the Bay affecting the country seriously. The observatory at Bangladesh University of Engineering and Technology (BUET) recorded 86 tremors of over 4 magnitude during January 2006-May 2009. Another four earthquakes took place with magnitude of over 5 during this period. The meteorological department detected at least 90 earthquakes taking place in the country between May 2007 and July 2008, nine of them above five on the Richter scale and epicenters of 95 percent being within a 600-kilometre radius of Dhaka city. Experts say that it is these minor tremors that indicate the possibility of much more powerful earthquakes hitting the country. According to a seismic zoning map prepared by BUET, 43 percent areas in Bangladesh are rated high risk, 41 percent moderate and 16 percent low (Ansary and Sharfuddin, 2002).

However, due to increasing number of bridges, buildings and industrial structures being built during the last two decades, assessment of seismicity in different regions in the country received considerable attention of engineers and scientists. There is lack of awareness not only among the public but also among the decision makers about the earthquake hazard in the country. A review of the available data shows that considerable seismic hazard exists for major parts of the country (Ansary and Sharfuddin, 2002).

The traditional seismic analyses are commonly realized by uniform ground motions at all supports. It means that, earthquakes are taken into account as same excitations with arrival times differences and spatial effects are disregarded. On the other hand, the researches and observations obtained from the past earthquakes have shown that the uniform ground motion assumption is not realistic for widely-spaced structures like bridges. Because, earthquake motions originated from bedrock level travel to ground surface with multicomponent and unequal spectral contents (amplitudes, phases etc.) due to refractions, reflections and various site properties. Asynchronous ground motions propagate in spatial varying form because of loss of correlations (coherency), wave passage effects (delay in arrival times), and local site properties. For 40 years, many investigations and analyses have been performed by various

researchers to understand the effects of asynchronous ground motions on behaviour of bridges. Furthermore, if the considered structure is too long then many parameters such as support distances, local site conditions would have larger influences on the behaviour in compared to short structures. Therefore, earthquakes vibrate a bridge system by multi-component load effects and nonuniform multi-support movements. Especially in long-span bridges, the effects of variability in time arrivals, amplitudes, phase angles and local site properties play critical role in defining the structural responses. In the earthquake motion, time delays between the supports results in different support movements which is named as quasi-static loads effects. As the distances between the supports increase, the coherence would decrease. That is to say, the effects of spatial varying ground motions become more significant. The effects of spatially varying earthquake ground motions (SVGEM) have been investigated by many researchers in the past decades with increasing attention. Under effects of stationary random vibrations, a response spectrum method was developed for the multiply supported structures (Der Kiureghian and Neuenhofer, 1991).

Dynamic response during earthquake is a very important factor for both the serviceability and safety of bridge structures. The controlling parameters that govern dynamic response of a bridge depend on different structural attributes of a particular bridge. Conventional structural design methods neglect the asynchronous earthquake effects. The effect of asynchronous earthquake may be prominent for heavy structures like bridges, resting on relatively soft soils. Damage sustained in recent earthquakes have also highlighted that the seismic behaviour of a structure is highly influenced not only by the response of superstructure, but also by the response of the foundation and ground as well.

Utilizing advanced analysis tools, study conducted by Crewe and Norman (2006) and Carnevale et. al. (2012) seeks to include the complex factor not often considered in seismic analysis: spatially varied seismic input with a range of incoherent cases. The factor is included due to increased understanding of the seismological characteristics of earthquakes and the higher displacement demand possible from asynchronous input, demonstrated in recent studies.

1.2 Objectives of the Study

The behavior of bridge under the influence of seismic load has been a major point of interest for engineers over a long period of time. The 1971 San Fernando earthquake was a major turning point in the development of seismic design criteria for bridges. Although significant advances have been achieved since that time in the design and construction of an earthquake resistant bridge, numerous gaps still remain in the understanding of the seismic behaviour of

bridges. In this study, we have used acceleration, velocity and displacement data recorded on the Bangabandhu Multi-Purpose bridge pile cap (horizontal direction) on June 16, 2004 and earthquake data of El Centro (1940) earthquake. The principal objectives of the present study are:

- i. To verify the bridge models in terms of Span to depth ratio, sectional efficiency, deflection limit, flexural capacity and stress limitation for static load.
- ii. To determine displacement variation due to synchronous and asynchronous motion considering damping properties of bearings and seismic devices.
- iii. To verify the bridge model considering asynchronous motion with bearing damping properties.
- iv. To study the displacement behaviour of 100m bridge if seismic isolation system does not function during earthquake.

1.3 Scope of the Study

The research work involves the seismic response of a box girder bridge models considering the earthquake effect. The following are the scopes of the study.

- i. The structural behaviour of the bridge is assumed to be linear ignoring other non-linearity.
- ii. Numerical finite element models are developed in CsiBridge V20.
- iii. The structural behaviour of the bridge is assumed to be linear ignoring other non-linearity.
- iv. The Depth variation and Bottom slab thickness variation of the bridge have been considered. However, horizontal and vertical curvatures of the bridge have not been considered.
- v. This design is only for concrete prestressed post-tensioned box Girder Bridge.
- vi. The bridge is straight.
- vii. The number of spans of the bridge is seven continuous spans with overhanging span resting on appropriate bearing
- viii. Linear time-history analysis is performed.
- ix. Seismic devices and bearings have been assigned for the bridge models. The bridge models are verified according to provisions in this study.

Chapter 2

LITERATURE REVIEW

2.1 Introduction

Bridge has been an essential type of structure for civilization. Now a days, it has become an integral part of modern life. But a large number of bridges were designed and constructed at the time where either bridge codes had no seismic provisions or when provisions were insufficient according to current standards. Reports show that, most of the bridges so far damaged in earthquake were constructed before 1971 and little or no seismic resistance consideration was present during design (Rafik and Xin, 2003). The vulnerability of pre-1971 bridges was especially evident in the 1971 San Fernando earthquake in California, 1989 Loma Prieta earthquake, the 1994 Northridge earthquake, the 2001 Nisqually earthquake and 2001 Bhuj earthquake (Siddique, 2006). Since then considerable changes have been done in the design codes considering seismic resistance. Still, there are some differences present in terms of modelling for seismic design and the actual situation. This chapter deals with box girder bridge, damages to bridges due to recent earthquakes, various types of bearing, various structural and seismic design provisions and analysis methods. Asynchronous motion and previous studies regarding asynchronous motion are also highlighted here.

2.2 Box Girder Bridge

A box girder bridge is a bridge in which the main beams comprise of girders in the shape of a hollow box. The box girder normally comprises either prestressed concrete, structural steel, or a composite of steel and reinforced concrete. The **Figure 2.1** shows Bangabandhu bridge which is composed of prestressed concrete. The box is typically rectangular or trapezoidal in cross-section. Box girder bridges are commonly used for highway flyovers and for modern elevated structures of light rail transport. Although normally the box girder bridge is a form of Beam Bridge, box girders may also be used on cable-stayed bridges and other forms (Smith and Hendy, 2002).

The box girder bridge was a popular choice during the road building expansion of the 1960s and many new bridge projects were in progress simultaneously. A serious blow to this was a sequence of three serious disasters, when new bridges collapsed in 1970 (West Gate Bridge and Cleddau Bridge) and 1971 (Koblenz Bridge). Fifty-one people were killed in these failures, leading in the UK to the formation of the Merrison Committee and considerable investment in new research into steel box girder behavior (Merrison Committee of Inquiry, 1973).



Figure 2.1: The Bangabandhu multipurpose bridge, Bangladesh (Source: BBA, 2019)

Most of the bridges still under construction at this time were delayed for investigation of the basic design principle. Some were abandoned or rebuilt as a different form of bridge altogether. Most of those that remained as box girder bridges such as Erskine Bridge were either redesigned or had additional stiffening added later. Some bridges were strengthened a few years after opening and then further strengthened years later. Although this was often due to increased traffic load as much as better design standards. The Irwell Valley Bridge of 1970 was strengthened in 1970 and again in 2000 (Smith and Hendy, 2002).

Long span concrete box girder bridges first appeared in the 1950's. From the beginning, this bridge type was built segmentally using the balanced cantilever method of construction with form travelers and cast-in-place segments. After half a century of developments, concrete box girder bridges have a positive track record that are widely used, and have reached spans of up to 988 ft.

At present, Shibampo Yangtze Bridge in China (**Figure 2.2**) has largest span among the box girder bridge which has a span of 330m. other notable long span box girder bridge include Stolmasundet Bridge in Norway (**Figure 2.3**) with a span of 301m. In Bangladesh, the largest long span bridge is the Bangabandhu multipurpose bridge.



Figure 2.2: Shibanpo Yangtze bridge (China) (span: 330m) (T.Y. Lin International, 2010)



Figure 2.3: Stolmasundet bridge (Norway) (span: 301m)

(Source: EXCA 2019)

Long span concrete girder bridges use a box cross-section as shown in Figure 2.4 because of its structural advantages. This section is able to resist both positive and negative moments present in continuous bridges because it has both top and bottom flanges. The large torsional

strength and rigidity of a closed section is favorable for resisting torsional moments due to curved alignments or eccentric live load. The box girder section requires less post-tensioning than other sections. The required post-tensioning is related to the efficiency of the section which can be measured by the ratio:

$$\rho = \frac{I}{Ay_t y_b}$$

Where I denote the moment of inertia, A the area and y_t , y_b the distances from the neutral axis to the top and bottom fibers. A typical box girder section has a ρ equal to 0.60 whereas for a rectangular section ρ is equal to 0.33. The only disadvantage of the box girder section is the cost associated with forming the section which is higher than for other cross sections. This additional cost is more than justified for long span lengths because a box section can be designed to reduce dead load to a minimum (Rodriguez, 2004).

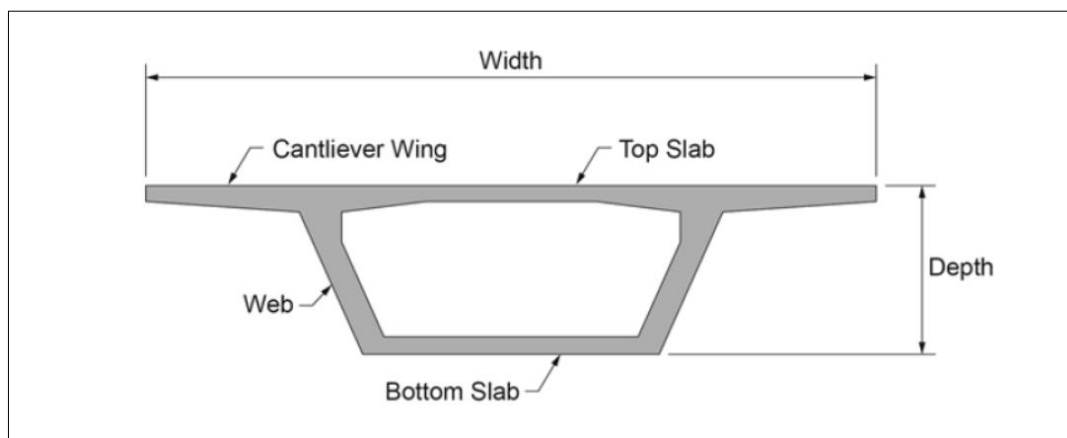


Figure 2.4: Cross section of single cell box girder bridge

The two-web box section has been used for widths up to 26 m (85 ft). Single box girder bridges with a large width to span ratio may lose efficiency due to the effect of shear lag, cross section distortion and transverse bending moments. To avoid these potential negative effects some bridges that are usually wider than about 50 ft, have been designed with other types of box sections. A two-cell, three-web section. This section has less shear lag and distortion than a single-cell section because the distance between webs is reduced. It also has smaller transverse bending moments due to the reduction in the transverse span. However, a three-web section is more difficult to build due to the fact that two internal forms are needed. Similar results can be achieved with the multiple box girders. Current trends in cross-section design lead to single cell box girders for increasingly wider bridges. Ribs or struts are used to provide additional transverse capacity (Rodriguez, 2004).

2.3 Segmental Construction

Balanced cantilever segmental construction shown in **Figure 2.5** for concrete box-girder bridges has long been recognized as one of the most efficient methods of building bridges without the need for falsework. This method has great advantages over other forms of construction in urban areas where temporary shoring would disrupt traffic and services below, in deep gorges and over waterways where falsework would not only be expensive but also a hazard. Construction commences from the permanent piers and proceeds in a “balanced” manner to midspan. The cantilevers are usually constructed in 3- to 6-m-long segments. These segments may be cast in place or precast in a nearby purpose-built yard, transported to the specific piers by land, water or on the completed viaduct and erected into place. Both methods have merit depending on the specific application (Chen and Duan, 2000).

Typical internal span-to-depth ratios for constant-depth girders are between 18 and 22. However, box girders shallower than 2 m in depth introduce practical difficulties for stressing operations inside the box and girders shallower than 1.5 m become very difficult to form. This sets a minimum economical span for this type of construction of 25 to 30 m. Constant-depth girders deeper than 2.5 to 3.0 m are unusual and therefore for spans greater than 50 m consideration should be given to varying-depth girders through providing a curved soffit or haunches. For haunch lengths of 20% to 25% of the span from the pier, internal span-to-depth ratios of 18 at the pier and as little as 30 at midspan are normally used (Chen and Duan, 2000).

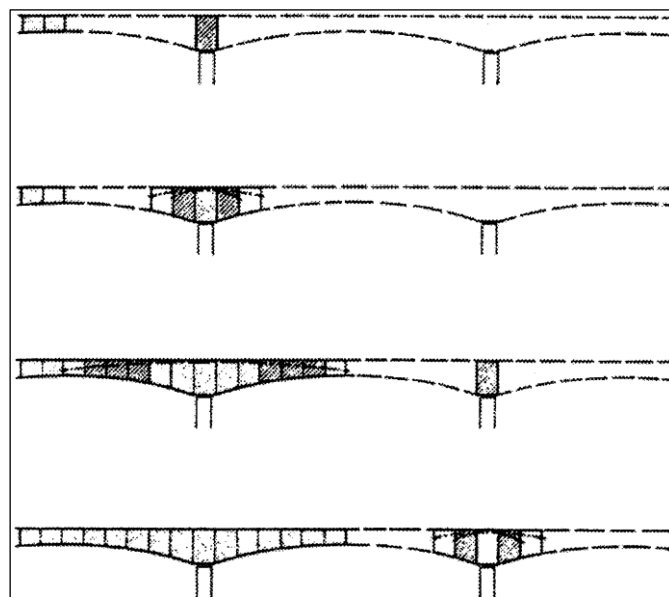


Figure 2.5: Balanced cantilever construction (Chen and Duan, 2000)

2.4 Bearings in Bridge

Bearings are structural devices positioned between the bridge superstructure and substructure. Transmission of load from superstructure to substructure and accommodating relative movements between superstructure and substructure are the principal function of bearing. Forces applied to a bridge bearing mainly include superstructure self-weight, traffic loads, wind loads and earthquake loads. Movements in bearing include translations and rotations, creep, shrinkage and temperature effect (Chen and Duan, 1993).

2.4.1 Types of Bearings

Sliding Bearing

A sliding bearing as shown in **Figure 2.6** utilizes on a plane metal plate sliding against another to accommodate translations. Sliding bearings can be used alone or as a component in other types of bearings. A guiding system may be added to a sliding bearing to control the direction of the movement (Chen and Duan, 1993).

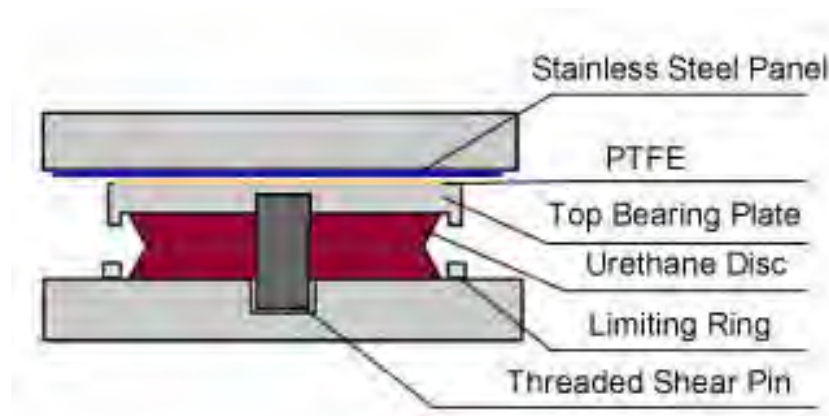


Figure 2.6: Sliding bearing (Chen and Duan, 1993).

Rocker and Pin Bearing

A rocker bearing as shown in **Figure 2.7** typically consists of a pin at top that facilitates rotations and a curved surface at the bottom that accommodates the translational movements. A pin bearing is a variety of fixed bearing that accommodates rotations through use of steel pin. Rocker and pin bearings are primarily used in steel bridges. (Stanton et al, 1993).

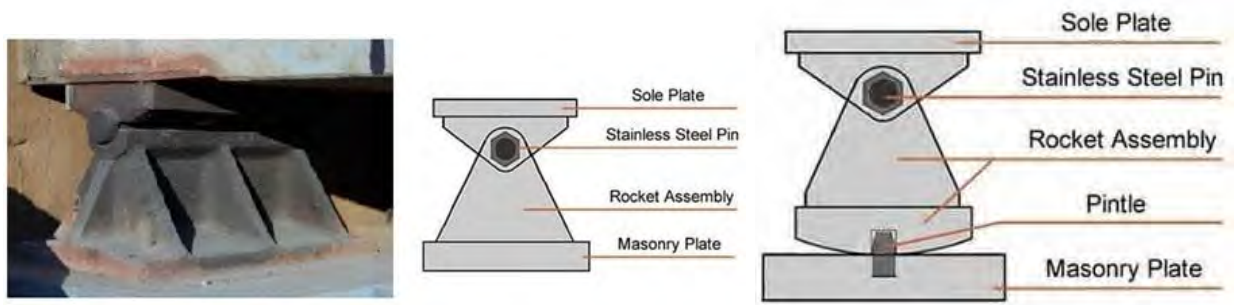


Figure 2.7: Rocker and pin bearing (Stanton et al, 1993).

Roller Bearing

Roller bearings are composed of one or more rollers between two parallel steel plates. Typical roller bearing is shown in **Figure 2.8**. Single roller bearings can facilitate both rotations and translations in the longitudinal directions, while a group of rollers would only accommodate longitudinal translations (Chen and Duan, 1993).



Figure 2.8: Roller bearing (Chen and Duan, 1993).

Elastomeric Bearing

An elastomeric bearing shown in **Figure 2.9** is made of elastomer (either natural or synthetic rubber). It accommodates both translational and rotational movements through the deformation of the elastomer. Elastomer is flexible in shear but very stiff against volumetric change. Under compressive load, the elastomer expands laterally. Elastomeric bearings are generally considered the preferred type of bearings because they are low cost and almost maintenance free (Chen and Duan, 1993).



Figure 2.9: Elastomeric bearing (Chen and Duan, 1993).

Curved Bearing

A curved bearing consists of two matching curved plates with one sliding against the other to accommodate rotations as shown in **Figure 2.10**. Lateral movements are restrained in a pure curved bearing and a limited lateral resistance may be developed through a combination of the curved geometry and the gravity loads (Chen and Duan, 1993).

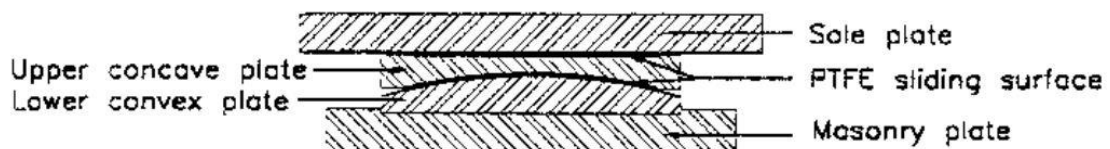


Figure 2.10: Curved bearing (Chen and Duan, 1993).

Pot Bearing

A pot bearing comprises of a plain elastomeric disk that is confined in a shallow steel ring or pot shown in **Figure 2.11**. Translational movements are restrained in a pure pot bearing and the lateral loads are transmitted through the steel piston moving against the pot wall. To accommodate translational movement, a PTFE sliding surface is used. (Chen and Duan, 1993).

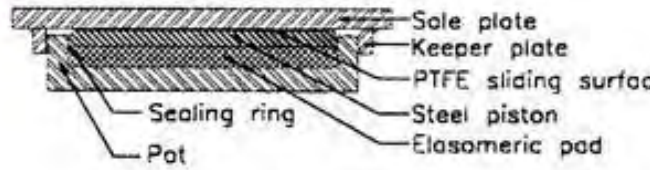


Figure 2.11: Pot bearing (Chen and Duan, 1993).

Disk Bearing

A disk bearing such as in **Figure 2.12** utilizes a hard elastomeric (Polyether urethane) disk to support the vertical loads and a metal key in the center of the bearing to resist horizontal loads. The rotational movements are accommodated through the deformation of the elastomer. (Chen and Duan, 1993).



Figure 2.12: Disk bearing (Chen and Duan, 1993).

2.4.2 Bearings Used in the Bangabandhu Bridge

The bearing and seismic isolation layout of a 7-span module of The Bangabandhu Multipurpose bridge is given in **Figure 2.13**. According to Castellano and Cestarollo (1999), FIP Industriale

have supplied the following seismic isolation components for the Bangabandhu Multipurpose bridge:

- i. Multidirectional Bearings VM 3300/850/400 (at the North Side)
- ii. Multidirectional Bearings VM 3000/850/400 (at the South Side)
- iii. Steel Hysteretic Dampers MEPOT 350/200
- iv. Steel Hysteretic Dampers MEP 350/200
- v. Multidirectional Bearings VM 900/800/50
- vi. Uni directional Bearings VU 850/800-200
- vii. Bumpers with a maximum load of 60 tons

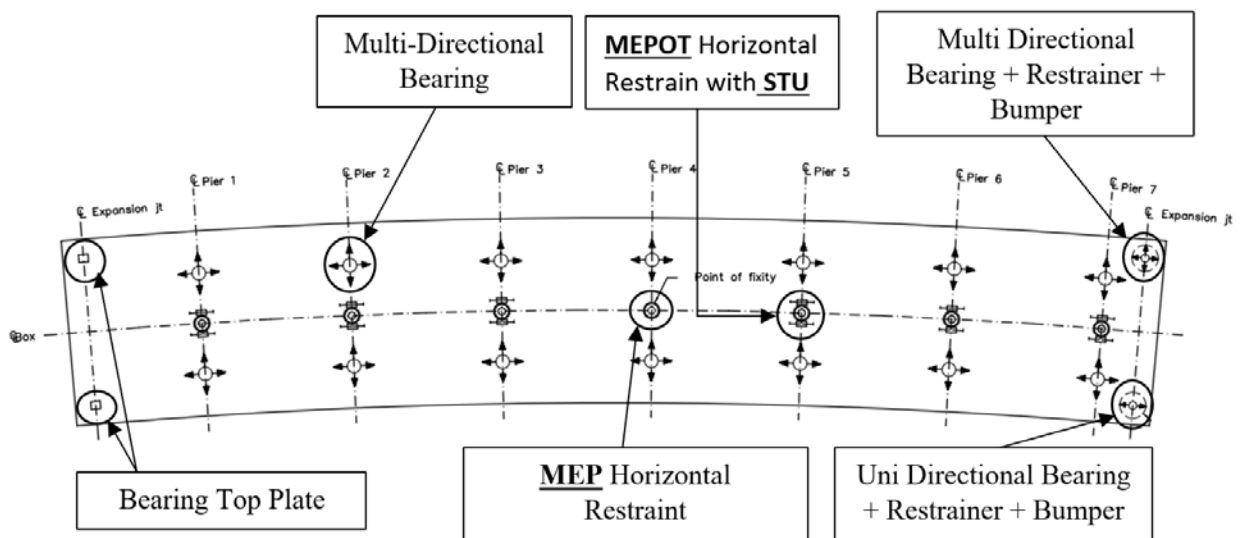


Figure 2.13: Bearing layout in 7 Span modules of The Bangabandhu multipurpose bridge

On the expansion points, there are seismic devices type MEPOT, capable of accommodating longitudinal deck displacements (due to thermal deformations, creep and shrinkage), due to the presence of Shock-Transmission Units (STUs) coupled in series to steel hysteretic dampers.

MEPOT type seismic device as shown in **Figure 2.14** comprises of 42 double taper spindles working in parallel, designed for a yield force approximately 80 kN each and a maximum force of 100 kN each at 200 mm displacement.

The STUs (Shock Transmission Unit) in each MEPOT device are two, with a nominal maximum force of 2100 kN each. They comprise double-action hydraulic cylinder-piston systems filled with silicon compound.

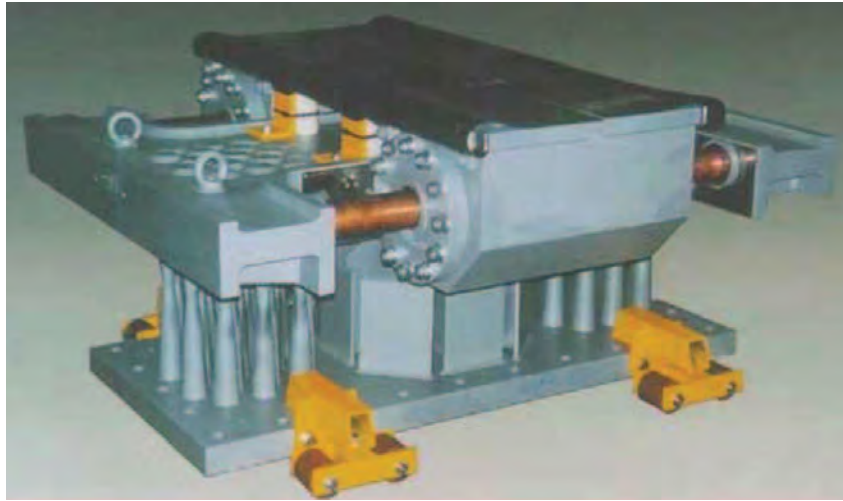


Figure 2.14: MEPOT with STUs (Source: FIP 2019)

Under service conditions, there is a fixed point on 4th pier where a seismic device type MEP is located. MEP also comprises of 42 double taper spindles working in parallel, designed for a yield force approximately 80 kN each and a maximum force of 100 kN each at 200 mm displacement. MEP type is identical except for the absence of STUs.

On the North Side on each pier, VASOFLON Multi-directional bearing (VM 3300/850/400) as shown in **Figure 2.15** with vertical capacity of 33,000 kN is used. Its allowable translation is ± 425 mm in longitudinal direction and ± 200 mm in transverse direction of the bridge.



Figure 2.15: Typical VASOFLON multi-directional bearing (Source: FIP 2019)

On the South side of each pier, VASOFLON Multi-directional bearing (VM 3300/850/400) with vertical capacity of 30,000 kN was used. Its allowable translational are same as that of multi-directional bearing used on the North Side.

On South side of both east and west end, Unidirectional bearing (VU 850/800-200) as shown in **Figure 2.16** is used. This type of bearing is only allowed to translate on longitudinal direction of the bridge. Its vertical capacity is 8500 kN with allowable longitudinal translation of ± 400 mm. It is able to transfer 2000 kN horizontal force in transverse direction.



Figure 2.16: Typical VASOFLON uni-directional bearing (Source: FIP 2019)

On North side of both east and west end, Multi-directional bearing (VM 900/800/50) is used. This type of bearing is only allowed to translate on both longitudinal and transverse direction of the bridge. Its vertical capacity is 9000 kN with allowable longitudinal translation of ± 400 mm and transverse translation of ± 25 mm.

In short, FIP Industriale have supplied unidirectional and multi-directional VASOFLON pot bearings with variable vertical load from 8500 to 11500 kN, installed on the West End and East End piers as well as at the Gerber girder connections.

FIP Industriale have also supplied special foam rubber bumpers to limit damage to the vertical girder interfaces due to possible hammering.

At any rate, under an extremely unlikely earthquake higher than the design-level, a stop-block intervenes with the onset of ± 250 mm transverse displacements. **Table 2.1** shows detailed properties of seismic devices.

Service loads (i.e., wind, braking actions, etc.) do not stress the dissipating elements owing to the use of "sacrificial restraints", designed to fail at a 500 kN horizontal load. Said sacrificial restraints impede any movements on those of the expansion type. In the event of a strong earthquake, the sacrificial restraints fail and the dampers are activated.

It is also stated that the bearing behavior during service condition and seismic conditions are different as sacrificial restraints are not present during seismic condition. **Figure 2.17** shows behavior of bearing system in both service and seismic condition. Also shock transmission unit play a major role during seismic condition.

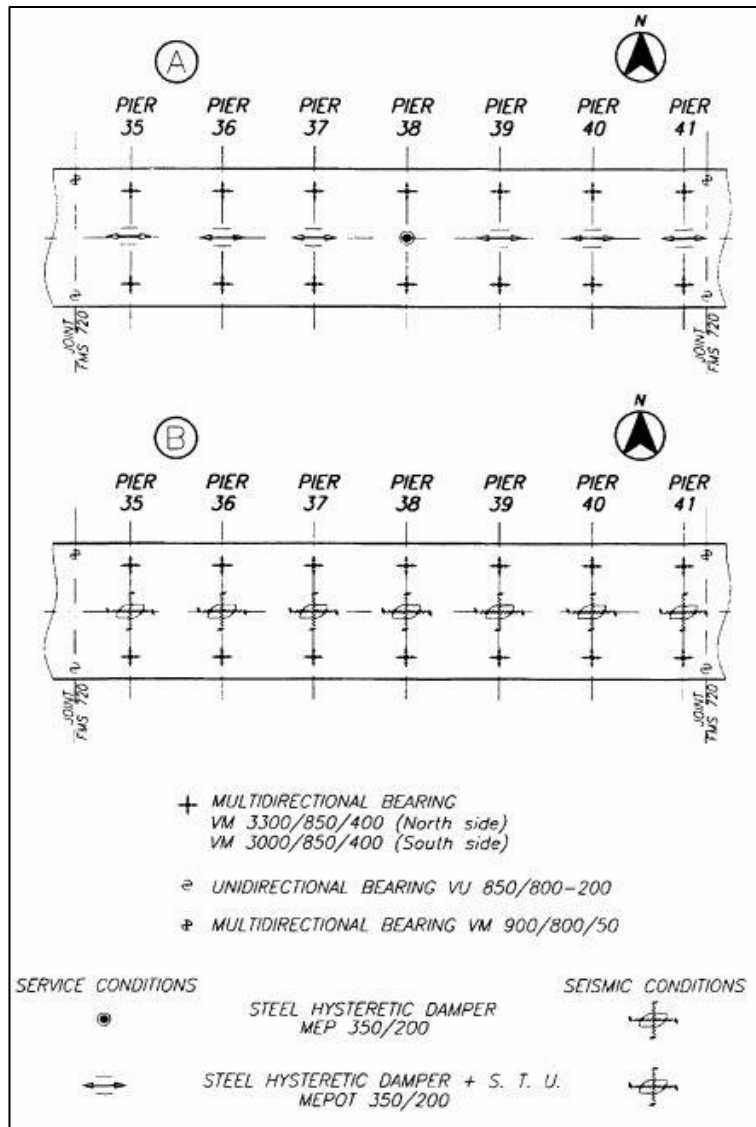


Figure 2.17: Bearing system of a typical girder of The Bangabandhu bridge
(A) service condition and (B) seismic condition

Table 2.1: Detailed properties of seismic devices used in The Bangabandhu Bridge

Name	Designation	Vertical Load Limit	Horizontal Load Limit	Horizontal Translation Limit		Stiffness (K)	
				Longitudinal	Transverse	Longitudinal	Transverse
		kN	kN	mm	mm	kN/mm	kN/mm
Steel Hysteretic Damper (MEP)	MEP 350/200		3500	± 200	± 200	17.50	17.50
Steel Hysteretic Damper+ STU (MEPOT)	MEPOT 350/200						
Multi Directional Bearing (North)	VM 3300/850/400	33000	5400	± 425	± 200	12.70	27.0
Multi Directional Bearing (South)	VM 3000/850/400	30000					
Uni Directional Bearing+ Restrainer +Bumper	VU 850/800-200	8500	2000	± 400	± 20	5.0	100.0
Multi Directional Bearing +Restrainer +Bumper	VM 900/800/50	9000	1800	± 400	± 25	4.50	72.0

2.5 Previous Records of Earthquakes

At the advent of recent earthquakes, bridges have shown below standard performance. In fact, some of the recently built bridges which are specifically designed for earthquake have collapsed or have been severely damaged (Wang, 2003). Earthquake risks in Bangladesh in recent times also pose threat for such severe damage to bridges.

2.5.1 Damages to Bridges in Recent Earthquakes

According to Priestley and Park (1984) bridges can be broadly grouped into three categories in terms of damage in recent earthquakes: (1) spans falling from piers under the seismically induced response displacement, due to inadequate seating provisions, and a lack of restraints from pier caps or adjacent spans; (2) failure of piers or piles in flexure or shear, resulting from the seismic inertia forces induced in the bridge superstructure; (3) failure of foundation materials (slumping of abutments, liquefaction of sandy foundations). The observed damage cannot be directly identified with the effect of asynchronous ground motion, as this aspect is not yet fully understood. Amongst the failures, some of unseating of spans are thought to be directly attributed to asynchronous input ground motion, or asynchronous motion at the tops of the piers (Wang, 2003).

Among these three categories, the unseating of bridge spans is a common type of seismic failure in bridges. The bridge girders move off their supports because the relative movement of the spans in the longitudinal direction exceeds the seating widths. Asynchronous ground displacement effects can play an integral part in this. However, the structural differences between sections separated by movement joints and the local soil conditions may increase the relative movements across the movement joints. Another case that may result in span unseating is when the spans are skewed. It has been observed that skewed spans develop larger displacements than right spans, as a consequence of a tendency for the skew span to rotate in the direction of decreasing skew, thus tending to drop off the supports at the acute corners. Spans unseating have been observed in most major earthquakes. Among them, some of the highlighted ones are described in the following.

Gulf of Alaska Earthquake (27th March, 1964; magnitude 8.5)

The steel trusses of the Copper River and north western Railroad Bridge near Round Island were shifted between a third and two-thirds of a meter movement according to USA National Oceanic and Atmospheric Administration (NOAA). **Figure 2.18** shows one of the displaced trusses, which pounded against an adjacent steel girder span. The girder span was moved, its

concrete pedestal was rotated, and the girder span almost fell into the river. Shortening indicated by buckling of the guardrail is clearly evident.



Figure 2.18: Damage to railroad bridges (Alaska earthquake, 1964)

Niigata Earthquake (16th June 16, 1964; magnitude 7.4)

The bridge shown in **Figure 2.19** had seven spans across the river, each supported by piers, consisting of structural steel girders carrying the reinforced concrete decks. Two of the piers collapsed. The corresponding spans of the bridge collapsed and dropped into the river. The successive spans toward the west bank also dropped while one end of each span remained connected at the top of successive piers. The construction was such that one end of the girders was fixed to a pier and the other end was free to slide longitudinally off the pier after about 30 cm of movement (NOAA).



Figure 2.19: Damage to Showa bridge (Niigata earthquake, 1964)

San Fernando Earthquake (9th February, 1971; magnitude 6.6)

The interchange between the I-5 (Golden State) and C-14 (Antelope Valley) was under construction at the time of the earthquake. (Figure 2.20 shows that the central portion of the curved, nine-span South Connector Overcrossing collapsed, which was structurally complete at the time of the earthquake. The collapsed section consisted of a two-span prestressed post-tensioned box girder supported by a central column and by reinforced concrete box sections at the ends. Although linkage restrainer bolts were provided across the movement joints in this bridge, they had insufficient strength to restrain the relative longitudinal movement (Fung et al., 1971).



Figure 2.20: Span collapse (San Fernando earthquake, 1971)

Guatemala Earthquake (4th February, 1976; magnitude 7.5)

Figure 2.21 shows the collapse of three central spans of the Agua Caliente Bridge on the road to the Atlantic Ocean. Both ground shaking and ground failure contributed to this collapse (NOAA).

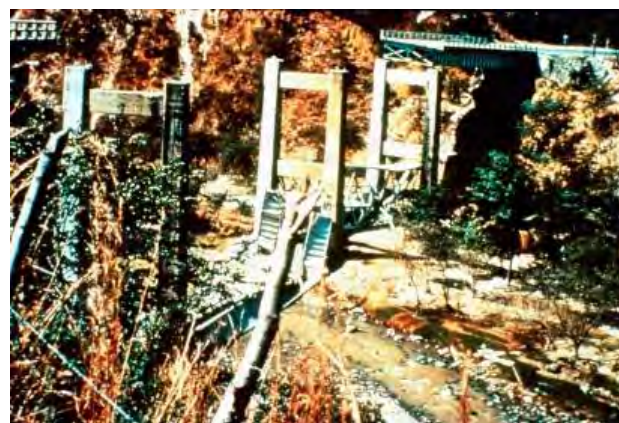


Figure 2.21: Agua Caliente bridge damaged (Guatemala earthquake, 1976)

Lorna Prieta Earthquake (17th October, 1989; magnitude 7.1)

Figure 2.22 shows damage of the San Francisco-Oakland bay bridge. At pier E-9 there is an abrupt change in the structural system, dimensions and spans. On the westward side, there is a span of 154m, where the truss has an overall height of 25.6m. On the eastward side, a shorter span of 88m exists, and the truss height is 12m. The collapsed 15m connecting span was simply supported on the two trusses mentioned above. Failure was due to relative motions between the two end trusses in excess of the 12.7 cm (5") provided by the seating length (EERI, 1990).



Figure 2.22: Oakland Bay bridge damaged by Lorna Prieta earthquake (EERI, 1990)

Costa Rica Earthquake (22nd April, 1991; magnitude 7.5)

Figure 2.23 shows span failure of a modern bridge in Costa Rica after the earthquake. The supports of the bridge were skewed at about 30° to the transverse axis, and the spans were thrown off the internal support in the direction of decreasing skew, due to relative displacement between the abutment and an internal pier at a site with soft soils (EERI, 1991).



Figure 2.23: Unseating of Rio Bananito bridge in 1991 Costa Rica earthquake

Northridge Earthquake (17th January, 1994; magnitude 6.8)

In this earthquake, several segments of the 1-5 and C-14 interchange collapsed again as shown in Figure 2.24 (EERI, 1995). This earthquake has a frequency peak of 0.838g Hz and shear force peak of 0.532g (Rahai and Arezoumandi, 2008).



Figure 2.24: Damage due to Northridge earthquake

Kobe Earthquake (17th January 17, 1995; magnitude 7.0)

Failure of the east link span to the 250m Nishinomiya-ko arch bridge as shown in **Figure 2.25** of the Wangan expressway resulted from Kobe earthquake (Priestley et al., 1995). This 50m simply supported span has unseated due to large movements of the arch bridge support. Elevated highways in Japan typically consist of single spans that have roller bearings at one end and are fixed at the other.



Figure 2.25: Unseating of Nishinomiya-ko bridge in Kobe earthquake (1995)

A number of these single spans fell off their supports as shown in **Figure 2.26** at the expansion joints because of the large longitudinal differential displacements induced between piers.



Figure 2.26: Collapsed sections of expressways in Kobe earthquake

The behavior exhibited by the long-elevated structures indicates that longitudinal seismic actions played an important part in their performance. In these cases, the damage appeared consistent with displacements being applied which were much greater than the strength or displacement capabilities of the components. It can therefore be concluded that the peak forces on these long-elevated bridges resulted from non-synchronous longitudinal ground displacement effects rather than the synchronous response of the structure to ground shaking. That is, the longitudinal ground displacement effects are caused by out of phase displacements

which occur as the seismic wave pass along the structures (Park et al., 1995). These deck collapse which were observed in these major earthquakes cannot be fully attributed to the asynchronous ground motion but it seems that non-uniform earthquake motions could play an important role in the seismic response of bridge and needs to be investigated further (Wang, 2003).

2.5.2 Risk of Earthquake in Bangladesh

In Bangladesh, number of bridge structures is growing at a rapid speed. So is the risk of occurrence of earthquake. Several small-scale earthquakes have hit this county very recently. Bangladesh at present is prone to a severe earthquake. Also, at past, various earthquake of large magnitude (Richter scale 7.0 or higher) shown in **Table 2.2** as epicenter situated within Bangladesh and India (close to Indo-Bangladesh border) have occurred (Ali and Choudhury, 1994). Some active fault lines surround this country as shown in **Table 2.3**. Considering major risks of earthquake failure as seen from other countries is fairly evident. Very few codes including Bangladesh National Building Code (BNBC) lack proper provision for earthquake analysis. Thus, assessment of responses of flyover bridges due to earthquake is becoming an important issue.

Table 2.2 : List of major earthquakes affecting Bangladesh (Ali and Choudhury, 1994)

Date	Name of Earthquake	Magnitude (Richter)	Distance of Epicenter from Dhaka (Km)
10 th January, 1869	Cacher Earthquake	7.5	250
14 th July, 1885	Bengal Earthquake	7.0	170
12 th June, 1897	Great Indian Earthquake	8.7	230
8 th July, 1918	Srimongol Earthquake	7.6	150
3 rd July, 1930	Dhubri Earthquake	7.1	250

Table 2.3: Tectonic Provinces and their Earthquake Potential (Ali and Choudhury, 1992)

Location of Fault Zone	Magnitude (Richter)	Maximum Credible Magnitude (Richter)	Depth of Focus (Km)
Assam	8.0	8.7	0-70
Tripura	7.0	8.0	0-70
Sub-Dauki	7.3	7.5	0-70
Bogra	7.0	7.5	0-70

2.6 Design Provision of Box Girder Bridge

Various codes are followed for designing box girder bridge across the world. Both structural provisions and seismic provisions are discussed in the following.

2.6.1 Structural Design Code

The design of a long span concrete box girder bridge takes place in the context of design codes and specifications. Traditionally these bridges have been designed for service stresses and then checked for ultimate capacity. In the United States first applicable design specification was first edition of the Guide Specifications for Design and Construction of Segmental Bridges published in 1989. A second edition followed in 1998. The AASHTO LRFD Bridge Design Specifications incorporates most of the provisions of the second edition of the Segmental Guide Specifications. A comparison of the AASHTO LRFD code with the first edition of the Guide Specifications for Design and Construction of Segmental Bridges reveals that AASHTO LRFD sets allowable stresses in compression higher than those included in the first edition of Segmental Guide Specifications. The allowable compressive stress for permanent loads changed from $0.40 f'_c$ to $0.45 f'_c$. This increase must be applied with caution since concrete creep accelerates for stresses exceeding $0.50 f'_c$. The Strength IV limit state, included in AASHTO LRFD, has a 1.5 load factor for dead load. This strength limit state may govern the design of long span structures with a high dead load to live load ratio. AASHTO LRFD also presents a new approach for checking shear capacity that can result in thinner webs. Also,

combination of truck and lane loads of LRFD code can result in higher ultimate bending moments for the top slab and the webs (Rodriguez,2004).

2.6.2 Seismic Design

Europe, Japan, New Zealand and the United States have made significant contribution to seismic design provision. Europe developed European Committee of Standardization (CEN) approved as part 2 to Eurocode 8 entitled “Earthquake Resistance Design of Bridges” in 1994 (CEN,1994). Japan published part V of Japan Road Association titled “Specification for Highway Bridges: Seismic Design” in 1990 (JRA, 1990). In New Zealand seismic design procedures are defined in Section 5 of the "Bridge Manual: Earthquake Resistant Design" (TNZ, 1994) issued by Transit New Zealand in 1994. At the present time, there are two national specifications for bridge design in the United States each containing seismic design provisions. Both are published by the American Association of State Highway and Transportation Officials (AASHTO). The first is a working-stress specification titled "Standard Specifications for Highway Bridges"; seismic requirements are contained in Division I-A: Seismic Design (AASHTO, 1992). The second is a limit-state specification, and is titled "LRFD Bridge Design Specifications" (AASHTO, 1994). The Department of Transportation of the State of California (Caltrans), has developed an independent set seismic specification that are published as a subset of "Bridge Design Specifications" and supplemented by "Memos to Designers" on an as-needed basis (Caltrans, 1995) (Buckle, 1996).

In case of Eurocode 8 part 2 recommends that bridges longer than 400m, or bridges built on significantly varying ground types, should be assessed under the effects of multiple support excitation (MSE). At present, the Eurocode 8 part 2 does not require bridges of the length being modelled to be analyzed for MSE if the ground conditions are homogenous (Crewe and Norman, 2006).

2.7 Analysis Method for Box Girder Bridges

Bridge is a complex system with various element. During designing a bridge, analysis is simplified by virtue of assumptions that establish relationship between behaviors of single element in the integrated structure. It is assumed that combination of the responses of these single elements represent the response of the whole structure. The accuracy and success of the method basically relies upon the quality of the assumptions made. There are several methods of analysis for only straight box-girder walls based on recommendation of American

Associations of State Highway Transportation Officials (AASHTO 2002) and Canadian Highway Bridge Design Code. These methods include (Mutsuddy, 2009):

- i. Finite-difference technique
- ii. Grillage analogy
- iii. Folded plate
- iv. Orthotropic Plate Theory
- v. Finite Strip
- vi. Finite Element Method
- vii. Thin walled beam theory

Among these methods finite element technique is applied to conduct this study.

2.7.1 Finite Element Method

Finite Element method (FEM) is an application of both methods of analysis and synthesis. In this procedure, a structure will be decomposed into element at first. Then, these elements are synthesized to create the reference structure. Structural problems can be solved from such decomposition and synthesis. (In recent decades, finite element method of analysis has exponentially become very popular for computational solution of complex problem in engineering.

Sisodiya et al. (1970) approximated the curvilinear boundaries of finite elements that is applied to model curved box-girders. This was done by a series of straight boundaries using parallelogram element. Chapman et al. (1971) analyzed steel and concrete box girder bridges using finite element method. Fam and Turkstra (1975) developed a finite-element scheme for static and free-vibration analysis of box girders with orthogonal boundaries and arbitrary combinations of straight and horizontally curved sections. Tiliouine and Ouanani (2012) presented a 3D finite element model of the Mascara box girder bridge (North Western Algeria) and performed time history analysis covering wide range of seismic hazard scenarios. Carnevale et. al. (2012) conducted a study producing both linear and nonlinear FEM modeling of bridge structure and then were subjected to different well-practiced analysis methods. Papadopoulos and Sextos (2018) developed a finite element model of Lissos bridge using SAP 2000 software and subjected that to anti-symmetric mode excitation to observe seismic response under asynchronous input motion. Another study where a continuous long-span bridge was modelled by finite element method and dynamic responses due to asynchronous motion and multiple support excitation were obtained by time history analysis (Saritaş, 2013).

Mwafy et. al. (2010) developed three different analytical model of an extended highway bridge across Mississippi river to investigate the consequences of ground motion spatial variability on the seismic response.

2.8 Structural Seismic Analysis

There are various ways for seismic analysis of a structure. But in most of the codes, response spectrum, time history analysis and others types are adopted. Among them, response spectrum and time history analysis are widely applied.

2.8.1 Response Spectrum Analysis

Response spectrum analysis (RSA) is a procedure for computing the statistical maximum response of a structure to a base excitation (or earthquake). Each of the vibration modes that are considered may be assumed to respond independently as a single-degree-of-freedom system. Various design codes specify response spectra which determine the base acceleration applied to each mode according to its period. Having determined the response of each vibration mode to the excitation, it is necessary to obtain the response of the structure by combining the effects of each vibration mode. Because the maximum response of each mode will not necessarily occur at the same instant, the statistical maximum response is taken as the square root of the sum of the squares of the individual response (Gazi, 2009).

2.8.2 Time History Analysis

Earthquake excitation is time dependent, highly irregular and arbitrary in nature. Usually earthquake excitation in the form of acceleration or displacement or velocity is recorded for a time interval of 0.02 to 0.005 seconds. In this dynamic analysis procedure, the response of a structure at every time interval is recorded for the whole earthquake period and the statistical average is represented. Because of its inherent complexities of the procedure and non-deterministic nature of the input ground motion, the analysis procedure has not become popular in the design houses for designing of the structures (Gazi, 2009). Time history analysis can be assigned in two ways. 1) Synchronous motion and 2) Asynchronous motion. In this study, asynchronous motion system has been conducted.

2.9 Asynchronous Motion

The asynchronous input accelerations are generally specified in one of the three ways while performing a time-history analysis with spatially varying input motions: (1) Selection of a ground motion array previously recorded in a setting similar to design situation at hand; 2)

generation of time-histories based on modelling of the seismic source and propagation of waves in an elastic medium; and (3) simulation of time-histories based on the random vibration approach. The theoretical, seismological approach based on the modelling of the seismic source and the propagation of waves through the soil is generally successful at low frequencies (less than 1 Hz) only. As an alternative, observed seismograms from small earthquakes can be used as empirical Green's functions in place of the theoretical functions (Wald et al., 1988). The empirical Green's functions allow an approximate inclusion of higher frequencies. The seismological approaches require detailed knowledge of the source mechanism and geological materials along the wave path, which is not always available. In earthquake engineering, the spatial variation is described by the coherency functions defined in terms of the cross-spectral density functions and the local power spectral density functions. Simulation techniques based on the random vibration theory (Shinozuka and Jan 1972; Spanos and Mignolet 1990; Ramadan and Novak 1993) are then used to generate spatially incoherent seismic ground motions matching the prescribed, or target, values of either the power spectral density and coherency function, or the cross-spectral density matrix.

2.10 Previous Studies on Asynchronous Motion

Tzanetos et al (2000) have conducted a study on inelastic dynamic response of RC Bridges Subjected to Spatial Non-Synchronous earthquake motion. In this study, two model structures of medium span Reinforced Concrete (RC) bridges are studied, subjected to different boundary conditions that influence the mode contributions. This is undertaken under transverse, longitudinal and vertical earthquake motion. The large volume of results, represented as displacement and force time-histories as well as Fourier amplitude spectra of the acceleration response, are distilled and used to assess the balance between dynamic de-tuning and static relative displacements. It is concluded that the conventional synchronous case provides conservative results for vertical vibrations. However, unconservative results, of up to 30%, are obtained for transverse and longitudinal response of short periods of structural vibrations, as well as cases where the higher modes of response are likely to be excited.

The RC bridge model is four span structure of total length 184m and straight in plan. The span between piers are 40m long while the two end spans between the abutments and adjacent piers are 32 m long. Deck is twin box prestressed concrete continuous construction and is supported on single columns of different heights.

The bearings are modeled using a single joint element with the pier attached to the first node and the deck attached to the second. The six degrees of freedom describing the relative motion

of two nodes are governed by six action-deformation curves. The longitudinal and transverse restraints are represented by linear curves. The stiffness is assigned as three orders of magnitude greater than the horizontal stiffness of the pier. Vertical restraint is also provided using the same factor applied to the axial stiffness of the pier. The rotational degrees of freedom are represented by a zero stiffness.

Both abutments are modelled as a single joint element where first node is attached to the deck and second is fully restrained. Start abutment is designed to restrict relative translation of the deck end diaphragm in both longitudinal and transverse directions. On the other hand, end abutment provides no restraint in the longitudinal translation. Rotations about the longitudinal axis (out-of-plane) are prevented while rotations about the transverse axis (in-plane) are free in both the abutments. Two different models are investigated with respect to the rotational restraint about the vertical axis (horizontal plane) at start abutment. The rotation is not restrained in the first model whilst the second model has a rotational restraint.

General conclusion in this study includes that factors like ground motion characteristics, symmetry of bridge deformed shape and frequency of fundamental mode of bridge with respect to dominant frequency of excitation determine whether the reduction in dynamic displacements is larger than the increase due to pseudostatic displacement. Also, synchronous case generally gives an upper bound of the maximum axial forces and a lower bound of the minimum axial forces at the piers. This paper indicates that frequency content of input motion in case of asynchronous case is unknown due to wave over-riding, which makes it difficult to the places where asynchronous motion is critical.

It is also concluded that non-synchronous motion in general tends to decrease the transverse response of the bridge. Hence, it was recommended to design bridges against synchronous motion and check the design for non-synchronous effects. This conclusion is limited to the particular geometry and boundary conditions investigated. The same trend was observed in this study for the transverse response of the pinned-pinned bridge.

Monti et al (1996) presents the results of an extensive numerical study on the nonlinear response of bridges subjected to multi-support seismic excitation and analyzed in the non-linear range under non-synchronous motion. The results show that displacement ductility demands in bridges designed by the reduction-factor method for a multi-support excitation are in good accordance with the selected value of reduction factor. The bridges designed for synchronous input and then checked for nonsynchronous motion exhibit an excess of strength in the central piers, whereas the opposite occurs for those close to the abutments, which may have displacement ductility demands larger than those requested under synchronous motion.

The bridge model considered is a six-span continuous deck with five piers of same height. The span length is 50 m. The deck is transversely hinged to the piers and the abutments. The piers that are acting as cantilever are considered fixed on the soil. The parameter considered in this study includes soil type, structural stiffness conducted by varying pier height, behaviour factor and coherency parameters. The three different pier heights are intended to produce three different degrees of bridge stiffness and have been chosen so as to get bridges with fundamental periods varying within rather large limits. The bridges were designed elastically for non-synchronous as well as synchronous ground motion for a PGA of 0.42g. Both linear and non-linear analyses are carried out.

The findings of this study include that incoherent motions lead to a decrease of the design forces, and hence to lower amounts of reinforcements, with respect to the synchronous ones. This result admits no exceptions for the cases considered. The amount of the decrease is variable, depending on the particular combination of the parameters. These given parameters, it varies from pier to pier, with a systematic trend to be larger for the central piers and practically nil for the lateral ones.

It is seen in this study that, increasing incoherency responses show a flattened shape, thus suggesting that higher modes excited by multi-support excitation. The case of decreasing incoherency of geometric nature and with typical natural period synchronous motion is critical in mid piers whereas asynchronous are critical in end pier. But margin between synchronous and asynchronous motion are not massive.

Crewe and Norman (2006) in their paper outlines the results of experimental tests that confirm that for bridges as short as 200m, multiple support excitation can have a significant effect on the response of the bridge. For the bridge configurations tested, the displacements caused by multiple support excitation were up to 36% larger than when multiple support excitation was not taken into consideration. To generate the multiple input motions to each of the piers the bridge model was shaken by five parallel single axis shaking tables. The response of the bridge to three different sets of input time histories are presented in this paper.

The prototype bridge is 200 m long with three piers at equal spacing. The physical tests were performed on a specially designed MSE test bed, which comprises of a set of 5 independent single axis shaking tables, specifically designed to allow simulation of any type of multi support excitation. Two types of input motion are used in this study. whilst the firm soil shows an increase in the response for the asynchronous case, the soft soil case shows a substantial

reduction in the response for the asynchronous case. This is partially due to the increased time delay and also due to the fact that different time histories generated from the same response spectrum can produce different responses when the inputs are asynchronous.

This paper concludes that the tests show that when a time delay is introduced between the input motions to each pier, there is a larger response in the first and third piers, whilst there is no reduction in response of the middle pier. This occurs because the synchronous input (with all piers exactly experiencing the same input motion) only excites the symmetrical first and third modes, whilst the time-delayed input excites all of the first three modes.

Sarıtaş (2013) studied a long span bridge having multi-support excitations were analyzed for the effects of spatially varying ground motions in terms of wave passage and local site response effects. Two types of dynamic analyses were performed: a) same or different soil conditions for all supports b) same ground motions but different arrival times for wave propagation. For evaluations, the results obtained by considering asynchronous ground motions were compared with those of the synchronous ground motions. From the comparisons, significant differences were observed in case of spatially varying ground motions and this case show that the assumption of synchronous ground motions and identical local site conditions are inadequate to represent the earthquake load and soil model. Therefore, earthquake motions and actual local site properties should be characterized by their inherent properties to obtain more realistic responses.

This study works with a five-span bridge with a box-girder having variable cross section in the form of V-shape and rectangular piers with hollow sections.

In this paper, it is seen that for no incidence angle, longitudinal base responses are very close for both synchronous and asynchronous motion. It is also seen that maximum responses are seen in the adjacent support of the ends.

This study concludes that, Delays in wave arrival affect the dynamic behaviour of the bridge system. When the velocity of the wave decreases, deck-displacements generally decrease as well and the deviations become more significantly according to results in case of infinite velocity. Also, Maximum response quantities of the piers appeared for the lowest velocities. The most unfavorable response quantities were observed for the earthquake motion on principal axis of the structural system.

Carnevale et. al. (2012) have seen that the seismic motion is characterized by temporal and spatial variability, that become significant in structures with long longitudinal development,

such as bridges and viaducts. In those cases, the differential displacements of the supports may have adverse effects, either on the pier responses either on the deck deformations. Asynchronous and synchronous dynamic analyses on continuous-span bridges have been carried out using the finite element method.

The bridge model is characterized by a continuous deck. The bridge is subjected to linear and non-linear dynamic analyses. The length of each deck is 40m. There is a total of 6 piers in the bridge model where pier dimensions are differed to differ natural period of the bridge. The bridge piers have slenderness in the range of 2-15; the bridge decks, modelled with a continuous rectangular equivalent section, are representative of one, three or six lanes.

To assess when considering the synchronous action becomes disadvantageous, a parametric analysis, varying the geometry of the bridge and the soil foundation characteristics, has been conducted. The bridges were subjected to sets of artificial accelerograms Analysis shows asynchronous input motions have a significant effect on the response of the bridges that may be more severe than those from synchronous inputs. This behavior becomes more significant when the natural period of bridge increase and the soil characteristics worsen. The geometry variability is obtained varying the ratio between the pier and the deck stiffness, and then the bridge natural period. The linear analyses highlight that the asynchronous response may be caught superimposing the inertial forces to the pseudo-static effects.

In this study, Non linear analyses for asynchronous dynamic behaviour due to different spatially varying ground motion sets has also been carried out. This shows for soil type A dirt of at the piers It shows while considering only an individual synchronous response, synchronous motion is critical in the middle piers while asynchronous motion is critical in the external piers. It is also stated that considering only synchronous motion may be unsafe, especially for external piers for other cases also.

Burdette et.al. (2008) have conducted a study analysis of proposed design example for the second international workshop on seismic design of bridges (Priestly, 1994) was conducted. This prestressed concrete bridge was supported by eight piers and two abutments with a total length of 344 m rotating 98 deg. The piers consist of 1 m diameter single column bents supporting a prestressed concrete twin box girder superstructure with sliding bearings, which allow rotation and longitudinal motion, but are restrained transversely.

The study bridge has eight bridge piers and was subjected to 11 earthquake events at each coherency level, providing 88 opportunities for piers to exceed this limit. Here a nominal lateral

deflection limit of 1.5 times the design synchronous deflection was defined as damaging limit for asynchronous deflection. Results comparing the effect of the two sources of asynchronous earthquake input investigated on the curved study structure indicate that geometric incoherence results in greater response amplification than wave arrival delay for the concrete study structure. Severe geometric incoherence alone resulted in 30% of the piers exceeding the 1.5 displacement limit, compared with 8% with only wave passage effect. This notable difference in response amplification is likely due to the nature of each of these incoherence sources. The wave passage effect simply results in adjacent support points following the same deflection record with a short delay, limiting the pseudo static deflection possible. Geometric incoherence, however, produces slightly different displacement records at adjacent piers due to random reflection and refraction. Thus, adjacent displacement records can vary more significantly, resulting in larger pseudo static deflections and greater response amplification compared with synchronous input.

In this study, it is also seen that for curve bridge model wave passage effect of asynchronous motion in the longitudinal direction, synchronous infinity-infinity is dominant in the mid piers such as pier 5 and 6 where in pier 8 and 9, asynchronous infinity-30 far outweighs in effect.

Most of the studies suggest that, bridges should be designed for synchronous motion and then checked for asynchronous motion. Responses in due to synchronous motion govern in middle spans whereas asynchronous motion governs at end spans. In studies conducted on asynchronous motion, assigned bearing properties are either not clearly defined or out of scope of the study. Also, bridge models are not verified by different provisions are not also thoroughly conducted.

Chapter 3

MODELLING OF THE BRIDGE

3.1 General

In this study, three individual models of different span module lengths are established. The commercially available software Csi Bridge 20 is used in this study for modelling the bridges. The geometry of the models is based on the Bangabandhu bridge. Their dimensions are modified to satisfy structural design provisions. The bridge models are analyzed by finite element method. The elements adopted for modelling described below. The modeling specifications and assignments are explained in this chapter.

3.2 Modelling Elements

Different modelling element such as frame element, link element, tendon element and shell element are assigned to model various component of bridge span modules. Different elements have distinct properties and local axes.

3.2.1 Frame Element

The Frame element is a very powerful element as it can be used to model beams, columns, braces and trusses in planar and three-dimensional structures. It uses a general, three-dimensional, beam-column formulation which includes the effects of biaxial bending, torsion, axial deformation and biaxial shear deformations (Bathe and Wilson ,1976). Each Frame element may be loaded by gravity (in any direction), multiple concentrated loads, multiple distributed loads, strain and deformation loads and loads due to temperature change.

In this analysis, one pier frame section as shown in **Figure 3.1** is used. Concrete strength of pier and cap beam are assigned as 45 MPa (6500 psi). The section and stiffness of pier is varied in accordance with the necessity of the model.

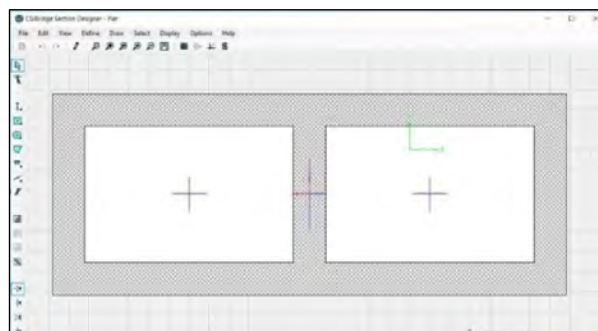


Figure 3.1: Pier section of bridge model

3.2.2 Shell Element

The Shell element is a type of area object that is used to model membrane, plate and shell behavior in planar and three-dimensional structures. This is a three or four-node formulation that combines membrane and plate bending behavior. A typical shell element is shown in **Figure 3.2**.

In this analysis, a shell element named ASEC1 is used for modelling box girder bridge with assigned concrete strength of 45 MPa (6500 psi). The thickness for membrane and bending is both assigned as 250mm.

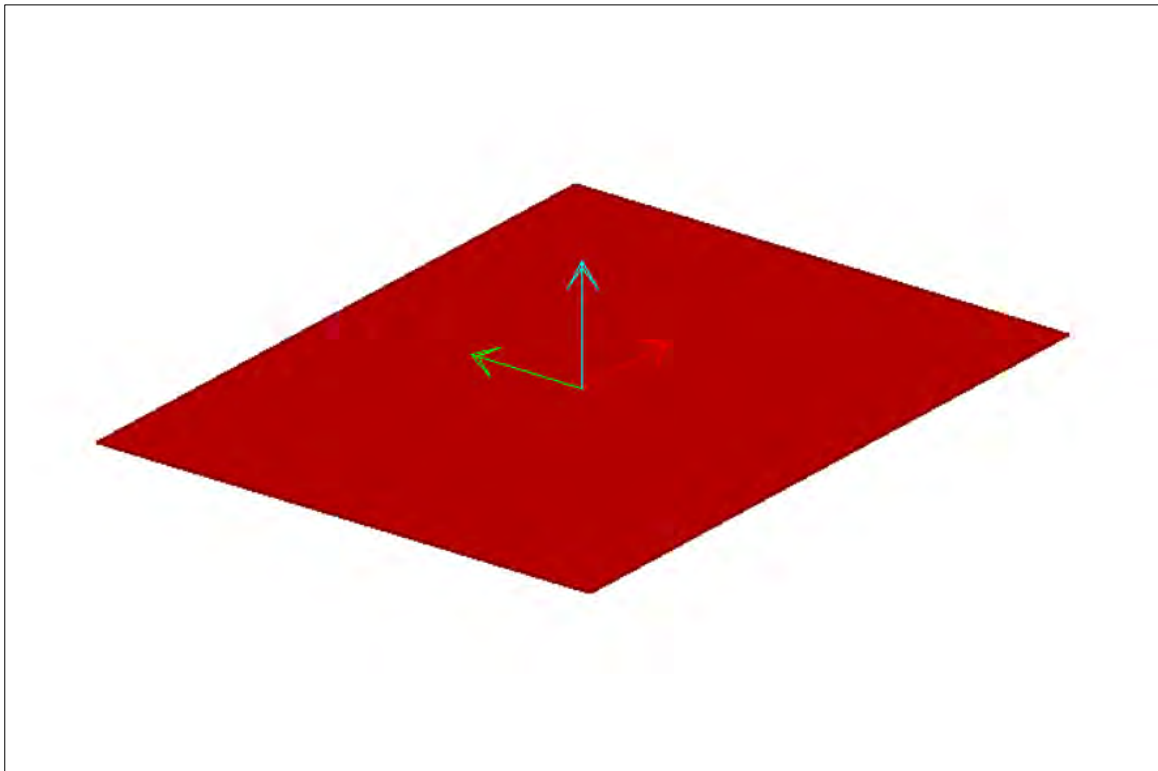


Figure 3.2: Typical Shell element

3.2.3 Link Element

The Link element is used to connect two joints together. The Support element is used to connect one joint to ground. A Support element is a one-joint grounded spring. Each link or support element may exhibit up to three different types of behaviour: linear, nonlinear and frequency-dependent. A typical link element and its directions are shown in **Figure 3.3**.

In this analysis, Multi Direc, Multi Direc End, Uni Direc and STU are used to model isolators such as Multidirectional, unidirectional bearings and Shock Transmission Unit respectively.

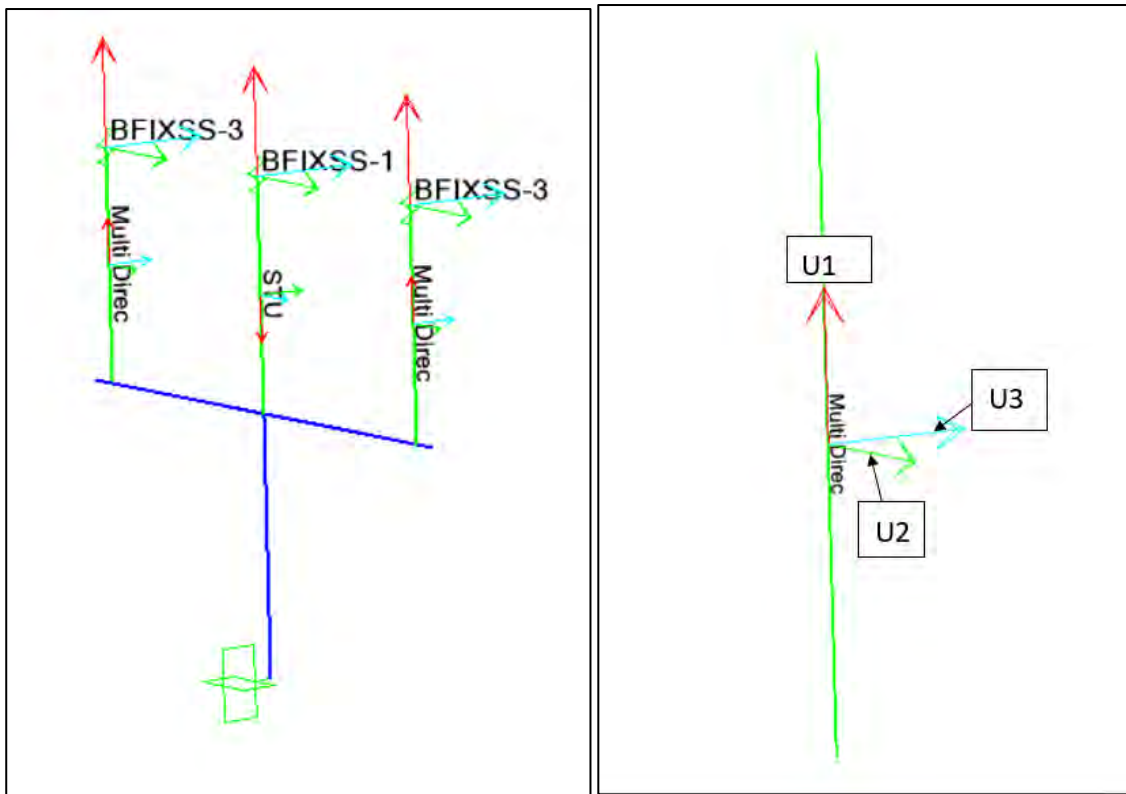


Figure 3.3: Typical link element and its direction

3.2.4 Tendon Element

Tendons are a special type of object that can be embedded inside other objects (frames, shells, planes, solids and solids) to represent effects of prestressing and posttensioning. These tendons attach to other objects through which they pass and impose load upon them. In this analysis, TT1, TB3 and TB3(2) are used to define tendon parameters. A typical tendon element is shown in Figure 3.4. Tendon duct template was assigned differently for top and bottom tendons. Tendon steel is taken to be grade 270. Tendon area is assigned as 3360 mm². But as force is assigned to these tendons, tendon area becomes irrelevant. Jacking is done from the start. Jacking force varied depending on the demand of the model. But bottom tendons and top tendons are as assigned individual forces to be coherent with the as-built drawing.

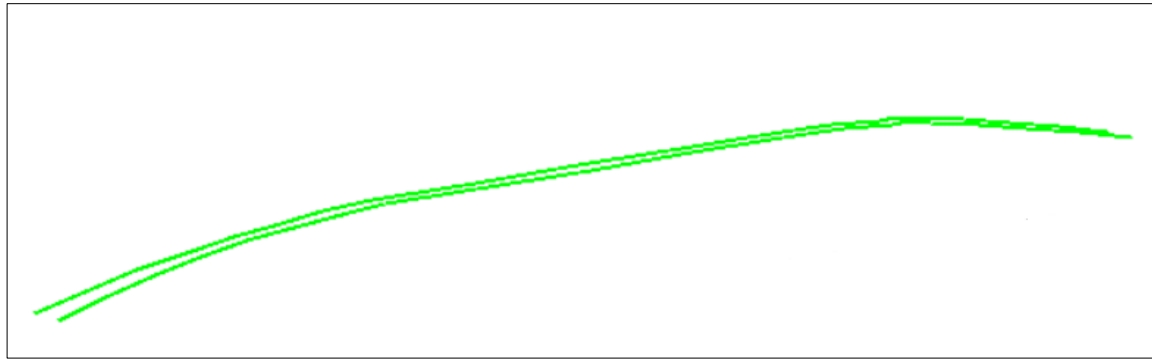


Figure 3.4: Typical tendon element

3.3 Salient Features of Bridges

Figure 3.5 shows schematic diagram of bridge model. The 3 bridge models have their distinctive features. But some of the salient features are highlighted in the following Table 3.1. These features include total length, bottom slab thickness, bottom width and so on. Typical span of Bangabandhu bridge is 99.375 m.

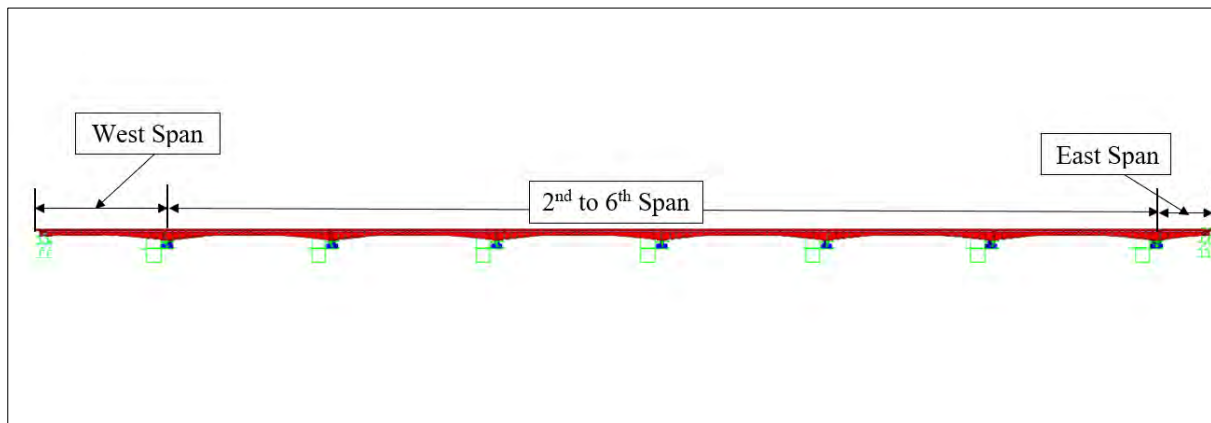


Figure 3.5: Schematic diagram of bridge model

Table 3.1: Salient Features of three bridge models

Typical Bridge Span	75 m	100 m	125m
Span Module (Nos)	7	7	7
Total Length	525m	700 m	870 m
West Span Length	55.78m	74.38m	91.30 m
2 nd to 6 th Span Length	74.531m	99.375m	124.375m
East Span Length	21.94 m	29.30 m	33.23 m
Typical Segment length	3000mm	4000mm	4000mm

Number of Lanes		Two Lane Two Way	Two Lane Two Way	Two Lane Two Way
Top Width		18.5m	18.5m	18.5m
Depth at Pier Top (D1)		4880 mm	6500 mm	8576 mm
Depth at Mid Top (D2)		2065 mm	3294 mm	3888 mm
Top Slab Thickness (t1)		250 mm	280 mm	350 mm
Bottom Width	Start to 0.375L (variable)	6268mm~8704mm	6229mm~8658mm	5264mm~7714mm
	0.375L to 0.625L	8704 mm	8658mm	7714mm
	0.625L to End (variable)	8704mm~ 6268 mm	8658mm~6229 mm	7714mm~5264 mm
Bottom Slab Thickness (t2)	Start to 0.25L (variable)	650mm~ 200mm	850mm~200mm	1060mm~250mm
	0.25L to 0.75L	200mm	200mm	250mm
	0.75L to End (Variable)	200mm~650mm	200mm~850mm	250mm~1060mm
Exterior Girder Thickness (t3)		400 mm	500 mm	625 mm
Concrete strength (as per design drawing)		45 MPa (6500 psi)	45 MPa (6500 psi)	45 MPa (6500 psi)

Among them the 100m model is described in details in this section. Descriptive information of other models is given in the appendix.

The bridge modelling is done in various steps. Some of the important steps are given in the following:

- i. Bridge Layout Step
- ii. Defining Layout Line
- iii. Defining Lanes
- iv. Defining Girder Section with Parametric Variations
- v. Defining abutment and Bent
- vi. Defining Seismic Isolation Properties
- vii. Assigning Prestress
- viii. Assigning Loading
- ix. Assigning Seismic Motion

3.4 Basic Features of the Bridge

All the three models have its own individual features. But as they are based on the same bridge, they are more or less similar. Here, elements of 100m bridge model is described as the representative of all the three bridge models.

3.4.1 Layout Line

At first, the bridge layout line is to be defined as shown in **Figure 3.6**. A 3D model of 100m span is shown in **Figure 3.7**. In this case, the quick start layout line is taken as straight and end station specified.

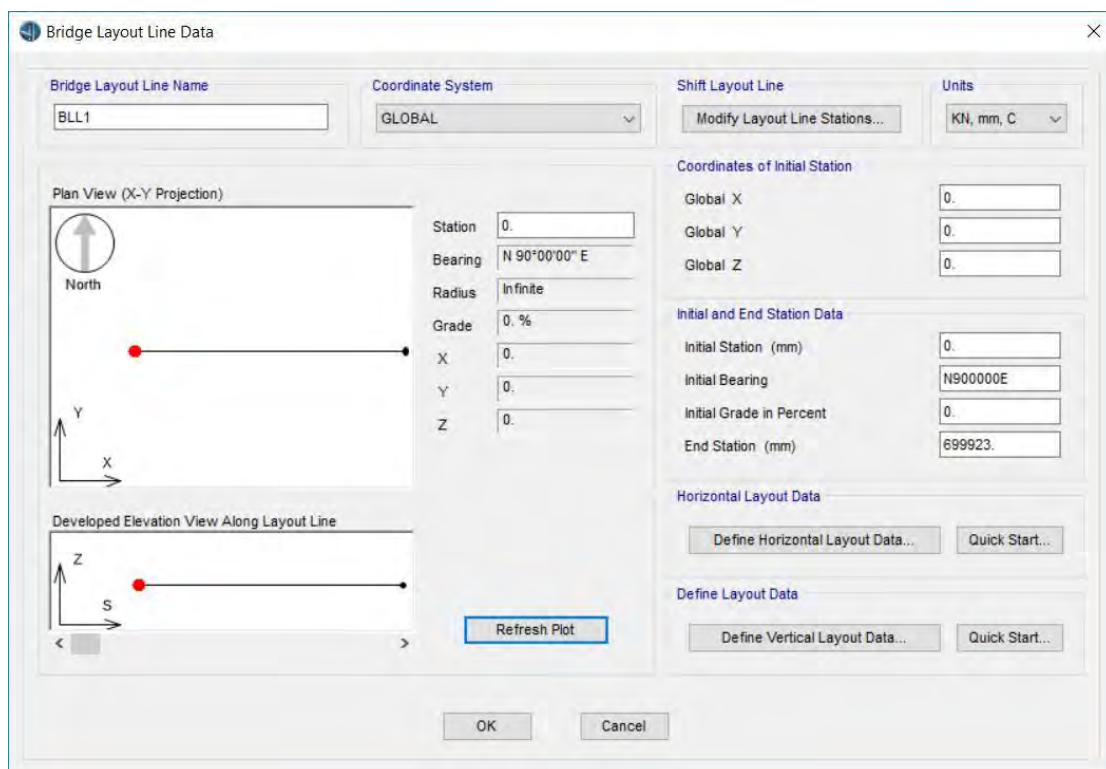


Figure 3.6: Bridge layout line data

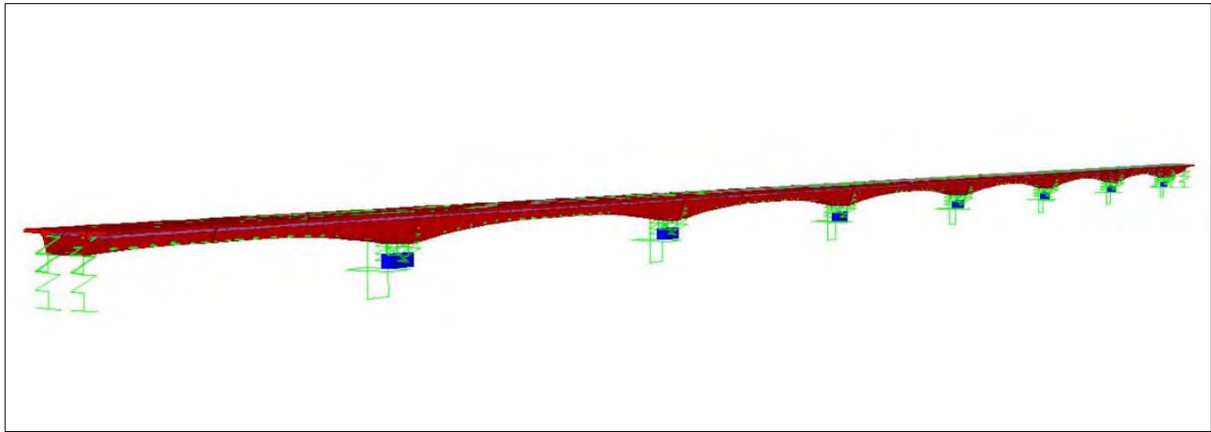


Figure 3.7: 3D model of 100m span module

3.4.2 Lane

There are four lanes defined in the models. They are shown in **Figure 3.8** and elevation view of lanes are shown in **Figure 3.9**.

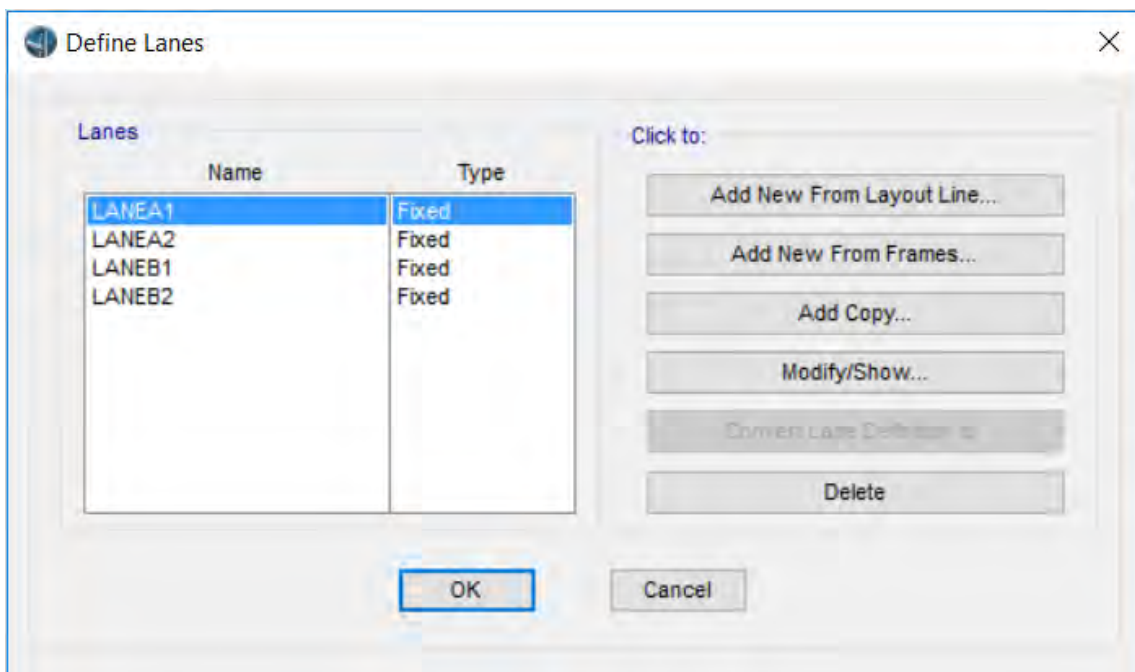


Figure 3.8: Definition of lane

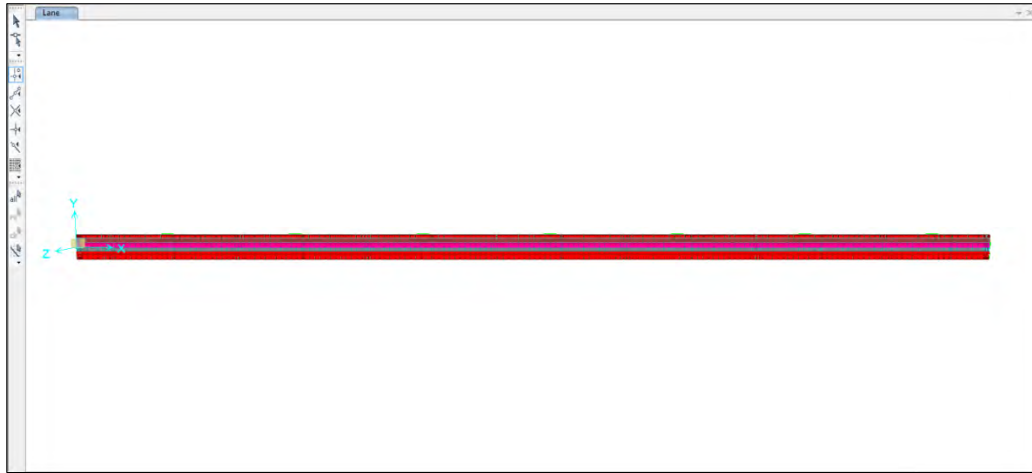


Figure 3.9: Elevation view of lane

3.4.3 Girder Section

The girder section has its section depth, slab thickness and section width parabolically varied based on 7-span module of The Bangabandhu multipurpose bridge. These variations are symmetrical to center line of segments only for typical segments. Assignment of girder section is shown in **Figure 3.10**. List of parametric variation assigned is shown in **Figure 3.11**.

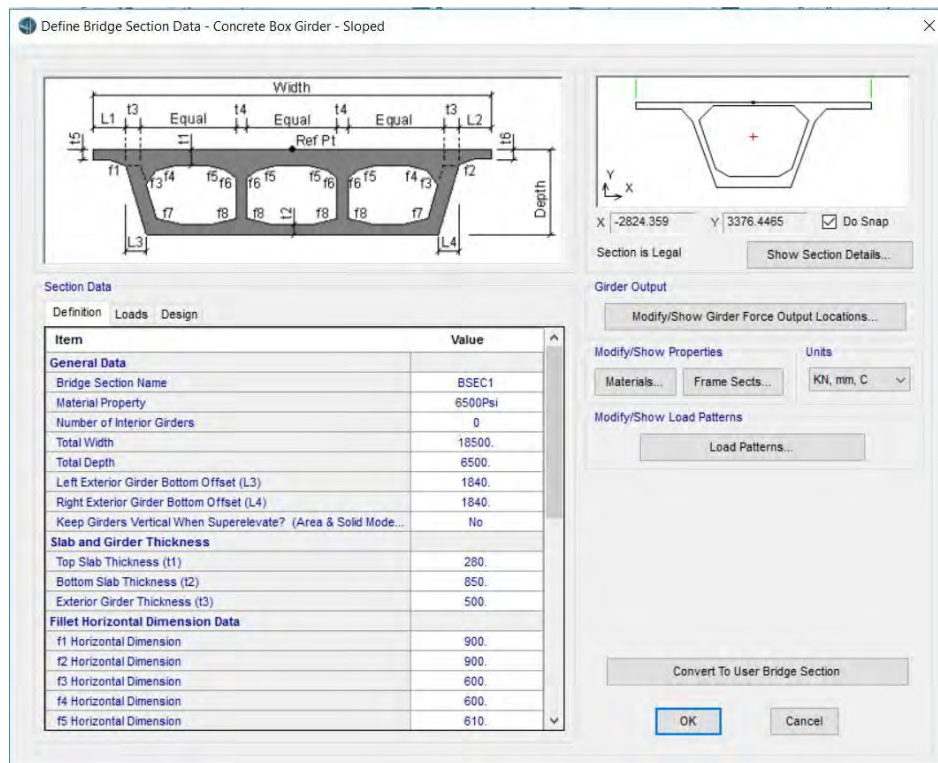


Figure 3.10: Typical cross section of girder

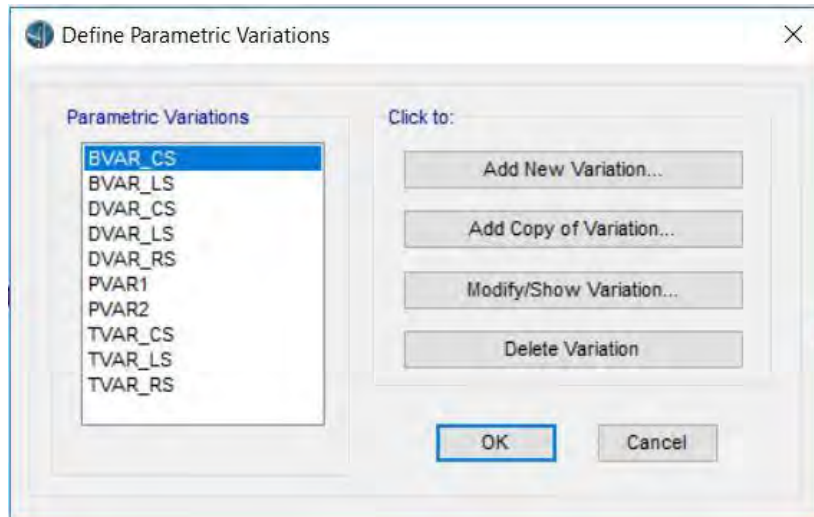


Figure 3.11: List of variation of deck sections

The west span bottom slab thickness varied parabolically as shown in **Figure 3.12**. Thus, it is varied in such a way from girder bottom slab thickness near 1st pier is maximum 850 mm. Then it reduced parabolically to minimum of 200 mm at mid-section as shown in **Figure 3.15**. In case of section depth at left segment, it varied parabolically from 1st pier as 6500 mm to 3892 mm at the end as shown in **Figure 3.13** to **Figure 3.14**. For left segment, section width starts at 5921 mm near piers and varies parabolically similar to segments as in **Figure 3.16**.

At the right segment, the bottom slab thickness was 850 mm at the pier, then it was assigned to decrease in parabolic way as shown **Figure 3.19**. The section depth at right segment varied from 6500 mm to 3604 mm at end as shown in **Figure 3.17** and **Figure 3.18**. For right segment, width starts at 5921 mm near piers and varies parabolically similar to typical segments as .

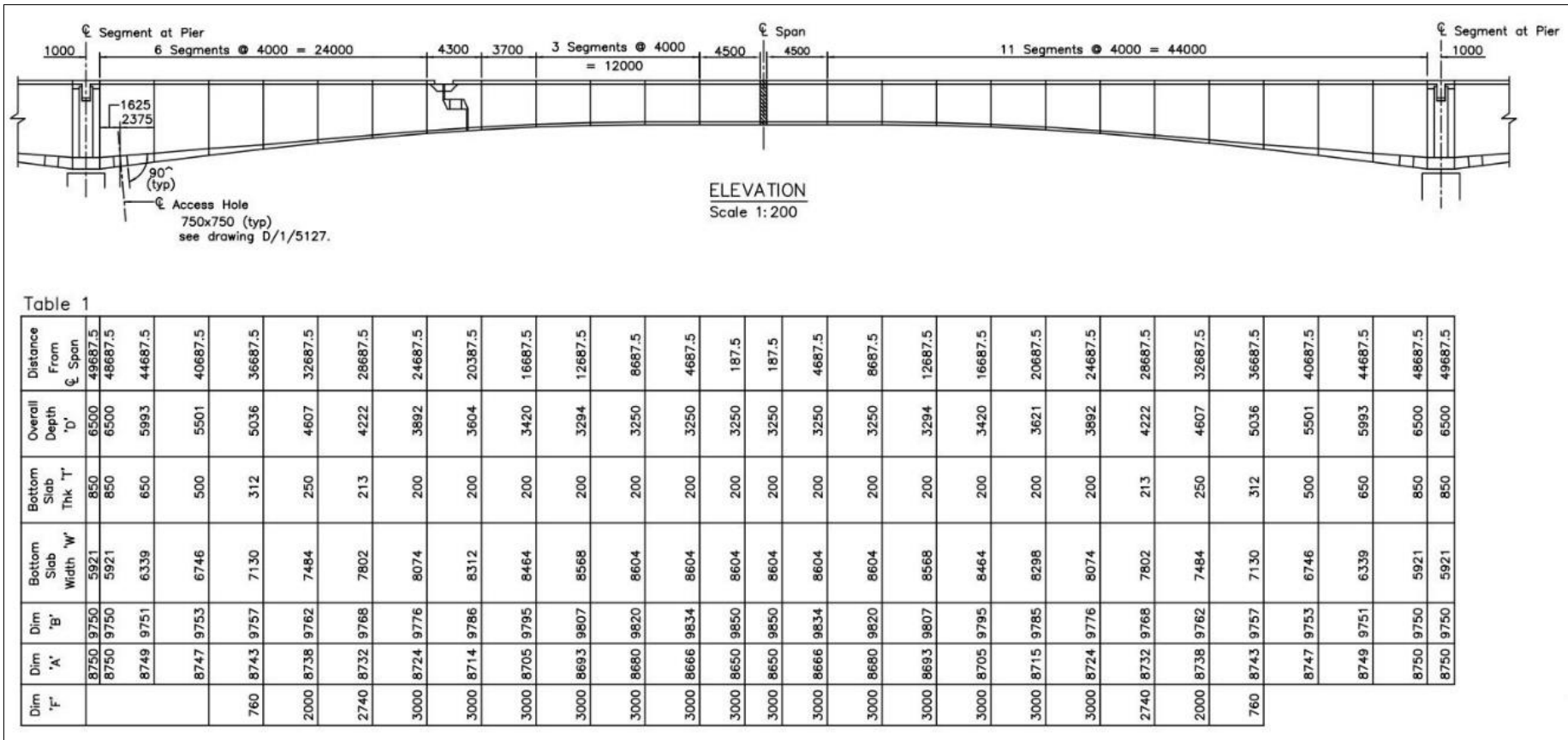


Table 1

Dim 'F'	Dim 'A'	Dim 'B'	Bottom Slab Width 'W'	Bottom Slab Thk 'T'	Overall Depth 'D'	Distance From ϕ Span
	8750	9750	5921	850	6500	49687.5
	8750	9750	5921	850	6500	49687.5
	8749	9751	6339	650	5993	44687.5
	8747	9753	6746	500	5501	40687.5
760	8743	9757	7130	312	5036	36687.5
2000	8738	9762	7484	250	4607	32687.5
2740	8732	9768	7802	213	4222	28687.5
3000	8724	9776	8074	200	3892	24687.5
3000	8714	9786	8312	200	3604	20387.5
3000	8705	9795	8464	200	3420	16687.5
3000	8693	9807	8568	200	3294	12687.5
3000	8680	9820	8604	200	3250	8687.5
3000	8666	9834	8604	200	3250	4687.5
3000	8650	9850	8604	200	3250	187.5
3000	8650	9850	8604	200	3250	187.5
3000	8666	9834	8604	200	3250	4687.5
3000	8680	9820	8604	200	3250	8687.5
3000	8693	9807	8568	200	3294	12687.5
3000	8705	9795	8464	200	3420	16687.5
3000	8715	9785	8298	200	3621	20687.5
3000	8724	9776	8074	200	3892	24687.5
2740	8732	9768	7802	213	4222	28687.5
2000	8738	9762	7484	250	4607	32687.5
760	8743	9757	7130	312	5036	36687.5
	8747	9753	6746	500	5501	40687.5
	8749	9751	6339	650	5993	44687.5
	8750	9750	5921	850	6500	49687.5
	8750	9750	5921	850	6500	49687.5

Figure 3.12: Elevation of expansion joint of 7 span module

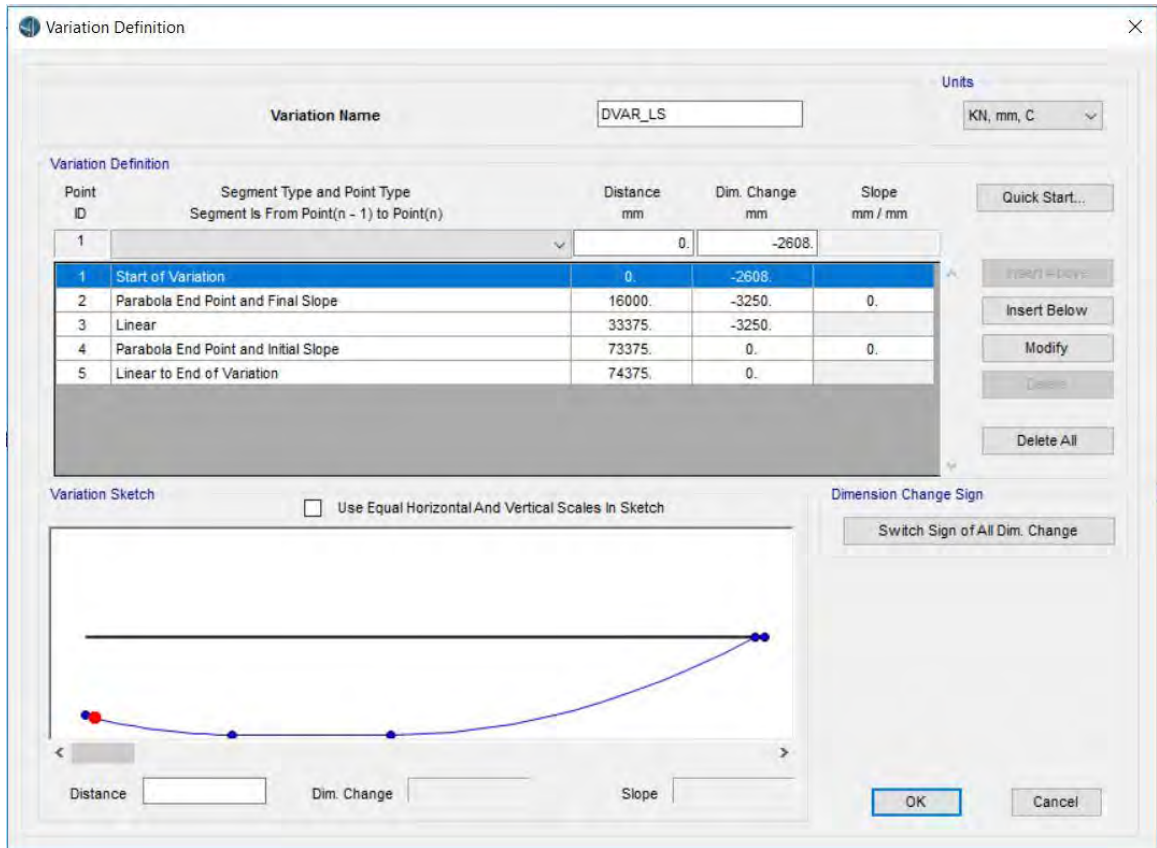


Figure 3.13: Depth variation of west span

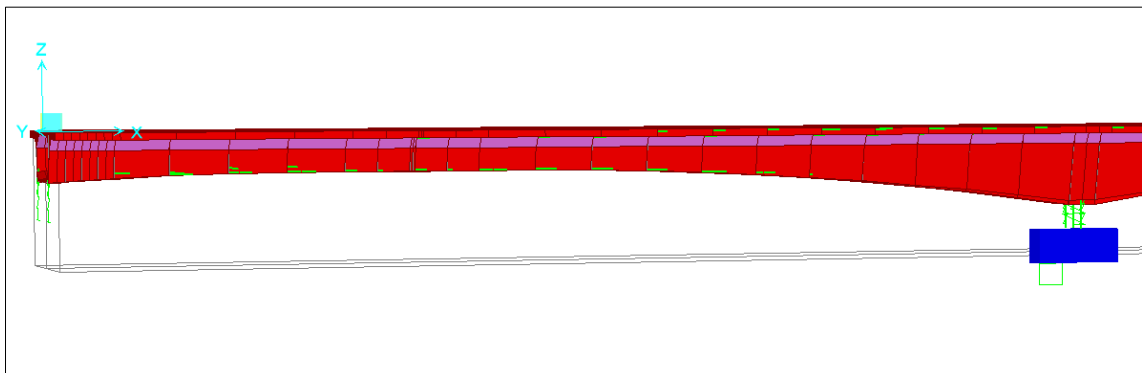


Figure 3.14: 3D view of section depth variation of west span

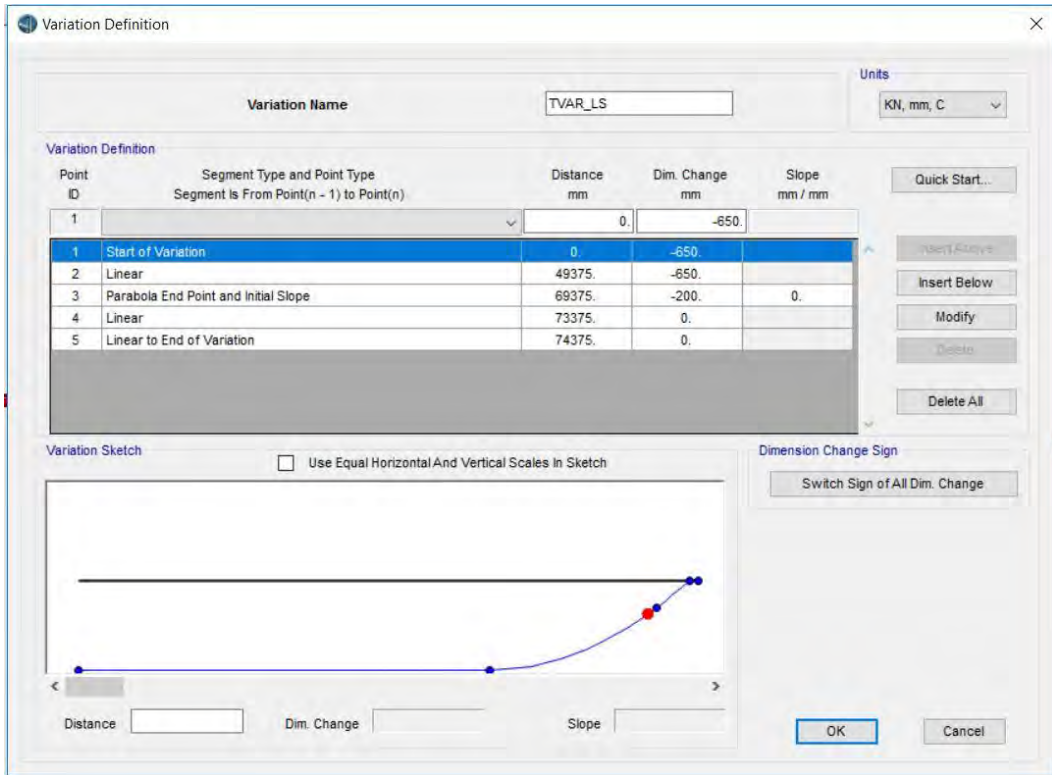


Figure 3.15: Bottom slab thickness variation of west span

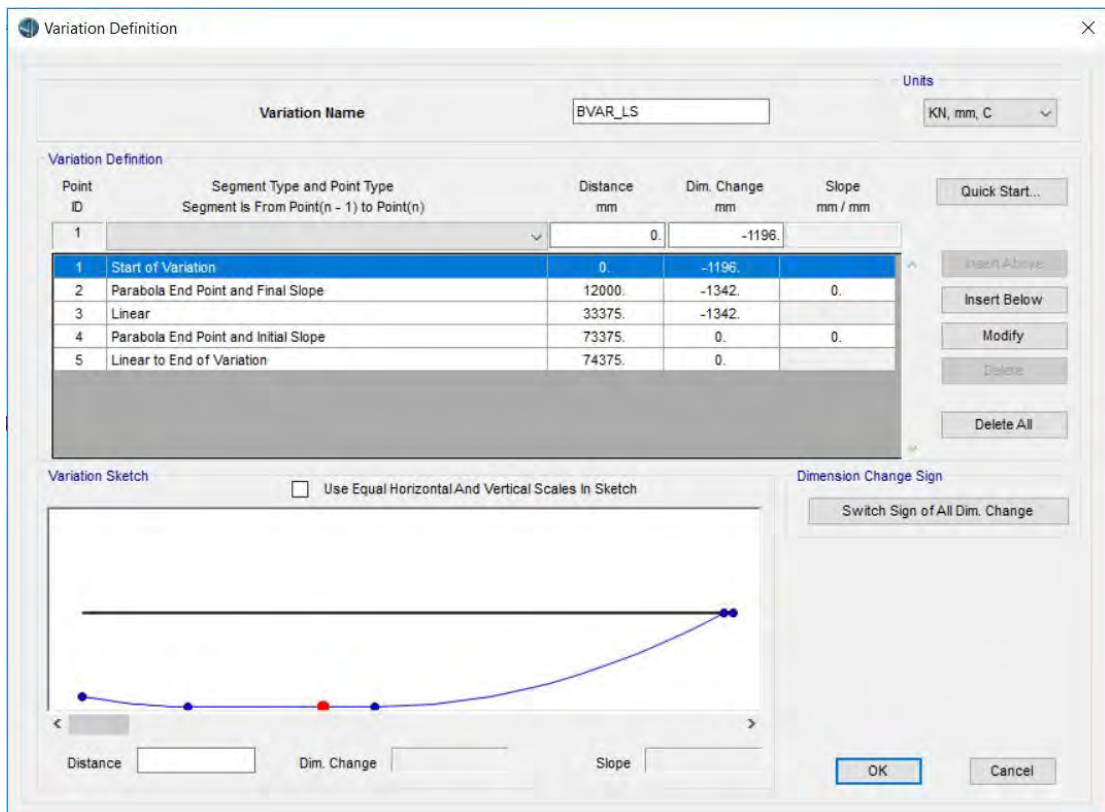


Figure 3.16: Cross section variation of west span

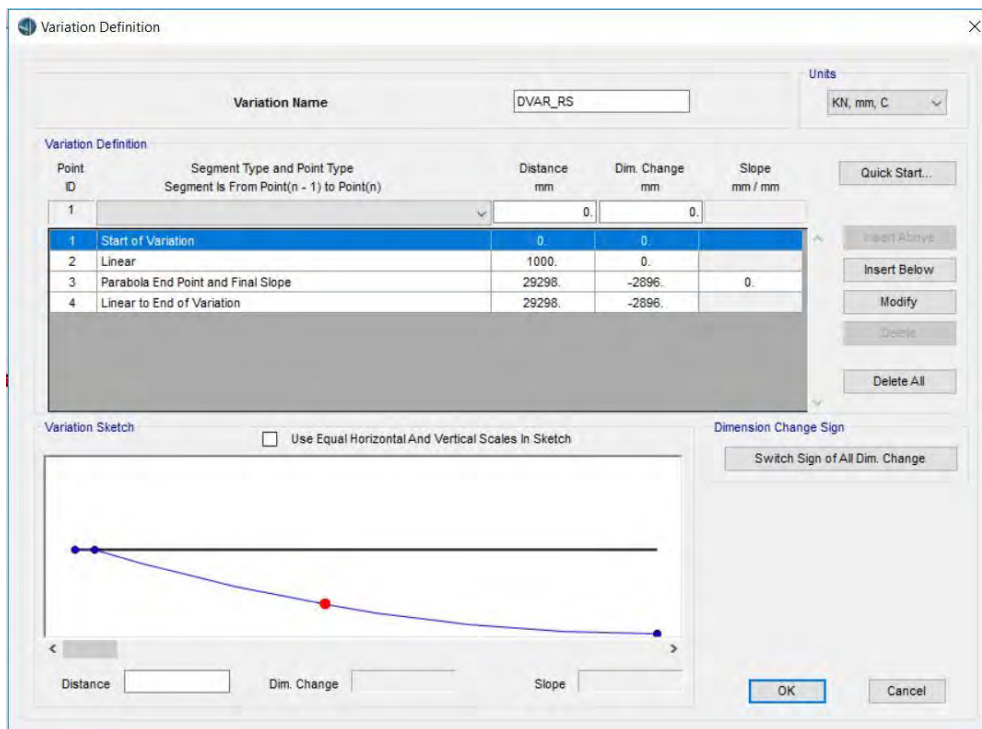


Figure 3.17: Section depth variation of east span

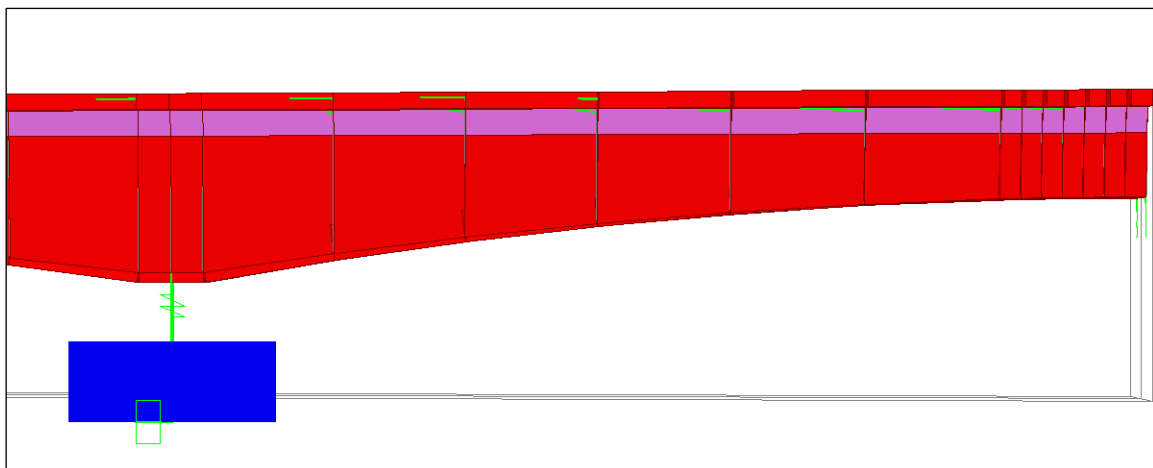


Figure 3.18: 3D view of section depth variation of east span

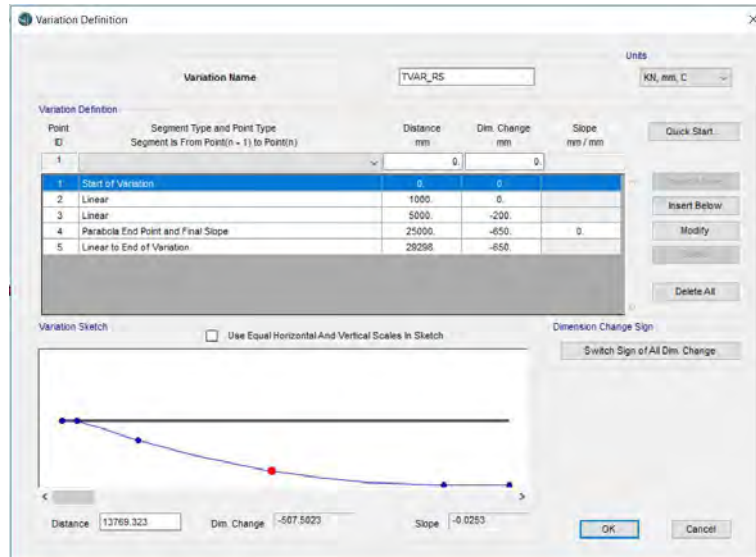


Figure 3.19: Bottom slab thickness variation of east span

Typical cross section in span and in pier are shown in **Figure 3.20** for typical span. Typical elevation of middle section is shown in **Figure 3.21**. For typical spans, girder bottom slab thickness is assigned as maximum of 850 mm at near the pier. Then it parabolically decreased to a constant depth of 200 mm at short length at middle of the span as shown in **Figure 3.25**. For section depth variation as shown in **Figure 3.22** and **Figure 3.23** at mid segments, maximum was at the pier which was 6500 mm. Then it was parabolically varied to reduce to 3250 at middle girders. For section width at typical segments, width start at 5921 mm from the piers and increased to a maximum of 8604 mm at middle part as shown in **Figure 3.24**.

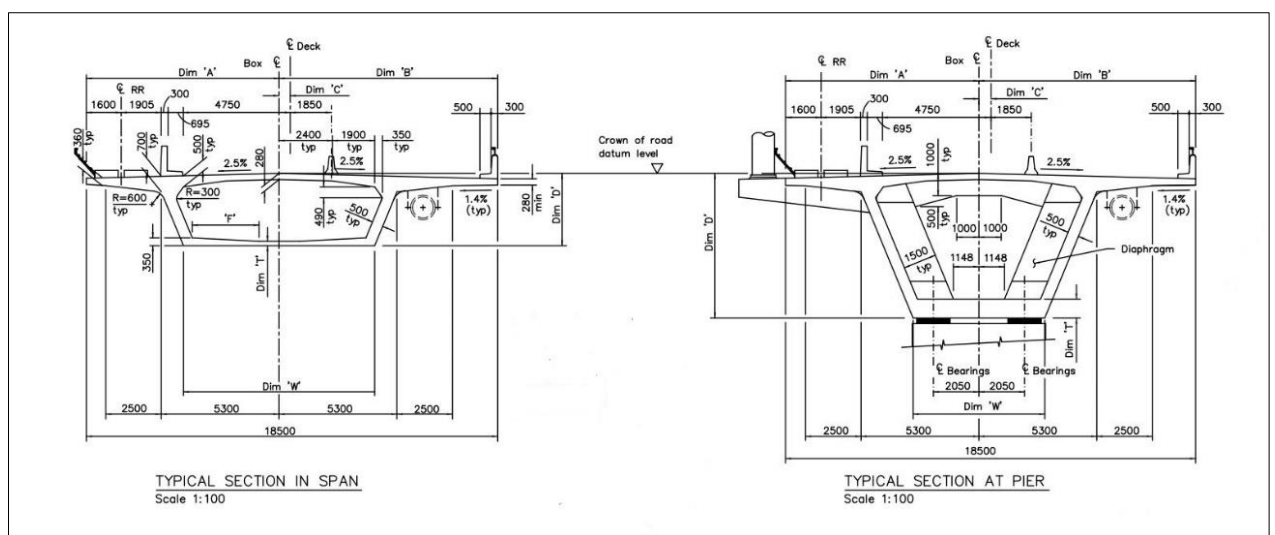


Figure 3.20: Cross section of typical span of 7 span module

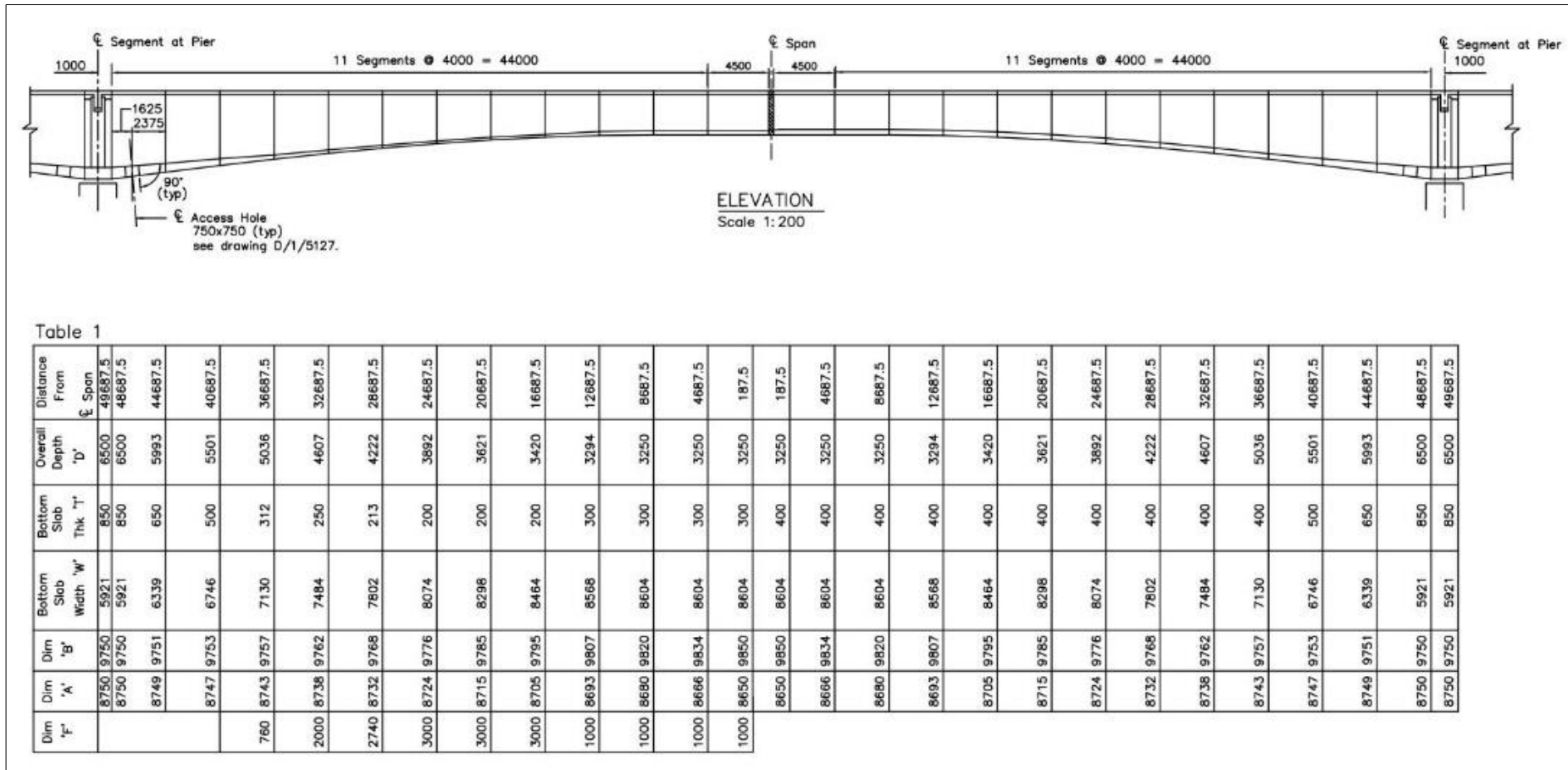


Figure 3.21: Elevation of typical span of 7 span module

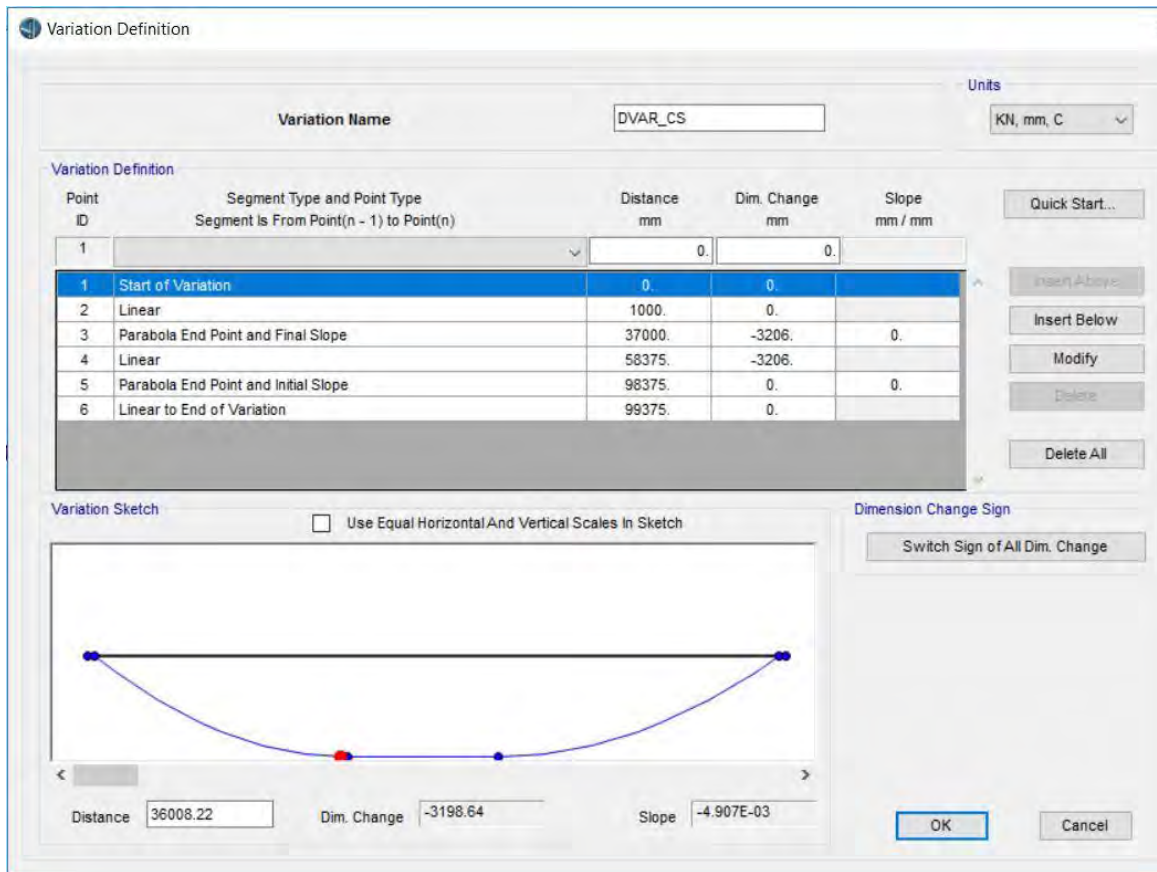


Figure 3.22: Section depth variation of typical segment

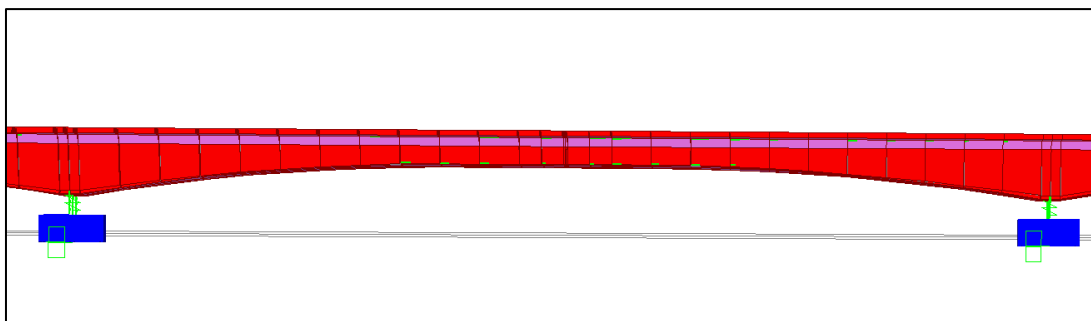


Figure 3.23: 3D view of girder depth variation of typical segment

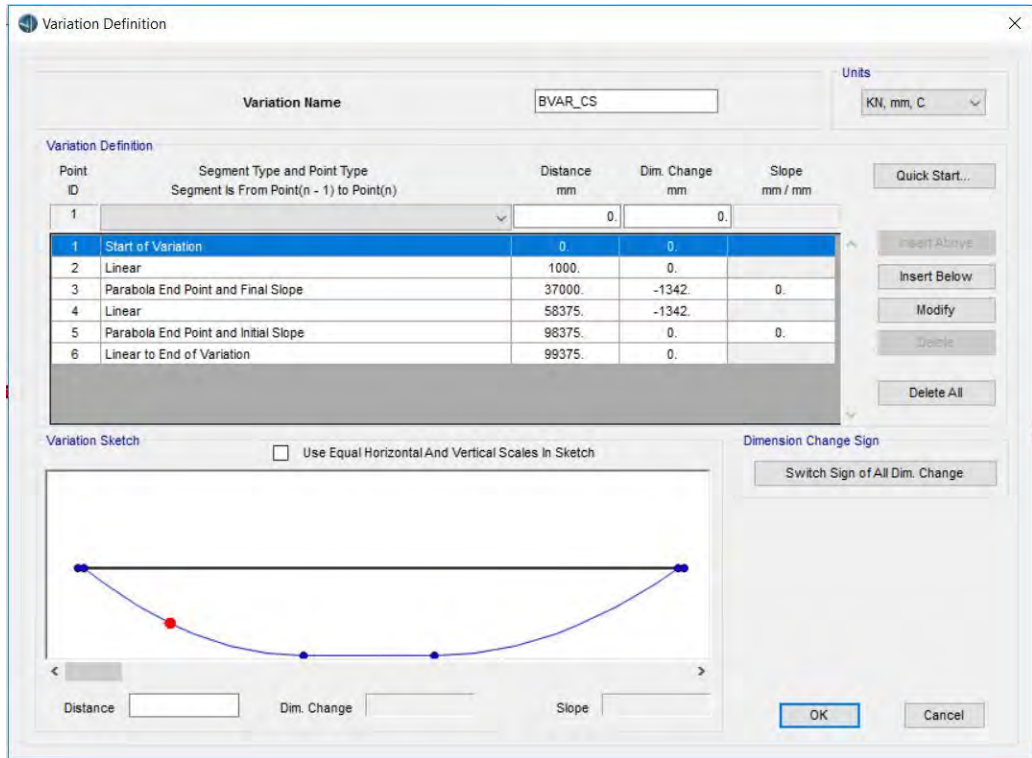


Figure 3.24: Girder width variation of typical segment

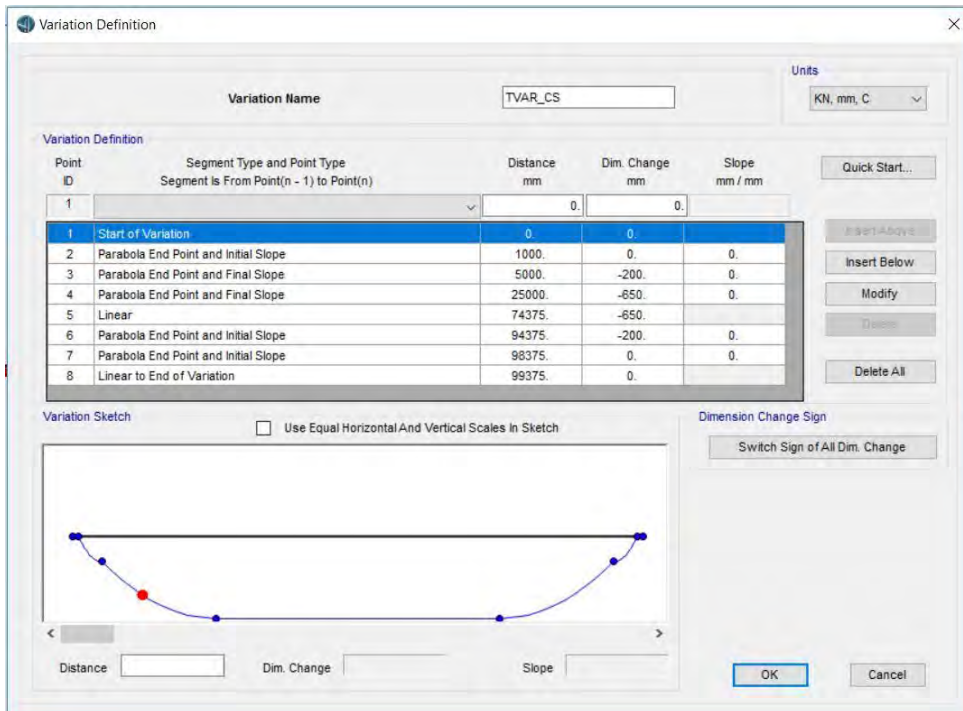


Figure 3.25: Bottom slab thickness variation of typical segment

3.4.4 Abutment and bent

The assignment of abutment is modelled in a simplistic way as shown in **Figure 3.26** and **Figure 3.27** such that the properties of bearings are simulated. Only, the physical properties are not in the scope for this study.

The screenshot shows the 'Bridge Object Abutment Assignments' dialog box for 'Start Abutment'. The 'Bridge Object Name' is 'BOBJ1' and the units are 'KN, mm, C'. The 'Start Abutment' tab is active. The 'Superstructure Assignment' section includes 'Support Name' (SA), 'Abutment Direction (Bearing Angle)' (Default), and 'Diaphragm Property' (None). The 'Substructure Assignment' section has 'Abutment Property' selected (BAPT1). The 'Substructure Location' section shows 'Elevation (Global Z)' (-4092) and 'Horizontal Offset' (0). The 'Bearing Assignment' section is set to 'General' with 'Bearing Property' (BBRG1), 'Restrainer Property at Bearing' (None), 'Elevation at Layout Line (Global Z)' (-3792), 'Rotation Angle from Bridge Default' (0), 'Number of Bearings for Bridge Section' (2), 'Uniform Spacing' (7864.8), and 'Offset from Section Ref. Point to Bearing Center' (0). A 'Modify/Show Overwrites...' button is present, and a note states 'No Overwrites Exist'.

Figure 3.26: Start abutment

The screenshot shows the 'Bridge Object Abutment Assignments' dialog box for 'End Abutment'. The 'Bridge Object Name' is 'BOBJ1' and the units are 'KN, mm, C'. The 'End Abutment' tab is active. The 'Superstructure Assignment' section includes 'Support Name' (NoSup), 'Abutment Direction (Bearing Angle)' (Default), and 'Diaphragm Property' (None). The 'Substructure Assignment' section has 'Abutment Property' selected (BAPT1). The 'Substructure Location' section shows 'Elevation (Global Z)' (-3804) and 'Horizontal Offset' (0). The 'Bearing Assignment' section is set to 'General' with 'Bearing Property' (BBRG1), 'Restrainer Property at Bearing' (None), 'Elevation at Layout Line (Global Z)' (-3504), 'Rotation Angle from Bridge Default' (0), 'Number of Bearings for Bridge Section' (2), 'Uniform Spacing' (7603.2), and 'Offset from Section Ref. Point to Bearing Center' (0). A 'Modify/Show Overwrites...' button is present, and a note states 'No Overwrites Exist'.

Figure 3.27: End abutment

Bent or pier was also done in the simplistic way as such detailing of the pier is out of scope of this study. Details of bent modeling is shown in **Figure 3.28** and **Figure 3.29**.

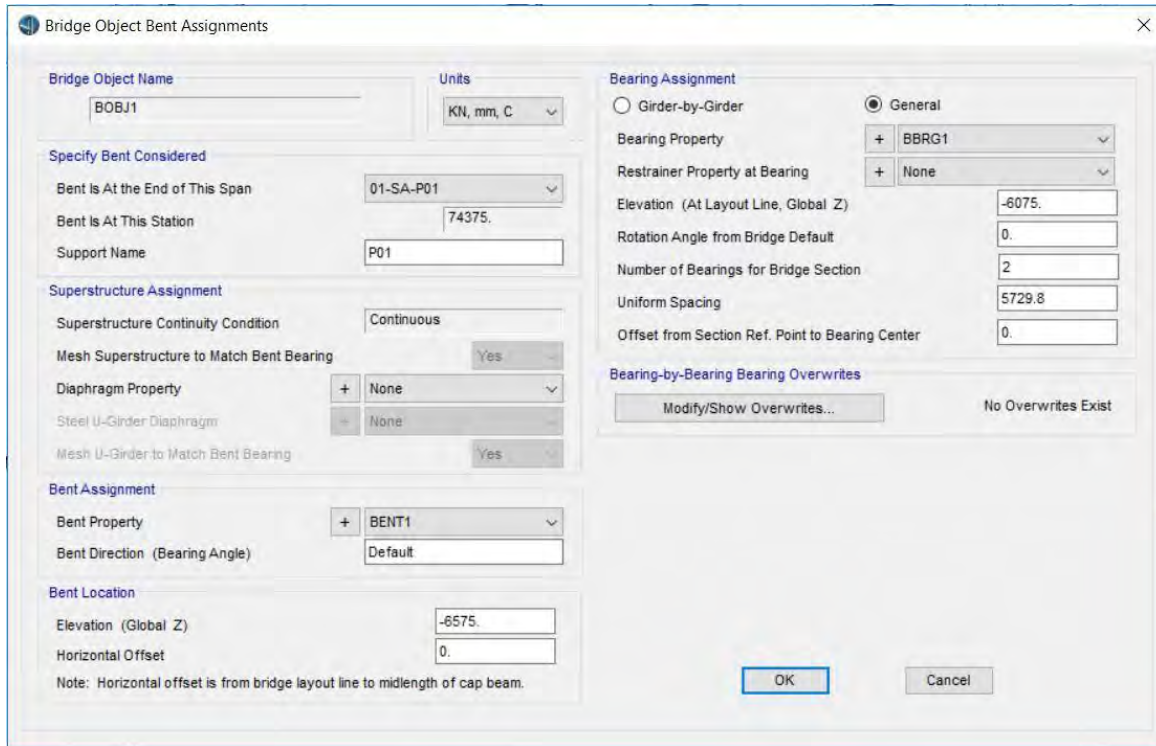


Figure 3.28: 1st bent assignment as representative of 7 bents

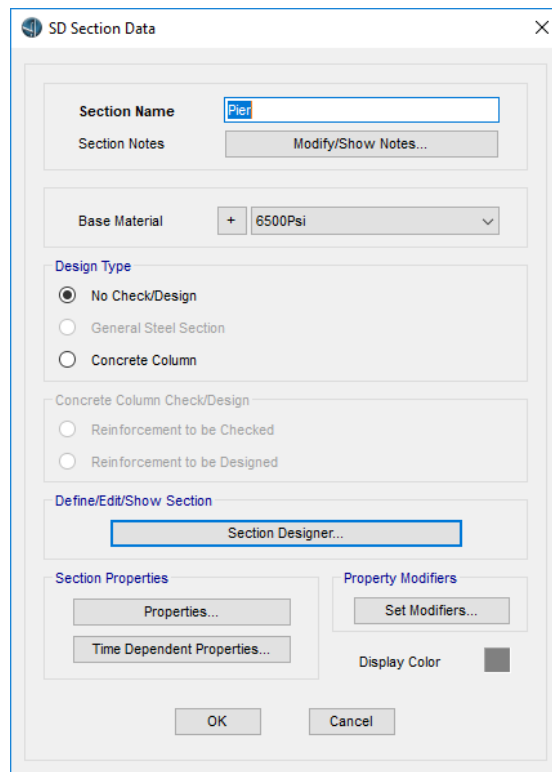


Figure 3.29: Pier modelling details

3.5 Bearing and Seismic Isolation

Bearing for a seven-span module of The Bangabandhu multipurpose bridge is shown in **Figure 3.30**. There are Steel Hysteretic Dampers (MEP and MEPOT), Unidirectional and Multidirectional bearing present. Sacrificial restrainers are not shown.

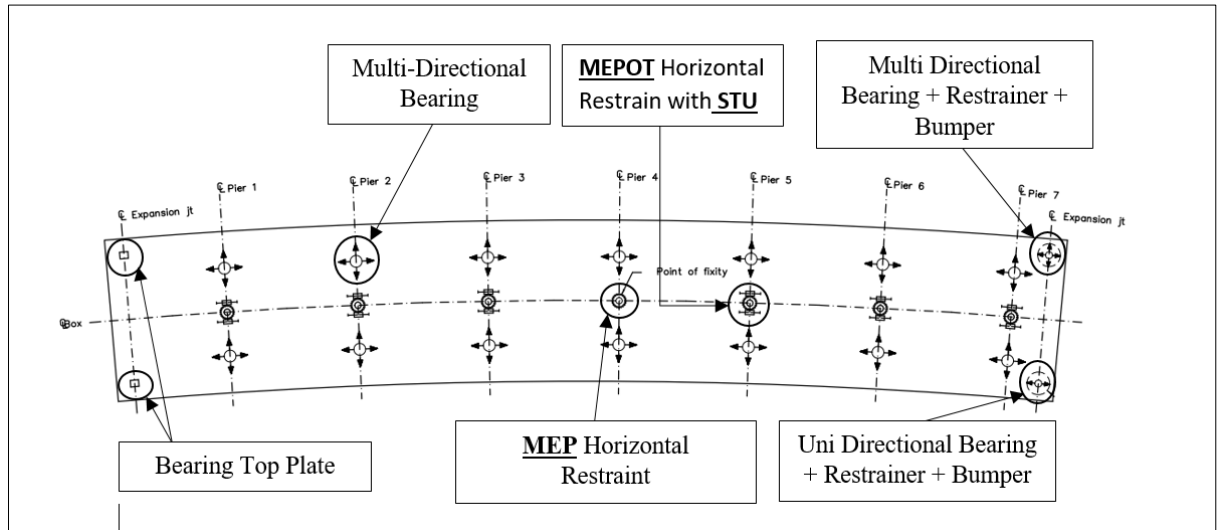


Figure 3.30: Bearing layout of 7-span module of The Bangabandhu bridge

3.5.1 Stiffness Properties of Seismic Devices

Stiffness properties of seismic isolation for 100m module which resembles Bangabandhu bridge are assigned by comparing with displacement limit of seismic isolators according to FIP Industriale. Seismic isolation stiffness is assigned in proportion to the span length for 75m and 125m span module based on 100m module. In **Table 3.2** detailed properties of seismic devices are shown. The assigned of properties for 100m bridge seismic devices are shown in **Table 3.3**. The detailed properties for 75m bridge seismic devices are shown in **Table 3.4** and assigned properties details are shown in **Table 3.5**. The detailed properties for 125m bridge seismic devices are shown in **Table 3.6** and assigned properties details are shown in **Table 3.7**. Here U1(red), U2(green) and U3(blue) are stiffness in vertical, transverse and longitudinal direction. R1, R2 and R3 are rotational stiffness about vertical, transverse and longitudinal axis.

Table 3.2: Detailed properties of seismic devices used in The Bangabandhu Bridge

Name	Designation	Vertical Load Limit	Horizontal Load Limit	Horizontal Translation Limit		Stiffness (K)	
				Longitudinal	Transverse	Longitudinal	Transverse
		kN	kN	mm	mm	kN/mm	kN/mm
Steel Hysteretic Damper (MEP)	MEP 350/200	-	3500	± 200	± 200	17.50	17.50
Steel Hysteretic Damper+ STU (MEPOT)	MEPOT 350/200						
Multi Directional Bearing (North)	VM 3300/850/400	33000	5400	± 425	± 200	12.70	27.0
Multi Directional Bearing (South)	VM 3000/850/400	30000					
Uni Directional Bearing+ Restrainer +Bumper	VU 850/800-200	8500	2000	± 400	± 20	5.0	100.0
Multi Directional Bearing +Restrainer +Bumper	VM 900/800/50	9000	1800	± 400	± 25	4.50	72.0

Table 3.3: Assignment of Seismic Isolation for 100m span module

For 100m Span module					
Name	Assigned Name	Stiffness (kN/mm)			Rotational Stiffness (R1, R2 and R3)
		U1 (Vertical)	U2 (transverse)	U3 (Longitudinal)	
Steel Hysteretic Damper (MEP)	STU	0	17.5	17.5	1.00E+11
Steel Hysteretic Damper+ STU (MEPOT)	STU	0	17.5	17.5	1.00E+11
Muti Directional Bearing (North)	Multi Direc	1.00E+08	27	12.7	1.00E+11
Muti Directional Bearing (South)	Multi Direc	1.00E+08	27	12.7	1.00E+11
Uni Directional Bearing+ Restrainer	Uni Direc	1.00E+08	100	5	1.00E+11
Multi Directional Bearing+ Restrainer	Multi Direc End	1.00E+08	72	4.5	1.00E+11

Table 3.4: Detailed properties of seismic devices used in 75m module

Name	Designation	Horizontal Load Limit	Horizontal Translation Limit		Stiffness (K)	
			Longitudinal	Transverse	Longitudinal	Transverse
		kN	mm	mm	kN/mm	kN/mm
Steel Hysteretic Damper (MEP)	MEP	-	-	-	13.125	13.125
Steel Hysteretic Damper+ STU (MEPOT)	MEPOT					
Multi Directional Bearing (North)	VM	-	-	-	7.76	16.5
Multi Directional Bearing (South)	VM					
Uni Directional Bearing +Restrainer +Bumper	VU	-	-	-	3.75	75
Multi Directional Bearing + Restrainer +Bumper	VM	-	-	-	2.25	36

Table 3.5: Assignment of Seismic Isolation for 75m span module

For 75m span module					
Name	Assigned Name	Stiffness (kN/mm)			Rotational Stiffness (R1, R2 and R3)
		U1 (Vertical)	U2 (transverse)	U3 (Longitudinal)	
Steel Hysteretic Damper (MEP)	STU	0	13.125	13.125	1.00E+11
Steel Hysteretic Damper+ STU (MEPOT)	STU	0	13.125	13.125	1.00E+11
Muti Directional Bearing (North)	Multi Direc	1.00E+08	16.5	7.76	1.00E+11
Muti Directional Bearing (South)	Multi Direc	1.00E+08	16.5	7.76	1.00E+11
Uni Directional Bearing+ Restrainer	Uni Direc	1.00E+08	75	3.75	1.00E+11
Multi Directional Bearing+ Restrainer	Multi Direc End	1.00E+08	36	2.25	1.00E+11

Table 3.6: Detailed properties of seismic devices used in 125m module

Name	Designation	Horizontal Load Limit	Horizontal Translation Limit		Stiffness (K)	
			Longitudinal	Transverse	Longitudinal	Transverse
		kN	mm	mm	kN/mm	kN/mm
Steel Hysteretic Damper (MEP)	MEP	-	-	-	21.875	21.875
Steel Hysteretic Damper+ STU (MEPOT)	MEPOT					
Multi Directional Bearing (North)	VM	-	-	-	15.875	33.75
Multi Directional Bearing (South)	VM					
Uni Directional Bearing+ Restrainer +Bumper	VU	-	-	-	6.25	125
Multi Directional Bearing +Restrainer +Bumper	VM	-	-	-	5.625	90

Table 3.7: Assignment of Seismic Isolation for 125m span module

For 125 m span module					
Name	Assigned Name	Stiffness (kN/mm)			Rotational Stiffness (R1, R2 and R3)
		U1 (Vertical)	U2 (transverse)	U3 (Long.)	
Steel Hysteretic Damper (MEP)	STU	0	21.875	21.875	1.00E+14
Steel Hysteretic Damper+ STU (MEPOT)	STU	0	21.875	21.875	1.00E+14
Muti Directional Bearing (North)	Multi Direc	1.00E+08	33.75	15.875	1.00E+14
Muti Directional Bearing (South)	Multi Direc	1.00E+08	33.75	15.875	1.00E+14
Uni Directional Bearing+ Restrainer	Uni Direc	1.00E+08	125	6.25	1.00E+14
Multi Directional Bearing+ Restrainer	Multi Direc End	1.00E+08	90	5.625	1.00E+14

3.5.2 Damping properties of Seismic Devices

Damping is provided by steel hysteric damper of both MEP and MEPOT types due to spindles present. The spindle (single or double-taper) is one of the dissipating elements typically used by FIP Industrial to achieve steel hysteric dampers. (Castellano and Cestarollo, 1999). **Figure 3.31** shows hysteresis loop for four full-scaled spindles.

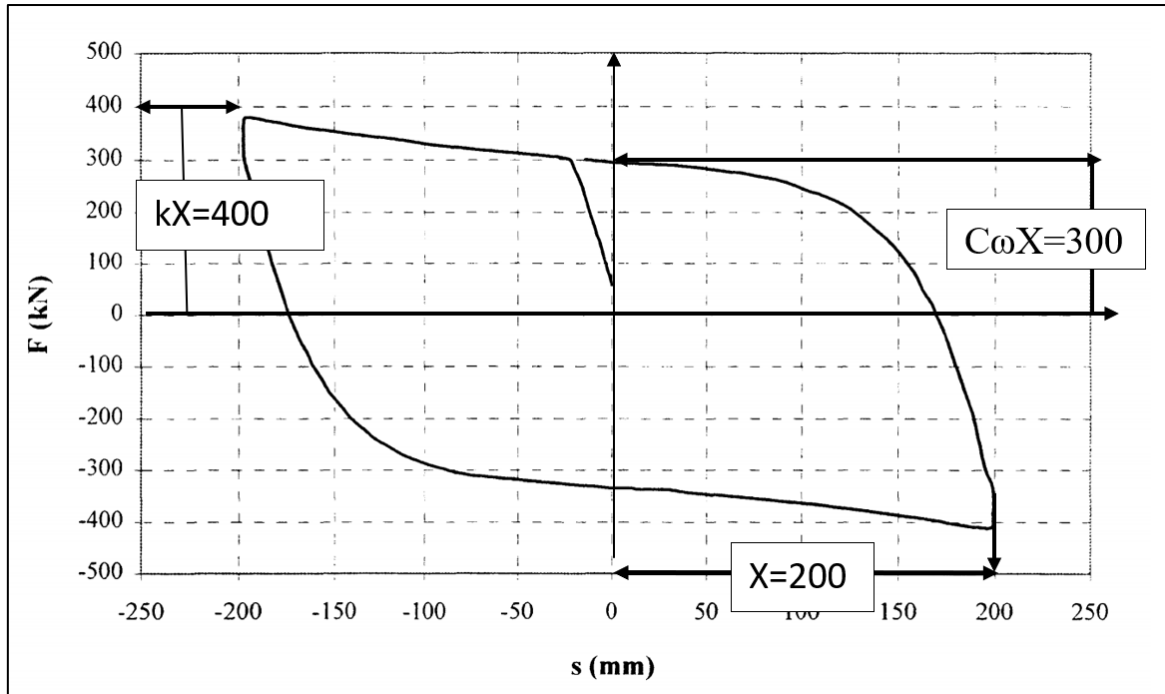


Figure 3.31: Force vs displacement measured on four spindles (Castellano and Cestarollo, 1999)

$$\xi = \frac{C\omega}{k}$$

$$C = 2m\omega\xi$$

Here,

ξ =damping ratio, ω = angular frequency, f = predominant frequency, k = Stiffness, C = Damping Co-efficient

From Graph,

$$X=200$$

$$C\omega X=300 \Rightarrow C\omega = \frac{300}{200} = 1.5$$

$$kX=400 \Rightarrow k=2$$

$$\xi = \frac{C\omega}{k} = \frac{1.5}{2} = 0.75$$

For 100 m bridge span module,

Predominant Frequency of El-Centro, $f=1.47$ Hz,

Stiffness of steel hysteretic damper, $k=17.5$ kN/mm

$$\text{Damping Co-efficient, } C = 2m\omega\xi = 2 \frac{k}{\omega} \xi = 2 \frac{k}{2\pi f} \xi = \frac{2 \times 17.5 \times 0.75}{2\pi \times 1.47} = 2.84 \text{ kNs/mm}$$

As predominant frequency for El-Centro is 1.47 Hz, predominant frequency for earthquake data found on Bangabandhu bridge in June 16, 2004 is 2 Hz (Rahman, 2008). Damping properties assigned in all the bridge span modules for both the earthquake data are shown in **Table 3.8**.

Table 3.8: Damping properties of steel hysteretic dampers

Earthquake Data	Damping Co-efficient Assigned in Span Modules (kN s/mm)		
	75 m	100 m	125m
Bangabandhu Bridge	1.57	2.09	2.61
El-Centro	2.13	2.84	3.55

3.5.3 Assignment of Seismic Devices

List of assigned seismic devices models are shown in **Figure 3.32**. Among the Multidirectional bearing assignment is shown in **Figure 3.33** and **Figure 3.34**.

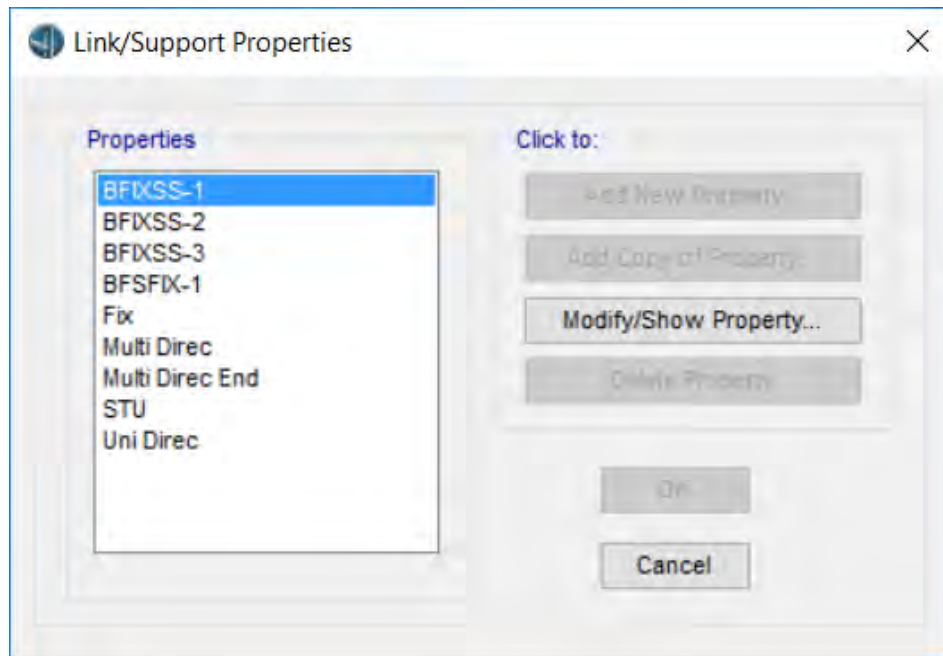


Figure 3.32: Assigned seismic devices

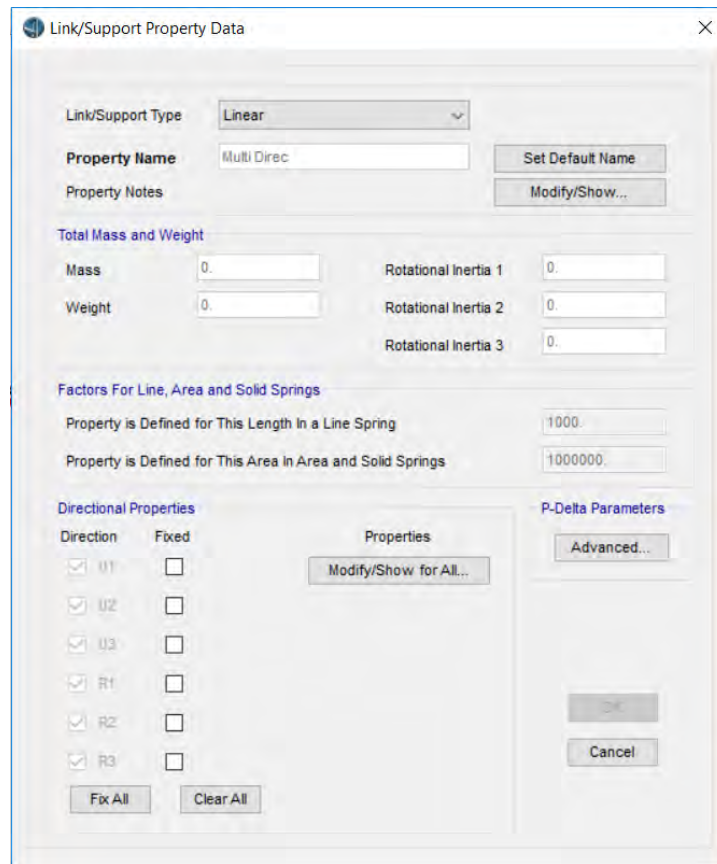


Figure 3.33: Multidirectional bearing data

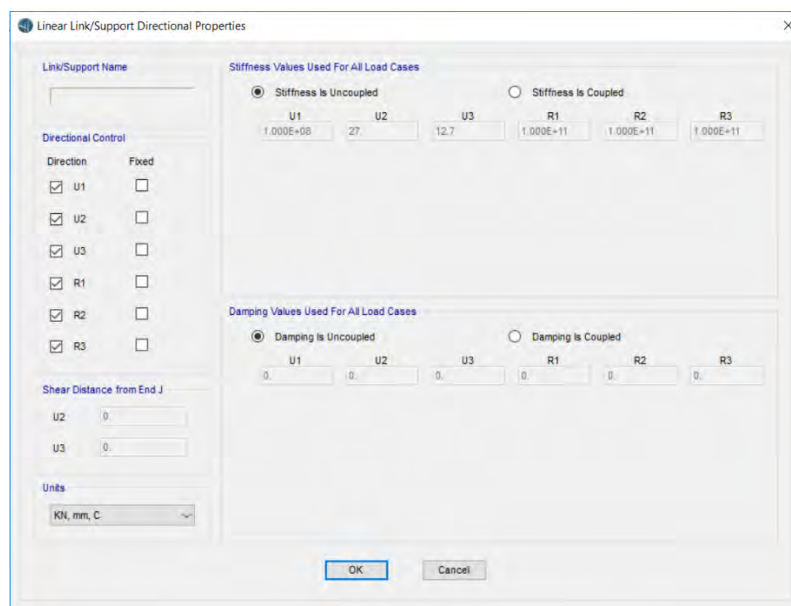


Figure 3.34: Multidirectional bearing properties

3.6 Prestress

Prestress tendons are configured on the model based on prestressing done on the Bangabandhu bridge as built drawing. However, due to some limitations, tendon configuration could not be fully replicated. The scheme of tendon 100 m bridge model is described as a representative for all the three models. Tendon configurations are equivalent for 75m and 125m span modules with minor adjustment for satisfying structural requirement. **Figure 3.35** to **Figure 3.38** show the tendon profile of the Bangabandhu bridge of a 7-span module.

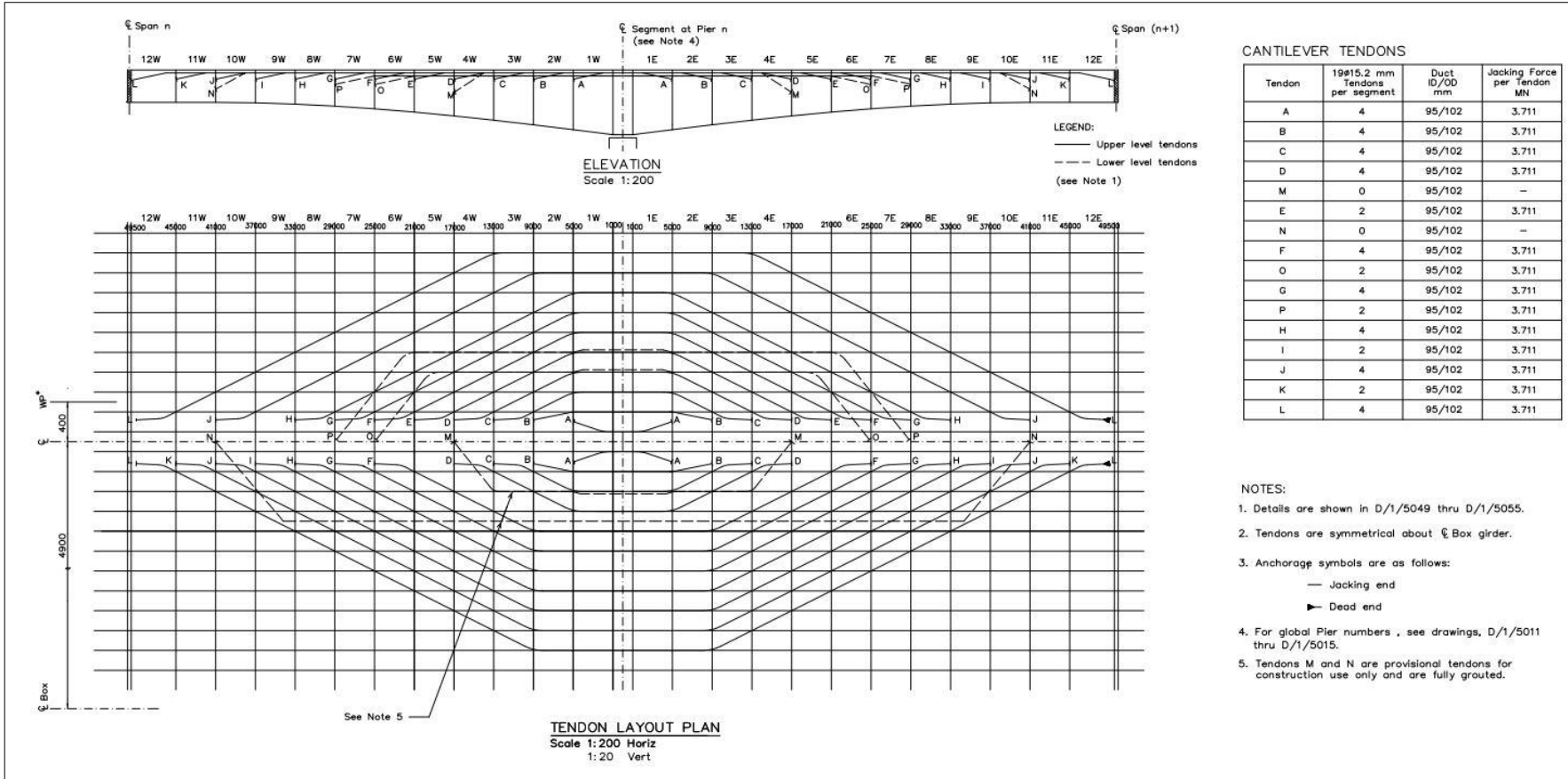


Figure 3.35: Top tendon profile (typical cantilever span)

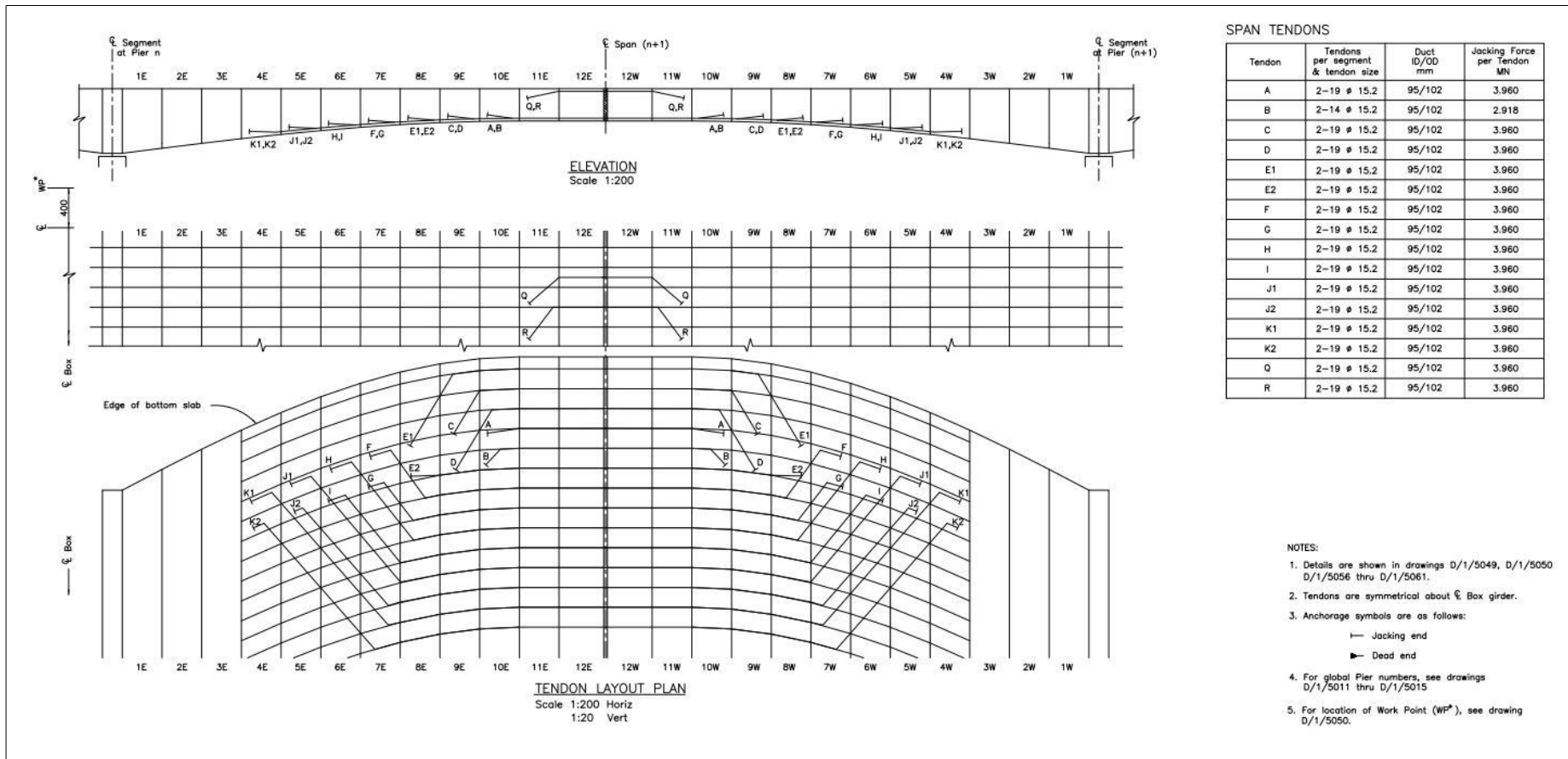


Figure 3.36: Bottom tendon profile (typical cantilever span)

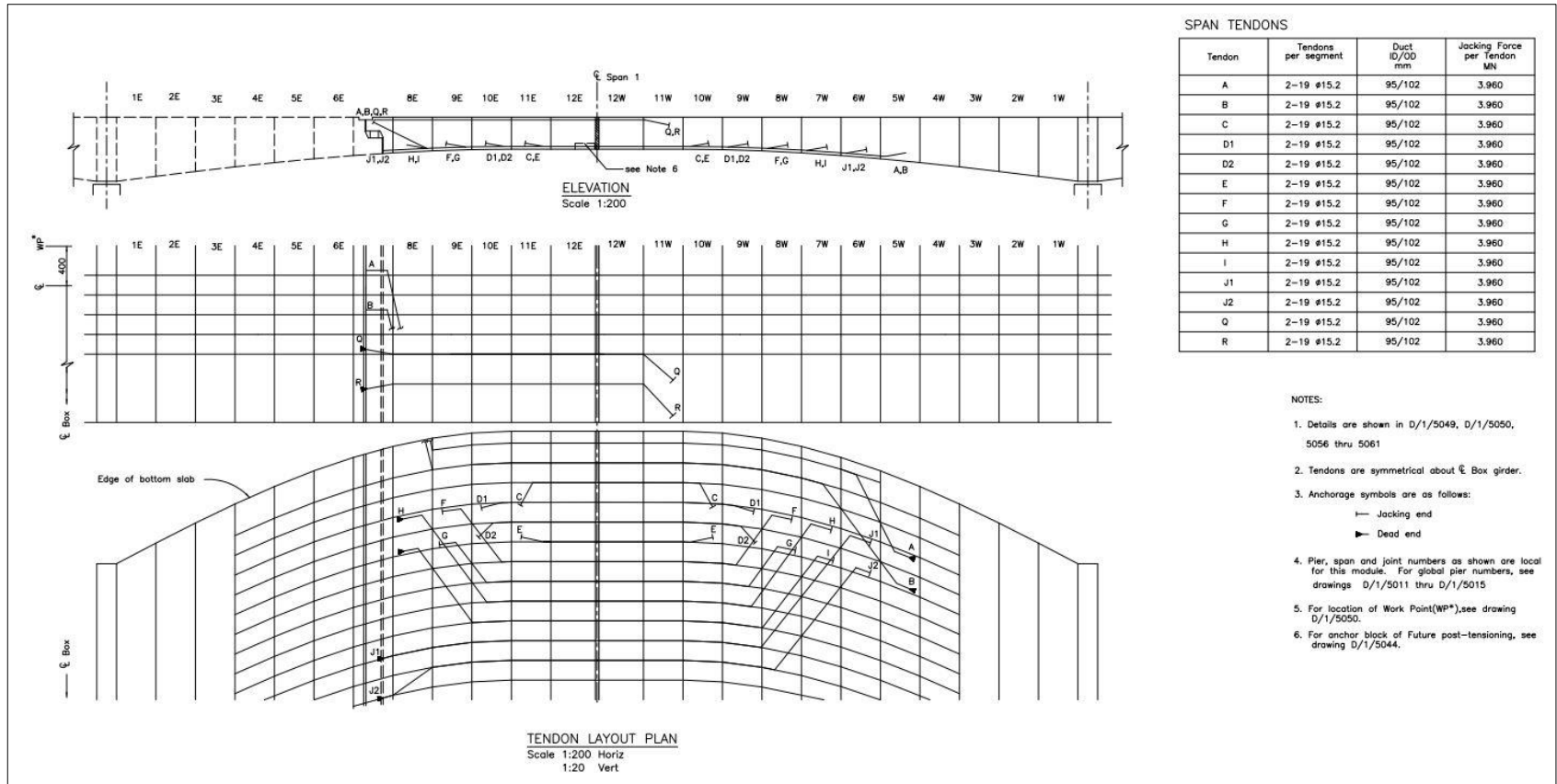


Figure 3.37: Tendon profile (west span)

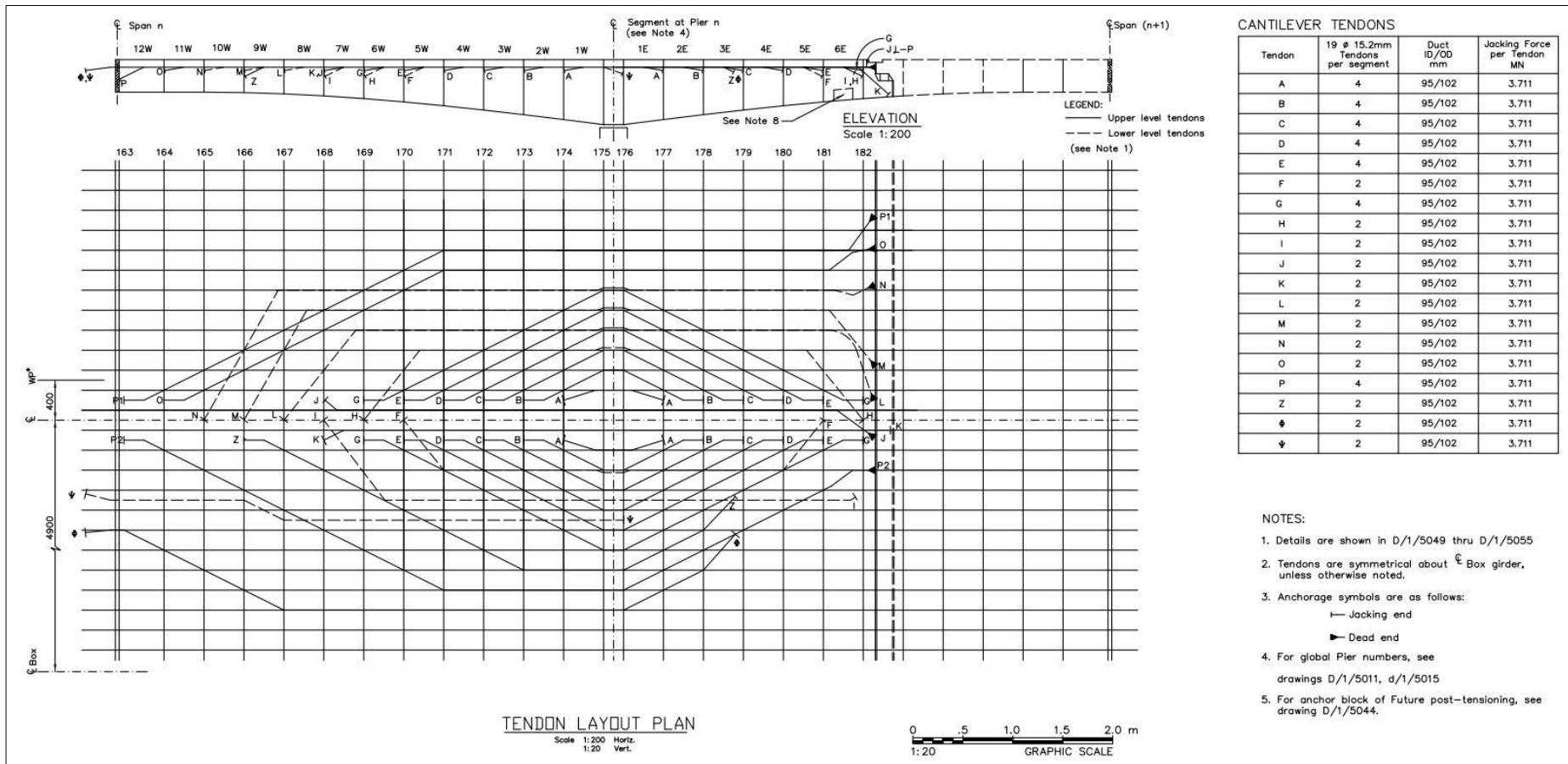


Figure 3.38: Tendon profile (east span)

In the Bangabandhu bridge, all the tendon profile is mirrored with respect to the center line of girder cross section. **Figure 3.39** to **Figure 3.42** show assignment of tendon at top for a typical segment. At the top tendon profile of a cantilever span, 24 tendons are modelled with respect to center line making it total 48 tendons at the top of a cantilever span. The working point for jacking force is modelled based on actual design.

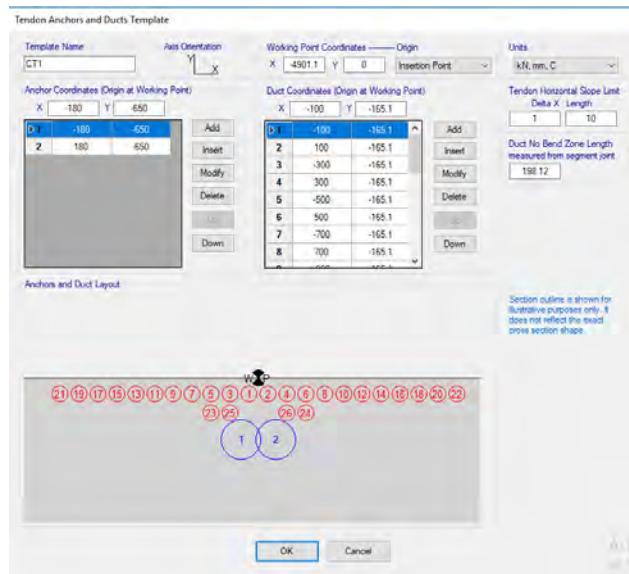


Figure 3.39: Cantilever tendon duct layout plan

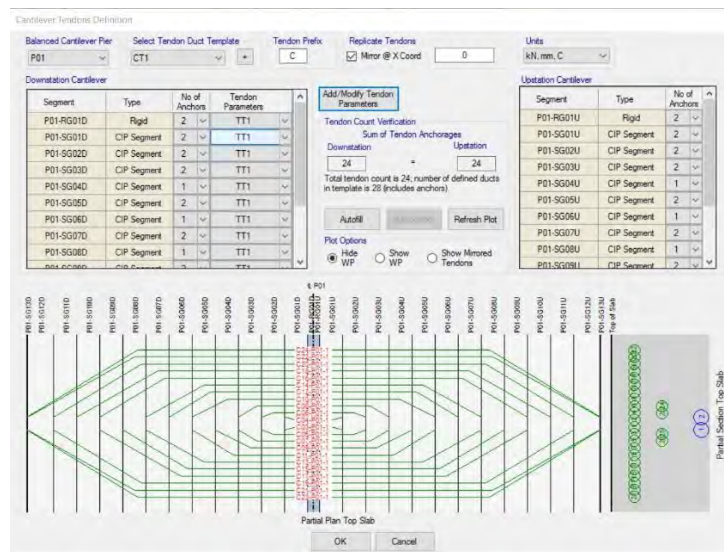


Figure 3.40: Top cantilever tendon

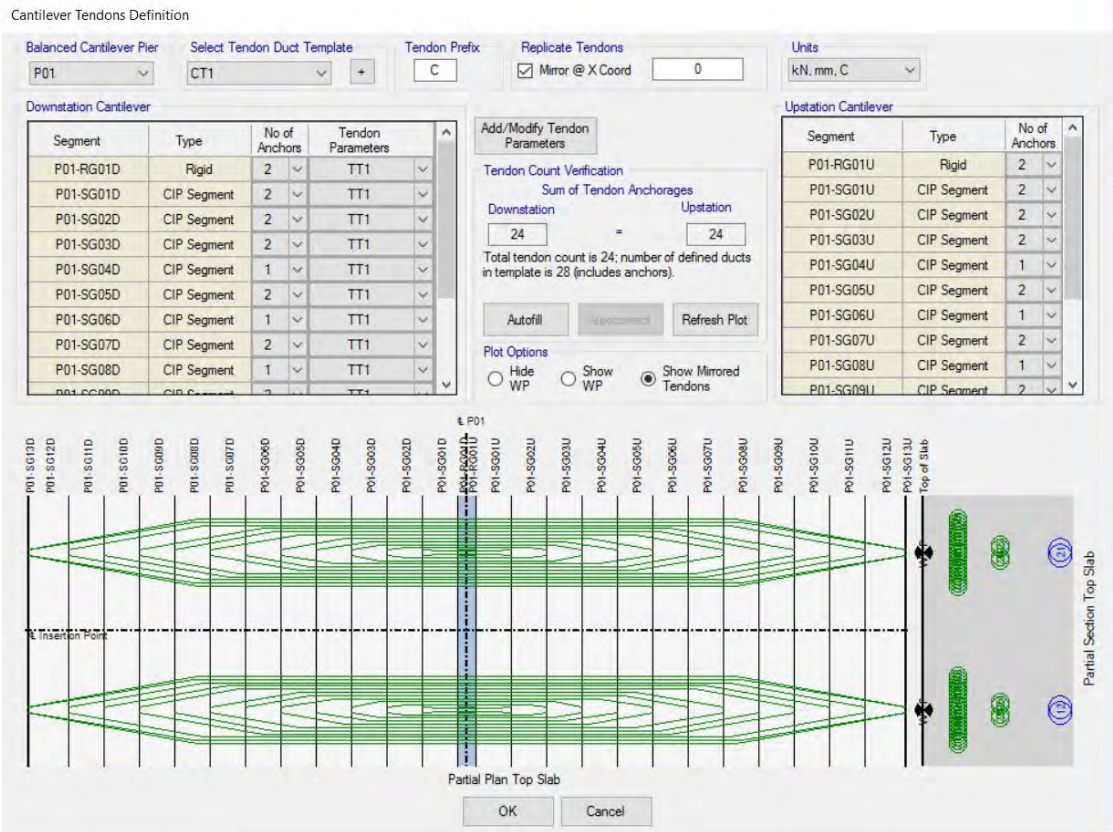


Figure 3.41: Top cantilever tendon (mirrored tendons)

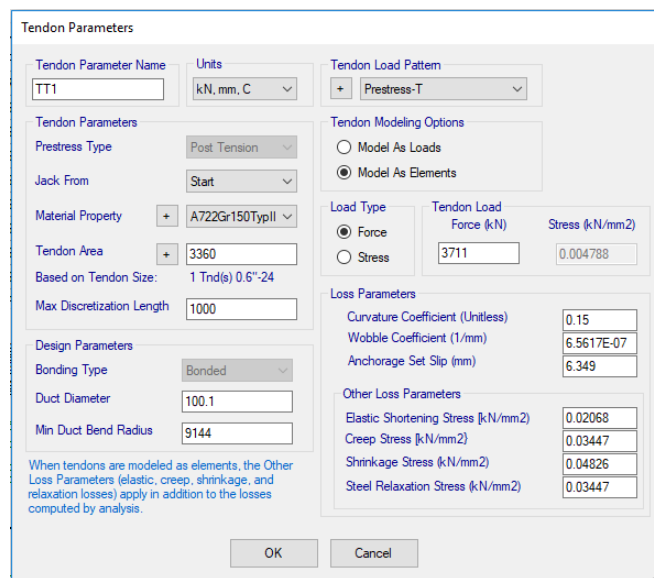


Figure 3.42: Top cantilever tendon parameter (TT1)

For bottom tendon profile of a typical span, 18 tendons are modelled in place of 26 as provided in the design. **Figure 3.43** and **Figure 3.44** show assignment of tendon at bottom

for a typical segment. This is due to the limitation that total 26 tendons cannot be modelled in Csi Bridge 20 at the bottom. The configurations of the tendons are according to the design.

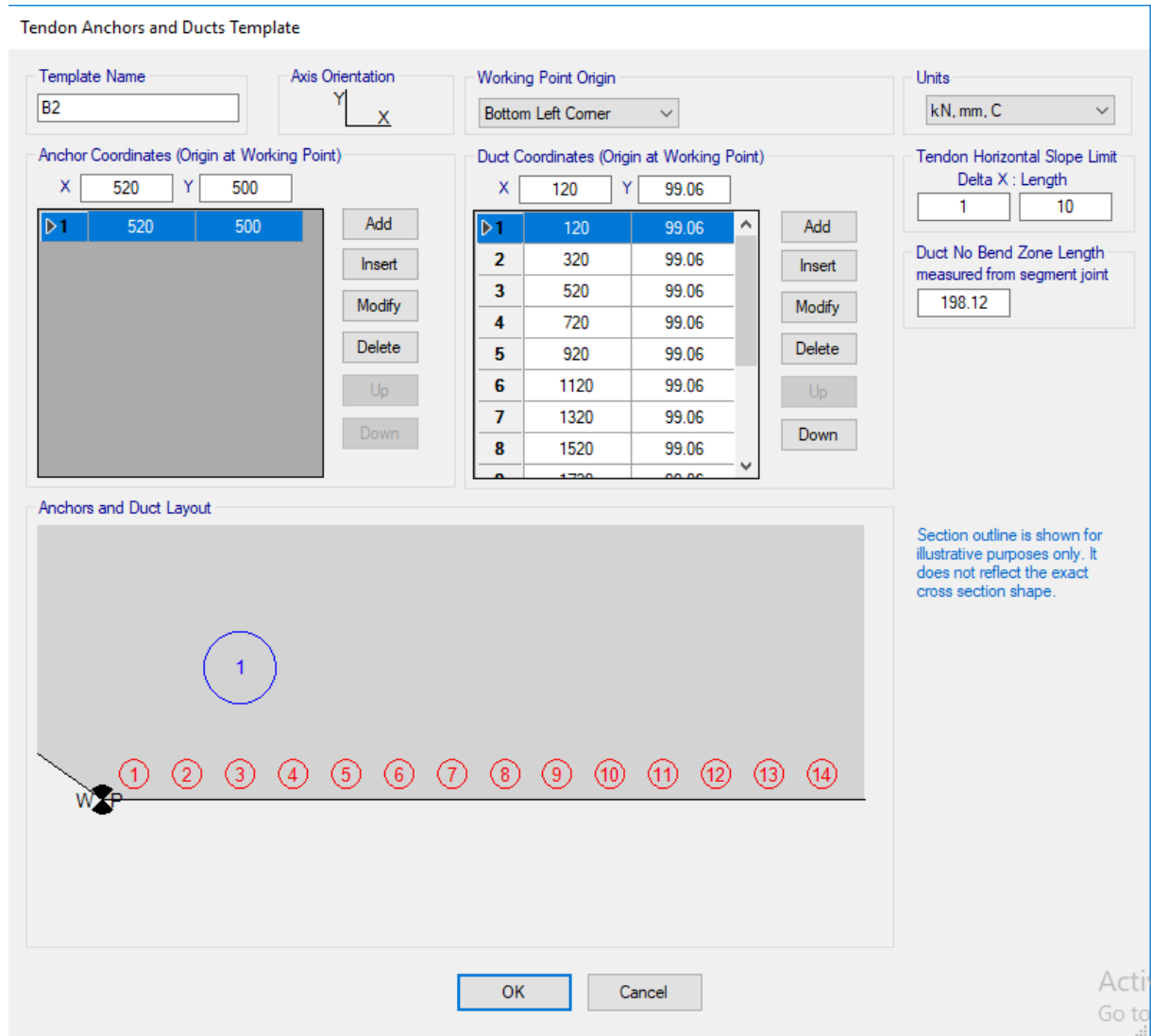


Figure 3.43: Typical bottom tendon duct layout

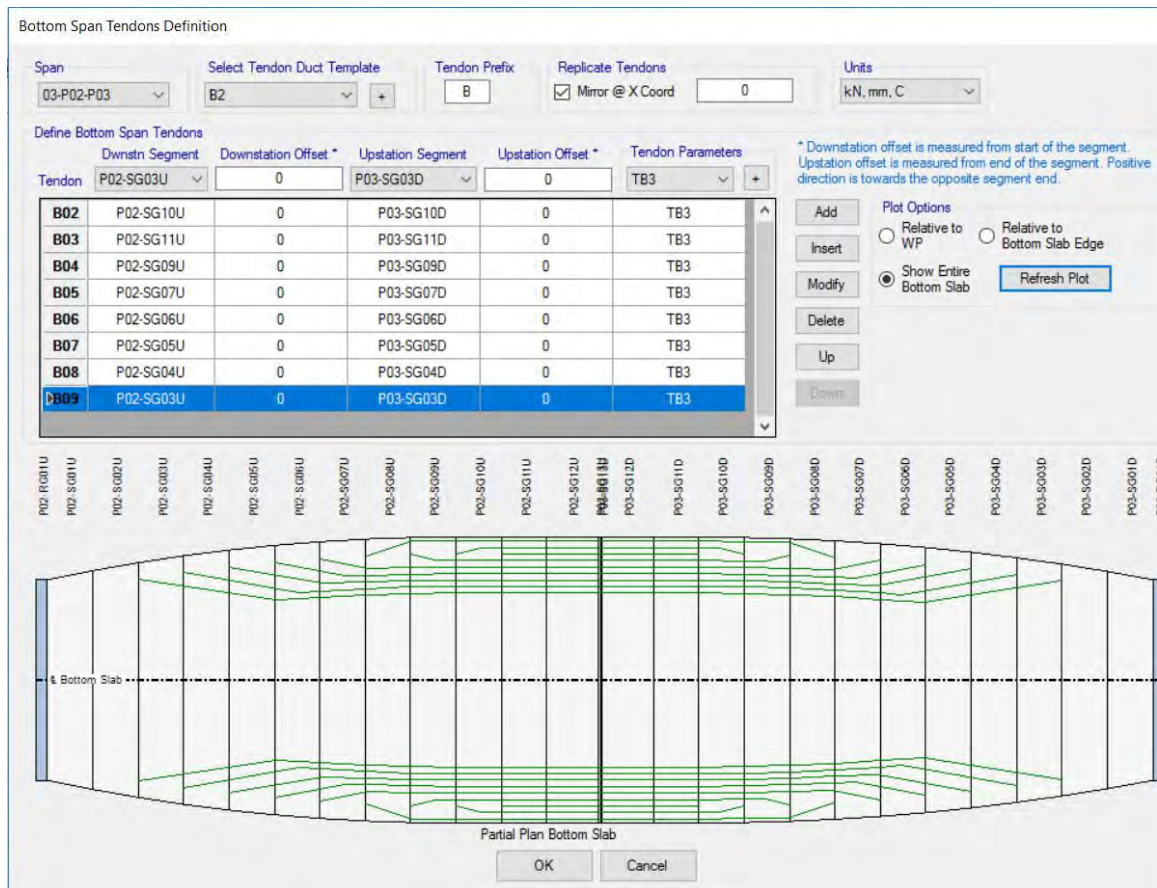


Figure 3.44: Typical Bottom tendon layout

Figure 3.45 to **Figure 3.47** show assignment of tendon on the left segment. On the left segment, the bottom tendon profile is such that 7 tendons are added starting from the end of the segment. At the top of left segment, another 4 tendons were applied starting from the end of the segment. On the left segment, the bottom tendons are applied with jacking force 7920 kN. At the top, total 4 tendons with jacking force of 3960 kN were applied.

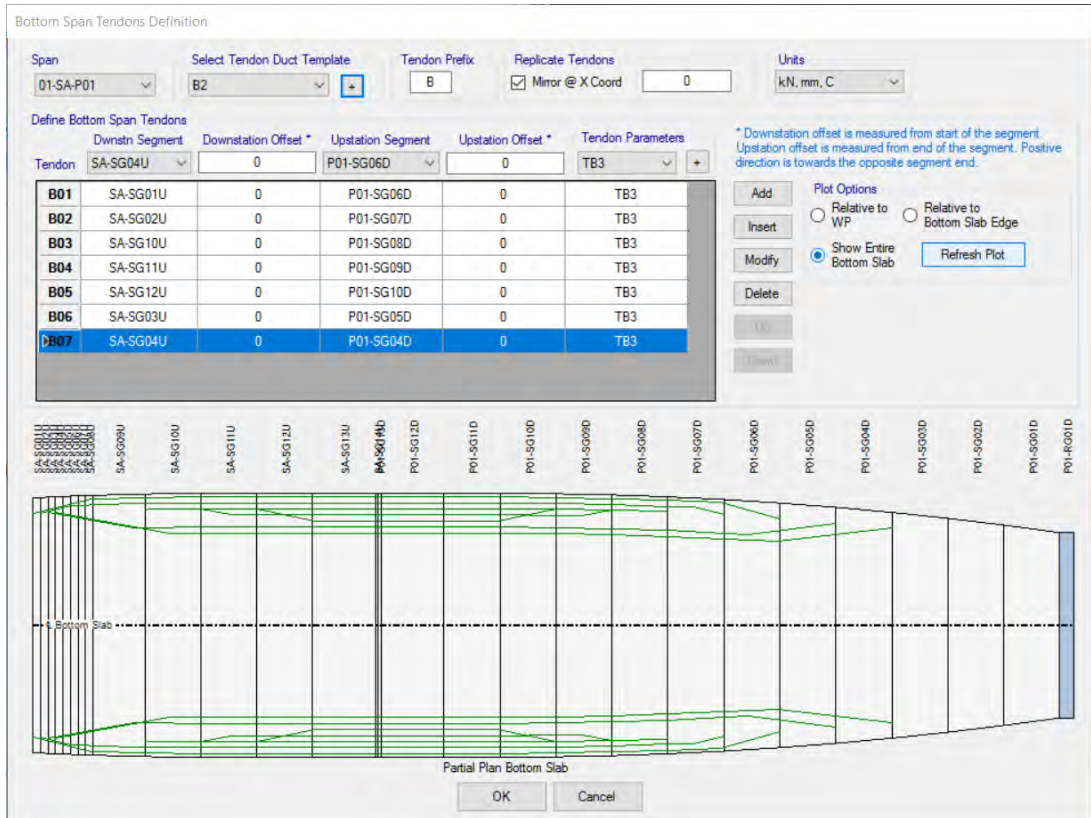


Figure 3.45: West span bottom tendon layout of entire bottom slab

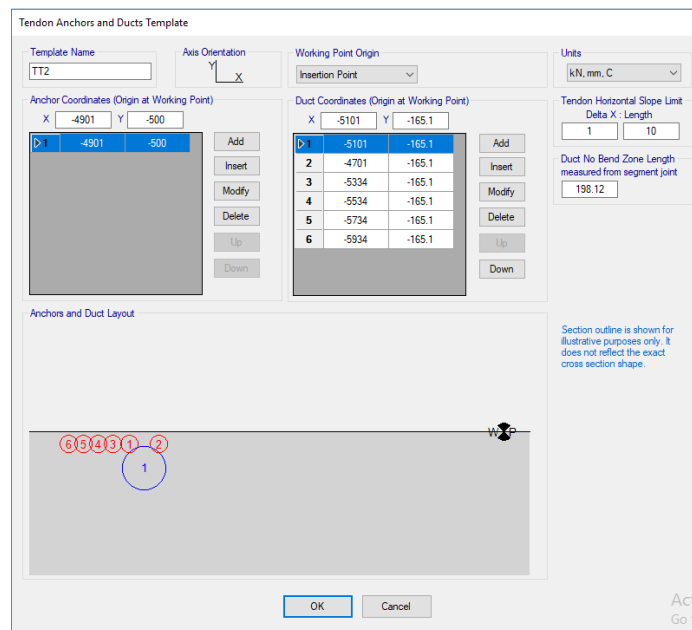


Figure 3.46: West span top tendon duct layout

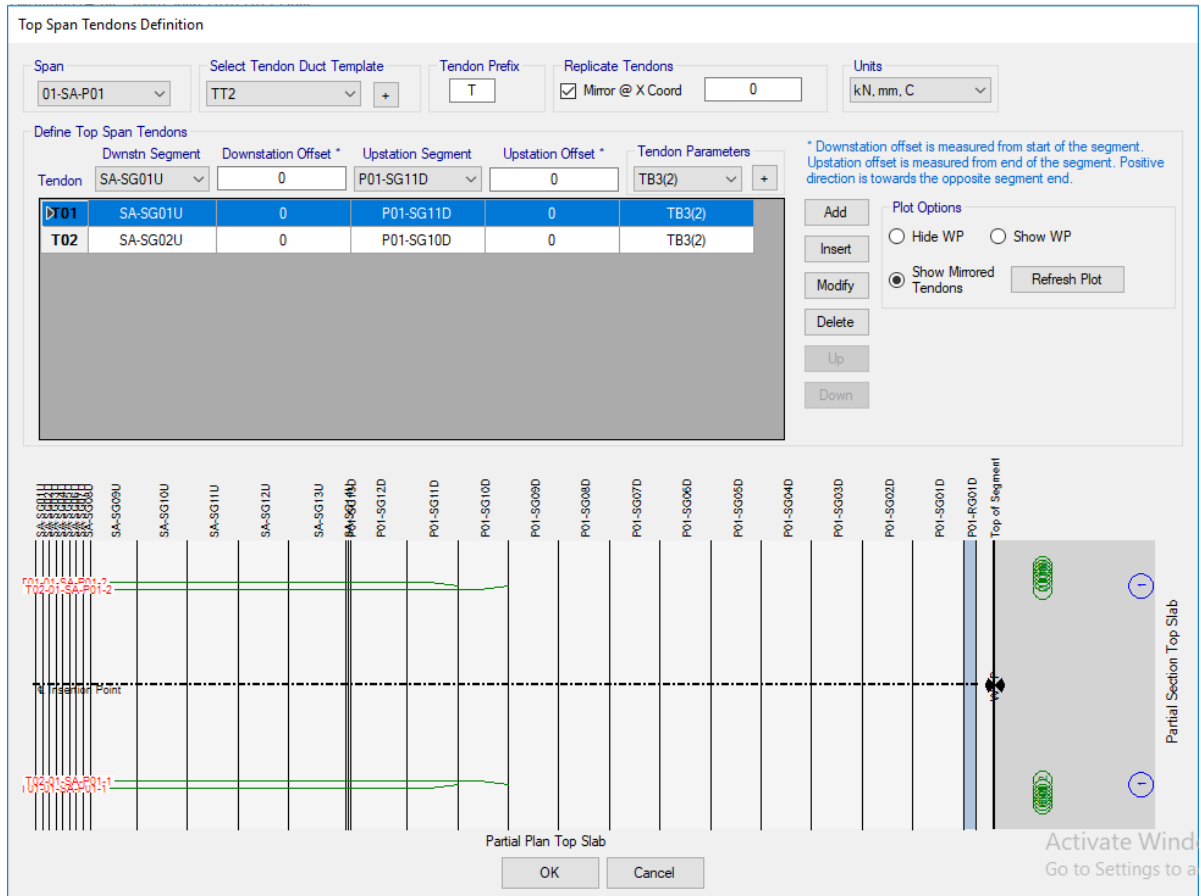


Figure 3.47: Left segment top tendon layout

As tendon configuration could not be fully replicated, loads are modified to ensure that structural requirements are fulfilled. **Figure 3.48** and **Figure 3.49** show tendon parameters assigned in 100m span module. In one cantilever segment 48 tendons on one side of center line are assigned with jacking force of 3711 kN at each according to the as-built drawing. But for the bottom tendons, it was not possible to assign 26 tendons in total similar to as built drawing due to software limitation. Thus, 9 tendons in total are applied at bottom with adjusted force of 7920 kN at each tendon. As jacking force was assigned, section area of the tendon is not an issue.

Tendon Parameters

Tendon Parameter Name: TB3 Units: kN, mm, C

Tendon Load Pattern: + Prestress-B

Tendon Parameters

Prestress Type: Post Tension

Jack From: Start

Material Property: + A416Gr270

Tendon Area: + 3360

Based on Tendon Size: 1 Tnd(s) 0.6"-24

Max Discretization Length: 1000

Design Parameters

Bonding Type: Bonded

Duct Diameter: 100.1

Min Duct Bend Radius: 9144

When tendons are modeled as elements, the Other Loss Parameters (elastic, creep, shrinkage, and relaxation losses) apply in addition to the losses computed by analysis.

Tendon Modeling Options

Model As Loads

Model As Elements

Load Type Tendon Load

Force Force (kN) Stress (kN/mm²)

Stress 7920 0.004788

Loss Parameters

Curvature Coefficient (Unitless): 0.15

Wobble Coefficient (1/mm): 6.5617E-07

Anchorage Set Slip (mm): 6.349

Other Loss Parameters

Elastic Shortening Stress [kN/mm²]: 0.02068

Creep Stress [kN/mm²]: 0.03447

Shrinkage Stress [kN/mm²]: 0.04826

Steel Relaxation Stress [kN/mm²]: 0.03447

OK Cancel

Figure 3.48: Bottom tendon parameter (TB3)

Tendon Parameters

Tendon Parameter Name: TB3(2) Units: kN, mm, C

Tendon Load Pattern: + Prestress-B

Tendon Parameters

Prestress Type: Post Tension

Jack From: Start

Material Property: + A416Gr270

Tendon Area: + 3360

Based on Tendon Size: 1 Tnd(s) 0.6"-24

Max Discretization Length: 1000

Design Parameters

Bonding Type: Bonded

Duct Diameter: 100.1

Min Duct Bend Radius: 9144

When tendons are modeled as elements, the Other Loss Parameters (elastic, creep, shrinkage, and relaxation losses) apply in addition to the losses computed by analysis.

Tendon Modeling Options

Model As Loads

Model As Elements

Load Type Tendon Load

Force Force (kN) Stress (kN/mm²)

Stress 3960 0.004788

Loss Parameters

Curvature Coefficient (Unitless): 0.15

Wobble Coefficient (1/mm): 6.5617E-07

Anchorage Set Slip (mm): 6.349

Other Loss Parameters

Elastic Shortening Stress [kN/mm²]: 0.02068

Creep Stress [kN/mm²]: 0.03447

Shrinkage Stress [kN/mm²]: 0.04826

Steel Relaxation Stress [kN/mm²]: 0.03447

OK Cancel

Figure 3.49: West span top span parameter (TB3(2))

3.7 Loads

The following loads has been considered in the three bridge models:

- i. Dead load (self-weight)
- ii. Superimposed dead loads (wearing course, railing)
- iii. Live loads

3.7.1 Dead Loads

Self-weight of the model was not taken as a lump of mass. Rather, all the element such as shell or solid elements are loaded by gravity load. Thus, self-weight is accounted for in the model automatically. Additionally, load due to wearing course is taken 30 lb/ft^2 in this study. Also, load due to railing is taken as 300 lb/ft at two sides of the deck and in the middle.

3.7.2 Live Loads

AASHTO guidelines for vehicle loads are followed in this study. The following vehicular loads are considered:

- i. HL 93 truck load
- ii. Lane Load

i. Truck Load

HL-93 is a truck load as shown in **Figure 3.50** consists of three axle loads; front axle load of 8 Kip and intermediate and rear axle load of 32 Kip each for semitrailer. The distance between Front and next axle is 14 ft, whereas distance between intermediate and rear axle ranges from 14-30 ft .In **Figure 3.50** rear axle range is denoted as V. Transverse spacing between centerline of wheel load is 6 ft with interior face of curb kept 2 ft and deck overhang for 1 ft.

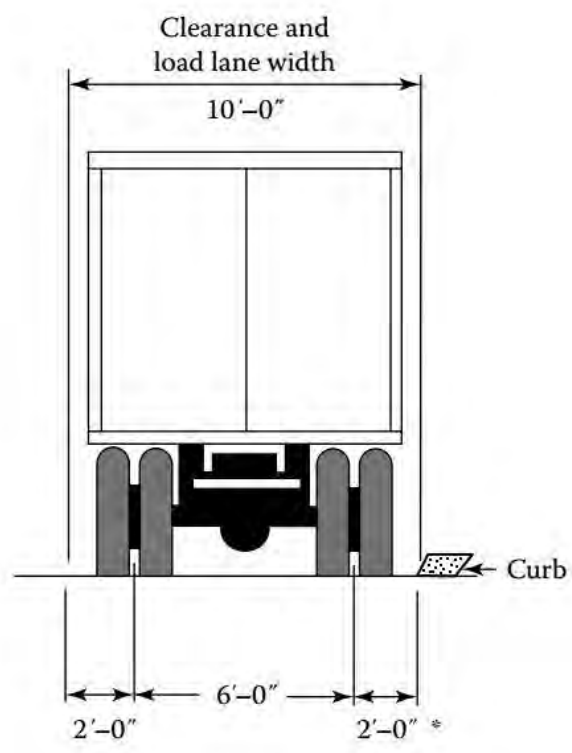
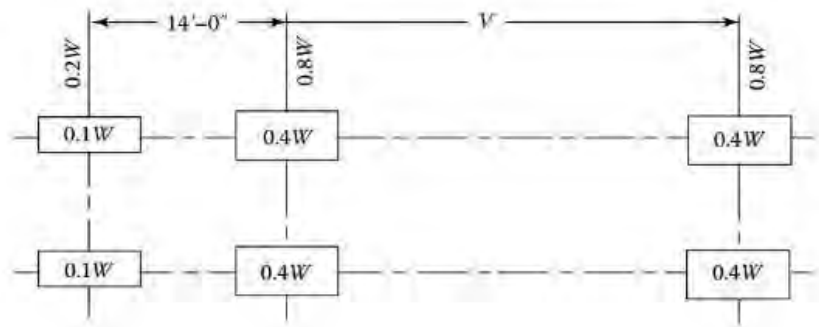
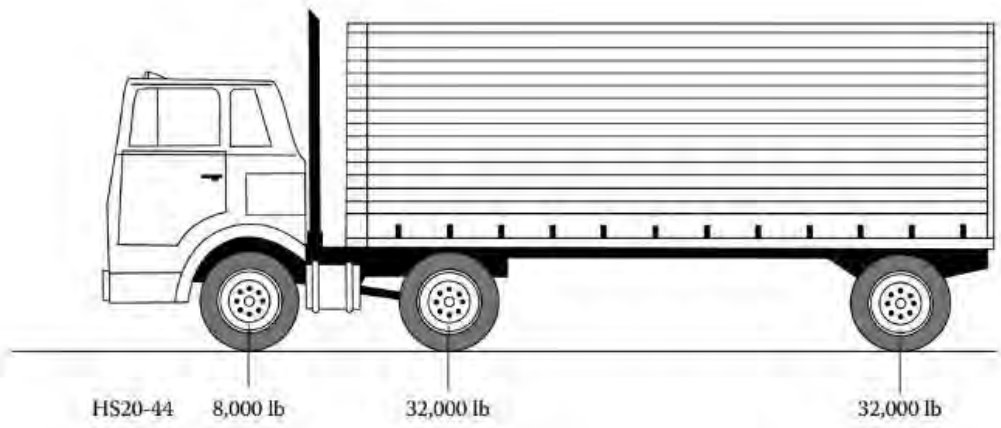


Figure 3.50: HL-93 loading

ii. Tandem Load

According to Taly (2015), for simple spans smaller than 40.27 ft the AASHTO tandem gives larger bending moment. For span greater than 40.27 ft, AASHTO truck produces larger bending moment. As the bridge structures in the study has span larger 40.27 ft, AASHTO tandem does not govern. Thus, it is omitted for the loading condition. The modeling of HL 93 used in this study are shown in Appendix A.

iii. Lane Load

According to AASHTO code, a load of 640 lb/ft is uniformly distributed in the longitudinal direction as a design lane load as show in **Figure 3.51**. Transversely, the design lane load is assumed to be distributed uniformly over 10 ft width. Details of modeling of lane load are shown in Appendix A.

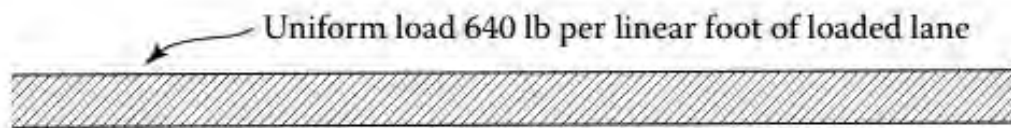


Figure 3.51: Lane load (AASHTO 2000)

3.8 Seismic Motion Data Input

Two earthquake data are used in this study. First one is data recorded on the pile cap of the Bangabandhu Multipurpose bridge in June 16,2004. Another one is the date of El-Centro earthquake (1940) with peak ground acceleration (PGA) of 0.35g. FIP Industriale provided seismic devices for seismic events with peak ground acceleration (PGA) of 0.47g (Castellano and Cestarollo, 1999). Design PGA for seismic isolation system in Bangabandhu bridge is 0.47g. For proper comparison between both earthquake data, both of them are scaled to PGA of 0.47g.

3.8.1 Seismic Data from The Bangabandhu Bridge with Scale Factor

In June 16,2004 data was recorded on the pile cap of the Bangabandhu bridge.

$$\text{Design PGA} = 0.47g = 461.07 \text{ cm/sec}^2$$

$$\text{Maximum Acceleration data found on Pier of The Bangabandhu bridge} = \underline{\underline{13.44 \text{ cm/s}^2}}$$

$$\text{Scale Factor} = \frac{461.07}{13.44} = \underline{\underline{34.31}}$$

Thus, scale factor of 34.31 is assigned for seismic input motion of both acceleration and displacement recorded on the pile cap of The Bangabandhu Multipurpose bridge.

In June 16,2004 the data recorded on the pile cap of The Bangabandhu Multipurpose bridge as peak ground acceleration vs time and displacement vs time are shown in **Figure 3.52** and **Figure 3.53** respectively.

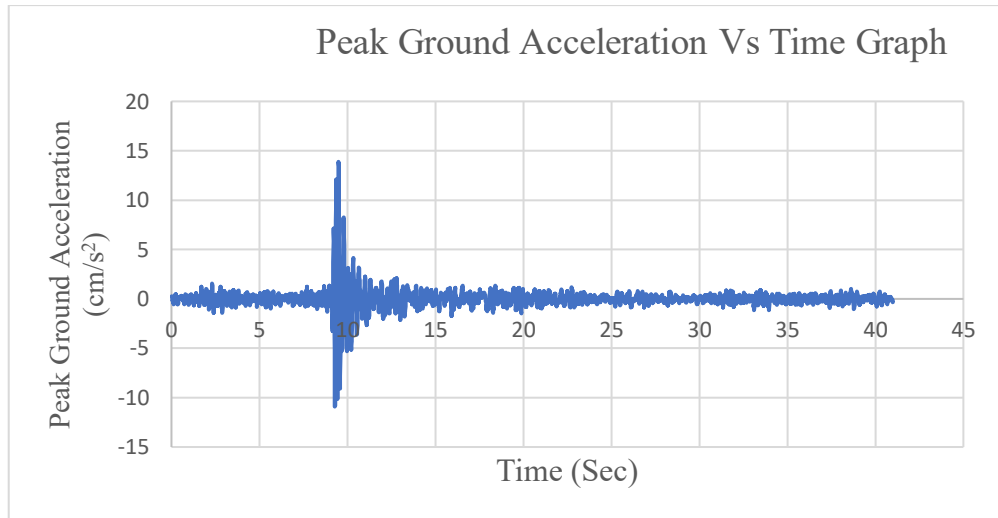


Figure 3.52: Peak ground acceleration vs time graph from The Bangabandhu bridge

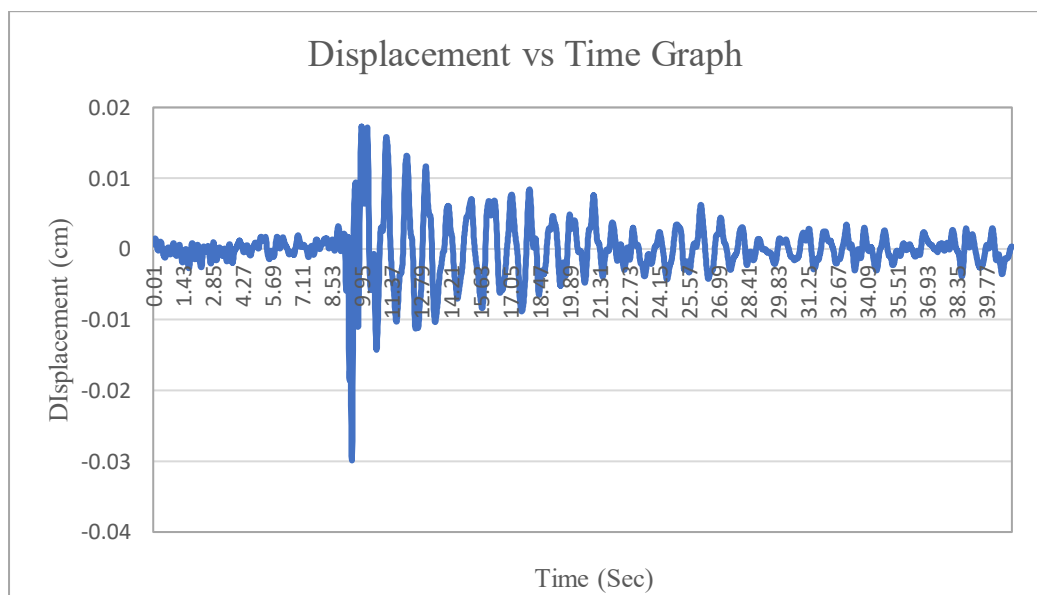


Figure 3.53: Displacement vs time data from The Bangabandhu bridge

3.8.2 El Centro Earthquake Data (1940)

El Centro is one of the most prominent earthquakes in history that occurred in 1940. It has a peak ground acceleration of 0.35 g. Earthquake data in terms of peak ground acceleration vs time and displacement vs time are shown in Figure 3.54 and Figure 3.55. Design PGA= $0.47g = 4.6107 \text{ m/s}^2$, Maximum Acceleration of El-Centro= 3.5 m/s^2 So, Scale Factor= $4.6107/3.5 = \underline{1.317}$.

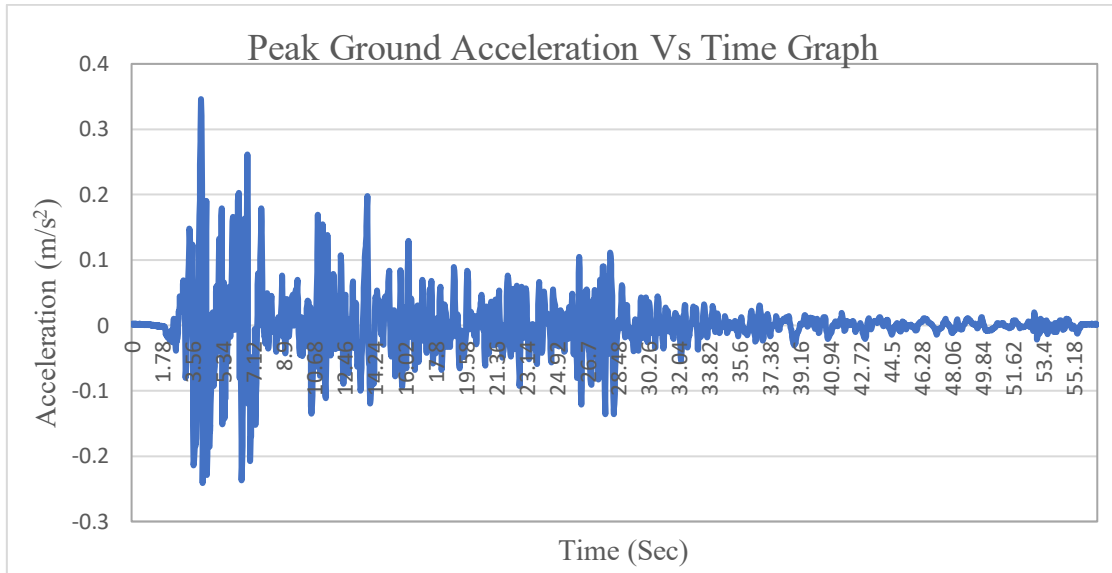


Figure 3.54: Peak ground acceleration vs time graph (El Centro, 1940)

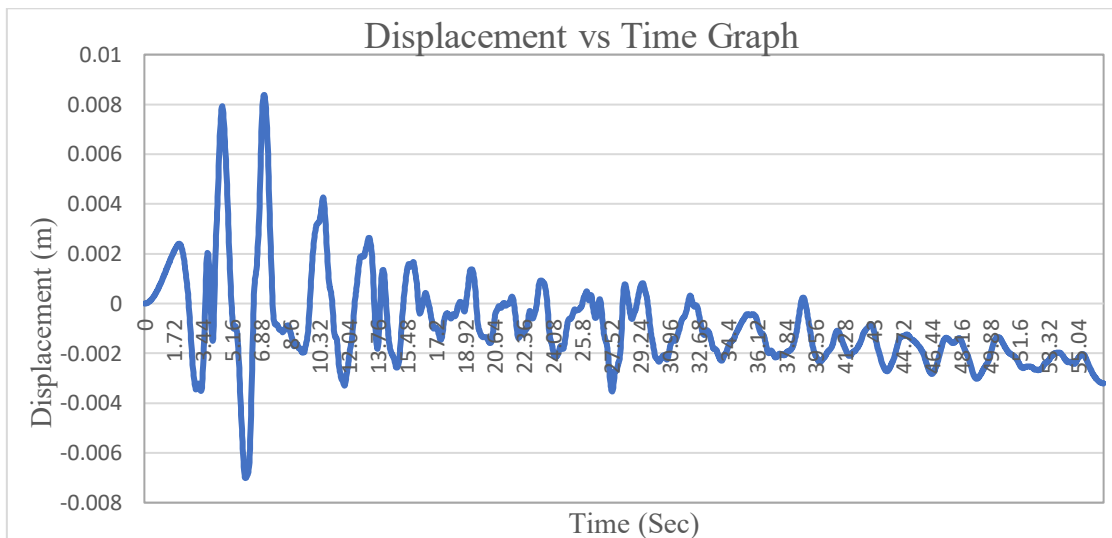


Figure 3.55: Displacement vs time data (El Centro, 1940)

3.8.3 Seismic Motion Input Assignment

Seven types of load cases due to earthquake are assigned in all the four bridge models. They are in the following:

- i. Synchronous motion
- ii. Asynchronous motion with 0.01 second time lag
- iii. Asynchronous motion with 0.05 second time lag
- iv. Asynchronous motion with 0.10 second time lag
- v. Asynchronous motion with 0.20 second time lag
- vi. Asynchronous motion with 0.50 second time lag
- vii. Asynchronous motion with 1.00 second time lag

Assignment of seismic motion input for 100m bridge model is given as a representative of the other bridge models. Since, seismic motion input is similar for all the bridge models.

For assigning seismic motion input of any type; at first, displacement is assigned at each pier and abutment. Displacement assigned in each pier and abutment are placed in their individual load pattern and load case as shown in **Figure 3.56** and **Figure 3.57**. The individual load patterns types are defined as quake whereas load cases are defined as linear static.

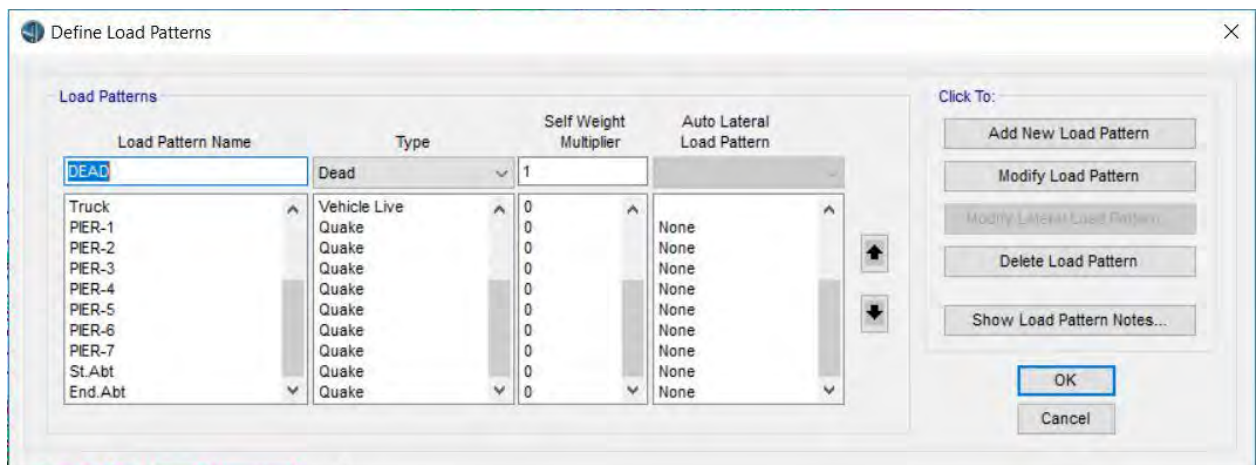


Figure 3.56: Abutment and pier displacement load pattern

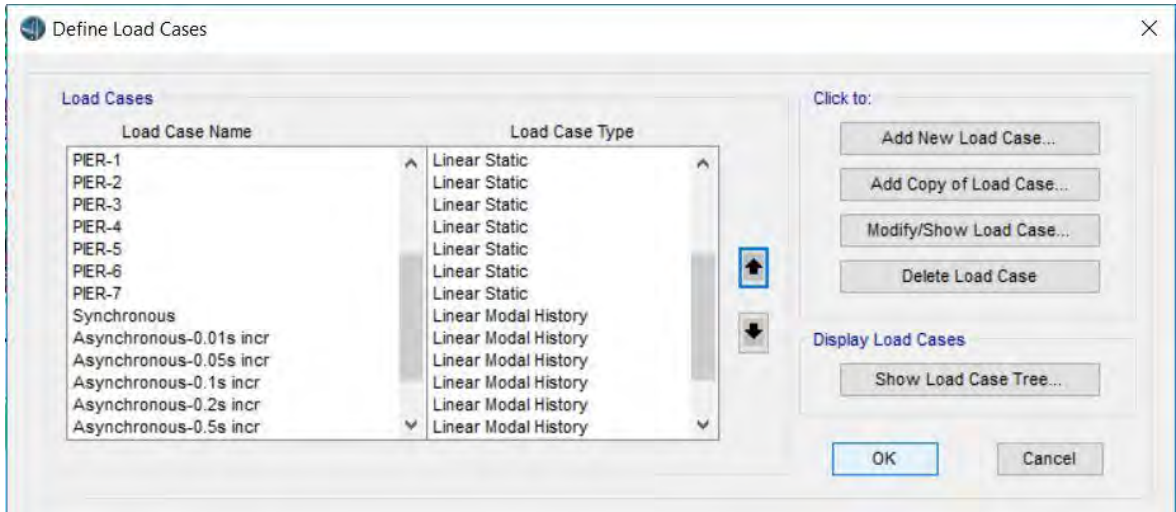


Figure 3.57: Abutment and pier displacement load pattern (2)

For applying synchronous earthquake motion; at first, particular load case with a type of linear modal history is defined. Acceleration vs time function data is assigned as a function as shown in **Figure 3.58**. This acceleration vs time data function is assigned to the defined synchronous load case with suitable scale factor either Longitudinal direction or transverse direction or both directions as shown in **Figure 3.59**.

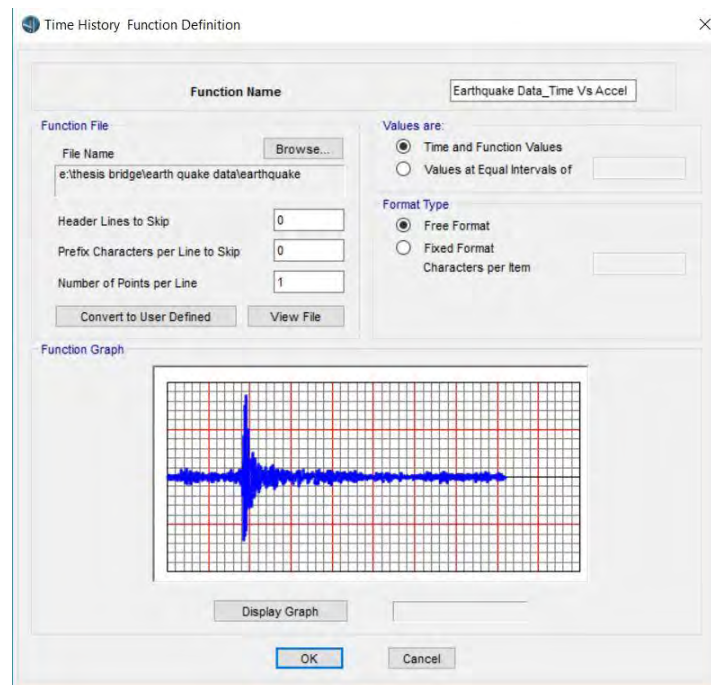


Figure 3.58: Acceleration vs time data for synchronous motion input

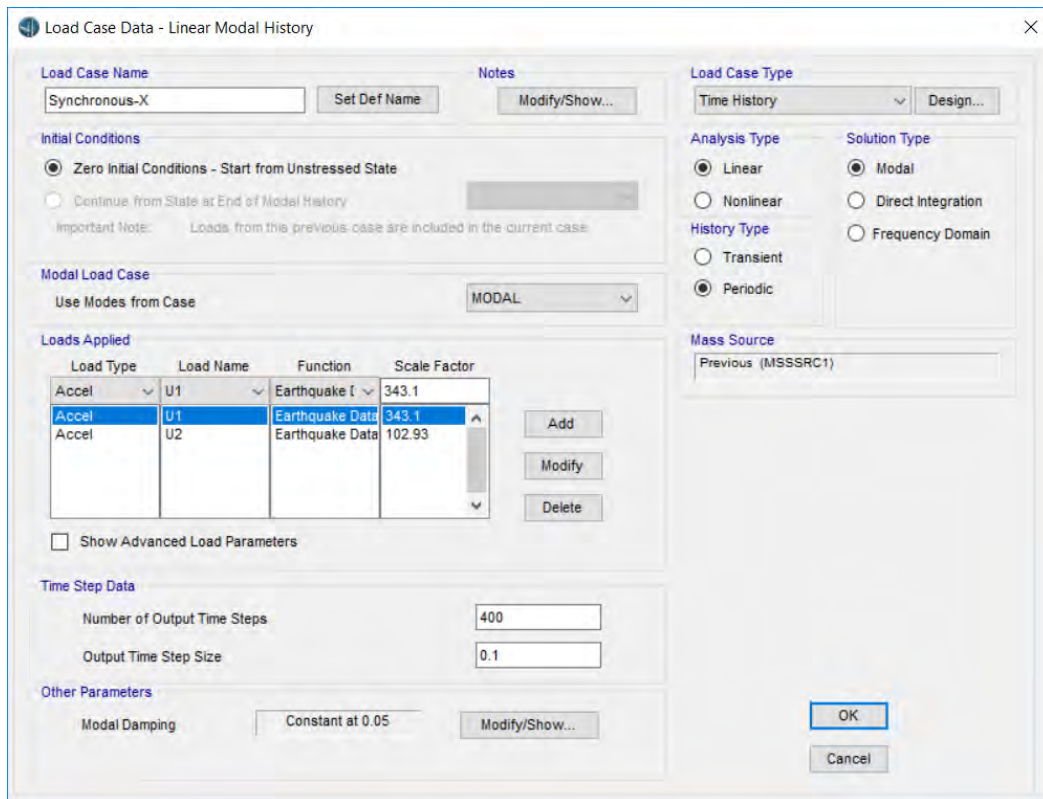


Figure 3.59: Synchronous motion load case example

For applying asynchronous earthquake motion; at first, particular load case with a type of linear modal history is to be defined. Displacement vs time function data is assigned as a function as shown in **Figure 3.60**. In a particular asynchronous load case, load patterns of all the displacements assigned starting from one abutment and ending with the other abutment as well as all the pier displacement in a sequence are assigned. displacement vs time function is assigned to all the assigned load patterns with suitable scale factor.

Arrival time of the displacement functions to the abutments and piers are assigned in cumulative increase in arrival time from start abutment with no arrival time to end abutment with maximum arrival time. This increase in arrival time simulates the asynchronous motion input as shown in **Figure 3.61**.

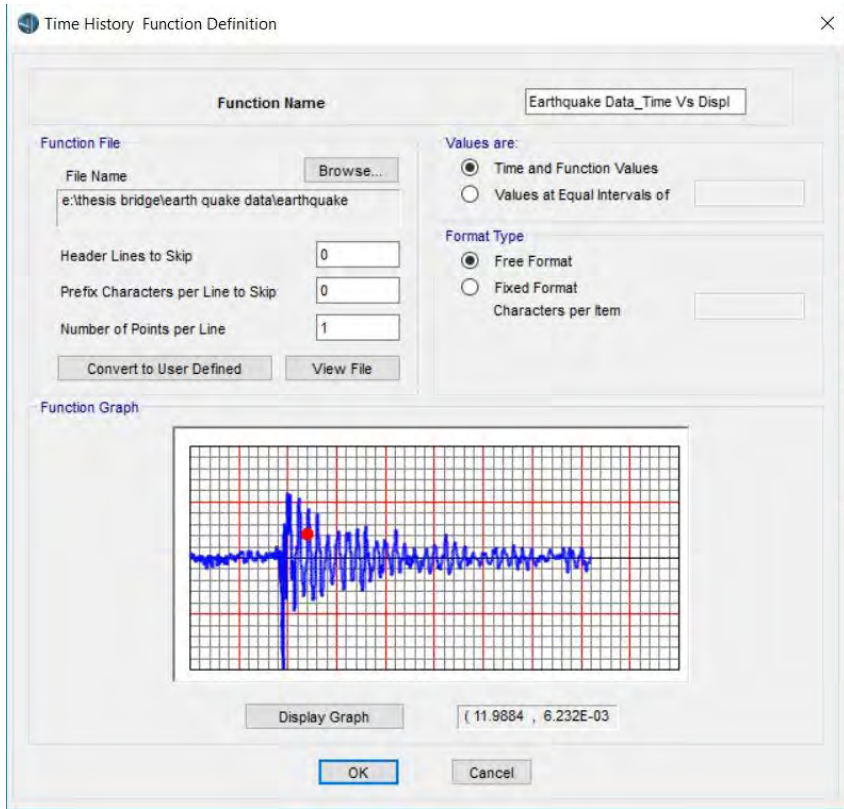


Figure 3.60: Displacement vs time data for asynchronous motion input

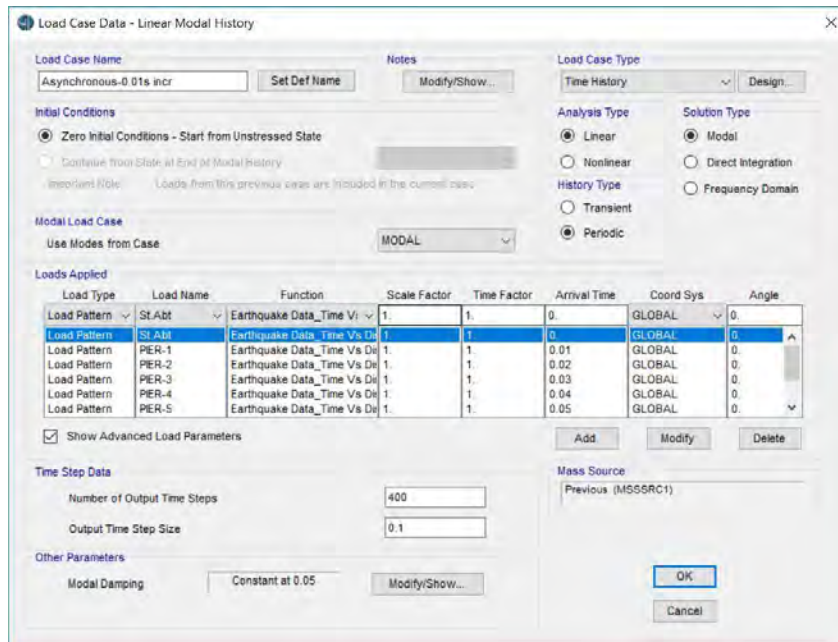


Figure 3.61: Load case for asynchronous motion input with 0.01 s time lag

Chapter 4

VERIFICATION OF BRIDGE ANALYSIS MODEL

4.1 Introduction

The bridge analysis models are verified on the basis of Span to depth ratio, sectional efficiency, deflection, flexural and stress capacity criteria. In this chapter, details about verification of the models is outlined.

4.2 Span to Depth Ratio

AASHTO LRFD Art. 2.5.2.6.3 provides optional deflection criteria for traditional constant depths, for constant depth super structure in terms of span-to-depth ratio. The **Table 4.1** below shows traditional minimum depths for constant depth superstructures.

Table 4.1: AASHTO LRFD Optional Deflection Criteria

Superstructure		Minimum Depth (Inc. Deck)	
Material	Type	Simple Spans	Continuous Spans
Concrete	Slabs with main reinforcement parallel to traffic	$\frac{1.2S + 10}{30}$	$\frac{S+10}{30} \geq 0.54 \text{ ft}$
	T-beams	0.070L	0.065L
	Box Beams	0.060L	0.055L
	Pedestrian structure beams	0.035L	0.033L
Prestressed Concrete	Slabs	0.030 L ≥ 6.5 in	0.027L ≥ 6.5 in
	Cast-in-place (CIP) box beams	0.045L	0.040L
	Precast I-beams	0.045L	0.040L
	Pedestrian structure beams	0.033L	0.030L
	Adjacent box beams	0.030L	0.025L
Steel	Overall depth of Composite I-beam	0.040L	0.032L
	Depth of I-beam portion of composite beam	0.033L	0.027L
	Trusses	0.1000L	0.1000L

This **Table 4.1** shows for pre-stressed concrete continuous span cast-in-place (CIP) box beams, minimum depth including deck is 0.040L where L is span length in feet. However, there is no specific provision for curved pre-stressed concrete bridge.

For spans up to 250 ft (75 m), constant depth section is typically utilized. However, when the span length is larger than 250 ft, a variable depth section is more economical and efficient. Span length over depth ratio (L/D) plays an important role in conceptual design as shown in **Figure 4.1**. The preliminary section depth is selected on the basis of the L/D ratio rule of thumb to establish the superstructure depth. The initial depth selected is continuously refined in the preliminary and final design (Chen and Duan, 2014).

For span greater than 250ft, the equation of span-to-depth ratio is

$$\frac{L}{D_s} = 15 \sim 18$$

$$\frac{L}{D_M} = 35 \sim 45$$

Where,

L =Length of mid-span

D_s = Depth at Pier

D_M = Depth at centre of mid-span

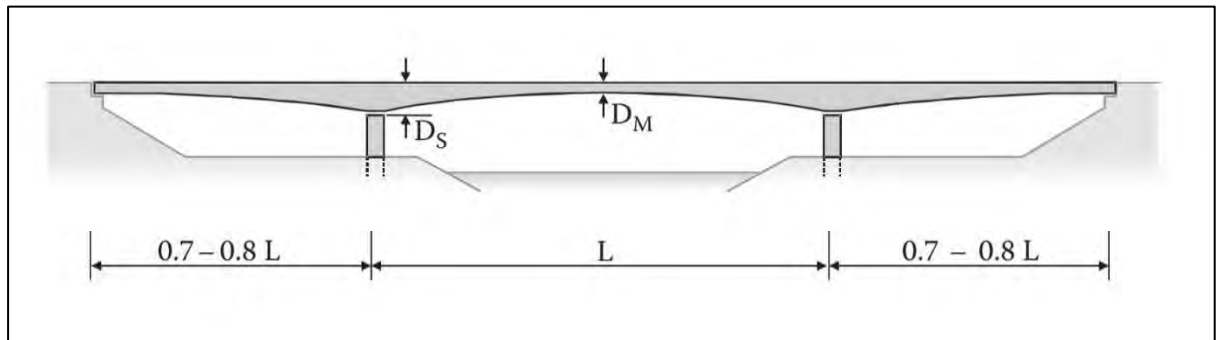


Figure 4.1: Span-to-depth ratio for variable depth bridge of span ≥ 250 ft.(Chen and Duan, 2014)

In the case of 100 m span module analysis model, which resembles the The Bangabandhu bridge,

Span Length, $L = 99.375$ m

Depth at pier, $D_s = 6.5$ m

Depth at centre of mid-span, $D_M = 2.919$ m

According to AASHTO LRFD criteria where for straight pre-stressed concrete CIP box beam

Minimum Depth = 0.040 L

In case of 75 m = 0.040 × 99.375 = 3.975 m < 6.5 m

According to Chen and Duan (2004), for variable depth,

$$\frac{L}{D_s} = \frac{99.375}{6.5} = 15.3$$

Which is between the ranges of 15 to 18. Thus, depth is within limit.

$$\frac{L}{D_M} = \frac{99.375}{2.919} = 34.1$$

Which is between the ranges of 35 to 45. Thus, depth is within limit.

In case of 75m span module,

Span Length, L = 74.531 m

Depth at pier, D_s = 4.88 m

Depth at centre of mid-span, D_M = 2.065 m

According to AASHTO LRFD criteria where for straight pre-stressed concrete CIP box beam

Minimum Depth = 0.040 L

In case of 75 m = 0.040 × 74.531 = 2.981 m < 4.88 m

According to Chen and Duan (2004), for variable depth,

$$\frac{L}{D_s} = \frac{74.531}{4.88} = 15.3$$

Which is between the ranges of 15 to 18. Thus, depth is within limit.

$$\frac{L}{D_M} = \frac{74.531}{2.065} = 36.1$$

Which is between the ranges of 35 to 45. Thus, depth is within limit.

For 125m span module,

Span Length, $L = 124.375$ m

Depth at pier, $D_s = 8.576$ m

Depth at centre of mid-span, $D_M = 3.888$ m

According to AASHTO LRFD criteria where for straight pre-stressed concrete CIP box beam

Minimum Depth $= 0.040 L$

In case of 125 m $= 0.040 \times 124.375 = 4.975$ m < 8.576 m

According to Chen and Duan (2004), for variable depth,

$$\frac{L}{D_s} = \frac{124.375}{8.576} \approx 14.5$$

Which is very close to the range of 15 to 18.

$$\frac{L}{D_M} = \frac{124.375}{3.888} = 32$$

Which is close to the ranges of 35 to 45.

4.3 Sectional Efficiency (Rodriguez, 2004)

Long span concrete girder bridges use a box cross-section because of its structural advantages. This section is able to resist both positive and negative moments present in continuous bridges because it has both top and bottom flanges. The large torsional strength and rigidity of a closed section is favorable for resisting torsional moments due to curved alignments or eccentric live load. The box girder section requires less post-tensioning than other sections. The required post-tensioning is related to the efficiency of the section which can be measured by the ratio:

$$\rho = \frac{I}{Ay_t y_b}$$

Where I denote the moment of inertia, A the area and y_t , y_b the distances from the neutral axis to the top and bottom fibers. A typical box girder section has a ρ equal to 0.60 whereas for a rectangular section ρ is equal to 0.33. The only disadvantage of the box girder section is the cost associated with forming the section which is higher than for other cross sections.

This additional cost is more than justified for long span lengths because a box section can be designed to reduce dead load to a minimum (Rodriguez, 2004).

In the case of 100 m span module analysis model, which resembles the Bangabandhu bridge, sectional properties are shown in Figure. Also, sectional efficiency check is show in Table

Table 4.2: Sectional Efficiency Check For 100m span module

For 100m span module		
Total Width	60.6955	ft
Total depth (at pier top)	21.3255	ft
Top Slab Thickness (t1)	0.9186	ft
Bottom Slab Thickness (t2)	2.7887	ft
Exterior Girder Thickness(t3)	1.6404	ft
Moment of Inertia, I [min]	15198.5	ft ⁴
Cross Sectional Area, A	221.737	ft ²
Distance of top fiber, Y _t	8.5465	ft
Distance of Bottom fiber, Y _b	12.779	ft
Efficiency Ratio, ρ	0.62759	

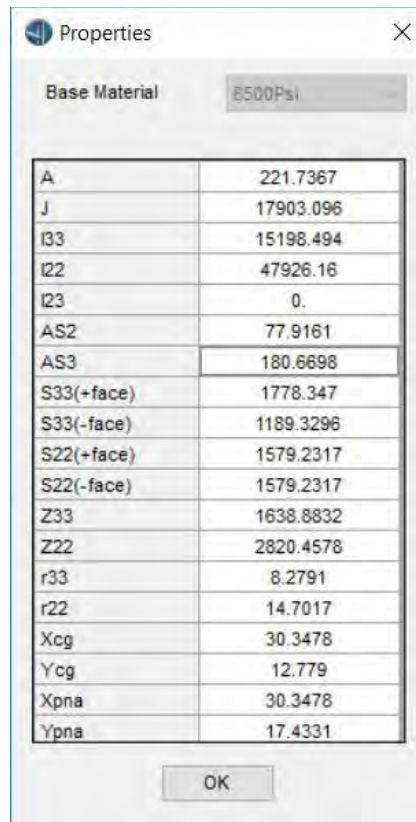


Figure 4.2: Sectional properties for 100 m span module

In In case of 75m span module, sectional properties are shown in **Figure 4.3**. Also, sectional efficiency check is show in **Table 4.3**.

Table 4.3 :Sectional Efficiency Check For 75m span module

75m span module		
Total Width	60.6955	ft
Total depth (at pier top)	16.0105	ft
Top Slab Thickness (t1)	0.9186	ft
Bottom Slab Thickness (t2)	2.1325	ft
Exterior Girder Thickness(t3)	1.4764	ft
Moment of Inertia, I [min]	6819.79	ft ⁴
Cross Sectional Area, A	182.447	ft ²
Distance of top fiber, Y _t	5.9365	ft
Distance of Bottom fiber, Y _b	10.074	ft
Efficiency Ratio, ρ	0.62503	

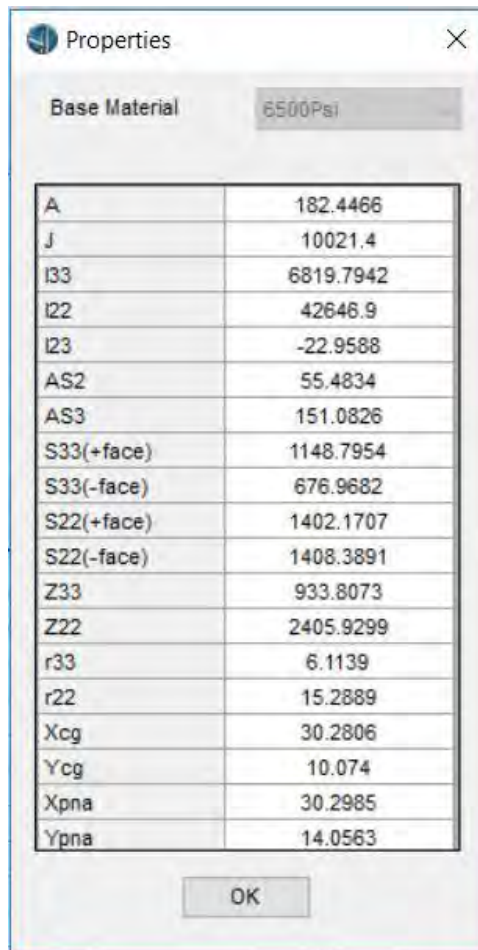


Figure 4.3: Sectional properties for 75 m span module

In In case of 125m span module, sectional properties are shown in **Figure 4.4**. Also, sectional efficiency check is show in **Table 4.4**.

Table 4.4 :Sectional Efficiency Check For 125m span module

For 125m span module		
Total Width	60.70	ft
Total depth (at pier top)	28.14	ft
Top Slab Thickness (t1)	1.15	ft
Bottom Slab Thickness (t2)	3.48	ft
Exterior Girder Thickness(t3)	2.05	ft
Moment of Inertia, I [min]	30352.62	ft ⁴
Cross Sectional Area, A	290.94	ft ²
Distance of top fiber, Y _t	11.30	ft
Distance of Bottom fiber, Y _b	16.84	ft
Efficiency Ratio, ρ	0.600	

Properties	
Base Material	6500Psi
A	290.9411
J	29791.64
I33	30352.617
I22	50268.58
I23	0.
AS2	118.0501
AS3	218.4464
S33(+face)	2723.2692
S33(-face)	1786.4118
S22(+face)	1656.4178
S22(-face)	1656.4178
Z33	2563.6945
Z22	3144.6752
r33	10.6384
r22	13.6907
Xcg	30.3478
Ycg	16.8353
Xpna	30.3478
Ypna	20.8646

Figure 4.4: Sectional properties for 125 m span module

4.4 Comparison with Deflection Criteria

In this section, deflection criteria due to dead load and vehicular load are verified according to corresponding provisions. Deflection due to service condition (dead load + live load + Prestress force) is also verified in this section.

4.4.1 Deflection Due to Dead Load

Dead load includes self-weight of structure, wearing course and railing. Maximum deflection due to dead load for 100m span module, which resembles the Bangabandhu bridge, is shown in **Table 4.5**. Also, maximum deflection due to dead load for 75m and 125 m span modules are also shown in **Table 4.5**.

Table 4.5: Maximum deflection due to dead load for three bridge modules

Span Module	Model Output (mm)
75 meters	78.9
100 meters	111.50
125 meters	130

4.4.2 Deflection Due to Vehicular Load

According to AASHTO LRFD code, deflection is a serviceability issue not a strength issue. Accordingly, service live loads (i.e. unfactored live loads) should be considered in calculating deflections. Deflection due to live load should be checked for two cases. They are:

- i. The live load portion of Load Combination Service I which is 1.00 Vehicular Live Load (LL) and 1.00 Vehicular dynamic load allowance (IM).
- ii. The live load criteria are taken from art. 3.6.1.3.2 of AASHTO for Optional Live Load Deflection Evaluation. It requires that the deflection should be taken as the larger of that resulting from design truck alone and that resulting from 25 percent of the design truck taken together with the design lane load.

For these cases, maximum deflection shall be taken as span/800.

In the case of 100 m span bridge analysis model, which resembles the Bangabandhu bridge, deflection due to vehicular load is shown in **Figure 4.5** and **Figure 4.6**. The magnitude of deflection and allowable limit is shown in Table 4.6.

In the case of 75 m span module analysis model, deflection due to vehicular load is shown in **Figure 4.7** and **Figure 4.8** .The magnitude of deflection and allowable limit is shown in **Table 4.7**.

In the case of 125 m span module analysis model, deflection due to vehicular load is shown in **Figure 4.9** and **Figure 4.10**.The magnitude of deflection and allowable limit is shown in **Table 4.8**.

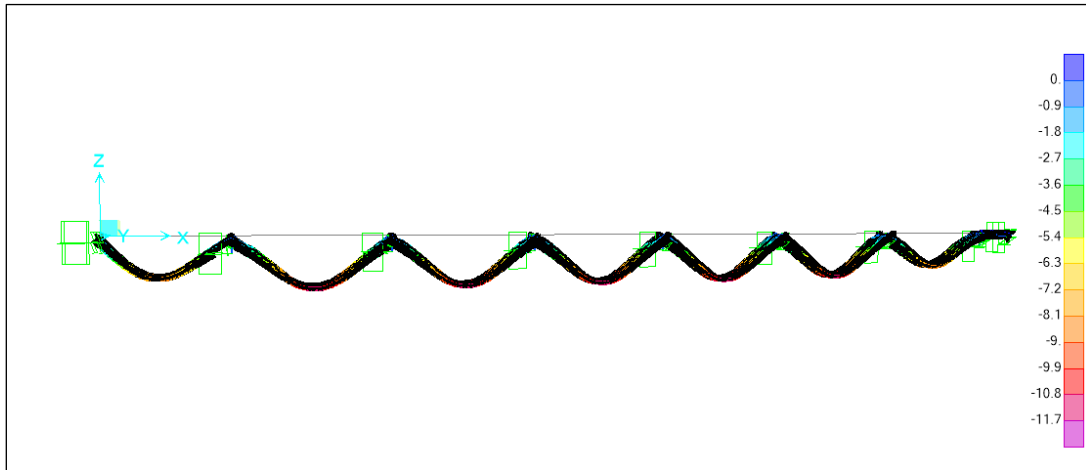


Figure 4.5: Deflection due to design truck load (100 m span module)

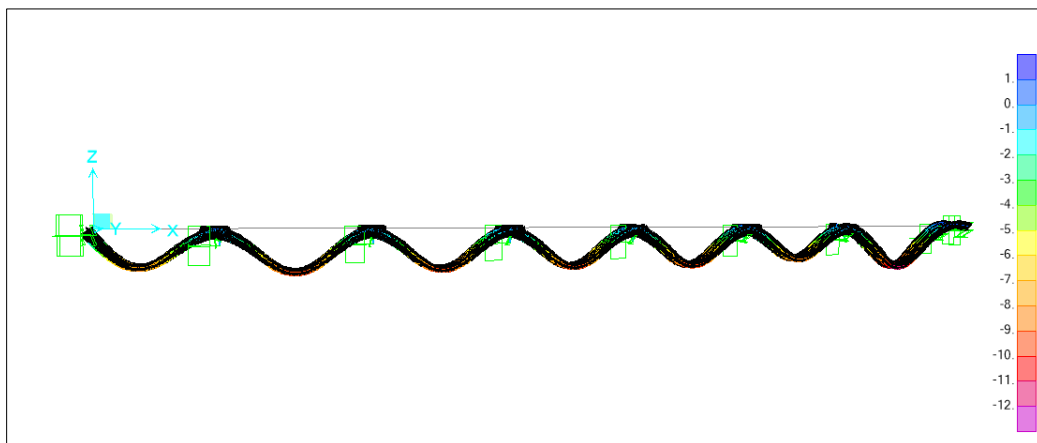


Figure 4.6: Deflection due to lane load + 0.25 truck load (100 m Span module)

Table 4.6: Deflection due to Live Load Check (100m)

Load Case	Allowable Deflection (mm)	Model Output (mm)
Design Truck Load+ Impact Load	124	11.7
Lane Load + 0.25 x Truck Load	124	12

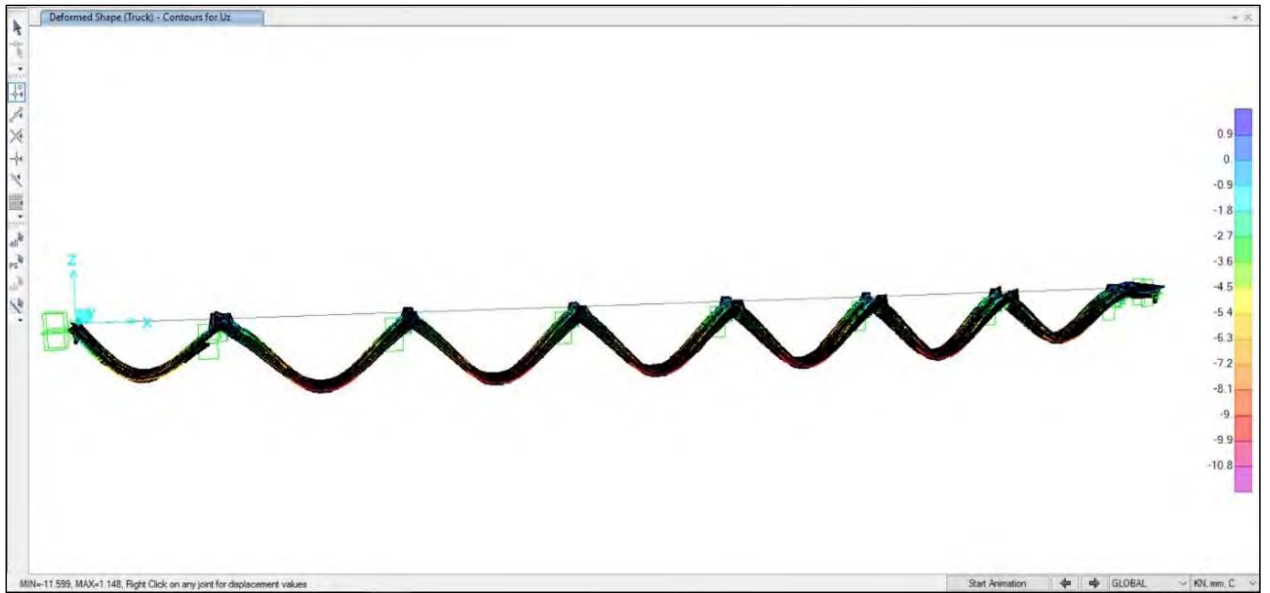


Figure 4.7: Deflection due to design truck load (75 m span module)

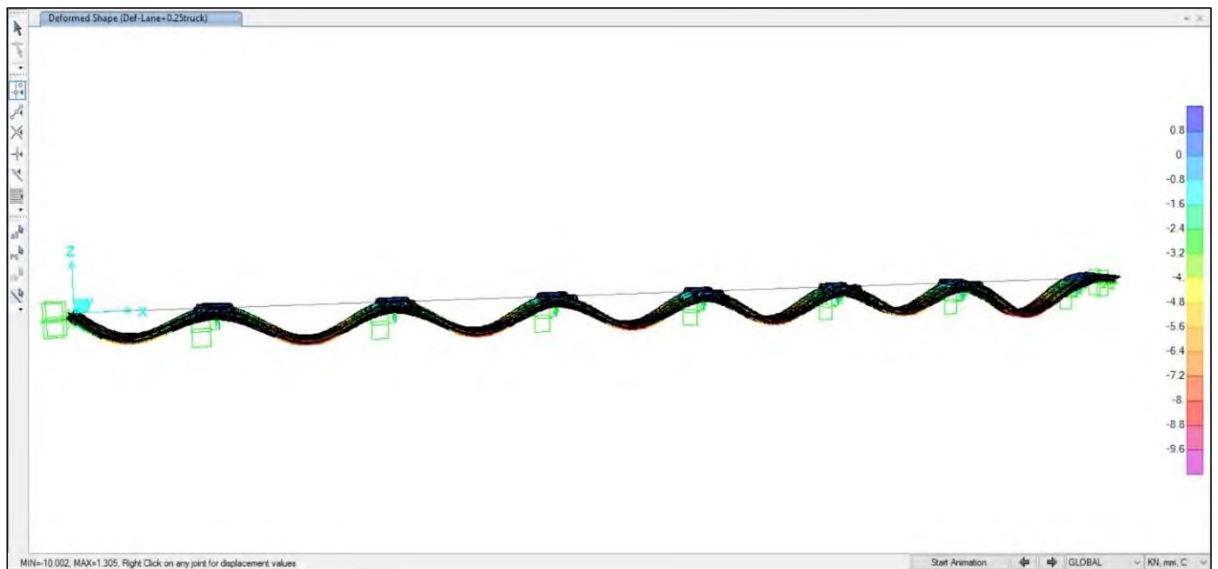


Figure 4.8: Deflection due to design lane load + 0.25 design truck load (75 m span module)

Table 4.7: Deflection due to Live Load Check (75m span module)

Load Case	Allowable Deflection (mm)	Model Output (mm)
Design Truck Load+ Impact Load	93	11.6
Lane Load + 0.25 x Truck Load	93	10.0

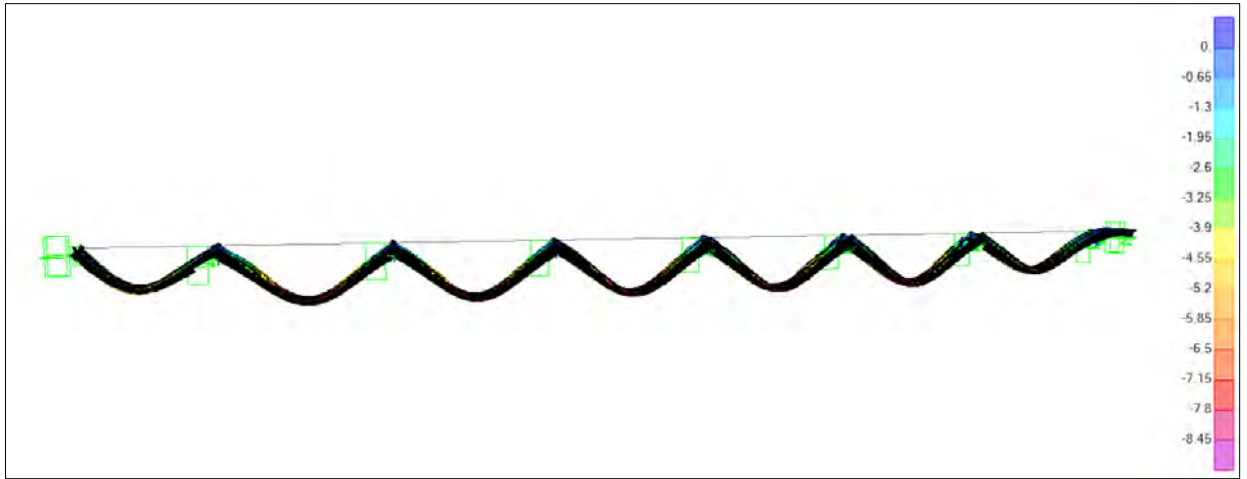


Figure 4.9: Deflection due to design truck load (125 m span module)

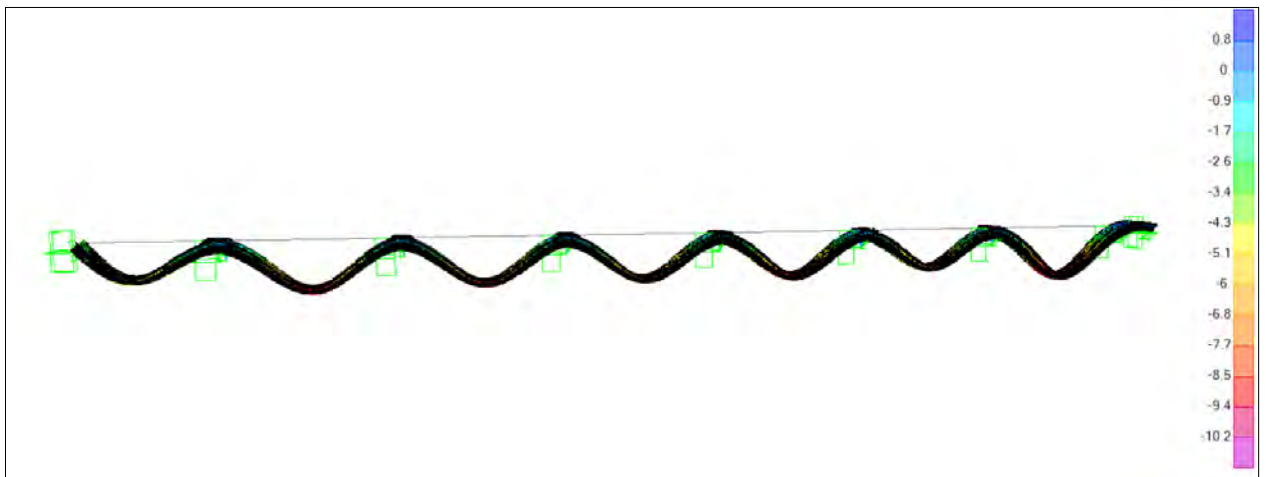


Figure 4.10: Deflection due to design lane load + 0.25 design truck load (125 m span module)

Table 4.8: Deflection due to Live Load Check (125m span module)

Load Case	Allowable Deflection (mm)	Model Output (mm)
Design Truck Load+ Impact Load	155	8.45
Lane Load + 0.25 x Truck Load	155	10.2

4.4.3 Total Deflection of Dead Load, Live Load and Prestress Force

In IS 1343-1980, deflection criteria are taken into consideration the prestress force. According to IS 1343-1980, maximum permissible deflection due to Dead load + Live load + Prestress force shall be taken as $\text{span}/350$ or ± 20 mm. In AASHTO code there is no limit for this case that's why Indian Standard (IS) is considered here.

Table 4.9 shows deflection due to dead load+ prestress force and deflection for dead load+ live load +prestress force for all three bridge modules. For 125m span module bridge deflection is slightly greater than the allowable limit which means prestressing force need to be adjusted.

Table 4.9: Deflection due to Dead Load + Live Load +prestress force

Load Case	Maximum Deflection (mm)		
	75m Module	100m Module	125m Module
Dead Load +Live Load +Prestress Force	12	15.3	24
Dead Load +Prestress Force	9.8	10.5	19.2

4.5 Flexure and Stress Check

AASHTO LRFD Art 5.9.4.2 mentions provision for both compression and tensile stress limit.

In segmentally constructed bridges due to sum of effective prestress and permanent loads, compressive stress limit is taken as $0.45 f'_c$ (MPa).

For segmentally constructed bridges, there are two provisions for longitudinal tensile stresses:

- i. In areas with bonded reinforcement sufficient to resist the tensile force in the concrete computed assuming an uncracked section, where reinforcement is proportioned using a stress of $0.5f_y$ not to exceed 205 MPa, limit can be taken as $0.5\sqrt{f'_c}$ (MPa).
- ii. For other areas without bonded reinforcement, no tension is allowed.

In the case of 100 m span module analysis model, which resembles the Bangabandhu bridge, flexural capacity check is shown in **Figure 4.11**. Bottom and top longitudinal stress check are shown in **Figure 4.12** and **Figure 4.13** respectively.

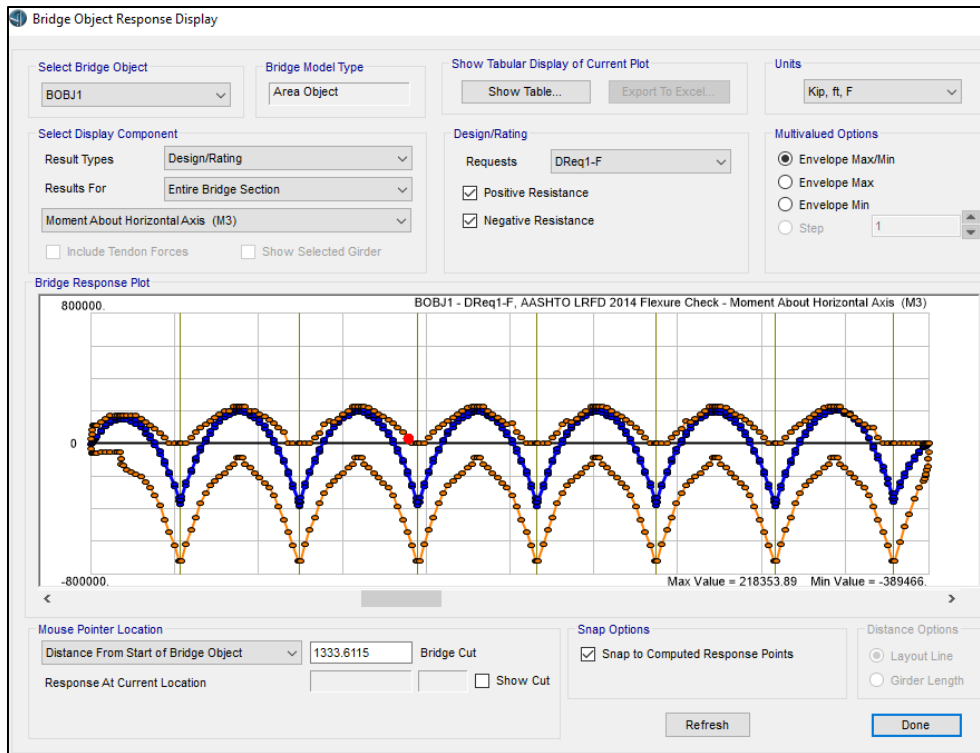


Figure 4.11: Flexural capacity check according AASHTO LRFD,2014 (100 m)

For 100m span module,

Maximum induced Positive Moment = 2, 18,628 Kip-ft

Maximum Positive Moment Capacity = 2, 28,771 Kip-ft

Maximum induced Negative Moment = 3, 89,466 Kip-ft

Maximum Negative Moment Capacity = 7, 21,387 Kip-ft

Thus, flexural capacity is within allowable capacity in case of 100m bridge span module.

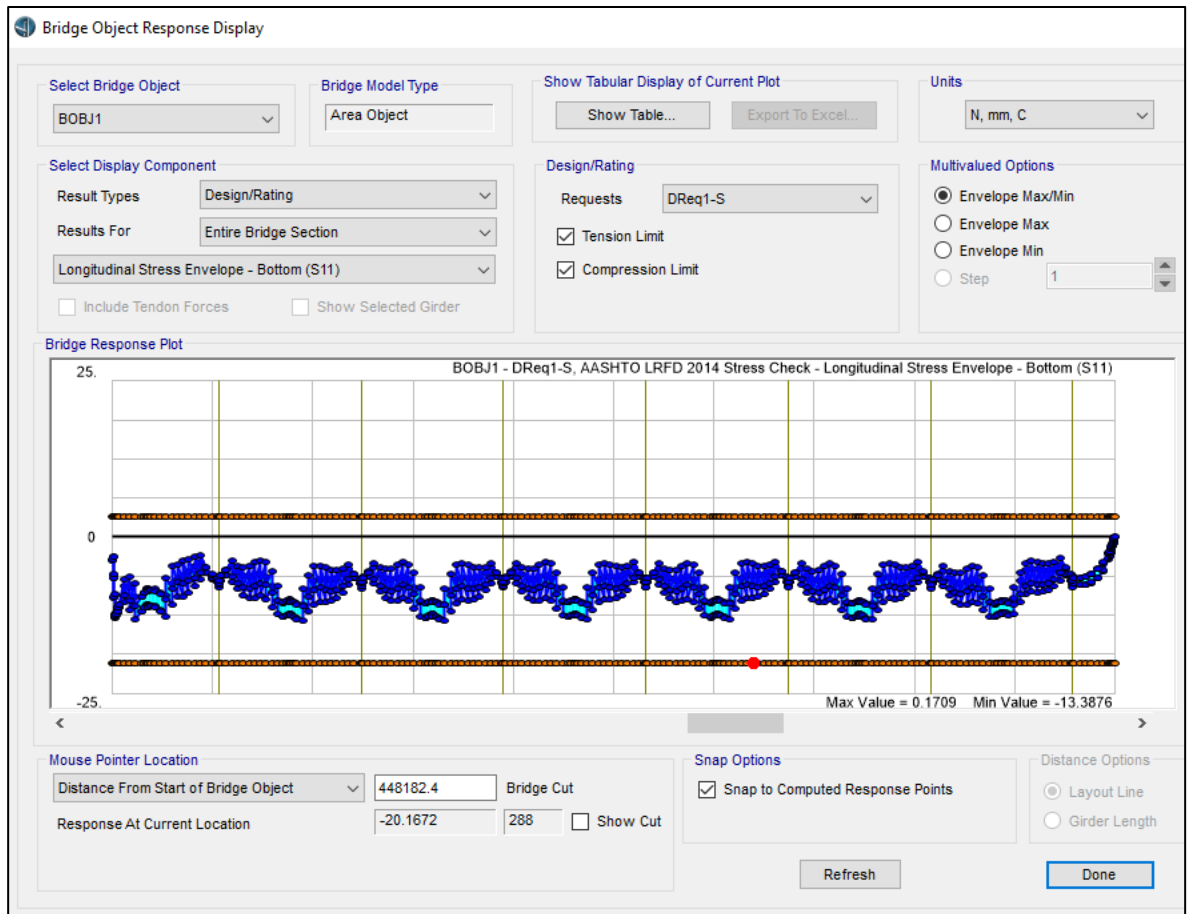


Figure 4.12: Bottom longitudinal stress capacity check (100 m)

For Bottom,

$$\text{Tensile Stress Limit} = 0.5\sqrt{f'_c}(\text{MPa}) = 0.5\sqrt{44.83} \text{ MPa} = 3.34 \text{ MPa}$$

Maximum Tensile Stress = 0 MPa

$$\text{Compressive Stress Limit} = 0.45 f'_c (\text{MPa}) = 0.45 \times 44.83 \text{ MPa} = 20.16 \text{ MPa}$$

Maximum Compressive Stress = 13.39 MPa

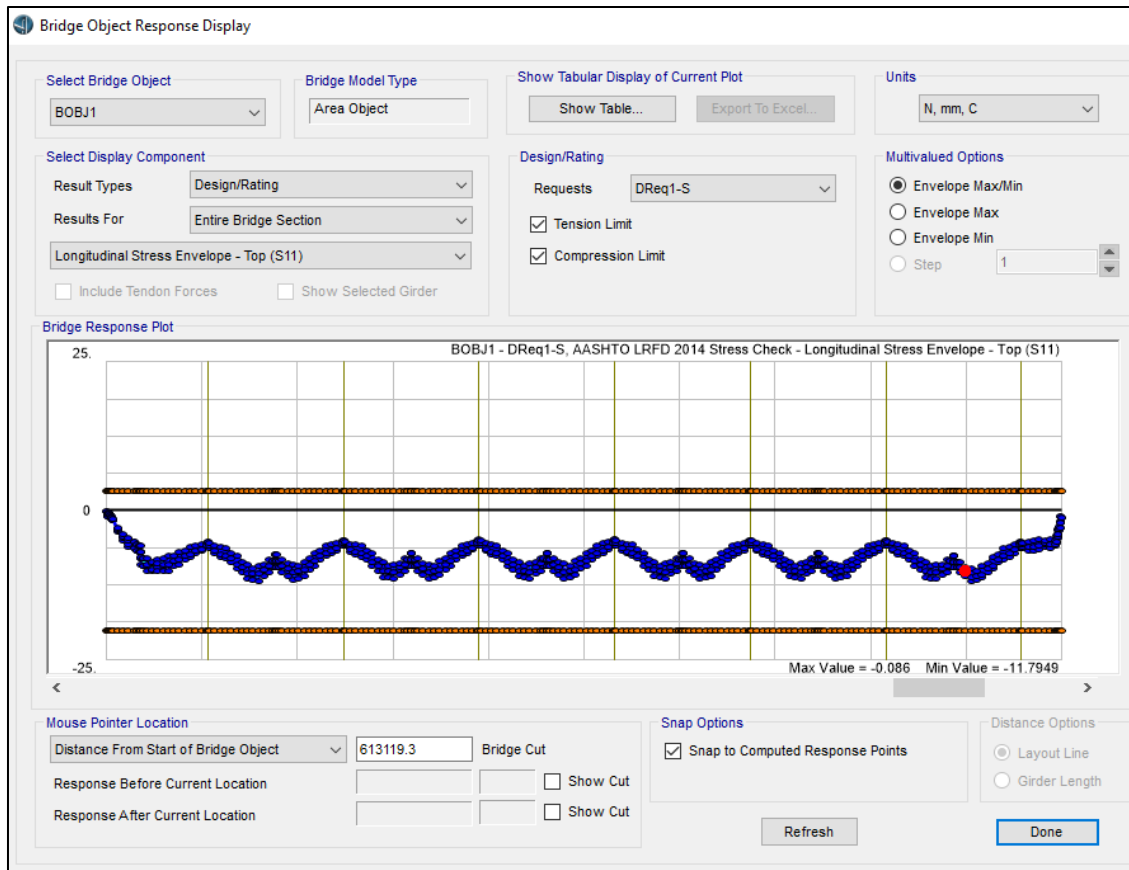


Figure 4.13: Top longitudinal stress capacity check (100 m)

For Top,

$$\text{Tensile Stress Limit} = 0.5\sqrt{f'_c}(\text{MPa}) = 0.5\sqrt{44.83} \text{ MPa} = 3.34 \text{ MPa}$$

$$\text{Maximum Tensile Stress} = 0 \text{ MPa}$$

$$\text{Compressive Stress Limit} = 0.45 f'_c (\text{MPa}) = 0.45 \times 44.83 \text{ MPa} = 20.16 \text{ MPa}$$

$$\text{Maximum Compressive Stress} = 11.79 \text{ MPa}$$

Tensile and compressive stress limit at top and bottom fibre of box girder section is within allowable limit for 100m bridge span module.

For 75 m span module, flexural capacity check is shown in **Figure 4.14**. Bottom and top longitudinal stress check are shown in **Figure 4.15** and **Figure 4.16** respectively.

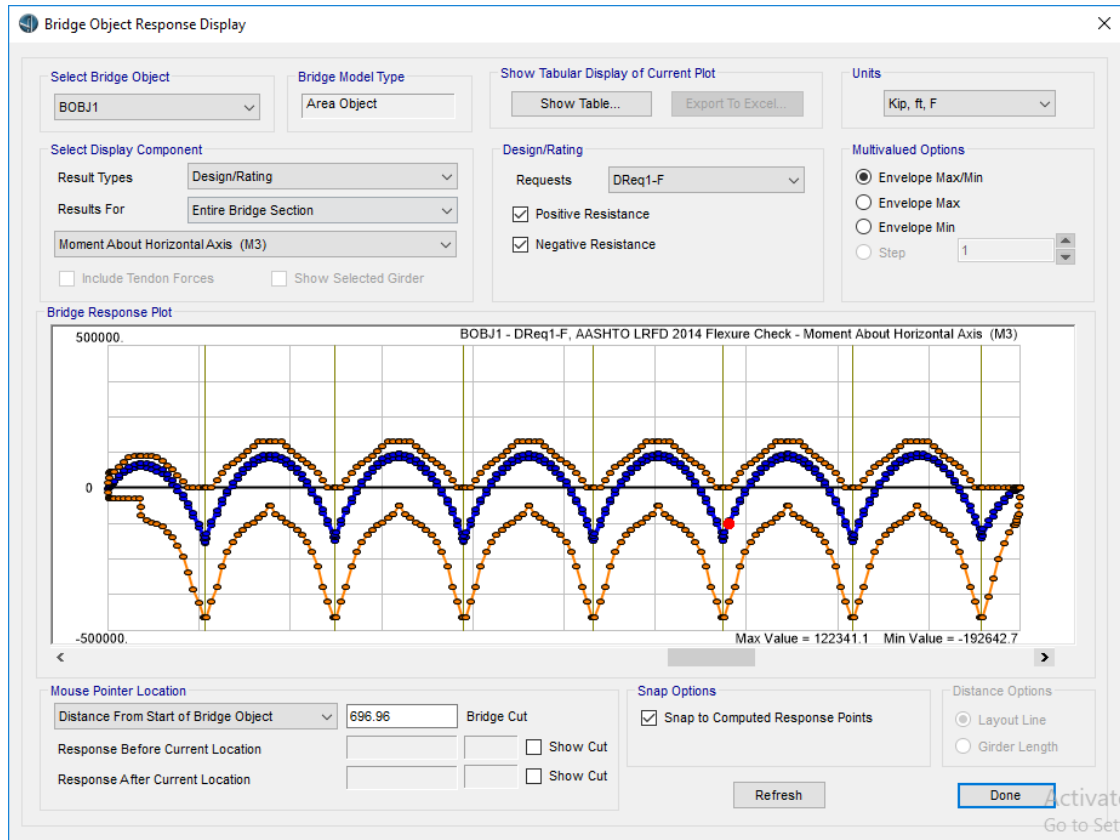


Figure 4.14: Flexural capacity check according AASHTO LRFD,2014 (75 m)

For 75m span module,

Maximum induced Positive Moment = 1, 22,341 Kip-ft

Maximum Positive Moment Capacity = 1, 65,047 Kip-ft

Maximum induced Negative Moment = 1, 92,642 Kip-ft

Maximum Negative Moment Capacity = 4,56,567 Kip-ft

Thus, flexural capacity is within allowable capacity in case of 75m bridge span module.

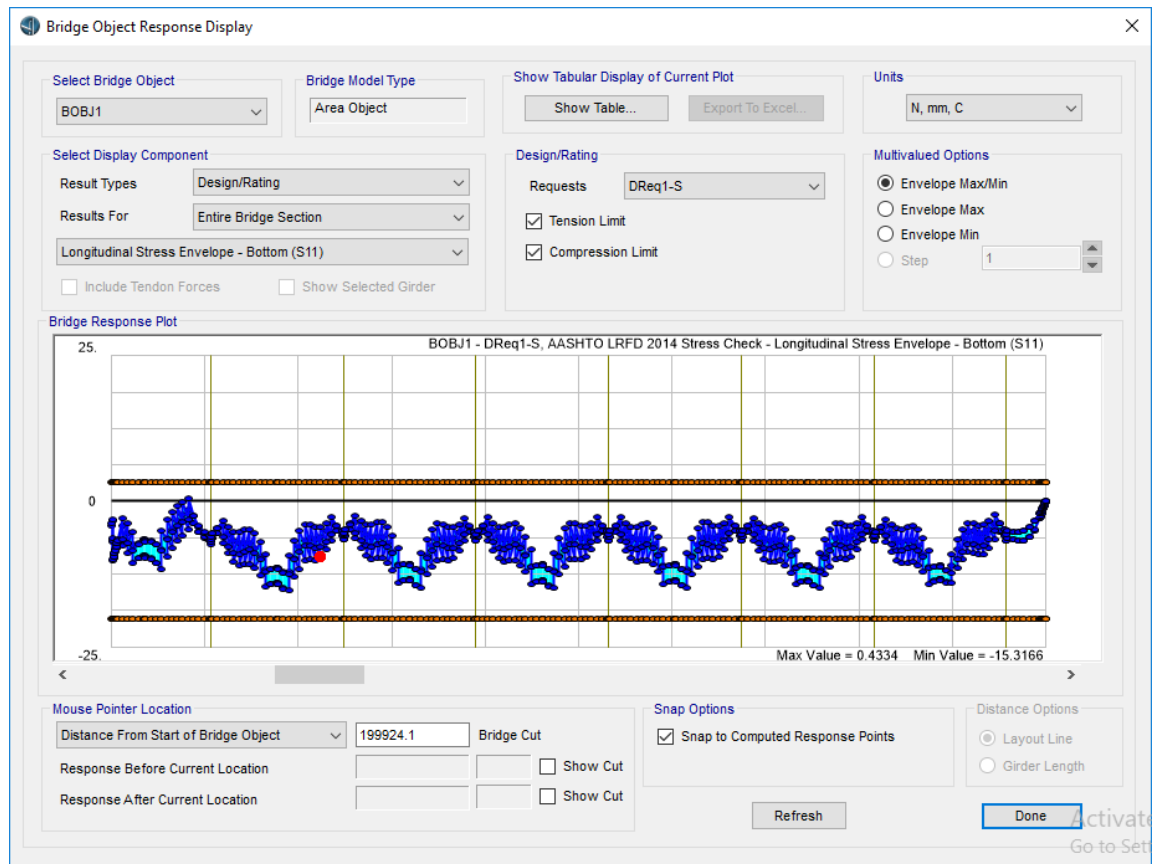


Figure 4.15: Bottom longitudinal stress capacity check (75 m)

Bottom Longitudinal Stress,

$$\text{Tensile Stress Limit} = 0.5\sqrt{f'_c}(\text{MPa}) = 0.5\sqrt{44.83} \text{ MPa} = 3.34 \text{ MPa}$$

$$\text{Maximum Tensile Stress} = 0 \text{ MPa}$$

$$\text{Compressive Stress Limit} = 0.45 f'_c (\text{MPa}) = 0.45 \times 44.83 \text{ MPa} = 20.16 \text{ MPa}$$

$$\text{Maximum Compressive Stress} = 15.32 \text{ MPa}$$

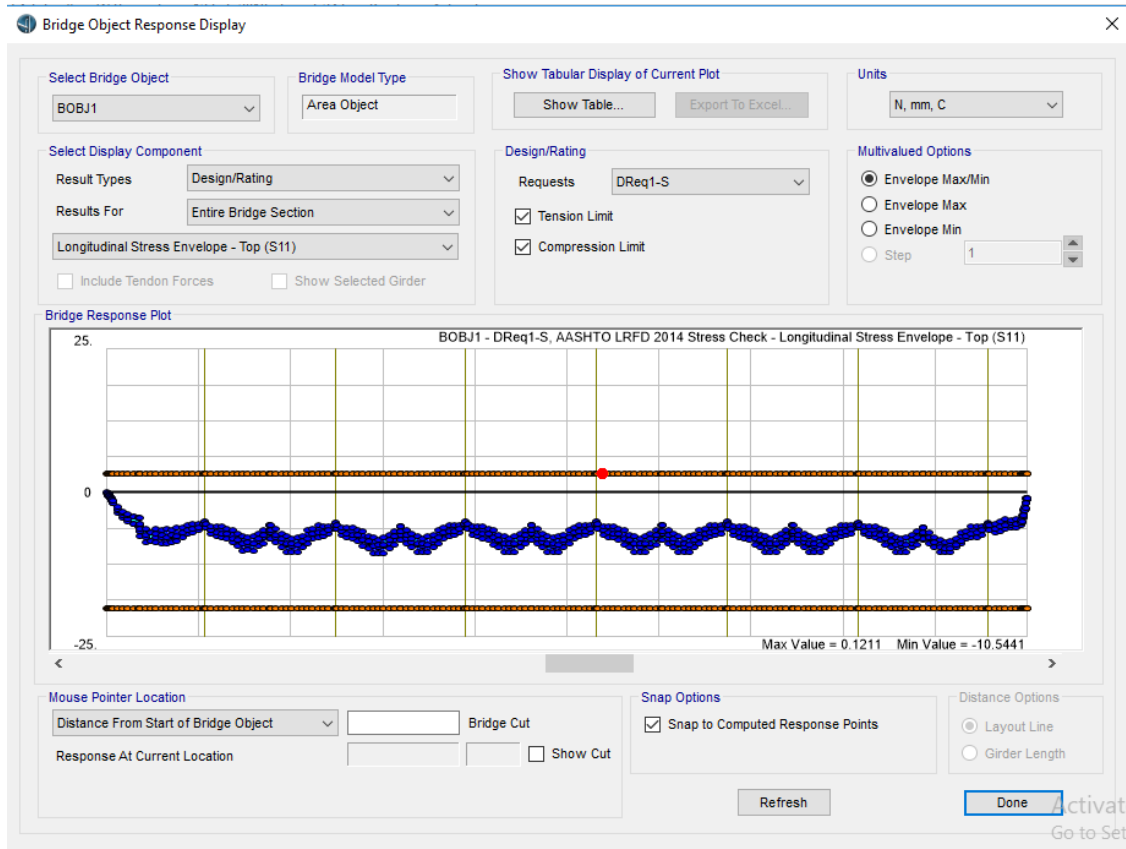


Figure 4.16: Top longitudinal stress capacity check (75 m)

Top Longitudinal Stress,

$$\text{Tensile Stress Limit} = 0.5\sqrt{f'_c}(\text{MPa}) = 0.5\sqrt{44.83} \text{ MPa} = 3.34 \text{ MPa}$$

$$\text{Maximum Tensile Stress} = 0 \text{ MPa}$$

$$\text{Compressive Stress Limit} = 0.45 f'_c (\text{MPa}) = 0.45 \times 44.83 \text{ MPa} = 20.16 \text{ MPa}$$

$$\text{Maximum Compressive Stress} = 10.54 \text{ MPa}$$

Tensile and compressive stress limit at top and bottom fibre of box girder section is within allowable limit for 75m bridge span module.

For 125 m span module, flexural capacity check is shown in **Figure 4.17**. Bottom and top longitudinal stress check are shown in **Figure 4.18** and **Figure 4.19** respectively.

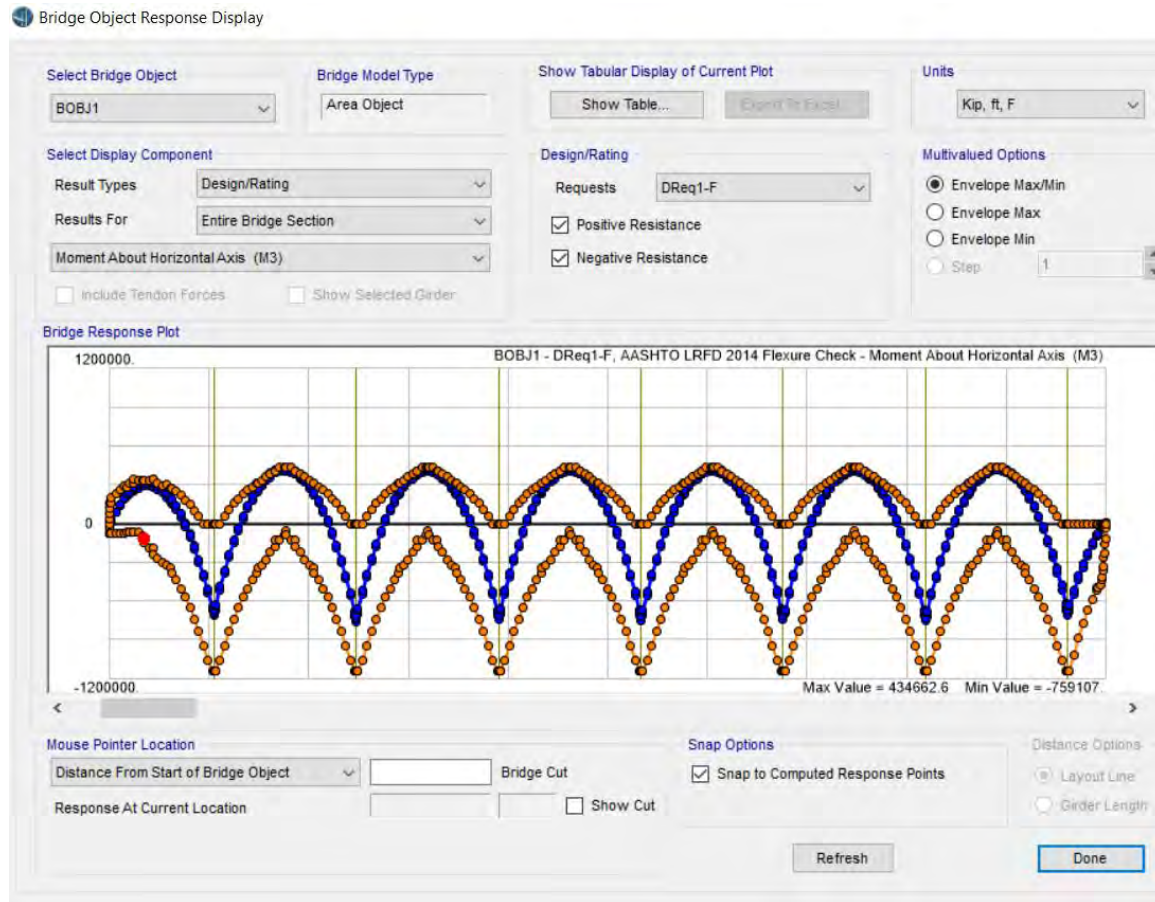


Figure 4.17: Flexural capacity check according AASHTO LRFD,2014 (125 m)

For 125m span module,

Maximum induced Positive Moment = 4, 34,662 Kip-ft

Maximum Positive Moment Capacity = 4,50,000 Kip-ft

Maximum induced Negative Moment = 7,59,107 Kip-ft

Maximum Negative Moment Capacity = 11,41,758 Kip-ft

Thus, flexural capacity is within allowable capacity in case of 125m bridge span module.

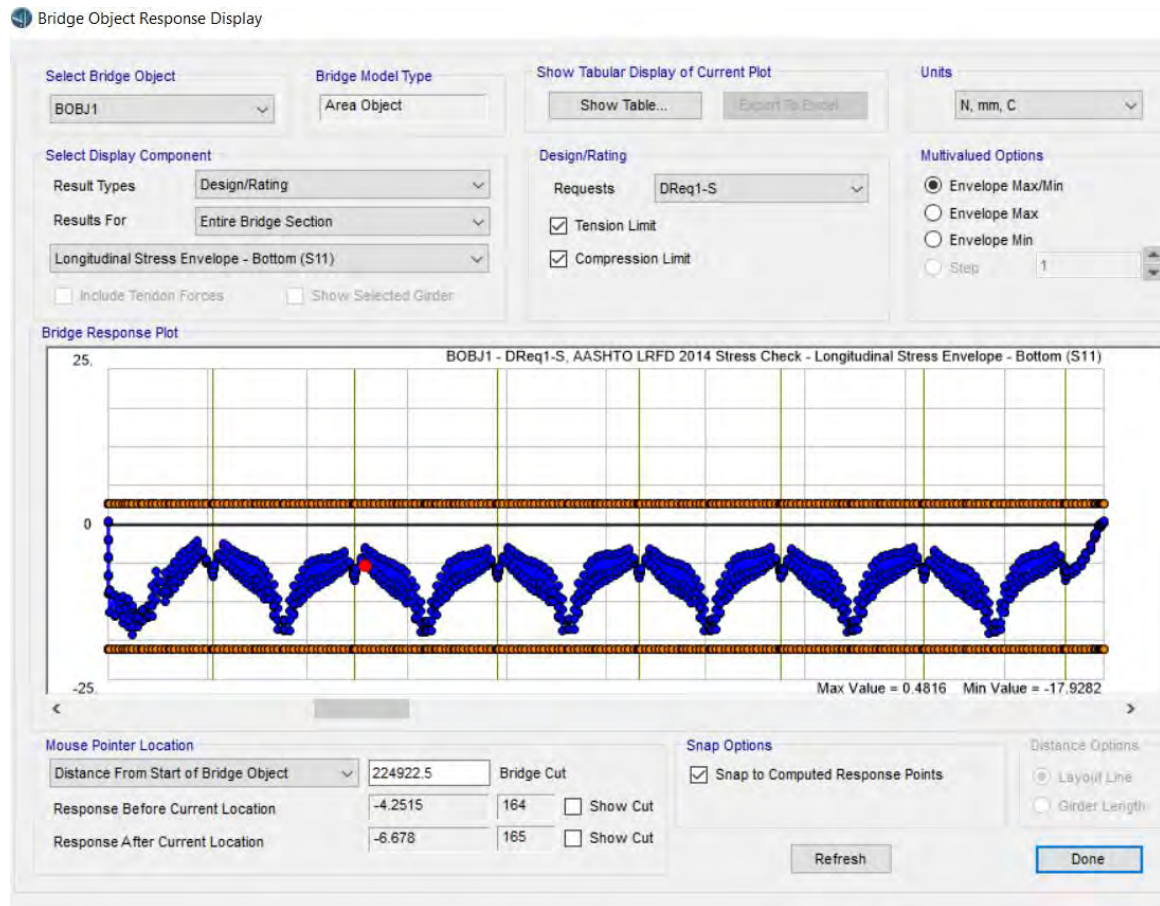


Figure 4.18: Bottom longitudinal stress capacity check (125 m)

Bottom Longitudinal Stress

$$\text{Tensile Stress Limit} = 0.5\sqrt{f'_c}(\text{MPa}) = 0.5\sqrt{44.83} \text{ MPa} = 3.34 \text{ MPa}$$

$$\text{Maximum Tensile Stress} = 0 \text{ MPa}$$

$$\text{Compressive Stress Limit} = 0.45 f'_c (\text{MPa}) = 0.45 \times 44.83 \text{ MPa} = 20.16 \text{ MPa}$$

$$\text{Maximum Compressive Stress} = 17.93 \text{ MPa}$$

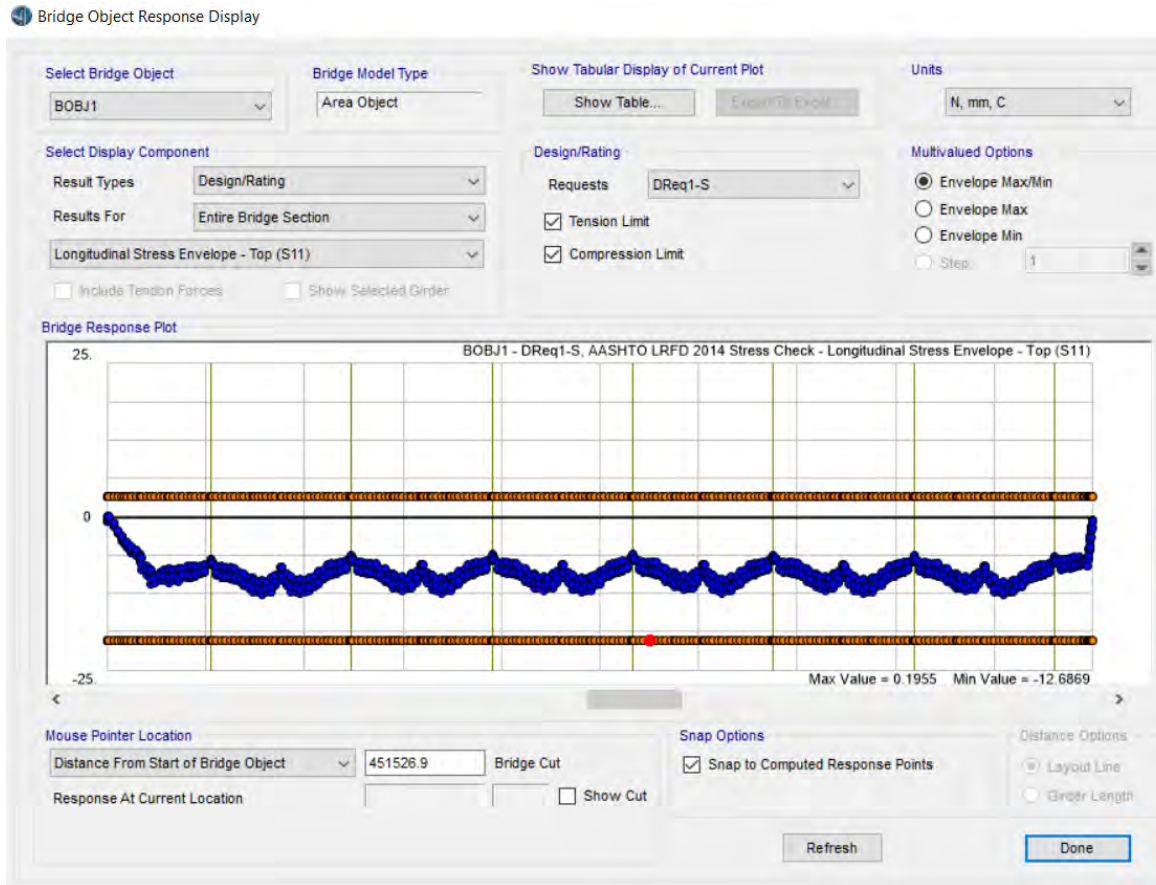


Figure 4.19: Top longitudinal stress capacity check (125 m)

Top Longitudinal Stress

$$\text{Tensile Stress Limit} = 0.5\sqrt{f'_c}(\text{MPa}) = 0.5\sqrt{44.83} \text{ MPa} = 3.34 \text{ MPa}$$

$$\text{Maximum Tensile Stress} = 0 \text{ MPa}$$

$$\text{Compressive Stress Limit} = 0.45 f'_c (\text{MPa}) = 0.45 \times 44.83 \text{ MPa} = 20.16 \text{ MPa}$$

$$\text{Maximum Compressive Stress} = 12.69 \text{ MPa}$$

Tensile and compressive stress limit at top and bottom fibre of box girder section is within allowable limit for 125m bridge span module.

4.6 100-meter Bridge Bearing Properties Verification

The properties of the bearing are assigned as such that the deflection of the bridges is similar to the suggested deflection for 100 m vertical and horizontal Deflections during earthquake of 0.47g according to Castellano and Cestarollo (1999) as shown in **Table 4.10**.

Table 4.10: Detailed properties of seismic devices in The Bangabandhu Bridge (100 m)

Name	Designation	Vertical Load Limit	Horizontal Load Limit	Horizontal Translation Limit (mm)		Stiffness (K)	
				Longitudinal	Transverse	Longitudinal	Transverse
		kN	kN	mm	mm	kN/mm	kN/mm
Steel Hysteretic Damper (MEP)	MEP 350/200	3500	3500	± 200	± 200	17.50	17.50
Steel Hysteretic Damper+ STU (MEPOT)	MEPOT 350/200						
Multi Directional Bearing (North)	VM 3300/850/400	33000	5400	± 425	± 200	12.70	27.0
Multi Directional Bearing (South)	VM 3000/850/400	30000					
Uni Directional Bearing+ Restrainer +Bumper	VU 850/800-200	8500	2000	± 400	± 20	5.0	100.0
Multi Directional Bearing +Restrainer+Bumper	VM 900/800/50	9000	1800	± 400	± 25	4.50	72.0

4.7 Verification of 100 Meter Model Based on Design Value

Verification of 100m model based on design value from T. Y. Lin International which is the designer of the Bangabandhu Multipurpose bridge.

4.7.1 Equivalent Static Force Method Verification

Input for equivalent static method in X (Longitudinal) direction and Y(transverse) direction is shown for 100 m bridge span module.

i. Input in Equivalent Static Force Method (X Direction)

Input details in equivalent Static force at X direction is shown in **Figure 4.20**. Ecc. Ratio is taken to be 0.05, Seismic zone factor (Z) is taken 0.47. Time period (Ct) is taken to be 0.035. Site coefficient is taken for 1.25. Importance factor is taken for 1. Numerical Coefficient (Rw) is taken to be 5. In Csi Bridge soil site coefficient 1.25 cannot be assigned. So, soil site coefficient is assigned 1.20 with scale factor ($1.25/1.20=1.0416$) 1.0416. According to R. Ahsan, M. M. Hasan and S. M. Reza (2010) the typical soil shear wave velocity (**Figure 4.22**) is 200-450 m/s up to 30m depth. As per BNBC (2014) the soil site class is SC (**Table 4.12**). And the soil site coefficient for soil type SC is 1.25 which shown in **Table 4.11**.

The image shows a software dialog box titled "1994 UBC Seismic Load Pattern". It is divided into several sections with input fields and radio buttons:

- Load Direction and Diaphragm Eccentricity:** Radio button selected for "Global X Direction". "Ecc. Ratio (All Diaph.)" is set to 0.05. There is an "Override Diaph. Eccen." button with "Override..." text.
- Seismic Coefficients:** Radio button selected for "User Defined". "Seismic Zone Factor, Z" is 0.47. "Site Coefficient, S" is 1.2. "Importance Factor, I" is 1.
- Time Period:** Radio button selected for "Program Calc". "Ct (ft) =" is 0.035. Other options are "Method A" and "User Defined".
- Factors:** "Numerical Coeff, Rw" is 5.
- Lateral Load Elevation Range:** Radio button selected for "Program Calculated". There are "Max Z" and "Min Z" input fields. A "Reset Defaults" button is present.

At the bottom right, there are "OK" and "Cancel" buttons.

Figure 4.20: EQx static force input (X direction)

ii. Input in Equivalent Static Force Method (Y Direction)

Input details in equivalent Static force at Y direction is shown in **Figure 4.21**. Ecc. Ratio is taken to be 0.05, Seismic zone factor (Z) is taken 0.47. Time period (Ct) is taken to be 0.035. Site coefficient is taken for 1.25. Importance factor is taken for 1. Numerical Coefficient (Rw) is taken to be 5. Soil site coefficient assignment procedure is discussed in above section.

The image shows a software dialog box titled "1994 UBC Seismic Load Pattern". It is divided into several sections for inputting seismic parameters:

- Load Direction and Diaphragm Eccentricity:** Radio buttons for "Global X Direction" and "Global Y Direction" (selected). A text box for "Ecc. Ratio (All Diaph.)" contains "0.05". An "Override Diaph. Eccen." button is labeled "Override...".
- Seismic Coefficients:** Radio buttons for "Per Code" and "User Defined" (selected). A text box for "Seismic Zone Factor, Z" contains "0.47". A dropdown menu for "Site Coefficient, S" is set to "1.2". A text box for "Importance Factor, I" contains "1".
- Time Period:** Radio buttons for "Method A", "Program Calc" (selected), and "User Defined". Next to "Program Calc" is a text box for "Ct (ft) =" containing "0.035".
- Lateral Load Elevation Range:** Radio buttons for "Program Calculated" (selected) and "User Specified". A "Reset Defaults" button is present. Below are text boxes for "Max Z" and "Min Z".
- Factors:** A text box for "Numerical Coeff, Rw" contains "5".

At the bottom right, there are "OK" and "Cancel" buttons.

Figure 4.21: EQy static force input (Y direction)

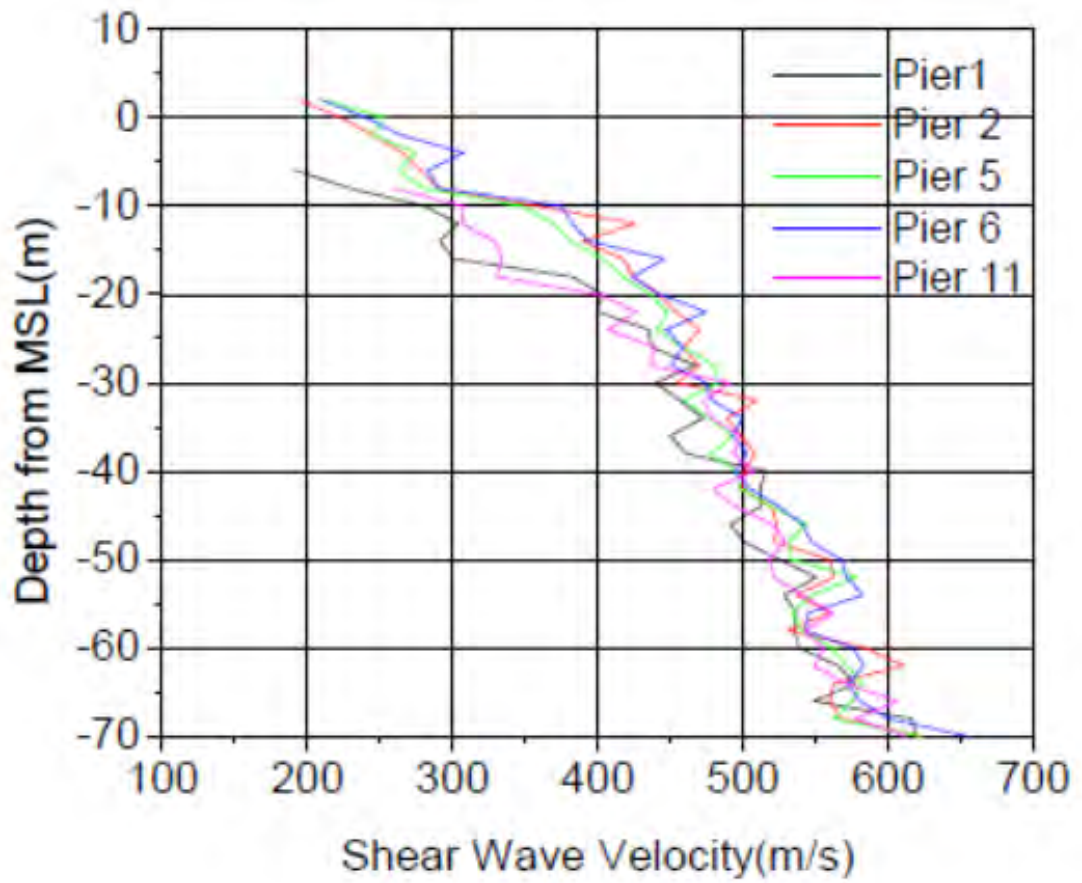


Figure 4.22: Soil shear wave velocity of different piers of Bangabandhu Bridge.

Table 4.11: Site dependent soil factor (BNBC, 2014)

Soil type	S	$T_B(s)$	$T_C(s)$	$T_D(s)$
SA	1.0	0.15	0.40	2.0
SB	1.2	0.15	0.50	2.0
SC	1.25	0.20	0.60	2.0
SD	1.35	0.20	0.80	2.0
SE	1.4	0.15	0.50	2.0

Table 4.12: Site classification based on soil properties (BNBC, 2014)

Site Class	Description of soil profile up to 30 meters depth	Average Soil Properties in top 30 meters		
		Shear wave velocity \bar{V}_s (m/s)	Standard Penetration Value, \bar{N} (blows/30cm)	Undrained shear strength, \bar{S}_u (kPa)
SA	Rock or other rock-like geological formation, including at most 5 m of weaker material at the surface.	> 800	--	--
SB	Deposits of very dense sand, gravel, or very stiff clay, at least several tens of metres in thickness, characterised by a gradual increase of mechanical properties with depth.	360 - 800	> 50	> 250
SC	Deep deposits of dense or medium dense sand, gravel or stiff clay with thickness from several tens to many hundreds of metres.	180 - 360	15 - 50	70 - 250
SD	Deposits of loose-to-medium cohesionless soil (with or without some soft cohesive layers), or of predominantly soft-to-firm cohesive soil.	< 180	< 15	< 70
SE	A soil profile consisting of a surface alluvium layer with V_s values of type C or D and thickness varying between about 5 m and 20 m, underlain by stiffer material with $V_s > 800$ m/s.	--	--	--
S ₁	Deposits consisting, or containing a layer at least 10 m thick, of soft clays/silts with a high plasticity index (PI > 40) and high water content	< 100 (indicative)	--	10 - 20
S ₂	Deposits of liquefiable soils, of sensitive clays, or any other soil profile not included in types SA to SE or S ₁	--	--	--

4.7.2 Verification of Horizontal Displacement

Horizontal displacement at seismic devices in case of equivalent static method and response spectrum method is verified. This displacement is compared with the allowable limit provided by T.Y. Lin international. In both the cases, displacement is compared with the allowable limit in longitudinal and transverse direction.

i. Horizontal Displacement Comparison for Equivalent Static Method

Maximum horizontal displacement for equivalent static loading (EQx) in X direction is shown in **Figure 4.23** and maximum horizontal displacement for equivalent static loading (EQy) in Y direction is shown in **Figure 4.24** for 100m span module.

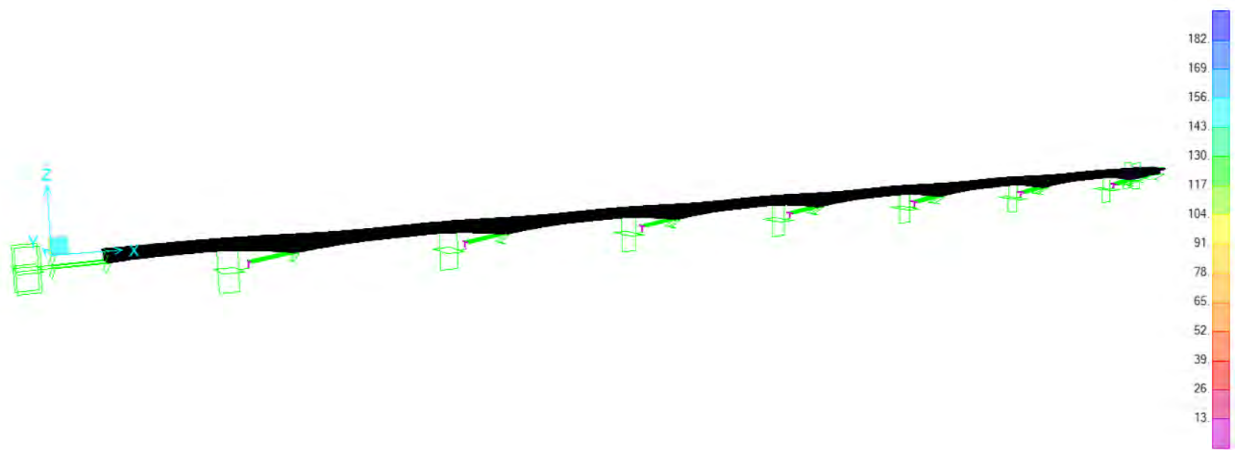


Figure 4.23: Displacement in X direction due to EX

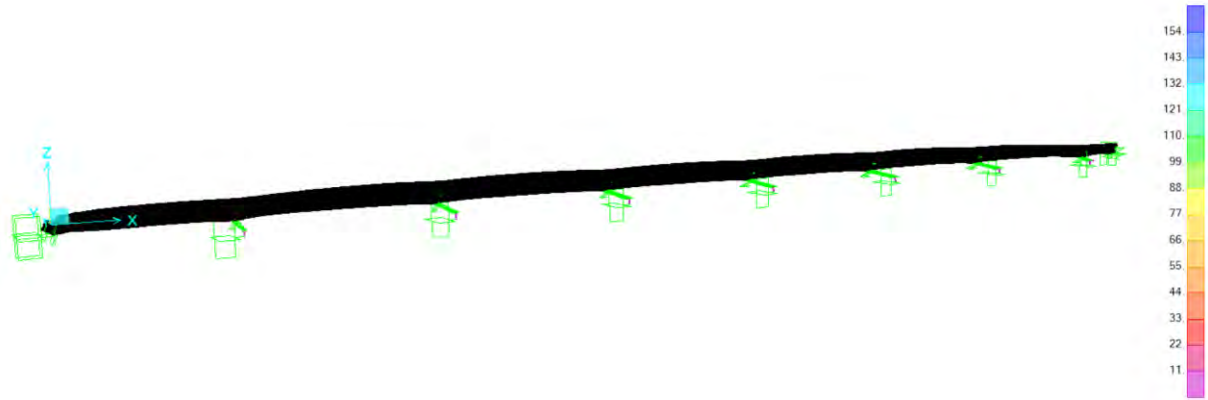


Figure 4.24: Displacement in Y direction due to EY

The maximum displacement due to EQX and EQY are shown in the **Table 4.13** along with design value provided by Castellano and Cestarollo (1999) and T.Y. Lin International. The observed displacements are within the allowable displacement capacity of the bearings (200mm). Observed maximum displacements for 75m and 125m module are shown in **Table 4.14**.

Table 4.13: Displacement Comparison with design value (100m span module)

Load Case	Maximum Displacement	Design Value
EQX	182 mm	200.00 mm
EQY	154 mm	200.00 mm

Table 4.14: Observed Maximum Displacement (75m and 125m module)

Load Case	Maximum Displacement	
	75 m module	125m module
EQX	196 mm	224 mm
EQY	168 mm	196 mm

4.7.3 Verification of Vertical load in Typical Multidirectional Bearing

From the Multidirectional bearing in the typical spans, it can be seen that Vertical load capacity is 33000 kN in North and 30000 kN in South Multidirectional bearing. The average of the capacity is 31500 kN Reaction in link property is found to be 31760 kN as shown in **Figure 4.25** which is close to design value in service condition.

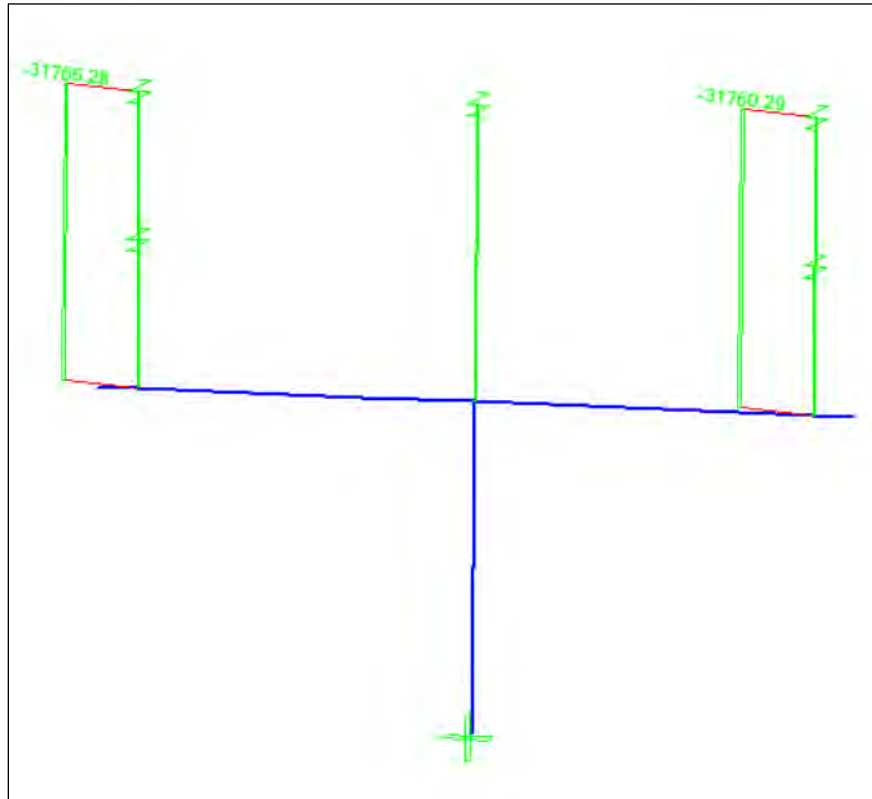


Figure 4.25: Vertical load in typical multi directional bearing in 100 m module

The summary of the verification of the 75m, 100m and 125m span module models are given in the Table 4.15 to

Table 4.17.

Table 4.15: Summary of Verification of 100m span module

100 m span module Analysis Model						
Verification Criteria		Provisional Limit	Source of Provision	Limit/Capacity	Actual	
1	Span to Depth Ratio	0.040 L	AASHTO LRFD (2014)	3.975	6.5	
		L/Ds= 15-18	Chen and Duan (2004)	15-18	15.3	
		L/Dm=35-45		35-45	34.1	
2	Sectional Efficiency	$\rho = \frac{I}{A_y t y_b}$	Rodriguez (2004)	around 0.60	0.62759	
3	Deflection (in mm)	Design Truck Load	Span/800	AASHTO LRFD (2014)	124	11.7
		Design Truck Load+ Impact Load	Span/800	AASHTO LRFD (2014)	124	11.7
		Lane Load + 0.25 x Truck Load	Span/800	AASHTO LRFD (2014)	124	12
		Dead Load + Live Load + Prestress Force	Span/800 or ± 20 mm	IS 1343-1940	± 20 mm	0 mm; -16.9 mm
4	Flexural Capacity (in Kip-ft)	Positive Moment	1.25 DL+ 1.25 Railing + 1.5 WC+	AASHTO LRFD (2014)	228,771	213,628
		Negative Moment	1.75 VL+ 1.00 Prestress	AASHTO LRFD (2014)	721,387	381,225
5	Stress Capacity (in MPa)	Tensile Stress	$0.5\sqrt{f'_c}$	AASHTO LRFD (2014)	3.34 MPa	Top: 0 Bottom: 0
		Compressive Stress	$0.45 f'_c$	AASHTO LRFD (2014)	20.16 MPa	Top: 10.54 Bottom: 15.32

Table 4.16: Summary of Verification of 75m span module

75 m span module analysis Model						
Verification Criteria		Provisional Limit	Source of Provision	Limit/Capacity	Actual	
1	Span to Depth Ratio	0.040 L	AASHTO LRFD (2014)	2.981	4.88	
		L/Ds= 15-18	Chen and Duan (2004)	15-18	15.3	
		L/Dm=35-45		35-45	36.1	
2	Sectional Efficiency	$\rho = \frac{I}{A_y y_b}$	Rodriguez (2004)	around 0.60	0.62503	
3	Deflection (in mm)	Design Truck Load	Span/800	AASHTO LRFD (2014)	93	11.6
		Design Truck Load+ Impact Load	Span/800	AASHTO LRFD (2014)	93	11.6
		Lane Load + 0.25 x Truck Load	Span/800	AASHTO LRFD (2014)	93	10.0
		Dead Load+ Live Load + Prestress Force	Span/800 or ± 20 mm	IS 1343-1940	± 20 mm	+14.9 mm; -13.8 mm
4	Flexural Capacity (in Kip-ft)	Positive Moment	1.25 DL+ 1.25 Railing + 1.5 WC+	AASHTO LRFD (2014)	165,047.8	122341.1
		Negative Moment	1.75 VL+ 1.00 Prestress	AASHTO LRFD (2014)	456,567.0	192,642.7
5	Stress Capacity (in MPa)	Tensile Stress	$0.5\sqrt{f'_c}$	AASHTO LRFD (2014)	3.34 MPa	Top: 0 Bottom: 0
		Compressive Stress	$0.45 f'_c$	AASHTO LRFD (2014)	20.16 MPa	Top: 11.79 Bottom: 13.73

Table 4.17: Summary of Verification of 125m span module

125 m span module analysis model						
Verification Criteria		Provisional Limit	Source of Provision	Limit/Capacity	Actual	
1	Span to Depth Ratio	0.040 L	AASHTO LRFD (2014)	4.975	8.576	
		L/Ds= 15-18	Chen and Duan (2004)	15-18	15	
		L/Dm=35-45		35-45	32	
2	Sectional Efficiency	$\rho = \frac{I}{A_y t_y b}$	Rodriguez (2004)	around 0.60	0.6	
3	Deflection (in mm)	Design Truck Load	Span/800	AASHTO LRFD (2014)	155	8.73
		Design Truck Load+ Impact Load	Span/800	AASHTO LRFD (2014)	155	8.73
		Lane Load + 0.25 x Truck Load	Span/800	AASHTO LRFD (2014)	155	10.42
		Dead Load + Live Load + Prestress Force	Span/800 or ± 20 mm	IS 1343-1940	± 20 mm	+8.9 mm; -17.1 mm
4	Flexural Capacity (in Kip-ft)	Positive Moment	1.25 DL+ 1.25 Railing + 1.5 WC+	AASHTO LRFD (2014)	4,50,000.0	4,34,662.6
		Negative Moment	1.75 VL+ 1.00 Prestress	AASHTO LRFD (2014)	11,41,758	7,59,107
5	Stress Capacity (in MPa)	Tensile Stress	$0.5\sqrt{f'_c}$	AASHTO LRFD (2014)	3.34 MPa	Top:0 Bottom:0
		Compressive Stress	$0.45 f'_c$	AASHTO LRFD (2014)	20.16 MPa	Top:12.69 Bottom: 17.93

Chapter 5

RESULTS AND DISCUSSIONS

5.1 Introduction

Earthquake data collected from The Bangabandhu bridge is applied with proper scale factor in the three models (75m, 100m and 125m model) with different time lag. Results from the bridge models are taken in terms of displacement along different position along longitudinal direction of bridge model for earthquake data at different time lag. The earthquake data for different time Lag are mentioned in the following:

- i. Synchronous Motion
- ii. Asynchronous motion with 0.01 sec time Lag
- iii. Asynchronous motion with 0.05 sec time Lag
- iv. Asynchronous motion with 0.10 sec time Lag
- v. Asynchronous motion with 0.20 sec time Lag
- vi. Asynchronous motion with 0.50 sec time Lag
- vii. Asynchronous motion with 1.00 sec time Lag

Propagation of shear wave velocity through various soil type causes this time lag. NEHRP soil type classification based on shear wave velocity is shown in **Table 5.1**. Corresponding shear wave velocity for different time lag in case of the three-bridge span module are given in **Table 5.2** to **Table 5.4**.

Table 5.1: NEHRP Soil Profile Type Classification

<i>Soil Type</i>	<i>Average Shear- Wave Velocity to 30 m Depth (\overline{V}_{s30})</i>
A	$\overline{V}_{s30} > 1500$ m/s, hard rock
B	$760\text{m/s} < \overline{V}_{s30} \leq 1500$ m/s, rock
C	360 m/s $< \overline{V}_{s30} \leq 760$ m/s, very dense soil and soft rock
D	180 m/s $< \overline{V}_{s30} \leq 360$ m/s, stiff soil
E	$\overline{V}_{s30} \leq 180$ m/s

Table 5.2: Time Lag vs Shear Wave Velocity (75 m)

Time Lag (Sec)	Span Length (m)	Soil Shear Wave Velocity (m/s)	Soil Type
0.01	75	7500	Hard rock
0.05	75	1500	Hard rock
0.1	75	750	Rock
0.2	75	375	Very Dense Soil and Soft Rock
0.5	75	150	Soft Soil
1	75	75	Soft Soil

Table 5.3: Time Lag vs Shear Wave Velocity (100 m)

Time Lag (Sec)	Span Length (m)	Soil Shear Wave Velocity (m/s)	Soil Type
0.01	100	10000	Hard rock
0.05	100	2000	Hard rock
0.1	100	1000	Rock
0.2	100	500	Very Dense Soil and Soft Rock
0.5	100	200	Very Dense Soil and Soft Rock
1	100	100	Soft Soil

Table 5.4: Time Lag vs Shear Wave Velocity (125 m)

Time Lag (Sec)	Span Length (m)	Soil Shear Wave Velocity (m/s)	Soil Type
0.01	125	12500	Hard rock
0.05	125	2500	Hard rock
0.1	125	1250	Hard rock
0.2	125	625	Very Dense Soil and Soft Rock
0.5	125	250	Stiff Soil
1	125	125	Soft Soil

Different seismic input cases are considered in this study. The cases where earthquake data assigned is from Bangabandhu bridge June 16, 2004 are shown in the following:

Case 1: Earthquake Data from Bangabandhu Bridge with point of fixity

Case 2: Wave Passage effect 100% in Longitudinal and 30% of Longitudinal in Lateral Direction

Case 3: Wave Passage effect in 100% in Lateral and 30% of Lateral in Longitudinal Direction

Case 4: Wave Passage effect in 100% in Longitudinal Direction

Case 5: Wave Passage effect 100% in Lateral Direction

Seismic input cases where data from El-Centro earthquake (1940) is assigned in the following:

Case 6: Wave Passage effect 100% in Longitudinal and 30% of Longitudinal in Lateral Direction for El-Centro (1940)

Case 7: Wave Passage effect 100% in Lateral Direction and 30% of Lateral in Longitudinal for El-Centro (1940)

Case 8: Wave Passage effect 100% in Longitudinal and 30% of Longitudinal in Lateral Direction for El-Centro (1940) when bearings are locked

5.2 100 m Model Results

The results of 100m span module are shown in graphs. All the graphs are in distorted scaled. Maximum displacement values for 75m and 125m modules are shown in tabular form.

5.2.1 Deck Displacement at Top Mid-Points Due to Load Case 1

Figure 5.1 to **Figure 5.3** show maximum displacements (longitudinal, transverse and vertical) due to wave passage effect along longitudinal direction. A point of fixity is considered at pier 4. The point of fixity is provided so that during service loads (i.e., wind, braking actions, etc.) do not stress the dissipating elements. The point of fixity is designed to fail at a 500 kN horizontal load. In the event of a strong earthquake, the sacrificial restraints fail and the dampers are activated. Data recorded on the pile cap of The Bangabandhu Multipurpose bridge in June 16,2004 is assigned in this case.

In **Figure 5.1** shows that longitudinal displacement is very insignificant. Pier 4 where point of fixity is present, displacement increase to both sides of the bridge. Here asynchronous 0.01s governs and maximum displacement is 0.165 mm. The displacement pattern throughout the bridge is not similar to the pattern of other wave passage effect cases. In the other wave passage effect cases in longitudinal direction, displacement is found to be same in all throughout the bridge. Such shows that point of fixity does have effect on the displacement pattern all throughout the bridge the maximum displacement for synchronous motion is found to be 0.14mm which is not significant enough to be considered in design checking. In **Figure 5.2** shows transverse displacement where maximum displacement found 0.00065 mm for synchronous motion. Here synchronous motion governs in most points. But from pier 1 to between pier 1 and pier 2 asynchronous motion governs. In this region, asynchronous motion responses are very close to each other. The magnitude of the displacement is not very significant to be considered. Displacement pattern is such that it started rising from around point of fixity.

In **Figure 5.3**, it shows that maximum vertical displacement is 0.63 mm which is between pier 5 and pier 6. Asynchronous 0.01s governs up to pier 4. After that, synchronous motion starts governing. Between pier 4 and pier 5 synchronous motion causes maximum displacement for this case. Same is in the region between pier 6 and pier 7 where maximum displacement due to synchronous motion is observed to be 0.5 mm which is not significant.

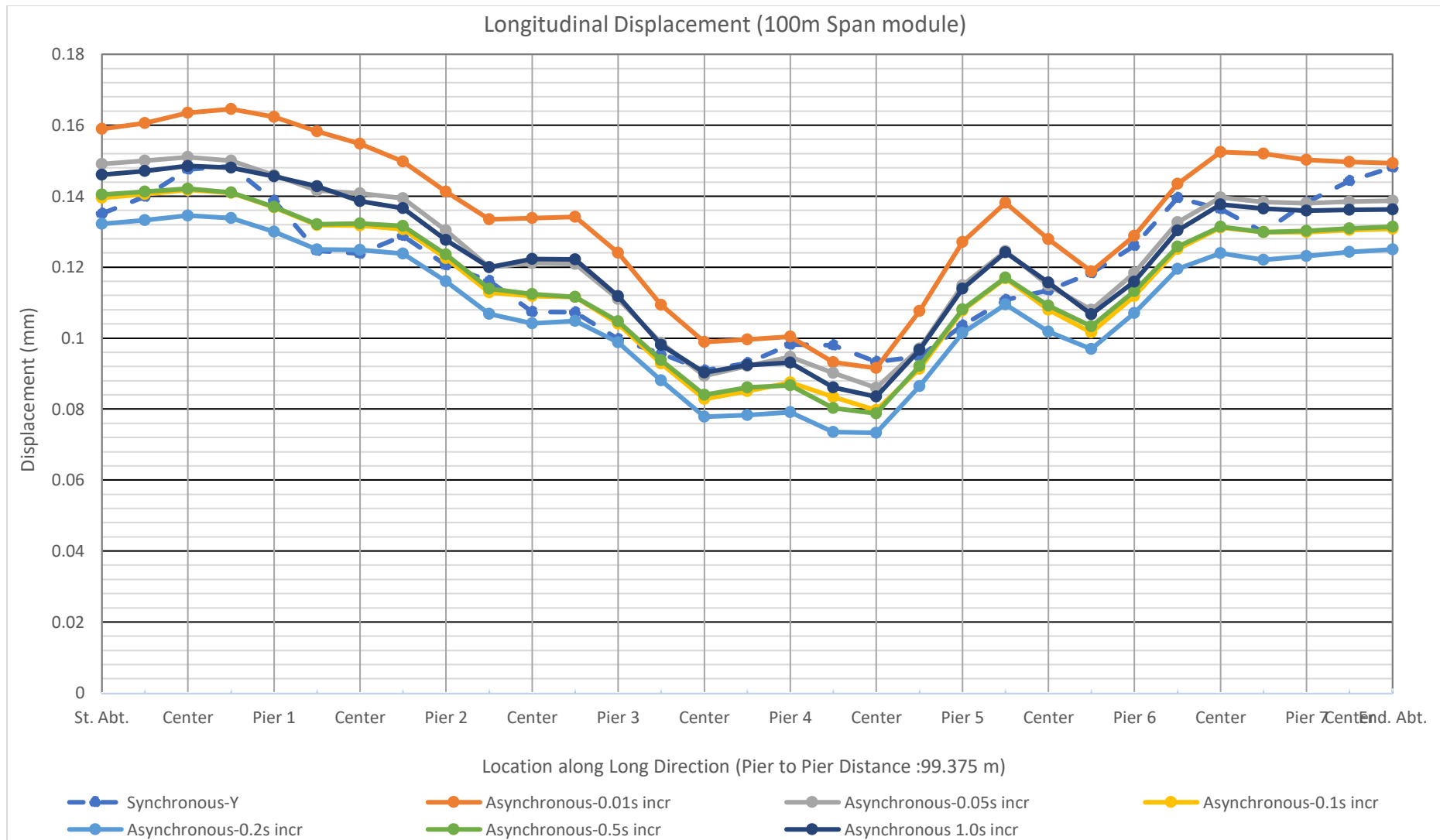


Figure 5.1: Maximum longitudinal displacement for load case 1 (100m span module)

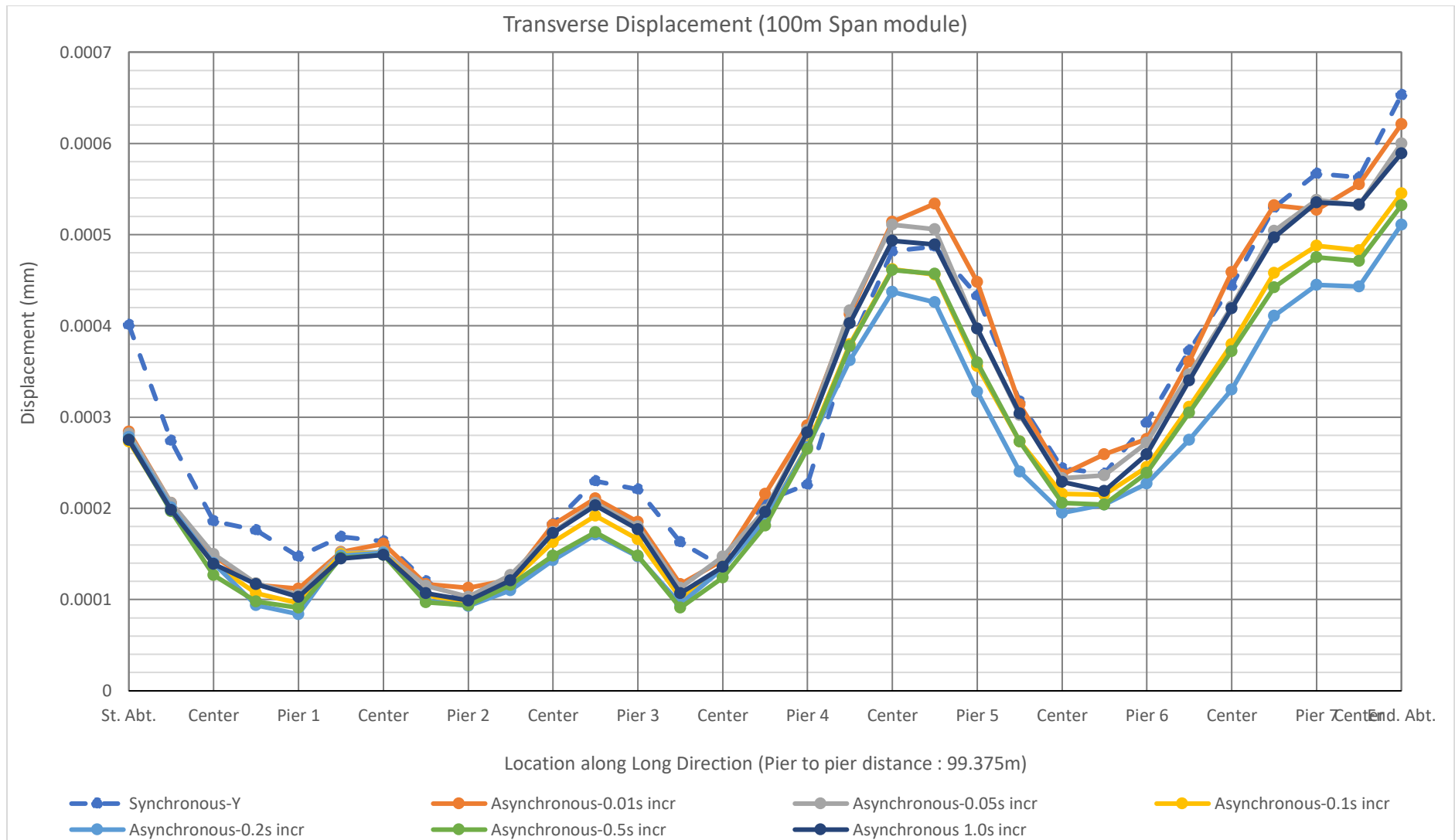


Figure 5.2: Maximum transverse displacement for load case 1 (100m span module)

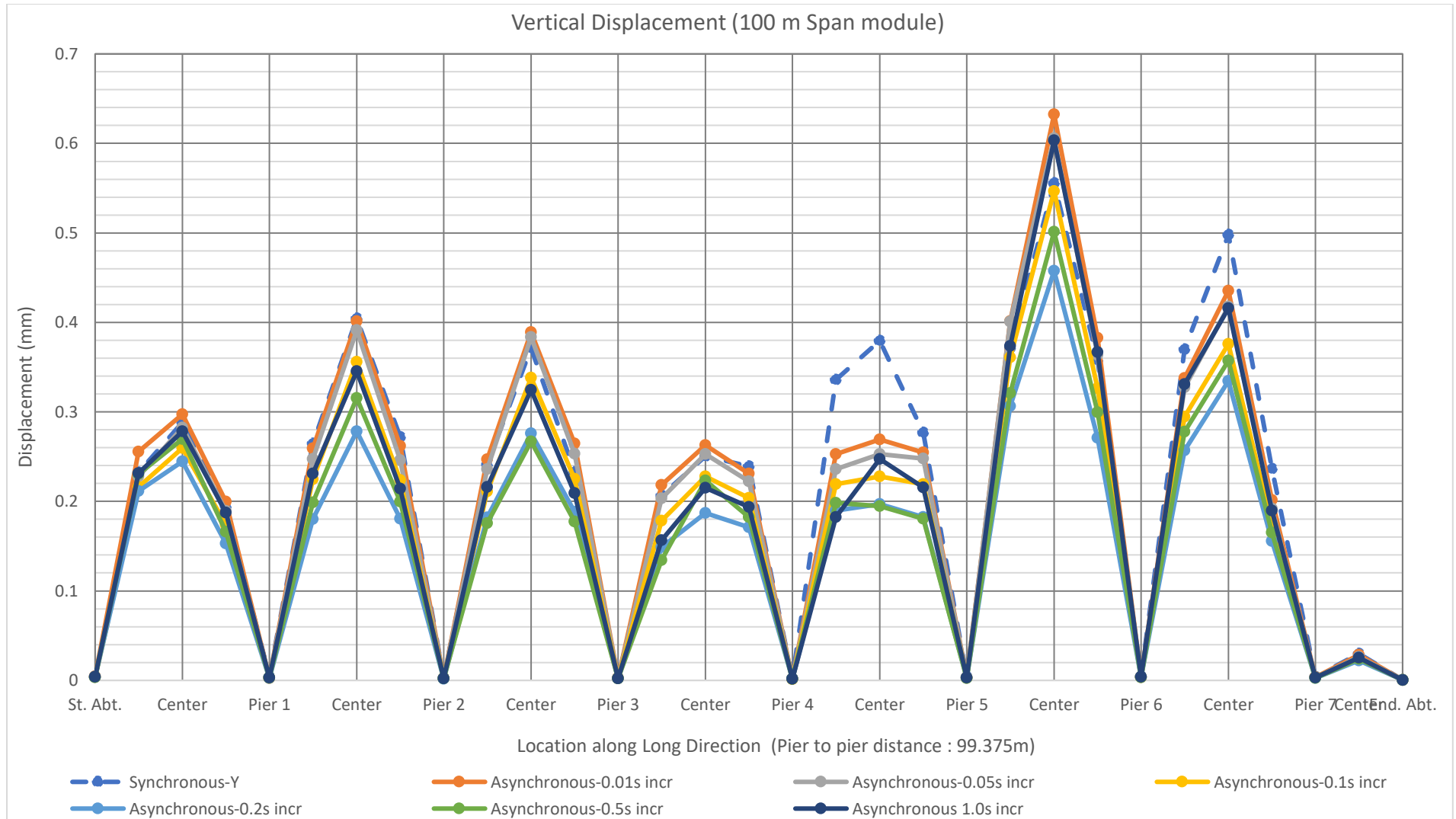


Figure 5.3: Maximum vertical displacement for load case 1 (100m span module)

5.2.2 Horizontal load at point of fixity

When wave passage effect is applied in longitudinal direction, maximum horizontal load of 509.86 kN is developed at point of fixity as shown in **Figure 5.4** . However, sacrificial restrainers are designed to fail at 500kN. This shows during that earthquake event the point of fixity is about to be damaged if wave passage effect is in longitudinal direction.

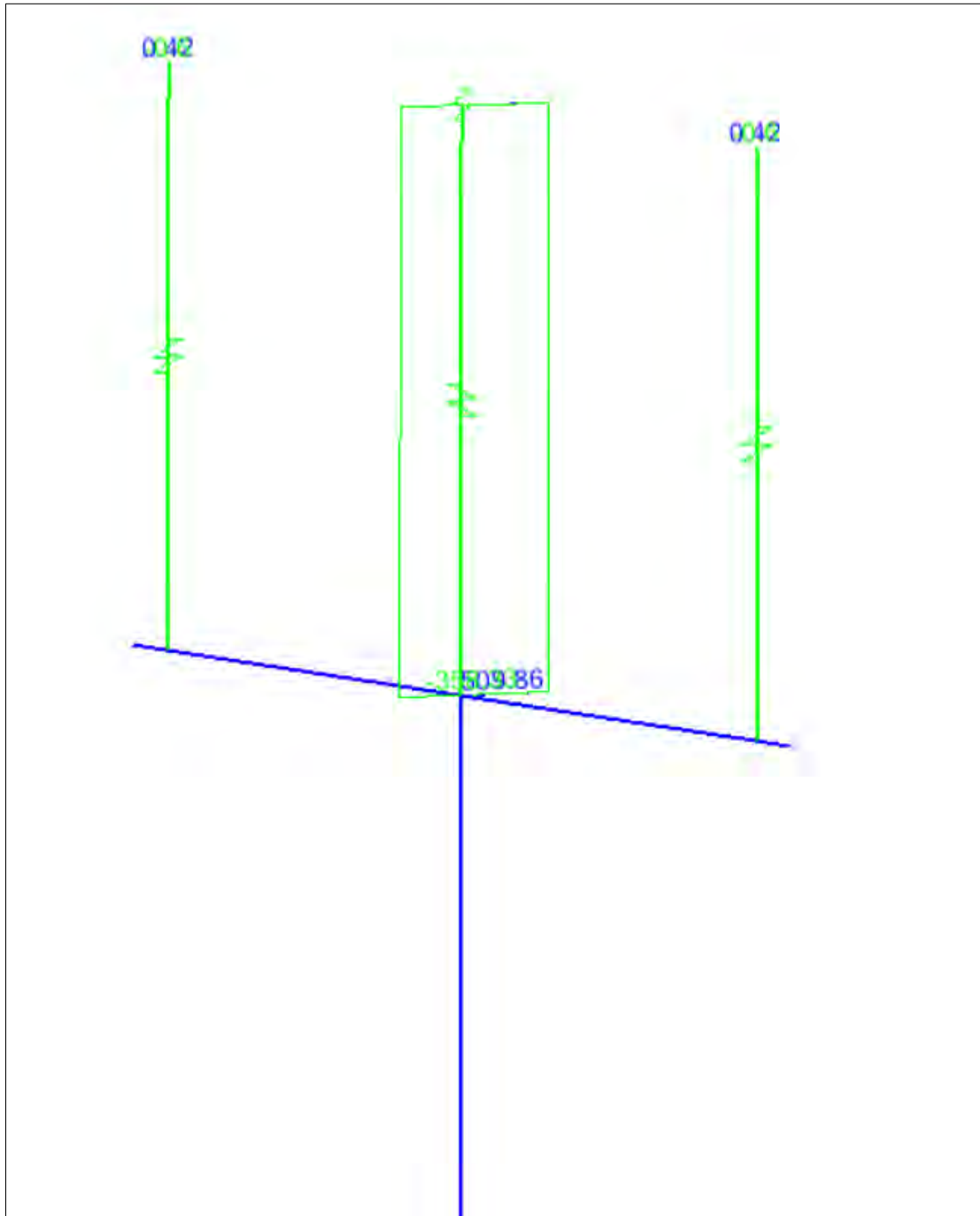


Figure 5.4: Horizontal load at point of fixity

5.2.3 Deck Displacement Due to Wave Passage Effect for Different Time Lag

The assigned earthquake data for all the 4 cases was recorded on the pile cap of The Bangabandhu Multipurpose bridge in June 16,2004. **Figure 5.5** to **Figure 5.7** show displacements (longitudinal, transverse and vertical) found due to wave passage effect in longitudinal direction and 30% effect assigned in lateral direction (Case 2). This wave passage effect configuration was assigned based AASHTO provision.

Figure 5.5 shows displacement at longitudinal direction. The displacement is constant all throughout the bridge for all seismic motion. Synchronous motion governs in this case and maximum displacement is found to 8.87 mm. Displacement due to synchronous motion is 1.9 times than that of asynchronous motion 0.01s. **Figure 5.6** shows displacement at transverse direction. The displacement in transverse direction is governed by synchronous motion in middle section (maximum displacement 3.66mm) of bridge model. But asynchronous 0.2s time lag governs (3.76mm) near the edges of the bridge model. **Figure 5.7** shows displacement at vertical direction. No displacement is there in piers but magnitude reaches maximum between two piers. In this case, asynchronous 0.5s motion governs and maximum displacement is 2 mm. Maximum displacement for asynchronous 0.5s motion is 7.4 times of synchronous motion.

Figure 5.8 to **Figure 5.10** show displacements (longitudinal, transverse and vertical) found due to wave passage effect in lateral direction and 30% effect assigned in longitudinal direction (case 3). This wave passage effect configuration was assigned based AASHTO provision.

Figure 5.8 shows displacement at longitudinal direction. The displacement is constant all throughout the bridge for all seismic motion. Synchronous motion governs in this case. Maximum displacement is found to be 2.66 mm Displacement due to synchronous motion is 1.9 times than that of asynchronous motion 0.01s.**Figure 5.9** shows displacement at transverse direction. The displacement in transverse direction is governed by synchronous motion in middle section (maximum displacement 12.2mm) of bridge model. But asynchronous 0.2s time lag governs (12.53 mm) near the sides of the bridge model. **Figure 5.10** shows displacement at vertical direction. No displacement is there in piers but magnitude reaches maximum between two piers. In this case, asynchronous 0.5s motion governs and maximum displacement is 0.6 mm. Maximum displacement for asynchronous 0.5s motion is 7.5 times of synchronous motion.

Figure 5.11 to **Figure 5.13** show displacements (longitudinal, transverse and vertical) found due to wave passage effect assigned in longitudinal direction only (Case 4). **Figure 5.11** shows displacement at longitudinal direction. The displacement is constant all throughout the bridge for all seismic motion. Synchronous motion governs in this case. Maximum displacement is found to be 8.9 mm Displacement due to synchronous motion is 1.9 times than that of asynchronous motion 0.01s. **Figure 5.12** shows displacement in transverse direction resembles having a fixity near pier 4. This is the centre of rotation. Maximum lateral displacement (-0.003mm and +0.003 mm) is found about centre of rotation for synchronous motion. **Figure 5.13** shows displacement at vertical direction. No displacement is there in piers but magnitude reaches maximum between two piers. In this case, asynchronous 0.5s motion governs and maximum displacement is 2 mm. Maximum displacement for asynchronous 0.5s motion is 7.4 times of synchronous motion.

Figure 5.14 to **Figure 5.18** show displacements (longitudinal, transverse and vertical) found due to wave passage effect assigned in lateral direction only (Case 5). **Figure 5.14** shows displacement at longitudinal direction which is very insignificant. The displacement is constant all throughout the bridge for all seismic motion. Asynchronous 0.2s motion governs in this case. Maximum displacement is found to be 0.0014 mm. Displacement due to Asynchronous 0.2s motion is 4.7 times than that of synchronous motion. **Figure 5.15** shows displacement at transverse direction. In this case, asynchronous 0.2s governs at the end segments. On the other hand, synchronous motion governs at middle sections of the bridge (maximum displacement 12.2 mm). Maximum displacement is found to be 12.53 mm for asynchronous 0.2s motion between pier 6 and pier 7. **Figure 5.18** shows displacement at vertical direction. No displacement is there in piers but magnitude reaches maximum between two piers. In this case, asynchronous 0.2s motion governs and maximum displacement is 0.01 mm. Maximum displacement for asynchronous 0.2s motion is 1.4 times of synchronous motion. **Figure 5.16** shows stress due to synchronous motion. It is seen that maximum stress is found to be 15.4 MPa (2240 psi) and is concentrated on expansion joints as in **Figure 5.17**. All throughout the bridge, stress is averaging 1.65 MPa (240 psi).

i. Wave Passage Effect for Case 2

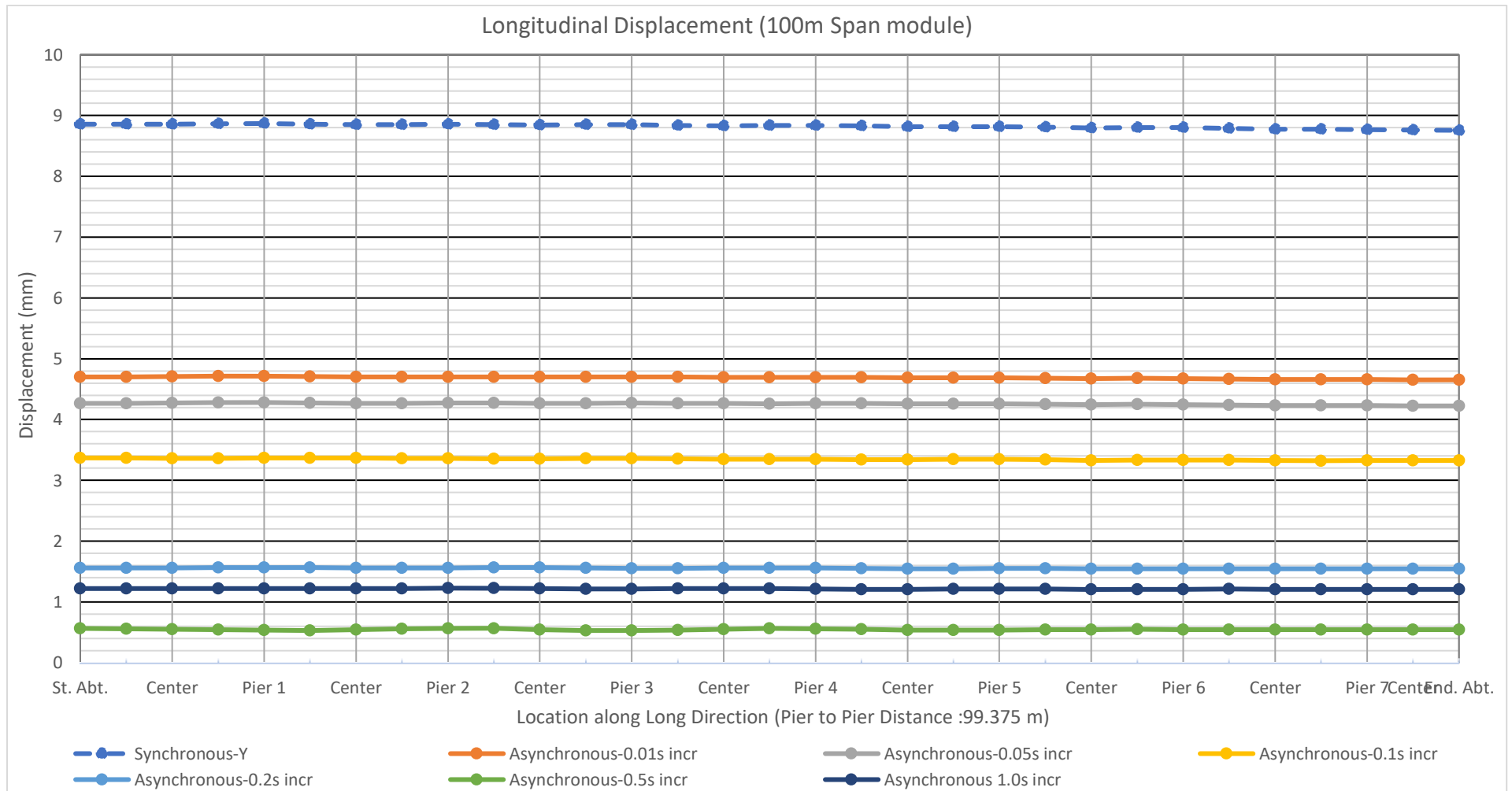


Figure 5.5: Maximum longitudinal displacement for load case 2 (100m span module)

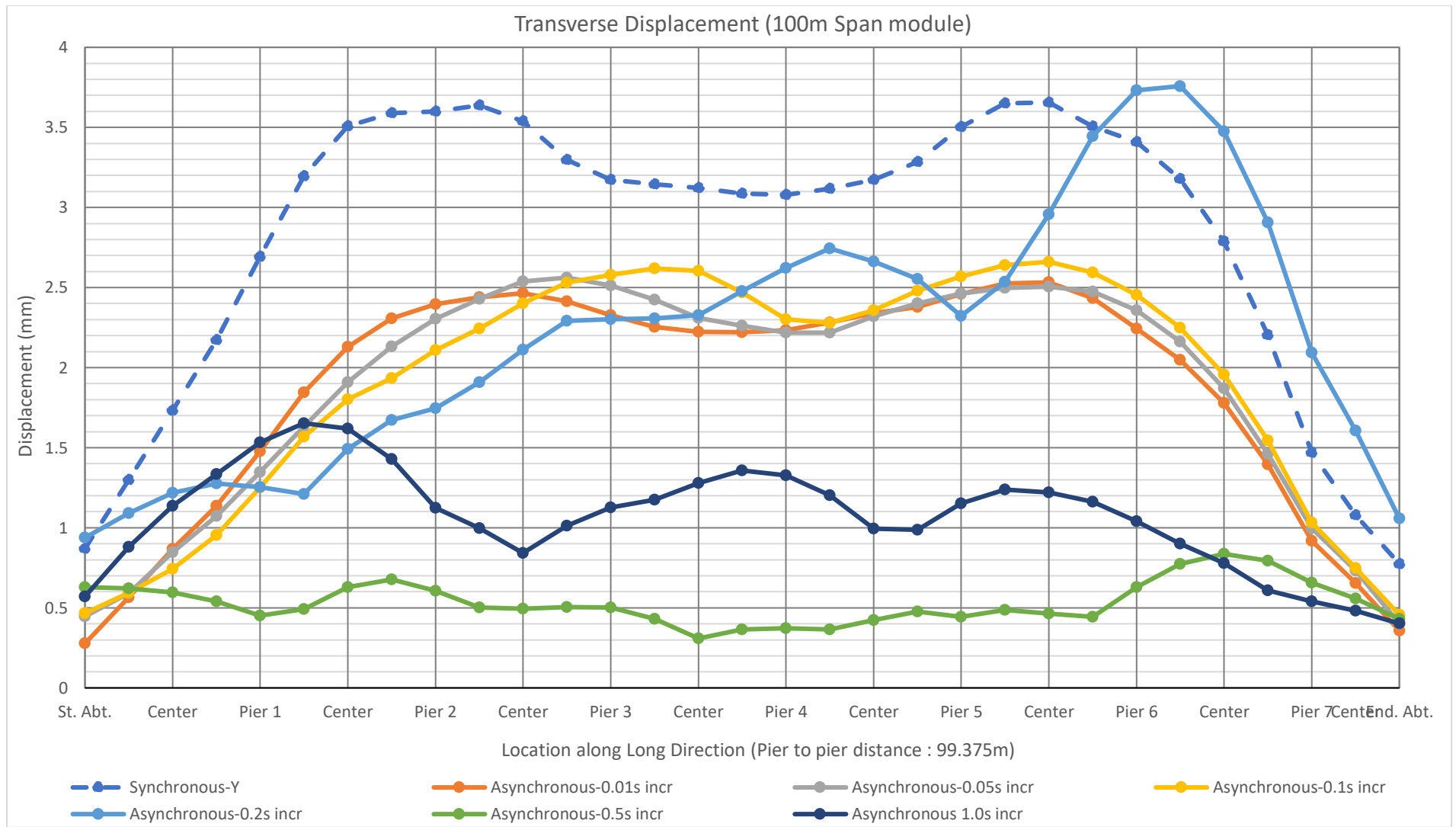


Figure 5.6: Maximum transverse displacement for load case 2 (100m span module)

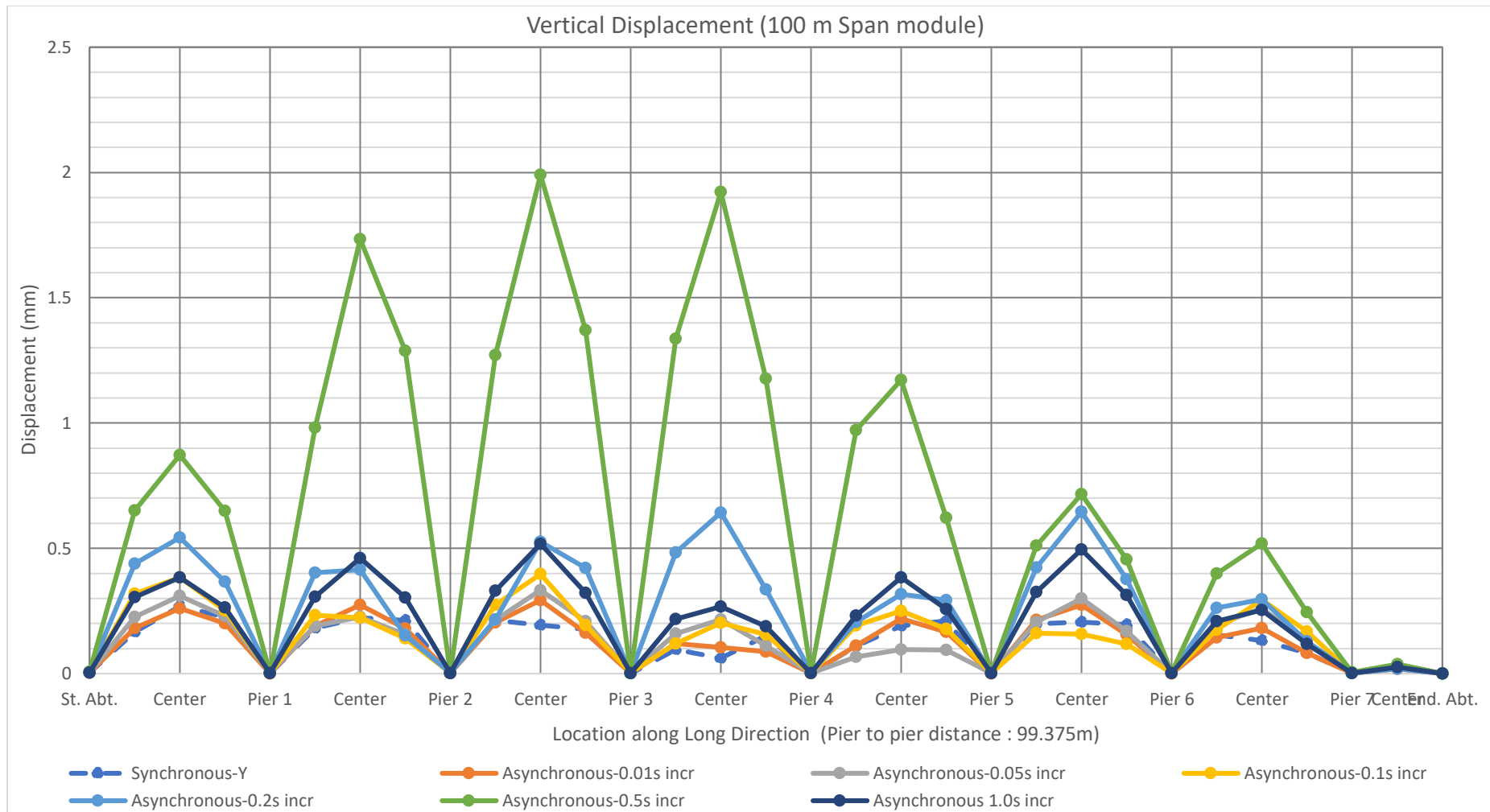


Figure 5.7: Maximum vertical displacement for load case 2 (100m span module)

Maximum displacements due to all seismic motion in all three bridge span modules for case 2 are shown in **Table 5.5**. For 75m span module, maximum longitudinal displacement is found to be 8.69mm by synchronous motion. The transverse displacement is also governed by synchronous motion (maximum displacement 3.97mm) of bridge. For vertical displacement asynchronous 0.5s time lag governs and maximum displacement is 2.26mm. Here asynchronous effect is 13.3 times the synchronous (0.17mm) effect.

For 125m span module, maximum longitudinal displacement is found to be 8.81 mm which is caused by synchronous motion. The displacement in transverse direction is also governed by synchronous motion (maximum displacement 3.82 mm). For vertical displacement asynchronous 0.5s time lag governs and maximum displacement is 1.5 mm. **Table 5.5: Maximum displacement for case 2 for three-bridge span modules**

Table 5.5: Maximum displacement for case 2 for three-bridge span modules

Case 2: 100% in Longitudinal + 30% Lateral									
Span Module	100m Span Module			75m Span Module			125m Span Module		
Seismic Motion Type	Maximum Displacement (mm)								
	Longitudinal Direction	Transverse Direction	Vertical Direction	Longitudinal Direction	Transverse Direction	Vertical Direction	Longitudinal Direction	Transverse Direction	Vertical Direction
Synchronous	8.87	3.66	0.27	8.69	3.97	0.17	8.81	3.82	0.2
Asynchronous-0.01s	4.71	2.53	0.3	4.66	2.79	0.14	3.23	2.1	0.2
Asynchronous-0.05s	4.28	2.56	0.33	4.27	2.87	0.22	3.04	2.04	0.25
Asynchronous-0.1s	3.37	2.66	0.4	3.3	3.06	0.28	2.54	2.01	0.32
Asynchronous-0.2s	1.57	3.76	0.66	1.52	3.36	0.4	1.73	2.29	0.7
Asynchronous-0.5s	0.57	0.84	2	0.58	0.54	2.26	0.54	1.34	1.5
Asynchronous 1.0s	1.23	1.65	0.52	1.24	1.41	0.26	0.81	1.2	0.51

ii. Wave Passage Effect for Case 3

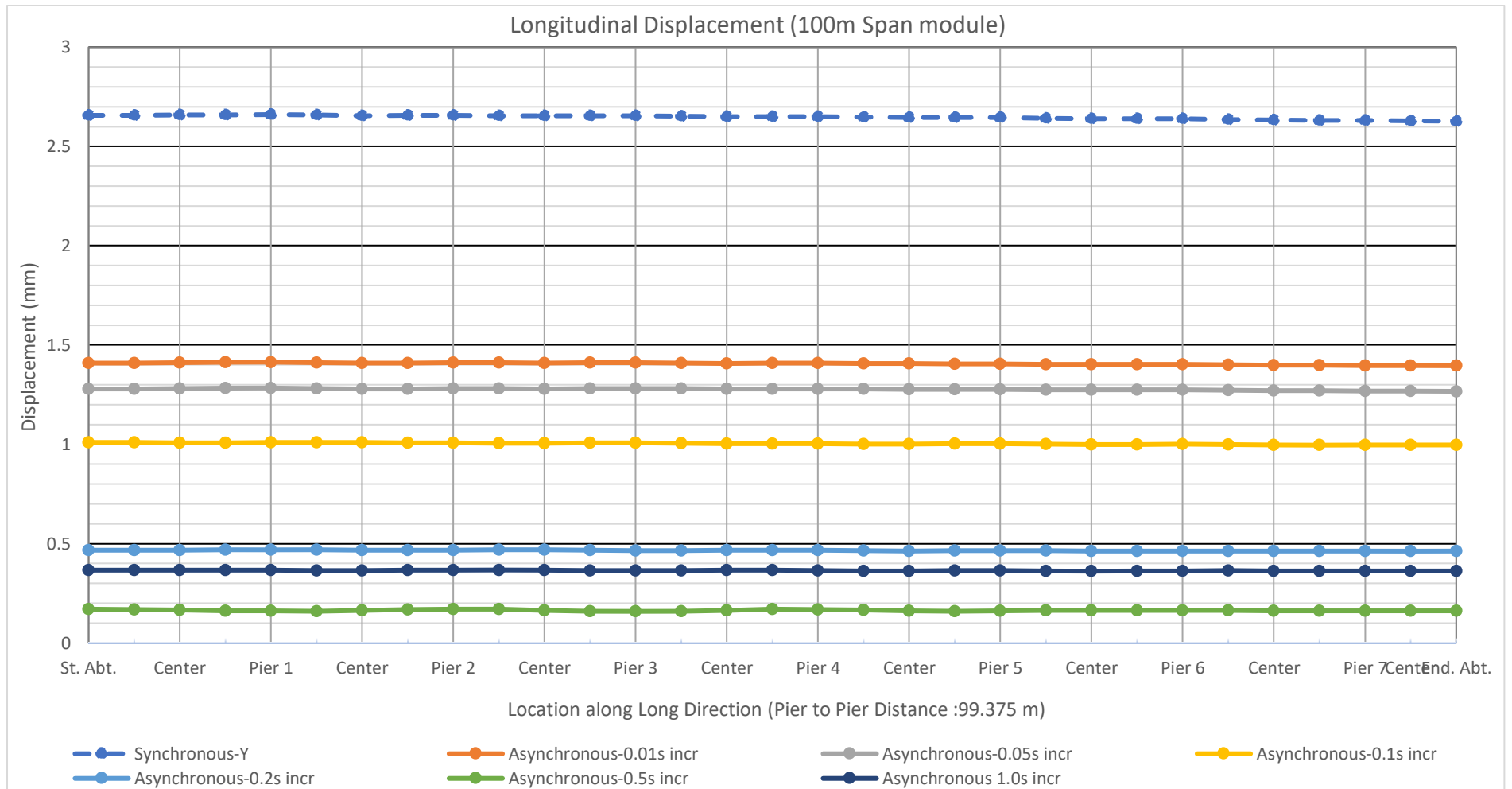


Figure 5.8: Maximum longitudinal displacement for load case 3 (100m span module)

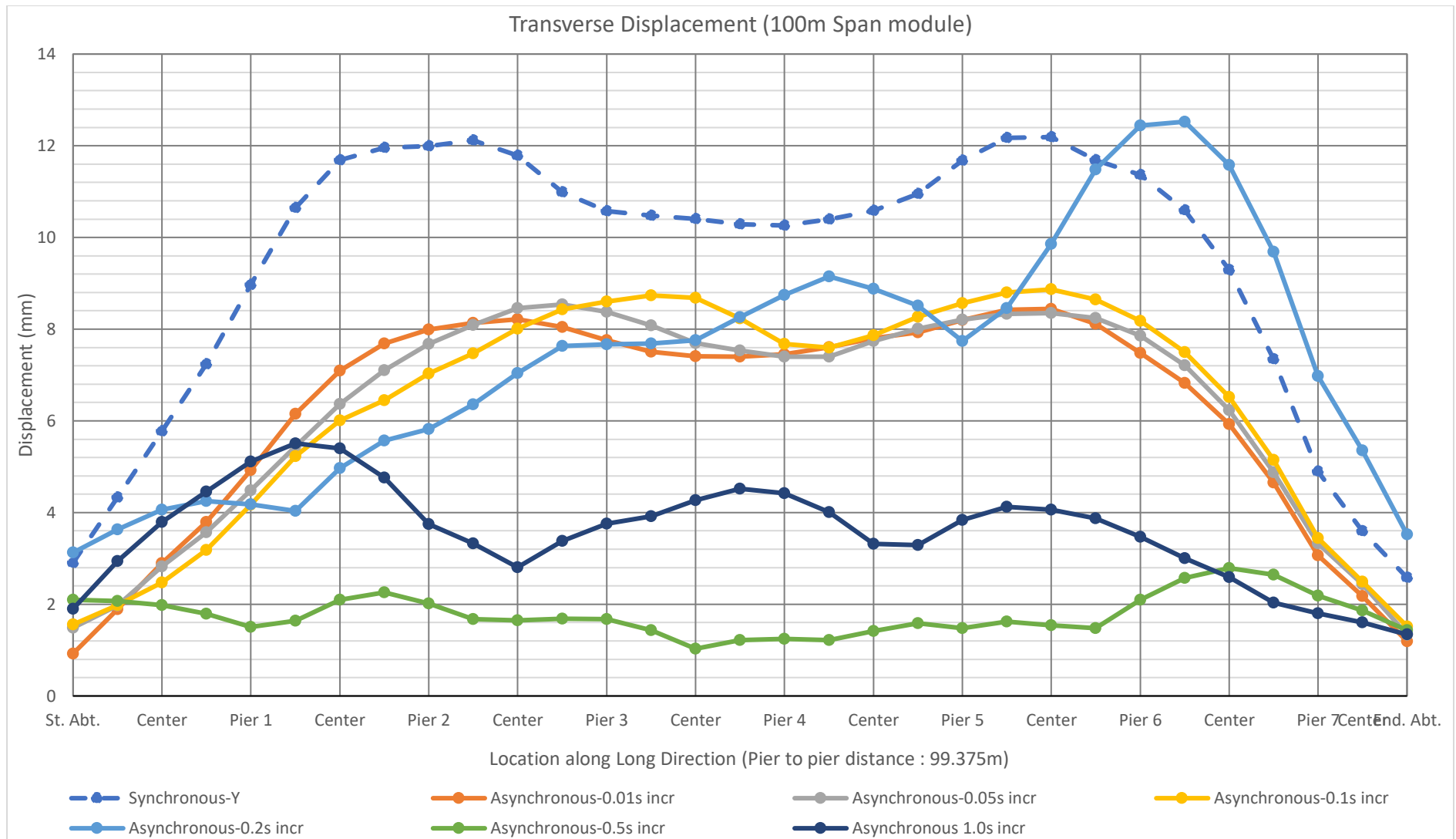


Figure 5.9: Maximum transverse displacement for load case 3 (100m span module)

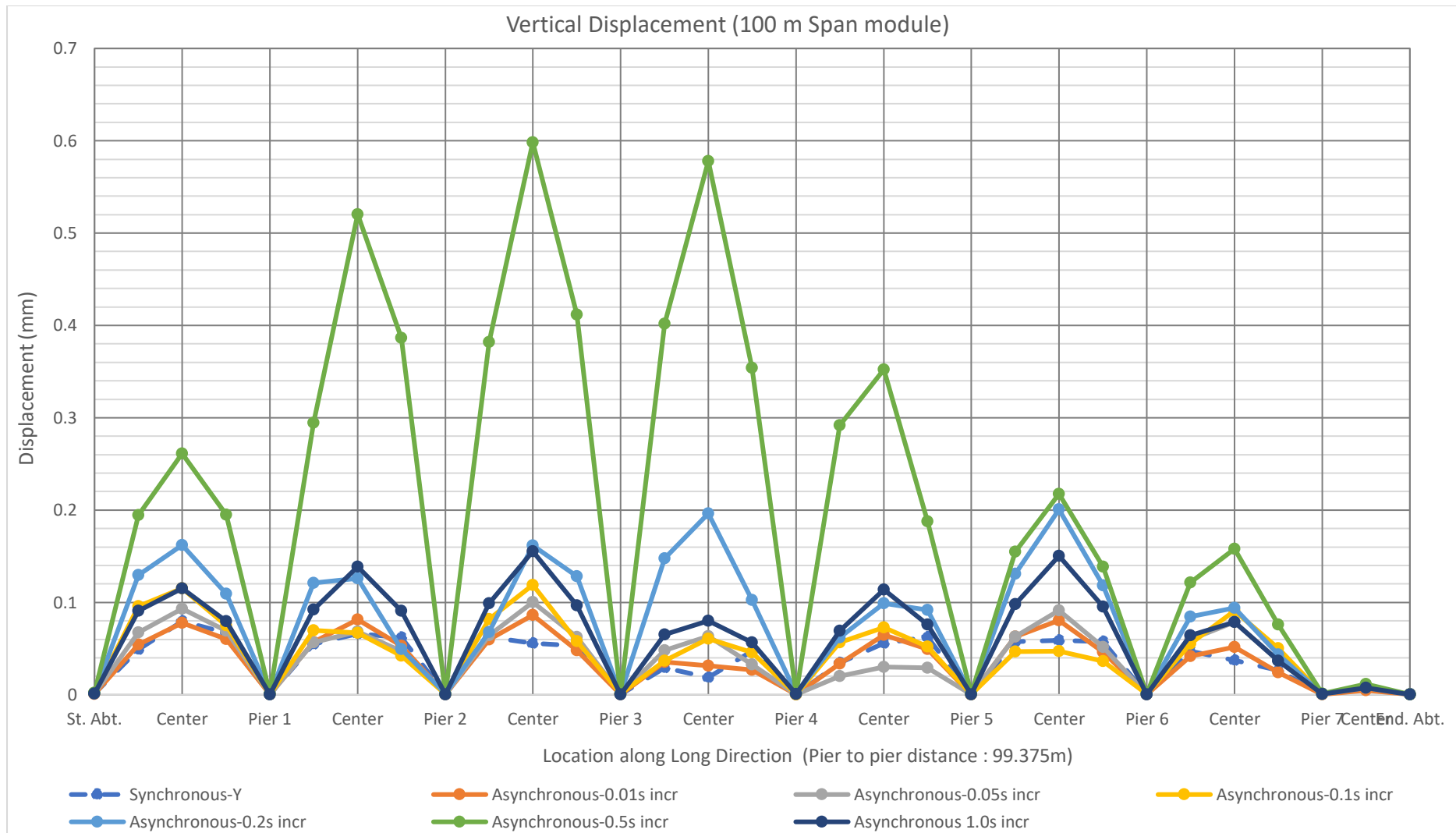


Figure 5.10: Maximum vertical displacement for load case 3 (100m span module)

Maximum displacements due to all seismic motion in all three bridge span modules for case 3 are shown in **Table 5.6**. For 75m span module, it is observed that maximum longitudinal displacement is found to be 2.61 mm which is caused by synchronous motion. The displacement in transverse direction is governed by synchronous motion throughout the bridge (maximum displacement 13.24 mm). For vertical displacement asynchronous 0.5s time lag governs and maximum displacement is 0.68mm, which is not significant.

For 125m span module, it is seen that maximum longitudinal displacement is found to be 2.64 mm caused by synchronous motion. Transverse displacement is governed by synchronous motion throughout the bridge (maximum displacement 12.73 mm). For vertical displacement asynchronous 0.5s time lag governs and maximum displacement is 0.45 mm, which is not significant.

Table 5.6: Maximum displacement for case 3 for three-bridge span modules

Case 3: 100% in Lateral + 30% of Lateral									
Span Module	100m Span Module			75m Span Module			125m Span Module		
Seismic Motion Type	Maximum Displacement (mm)								
	Longitudinal Direction	Transverse Direction	Vertical Direction	Longitudinal Direction	Transverse Direction	Vertical Direction	Longitudinal Direction	Transverse Direction	Vertical Direction
Synchronous	2.66	12.2	0.08	2.61	13.24	0.05	2.64	12.73	0.06
Asynchronous-0.01s	1.41	8.44	0.086	1.4	9.31	0.04	0.97	7	0.06
Asynchronous-0.05s	1.28	8.54	0.1	1.28	9.58	0.06	0.92	6.8	0.08
Asynchronous-0.1s	1	8.9	0.12	0.98	10.21	0.09	0.76	6.71	0.1
Asynchronous-0.2s	0.47	12.53	0.2	0.46	11.21	0.13	0.6	7.62	0.21
Asynchronous-0.5s	0.17	2.8	0.6	0.17	1.81	0.68	0.16	4.5	0.45
Asynchronous 1.0s	0.37	5.51	0.16	0.37	4.71	0.08	0.24	4	0.15

iii. Wave Passage Effect for Case 4

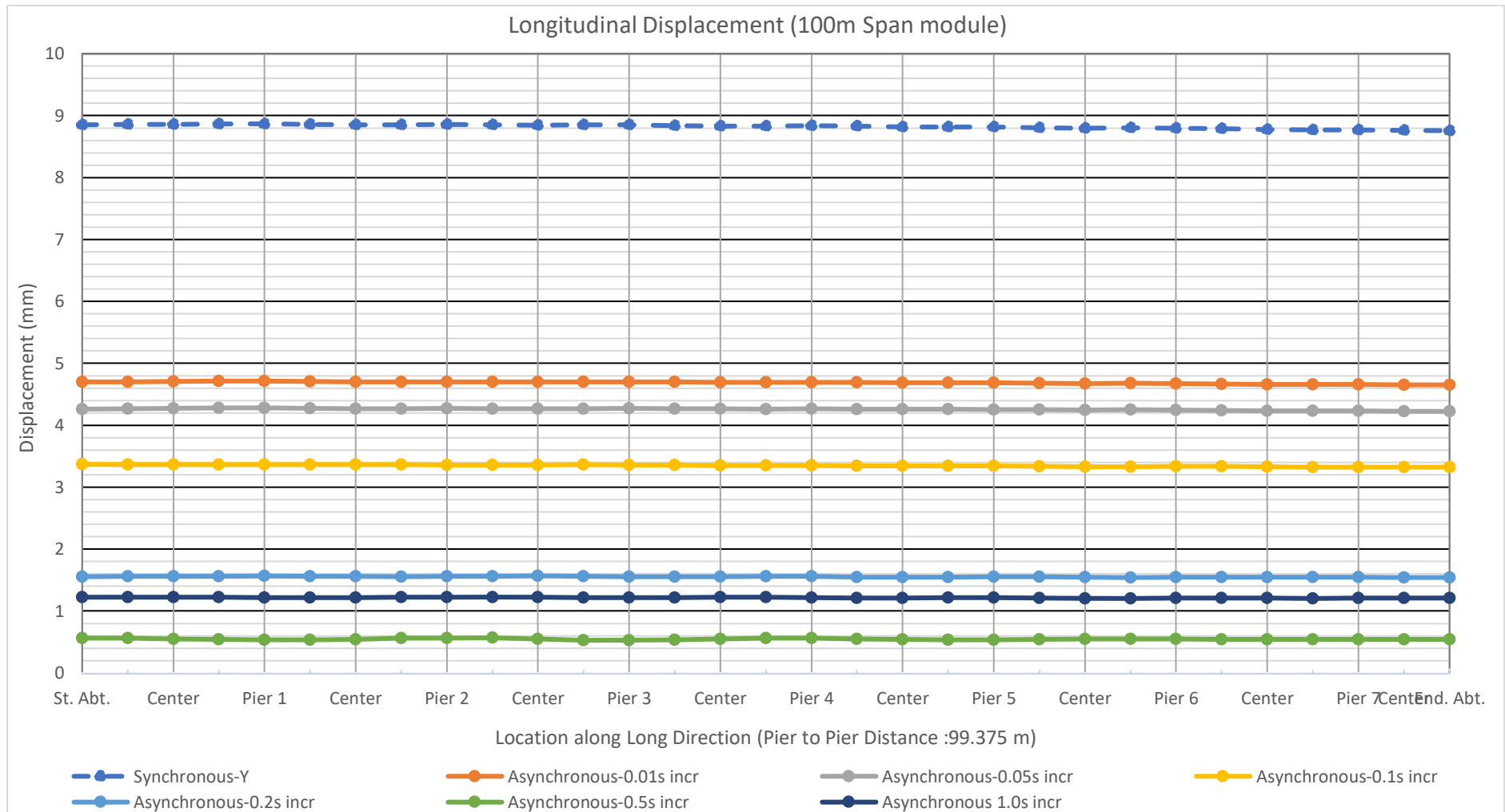


Figure 5.11: Maximum longitudinal displacement for load case 4 (100m span module)

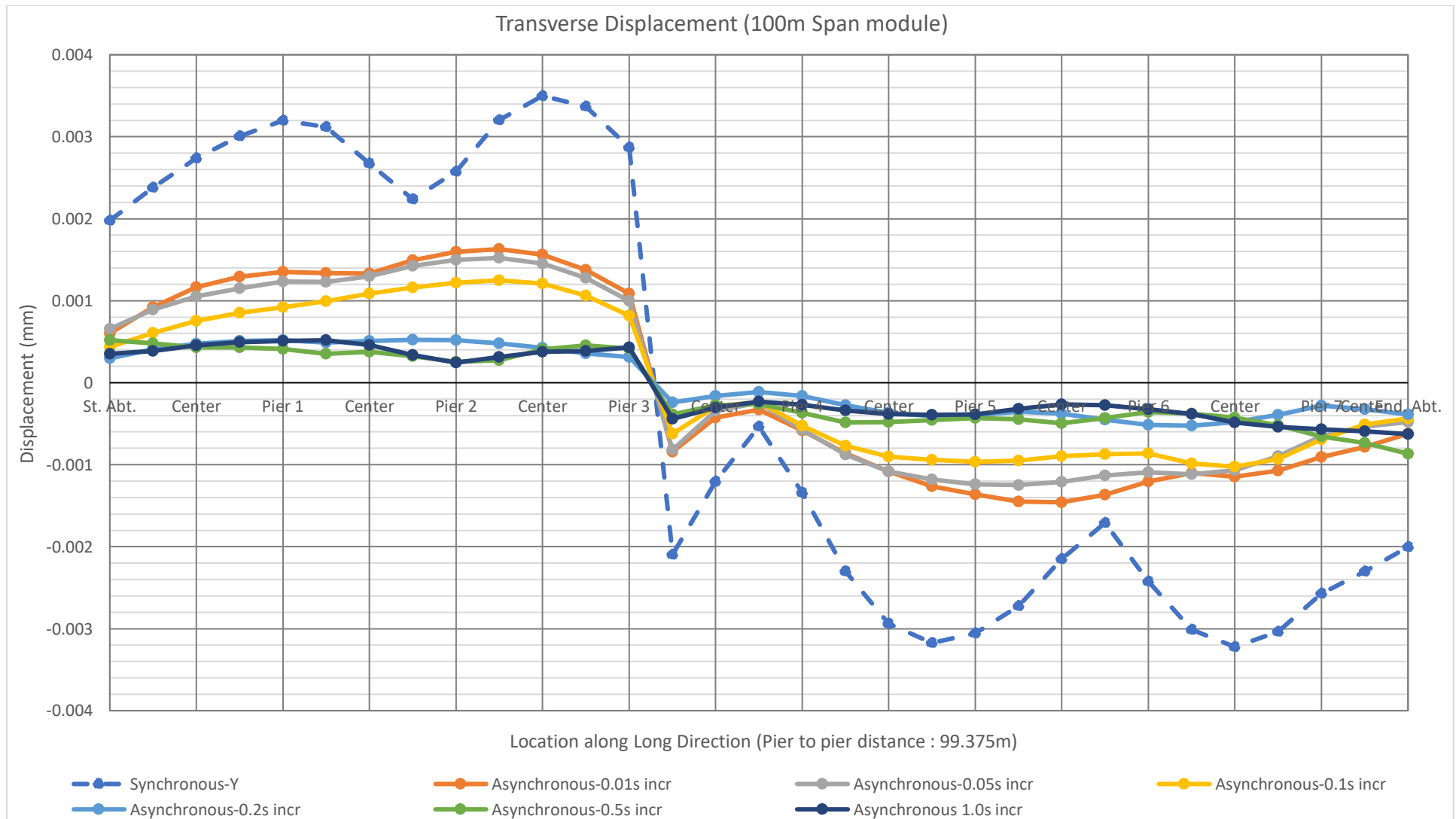


Figure 5.12: Maximum transverse displacement for load case 4 (100m span module)

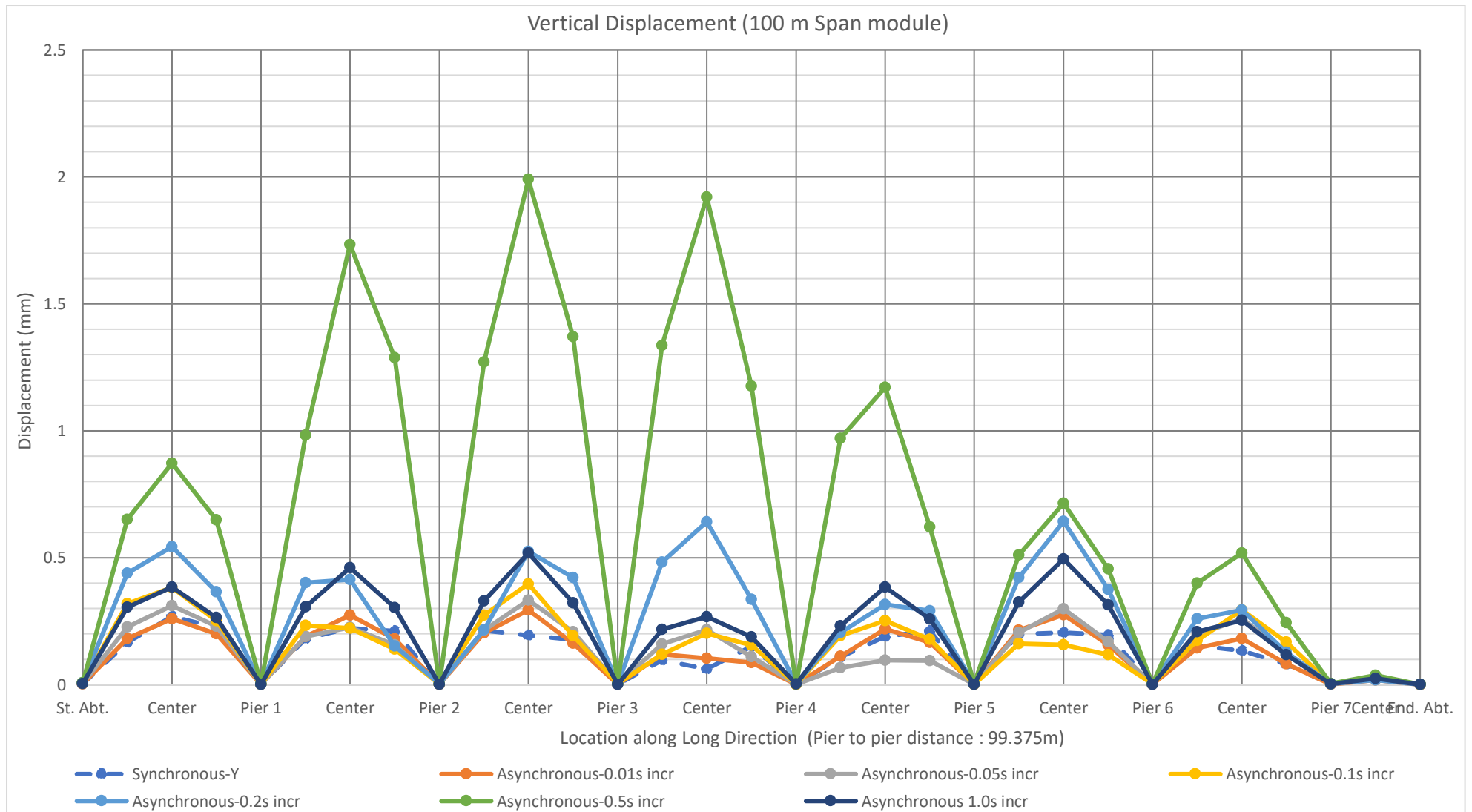


Figure 5.13: Maximum vertical displacement for load case 4 (100m span module)

Maximum displacements due to all seismic motion in all three bridge span modules for case 4 are shown in **Table 5.7**. For 75m span module, it is observed that in case 4 displacement in transverse direction resembles a fixity near pier 4. This is the centre of rotation. Maximum transverse direction is ± 0.010 mm for synchronous motion. Maximum longitudinal displacement is found to be 8.69 mm which is caused by synchronous motion. For vertical displacement asynchronous 0.5s time lag governs and maximum displacement is 2.26mm. Here asynchronous effect is 13.3 times of synchronous effect. For 125m span module, it is seen that in case 4 displacement in transverse direction resembles a fixity near pier 4. This is the centre of rotation. Maximum transverse direction is ± 0.0021 mm for synchronous motion. Maximum longitudinal displacement is found to be 8.82 mm which is caused by synchronous motion. For vertical displacement asynchronous 0.5s time lag governs and maximum displacement is 1.50mm. Here asynchronous effect is 7.5 times the synchronous effect.

Table 5.7: Maximum displacement for case 4 for three-bridge span modules

Case 4: 100% in Longitudinal									
Span Module	100m Span Module			75m Span Module			125m Span Module		
Seismic Motion Type	Maximum Displacement (mm)								
	Longitudinal Direction	Transverse Direction	Vertical Direction	Longitudinal Direction	Transverse Direction	Vertical Direction	Longitudinal Direction	Transverse Direction	Vertical Direction
Synchronous	8.9	± 0.003	0.27	8.69	± 0.010	0.17	8.82	± 0.0021	0.2
Asynchronous-0.01s	4.71	± 0.002	0.3	4.66	± 0.005	0.14	3.23	± 0.0010	0.2
Asynchronous-0.05s	4.28	± 0.002	0.33	4.27	± 0.005	0.22	3.04	± 0.0010	0.25
Asynchronous-0.1s	3.37	± 0.001	0.4	3.3	± 0.004	0.28	2.54	± 0.0009	0.32
Asynchronous-0.2s	1.57	± 0.001	0.64	1.52	± 0.002	0.4	1.73	± 0.0007	0.7
Asynchronous-0.5s	0.57	± 0.001	2	0.58	± 0.003	2.26	0.54	± 0.0004	1.5
Asynchronous 1.0s	1.23	± 0.001	0.52	1.24	± 0.001	0.26	0.81	± 0.0003	0.51

iv. Wave Passage Effect for Case 5

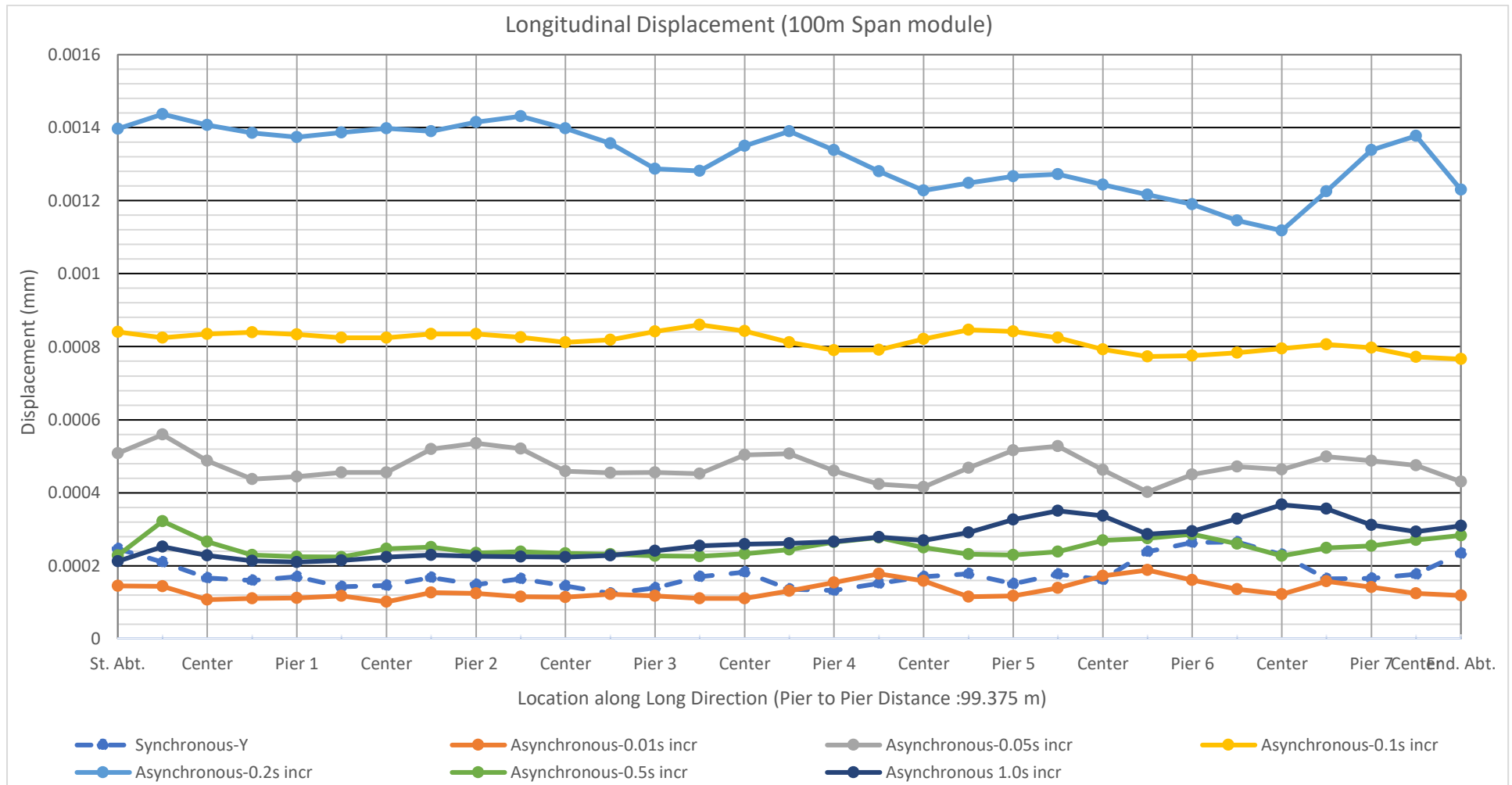


Figure 5.14: Maximum longitudinal displacement for load case 5 (100m span module)

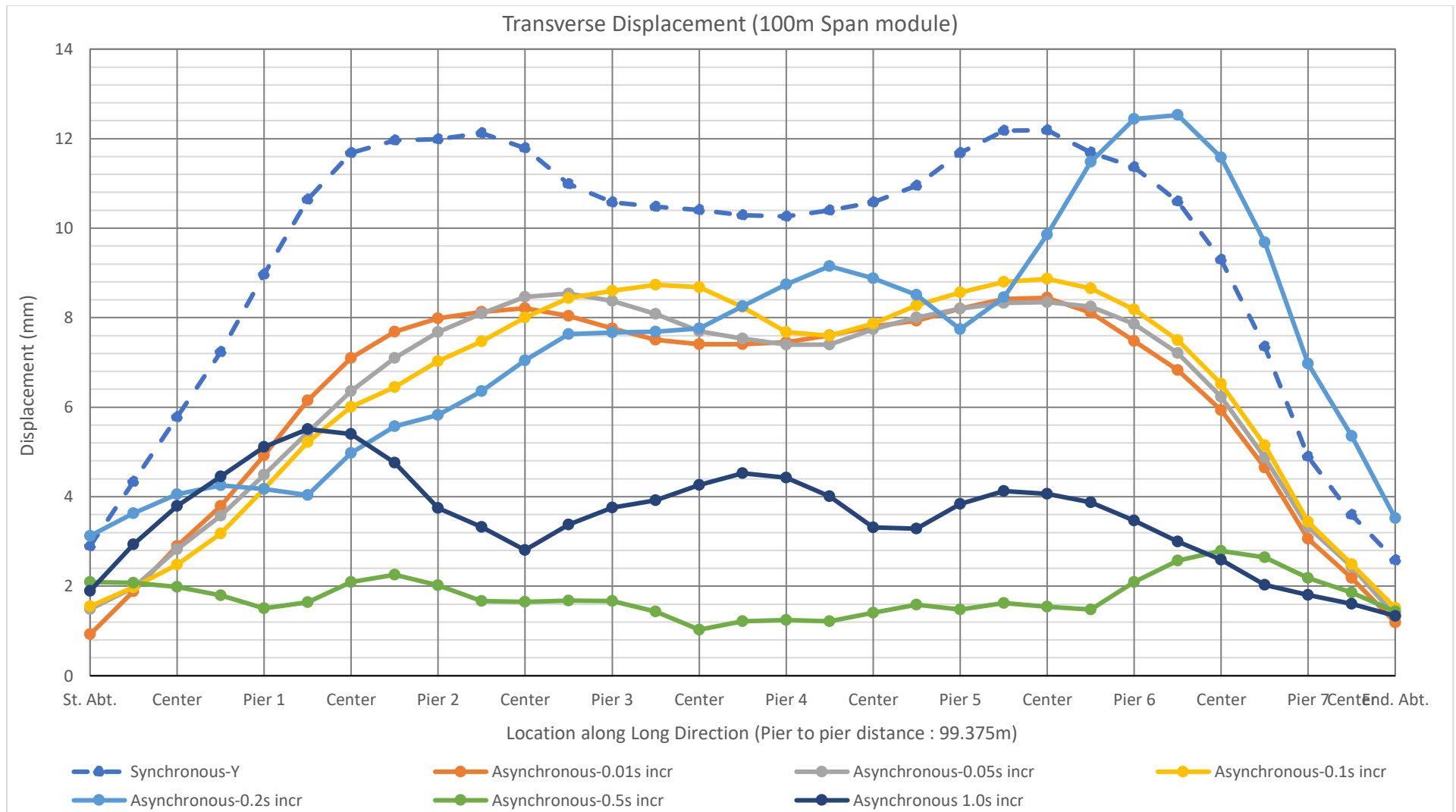


Figure 5.15: Maximum transverse displacement for load case 5 (100m span module)

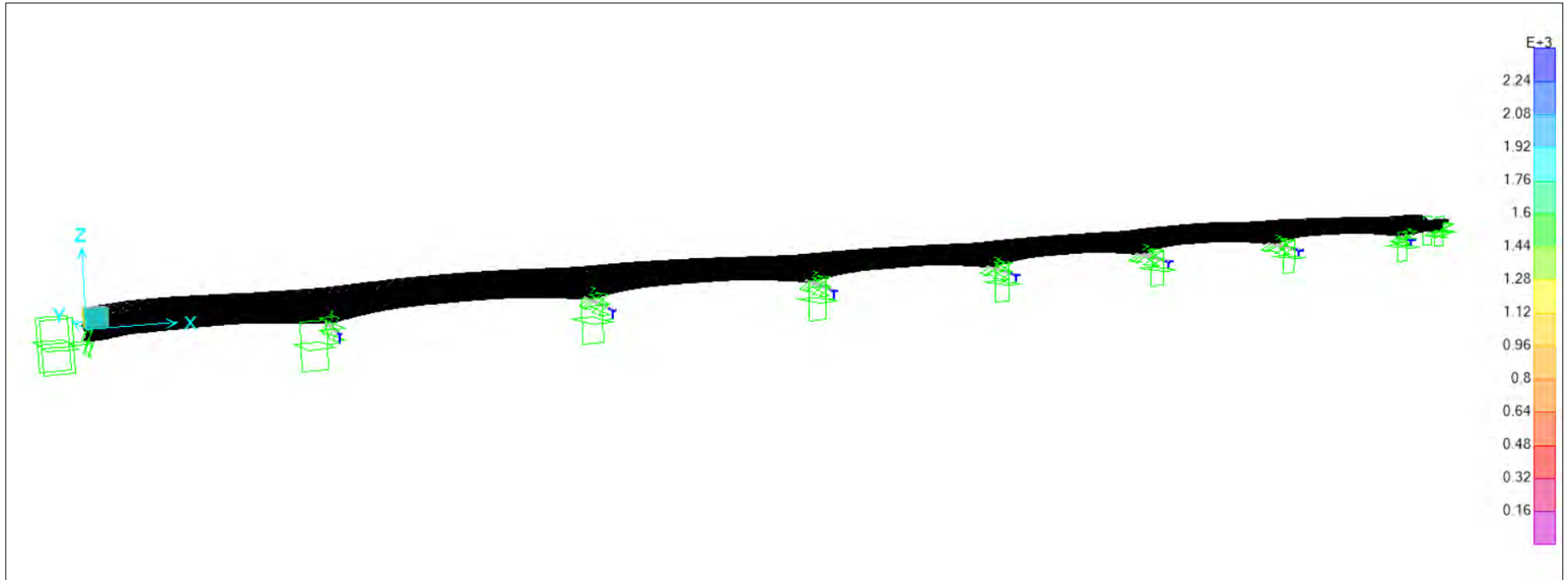


Figure 5.16: Stress due to synchronous motion (100m span module)

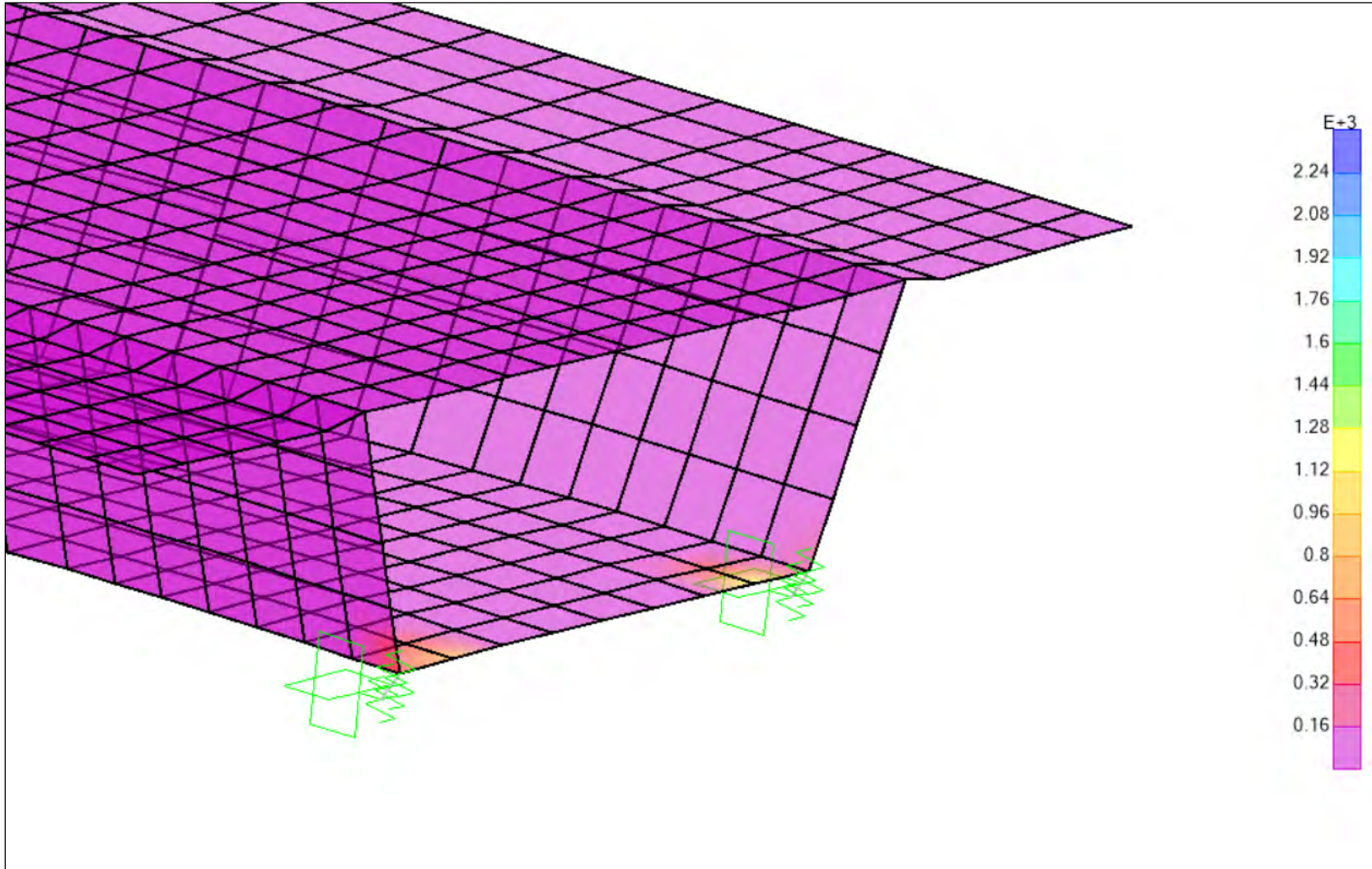


Figure 5.17: Stress Concentration at expansion joint bearing top due to synchronous motion (100m span module)

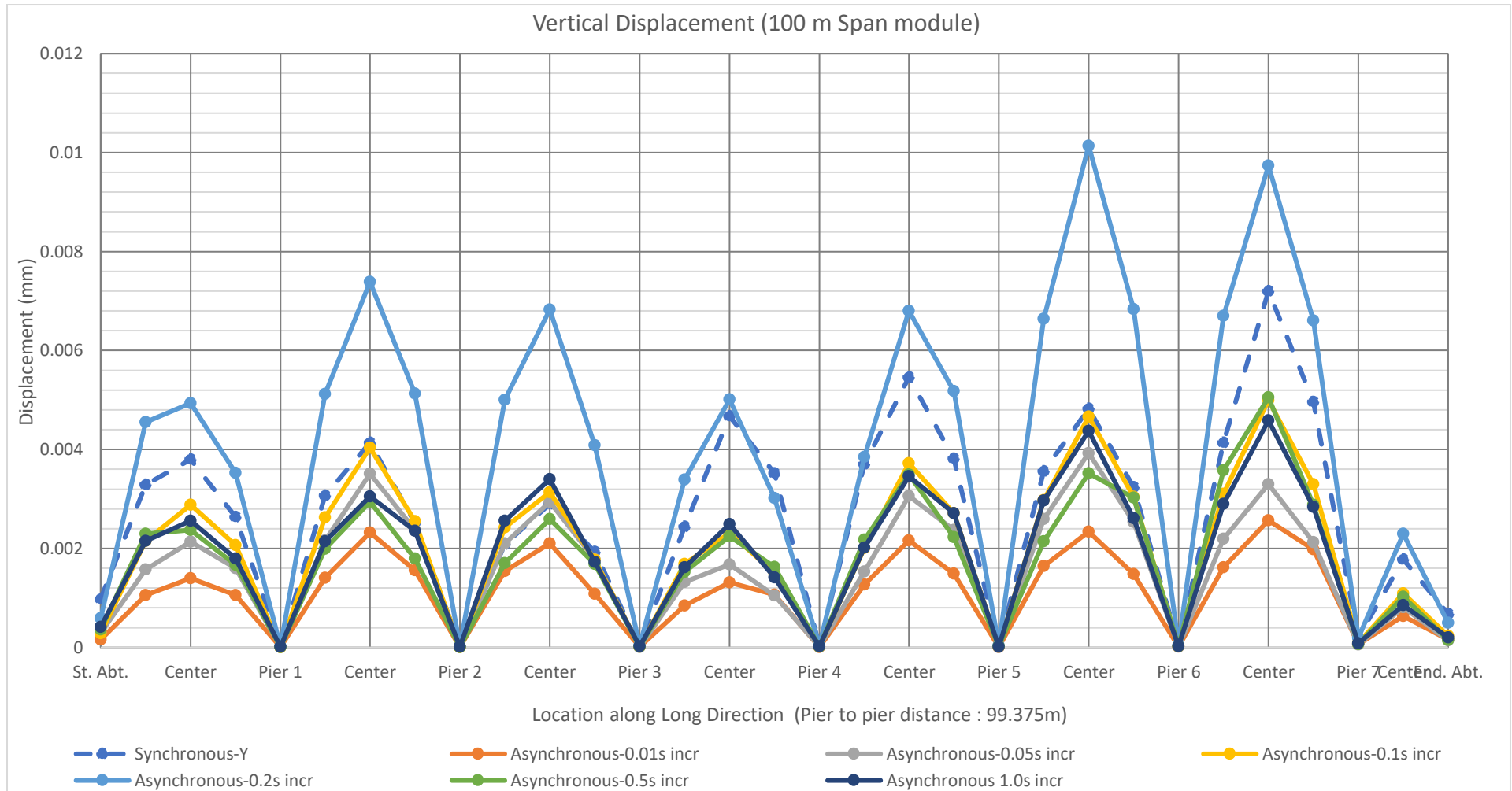


Figure 5.18: Maximum vertical displacement for load case 5 (100m span module)

Maximum displacements due to all seismic motion in all three bridge span modules for case 5 are shown in **Table 5.8**. For 75m span module, it is seen that maximum longitudinal displacement is found to be 0.01mm which is caused by asynchronous 0.2s time lag. The displacement in transverse direction is governed by synchronous motion (maximum displacement 13.24 mm) of bridge. Vertical displacement is not significant (asynchronous 0.20s time lag govern and maximum displacement found 0.037 mm).

For 125 m span module, it is seen that Maximum longitudinal displacement found to be 0.0008 mm which is caused by asynchronous 0.2s motion. The displacement in transverse direction is governed by synchronous motion (maximum displacement 12.73 mm). Vertical displacement is not significant (synchronous motion governs and maximum displacement found 0.08 mm).

Table 5.8: Maximum displacement for case 5 for three-bridge span modules

Case 5: 100% in Lateral Direction									
Span Module	100m Span Module			75m Span Module			125m Span Module		
Seismic Motion Type	Maximum Displacement (mm)								
	Longitudinal Direction	Transverse Direction	Vertical Direction	Longitudinal Direction	Transverse Direction	Vertical Direction	Longitudinal Direction	Transverse Direction	Vertical Direction
Synchronous	0.0003	12.2	0.007	0.001	13.24	0.033	0.0004	12.73	0.08
Asynchronous-0.01s	0.0002	8.44	0.003	0.001	9.31	0.012	0.0001	7	0.001
Asynchronous-0.05s	0.0006	8.54	0.004	0.002	9.6	0.012	0.0003	6.8	0.002
Asynchronous-0.1s	0.0009	8.9	0.005	0.004	10.21	0.008	0.0004	6.71	0.001
Asynchronous-0.2s	0.0014	12.53	0.01	0.005	11.21	0.037	0.0008	7.62	0.002
Asynchronous-0.5s	0.0003	2.8	0.005	0.001	1.81	0.008	0.0004	4.48	0.003
Asynchronous 1.0s	0.0004	5.51	0.005	0.001	4.71	0.013	0.0003	4	0.002

v. Wave Passage Effect for Case 8

Figure 5.19 to **Figure 5.21** show displacements (longitudinal, transverse and vertical) found due to wave passage effect in longitudinal direction and 30% effect of longitudinal direction assigned in lateral direction for El-Centro Earthquake data. In this model no seismic isolation was assigned.

Figure 5.19 shows displacement at longitudinal direction. Sudden increase in displacement at piers is observed. Longitudinal displacement is not same throughout the bridge as it fluctuates. Asynchronous motion 1.0s governs and maximum displacement is found to be 26.2 mm Maximum displacement for synchronous motion is 0.43 mm.

Figure 5.20 shows displacement at transverse direction. In this case, asynchronous 0.1s gives maximum displacement at most segment. But between pier 6 and pier 7, maximum displacement was found 62.07 mm for asynchronous 0.1s. Maximum displacement for synchronous motion is 32.51 mm. Displacement due to asynchronous motion is 1.91 times of synchronous motion.

Figure 5.21 shows displacement at vertical direction. No displacement is there in piers but magnitude reaches maximum between two piers. In this case, asynchronous 1.0 s motion governs and maximum displacement is 609.67 mm which extremely exceeds allowable limit. Maximum displacement due to synchronous motion is 9.78 mm which exceeds allowable limit. Maximum displacement for asynchronous 1.0s motion is 60 times of synchronous motion.

As 100m bridge is similar to that of a 7-span module of Bangabandhu bridge, it can be seen that present bearings are essential for proper functioning of the bridge during seismic event. In case of seismic isolation malfunction, displacement due to asynchronous motion will significantly exceed allowable displacement. Thus, maintenance of the bearings is critical for the seismic performance of Bangabandhu bridge.

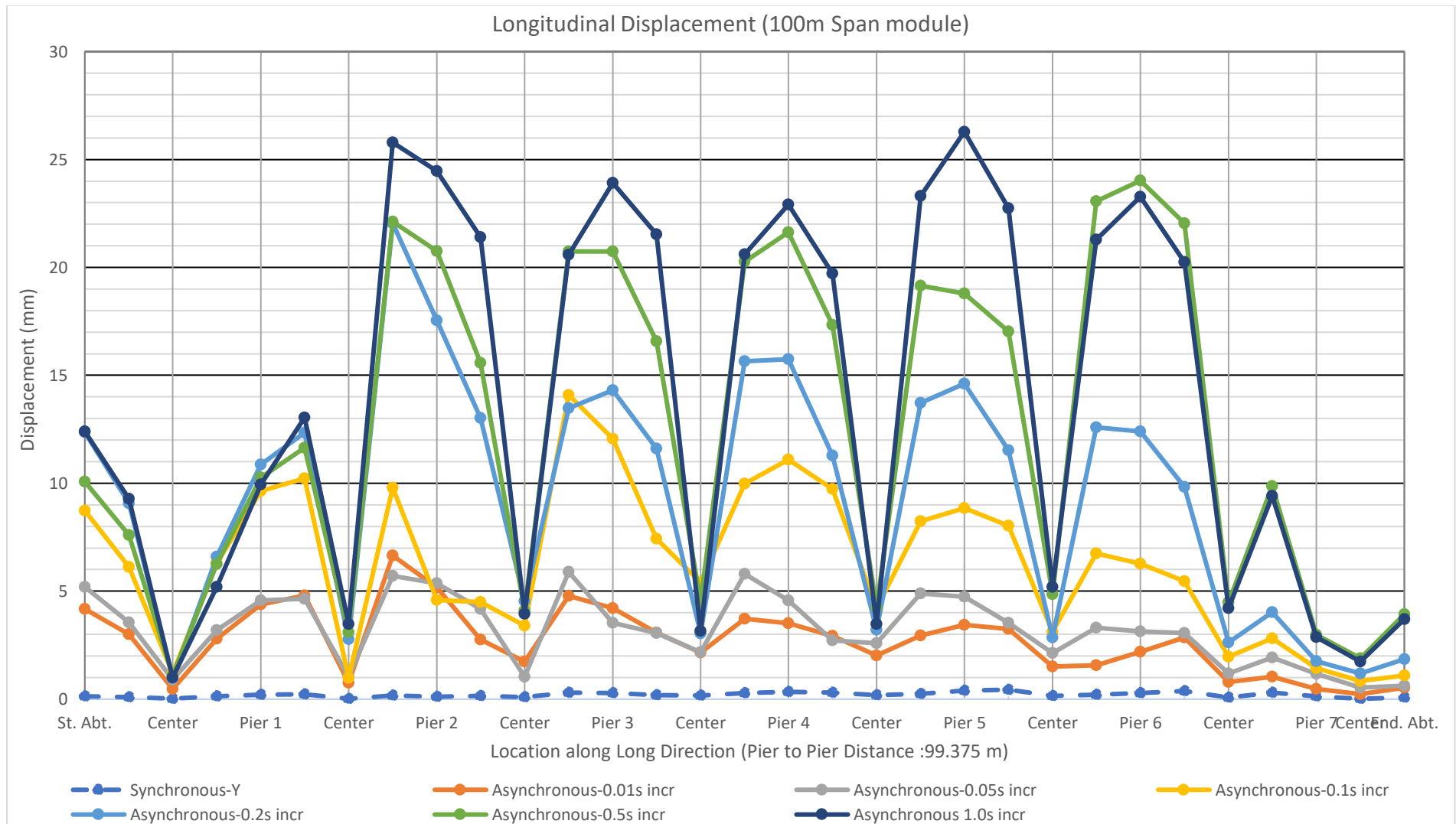


Figure 5.19: Maximum longitudinal displacement for load case 8 (100m span module)

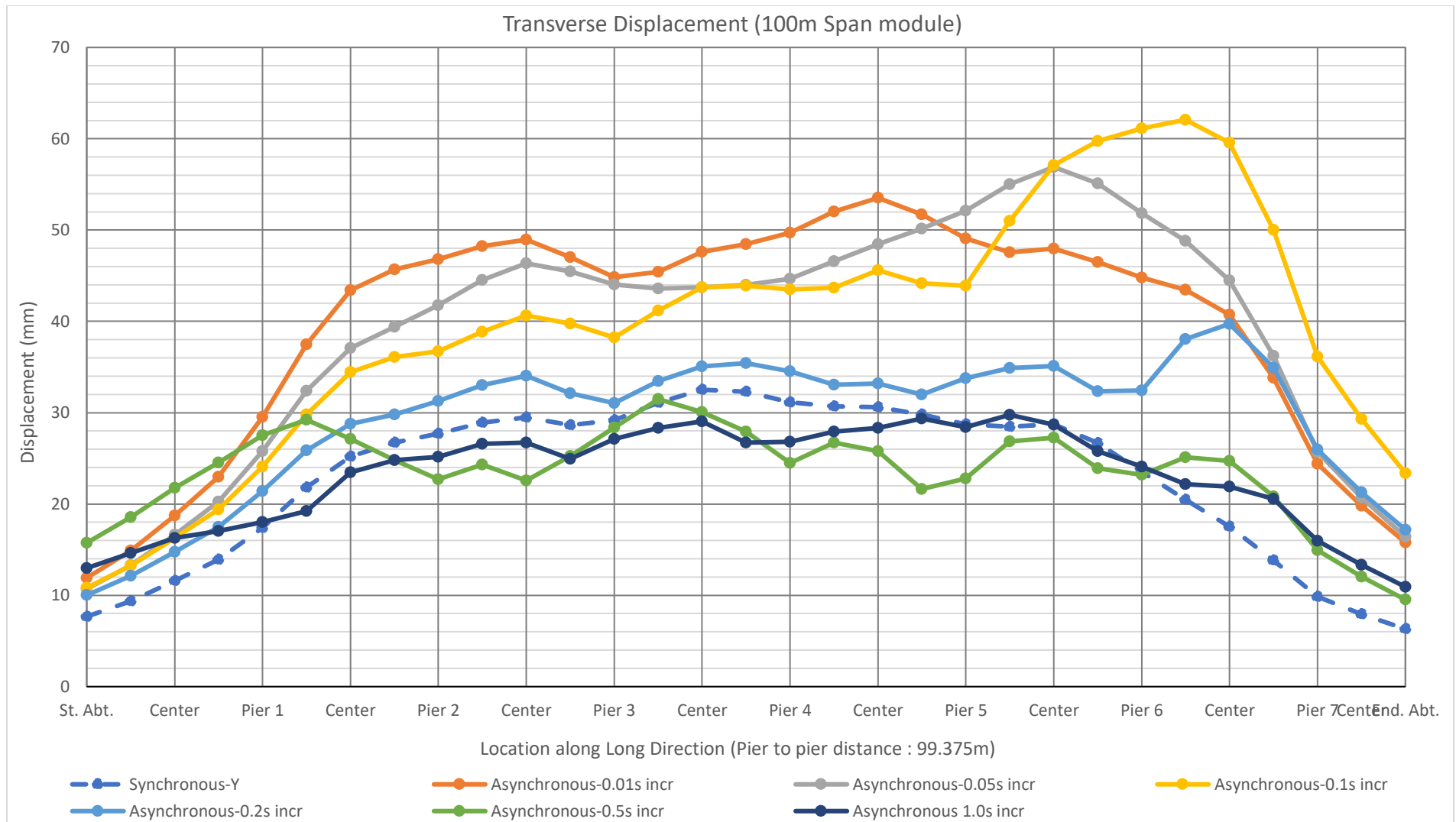


Figure 5.20: Maximum transverse displacement for load case 8 (100m span module)

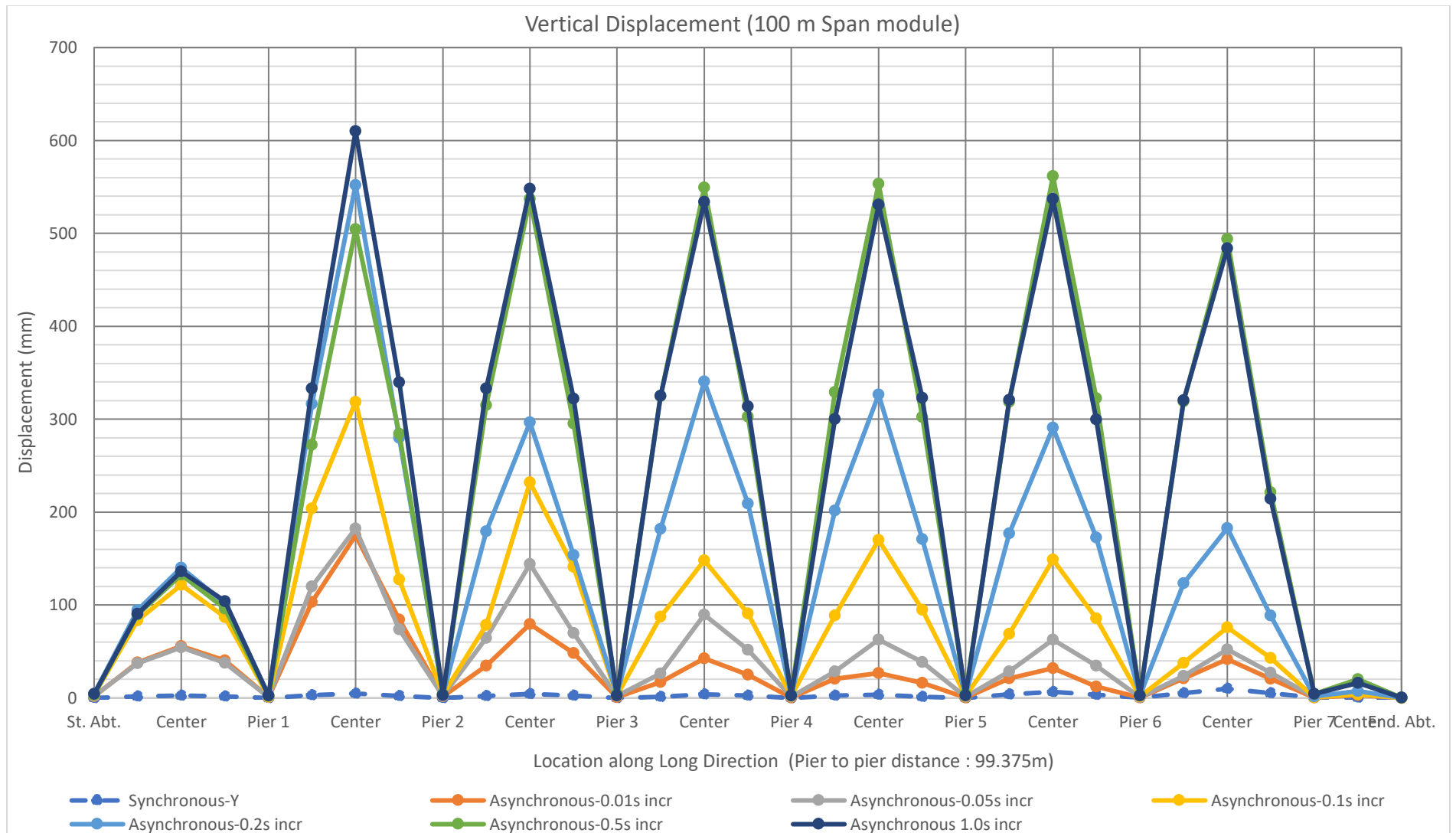


Figure 5.21: Maximum vertical displacement for load case 8 (100m span module)

5.2.4 El-Centro Earthquake Data Input

Figure 5.22 to **Figure 5.24** show displacements (longitudinal, transverse and vertical) found due to wave passage effect in lateral direction and 30% effect assigned in longitudinal direction (Case 6). This wave passage effect configuration was assigned based AASHTO provision. In this case, the assigned earthquake data was recorded from El-Centro earthquake in 1940 with scale factor of 1.317.

Figure 5.22 shows displacement at longitudinal direction. The displacement is constant all throughout the bridge for all seismic motion. Asynchronous 0.01s motion governs. Maximum displacement is found to be 201 mm for asynchronous 0.01s and 183.6mm for synchronous motion. **Figure 5.23** shows displacement at transverse direction. The displacement in transverse direction is governed by asynchronous 0.1s motion (maximum displacement 64.1 mm) of bridge model. **Figure 5.24** shows displacement at vertical direction. No displacement is there in piers but magnitude reaches maximum between two piers. In this case, asynchronous 1.0s motion governs and maximum displacement is 15.8 mm. Maximum displacement for asynchronous 1.0s motion is 3.1 times of synchronous motion.

Figure 5.25 to **Figure 5.27** show displacements (longitudinal, transverse and vertical) found due to wave passage effect in lateral direction and 30% effect assigned in longitudinal direction (Case 7).

Figure 5.25 shows displacement at longitudinal direction. The displacement is constant all throughout the bridge for all seismic motion. Asynchronous 0.01s motion governs in this case. Maximum displacement is found to be 60.3 mm for asynchronous 0.01s and 55.1 mm for synchronous motion. Displacement due to asynchronous 0.01 s motion is 1.1 times than that of synchronous motion. **Figure 5.26** shows displacement at transverse direction. The displacement in transverse direction is governed by asynchronous 0.1s time lag (maximum displacement is 214 mm). **Figure 5.27** shows displacement at vertical direction. No displacement is there in piers but magnitude reaches maximum between two piers. In this case, asynchronous 1.0 s motion governs and maximum displacement is 4.71 mm. Maximum displacement for asynchronous 1.0 s motion is 3.14 times of synchronous motion.

i. Wave Passage Effect for Case 6

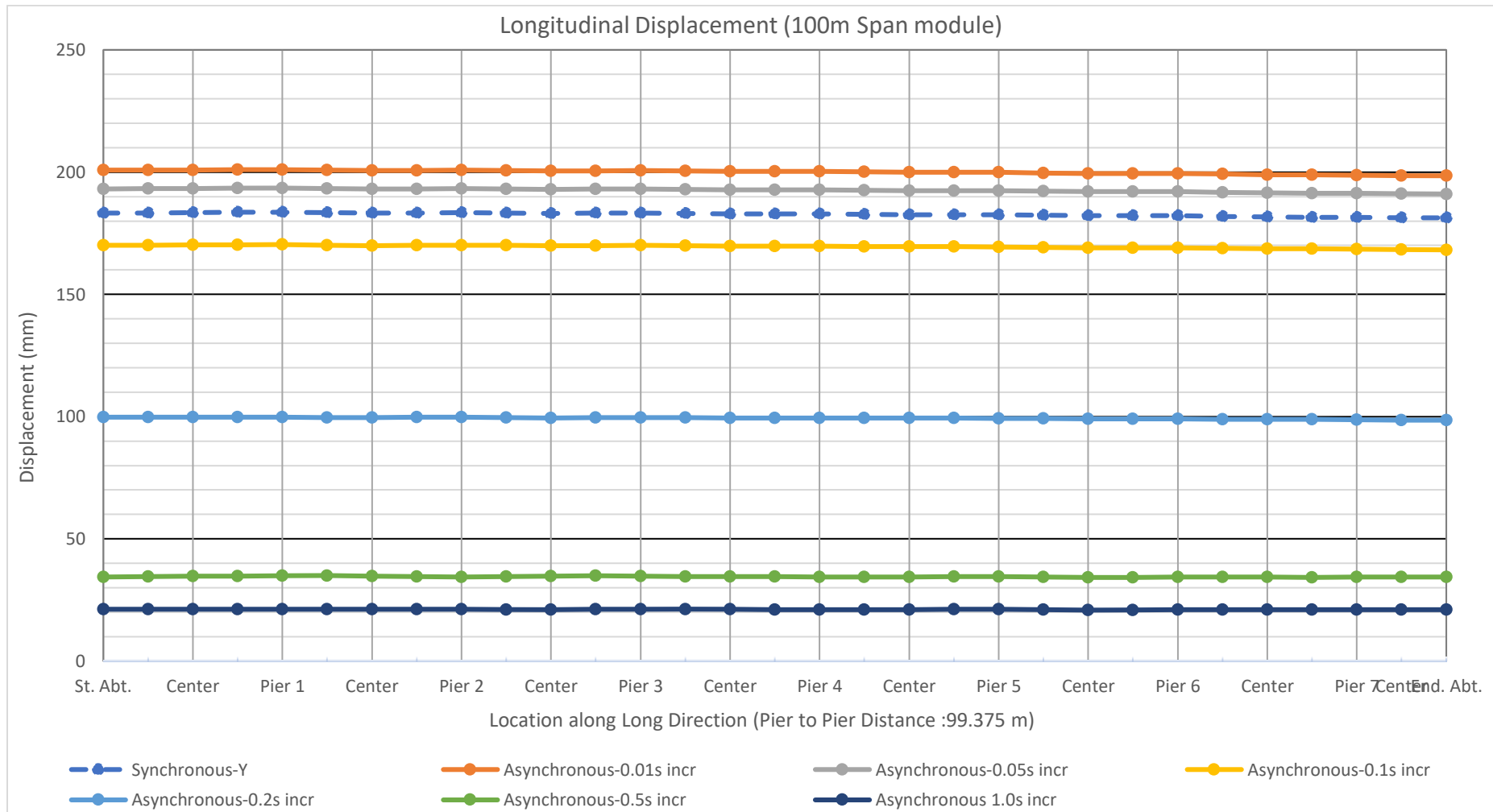


Figure 5.22: Maximum longitudinal displacement for load case 6 (100m span module)

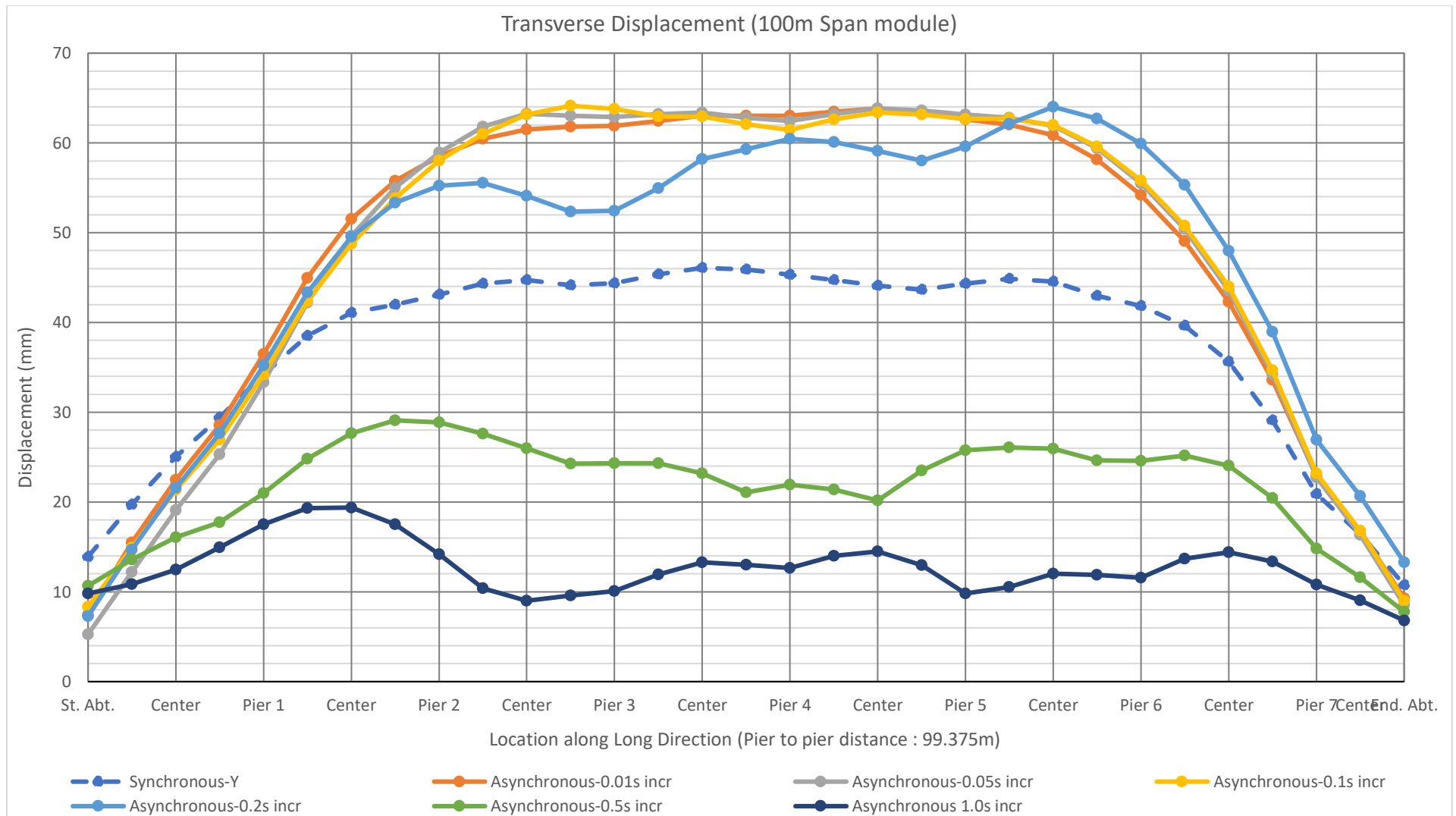


Figure 5.23: Maximum transverse displacement for load case 6 (100m span module)

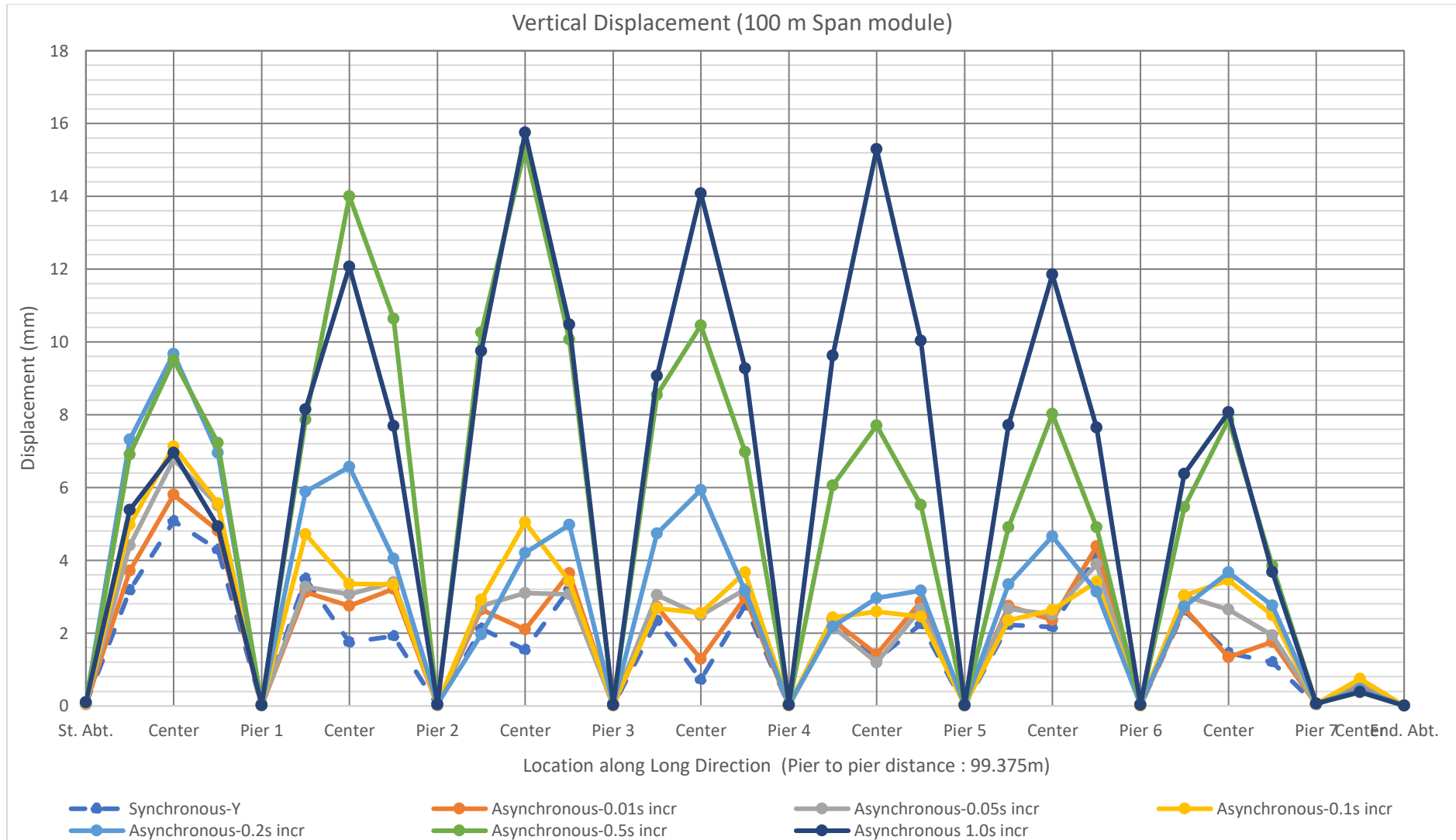


Figure 5.24: Maximum vertical displacement for load case 6 (100m span module)

Maximum displacements due to all seismic motion in all three bridge span modules for case 6 are shown in **Table 5.9**. For 75 span module, it is seen that Longitudinal Displacement is governed by Asynchronous 0.01s time lag (maximum displacement 193.7mm) compared to Synchronous motion (maximum displacement 175.2mm). In both cases, it is very near to allowable limit. Maximum transverse displacement is found for asynchronous 0.01s motion of 65.46mm. For vertical displacement asynchronous 0.5s lag governs and maximum displacement is 14.2mm. Here asynchronous 0.5s time lag effect is 5.1 times the synchronous effect (2.81 mm). For 125 span module, it is seen that Longitudinal Displacement is governed by synchronous 0.01s time lag (maximum displacement 245.5 mm) compared to asynchronous motion 0.01s (maximum displacement 233.4 mm). In both cases, displacement exceeds allowable limit. Maximum transverse displacement is found for asynchronous 0.01s motion of 82.5 mm. For vertical displacement asynchronous 1.0 s lag governs and maximum displacement is 13.73mm. Here asynchronous 0.5s time lag effect is 2.4 times the synchronous effect (5.74 mm).

Table 5.9: Maximum displacement for case 6 for three-bridge span module

Case 6: 100% in Longitudinal+30% Lateral Direction (El-Centro)									
Span Module	100m Span Module			75m Span Module			125m Span Module		
Seismic Motion Type	Maximum Displacement (mm)								
	Longitudinal Direction	Transverse Direction	Vertical Direction	Longitudinal Direction	Transverse Direction	Vertical Direction	Longitudinal Direction	Transverse Direction	Vertical Direction
Synchronous	183.6	46.1	5.1	175.2	48.21	2.81	245.5	74.3	5.74
Asynchronous-0.01s	201	63.8	5.8	193.7	65.46	3.16	233.4	82.5	5.9
Asynchronous-0.05s	193.5	63.8	6.8	186.5	63.5	3.45	224.4	81.5	5.83
Asynchronous-0.1s	170.4	64.1	7.1	164.2	60	3.96	201	80	4.71
Asynchronous-0.2s	100	64	9.7	96.03	56.45	5.24	124.7	79.3	7.3
Asynchronous-0.5s	35	29.1	15.3	33.76	17.5	14.2	41.4	51.2	13.73
Asynchronous 1.0s	21.3	19.4	15.8	20.46	13.44	8.28	24.5	20	18.5

ii. Wave Passage Effect for Case 7

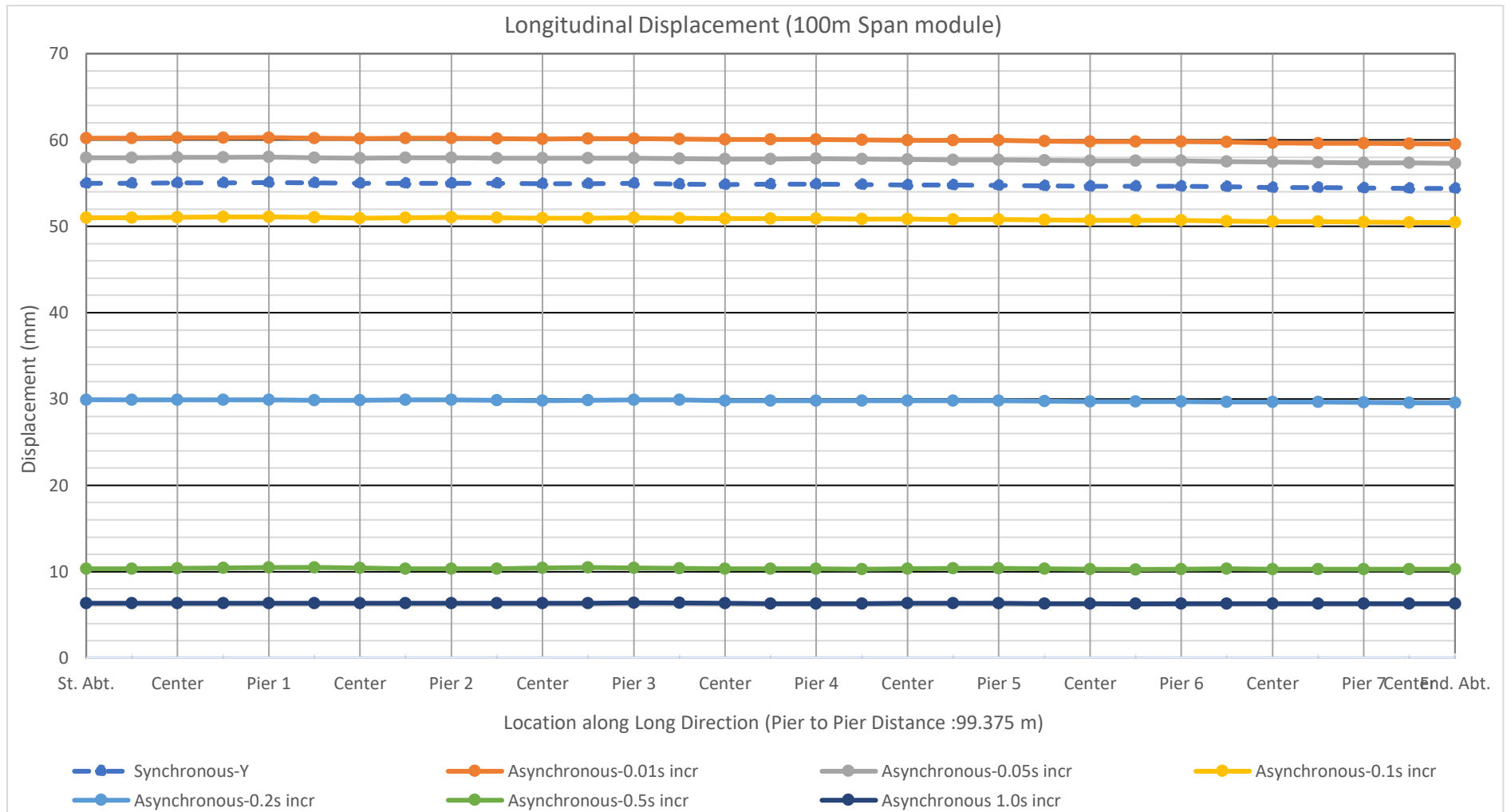


Figure 5.25: Maximum longitudinal displacement for load case 7 (100m span module)

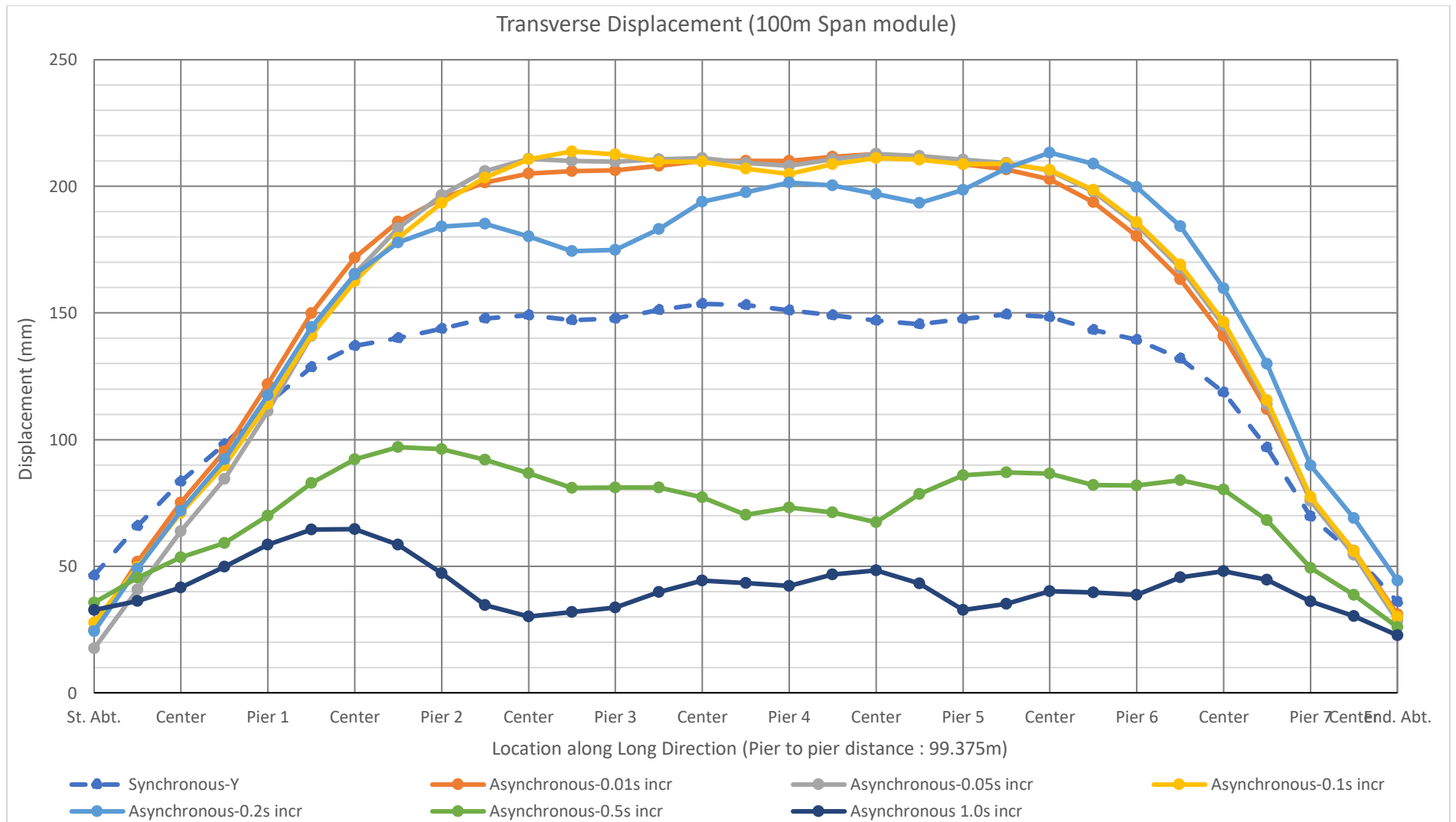


Figure 5.26: Maximum transverse displacement for load case 7 (100m span module)

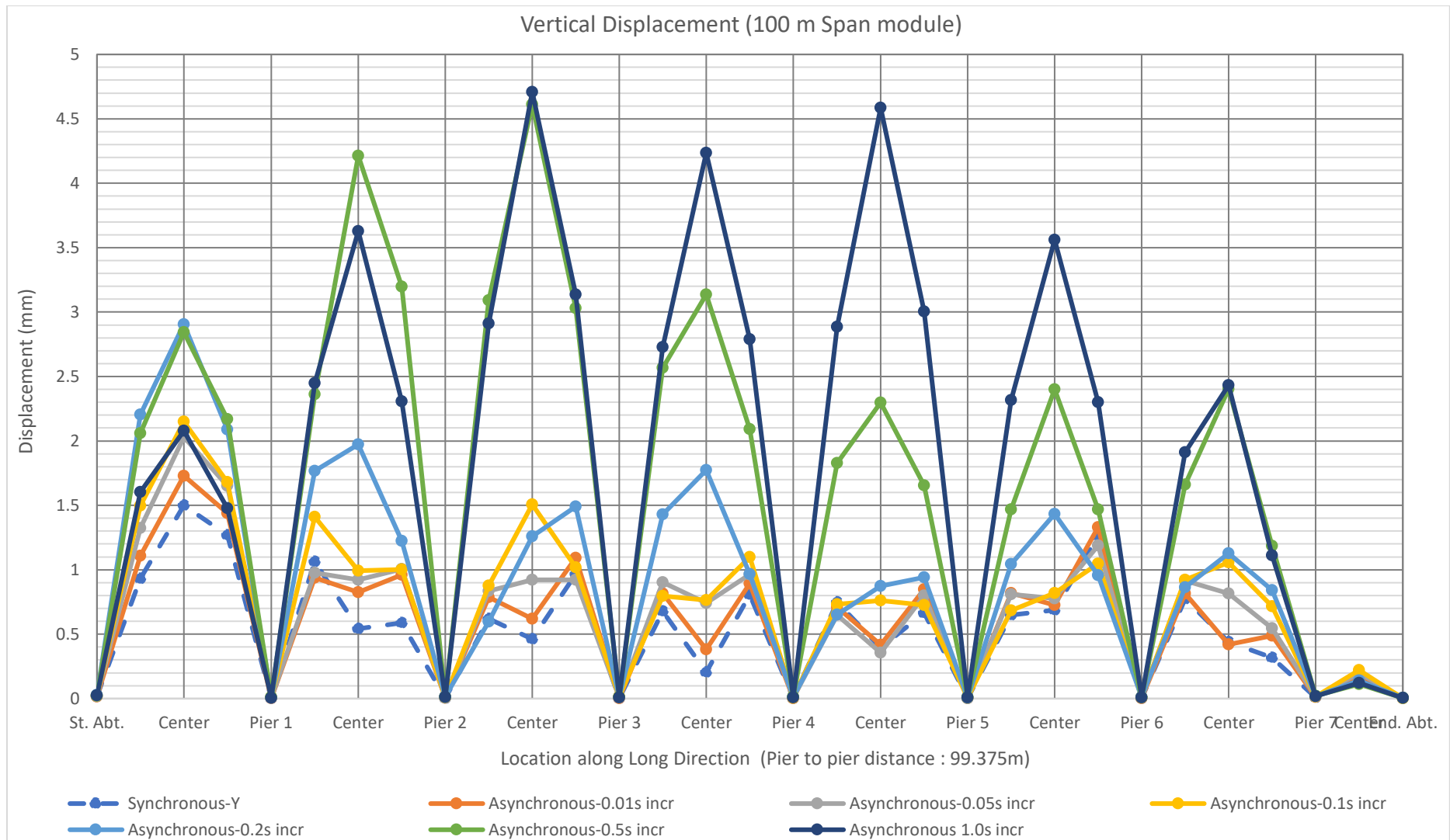


Figure 5.27: Maximum vertical displacement for load case 7 (100m span module)

Maximum displacements due to all seismic motion in all three bridge span modules for case 7 are shown in **Table 5.10**. For 75m span module, it is seen that Longitudinal Displacement is governed by Asynchronous 0.01s time lag (maximum displacement 58.15mm) compared to Synchronous motion (maximum displacement 52.55 mm). Maximum transverse displacement is found for asynchronous 0.01s motion of 218.2mm. In this case, it exceeds the allowable limit. For vertical displacement asynchronous 0.5s lag governs and maximum displacement is 4.27 mm. Here asynchronous 0.5s time lag effect is 5 times the synchronous effect (0.85 mm).

For 125m span module, it is seen that Longitudinal Displacement is governed by synchronous motion (maximum displacement 73.6 mm) compared to asynchronous motion 0.01s (maximum displacement 70 mm). Maximum transverse displacement is found for asynchronous 0.01s motion of 275 mm compared to synchronous motion of 247.5mm. In both cases, displacement exceeds allowable limit. For vertical displacement asynchronous 1.0 s lag governs and maximum displacement is 5.55mm. Here asynchronous 1.0 s time lag effect is 3.2 times the synchronous effect (1.75 mm).

Table 5.10: Maximum displacement for case 7 for three-bridge span module

Case 7: 100% in Lateral Direction + 30% Lateral (El-Centro)									
Span Module	100m Span Module			75m Span Module			125m Span Module		
Seismic Motion Type	Maximum Displacement (mm)								
	Longitudinal Direction	Transverse Direction	Vertical Direction	Longitudinal Direction	Transverse Direction	Vertical Direction	Longitudinal Direction	Transverse Direction	Vertical Direction
Synchronous	55.1	153.6	1.5	52.55	160.7	0.85	73.6	247.7	1.75
Asynchronous-0.01s	60.3	212.8	1.73	58.15	218.2	0.95	70	275	1.78
Asynchronous-0.05s	58	212.8	2.03	56	211.65	1.04	67.3	271.5	1.75
Asynchronous-0.1s	51.1	214	2.15	49.22	199.62	1.21	60.3	266.4	1.41
Asynchronous-0.2s	30	213.3	3	28.8	188	1.6	37.4	264.3	2.2
Asynchronous-0.5s	10.5	97	4.61	10.11	58.31	4.27	12.4	171	4.13
Asynchronous 1.0s	6.4	64.6	4.71	6.12	44.82	2.56	7.3	66.5	5.55

5.3 Modal Participation Mass Ratios and Time Period

In the **Table 5.11** Modal participation and period for different modes in 75 m bridge. In **Table 5.12** Modal participation and period for different modes in 100 m bridge. In **Table 5.13** Modal participation and period for different modes in 125 m bridge.

Table 5.11: Modal Participating Mass Ratios (75 m)

Mode	Period	Frequency	UX	UY	UZ	Sum UX	Sum UY	Sum UZ
Unitless	Sec	Cyc/sec	Unitless	Unitless	Unitless	Unitless	Unitless	Unitless
1	1.97	0.51	0.93	0.00	0.00	0.93	0.00	0.00
2	1.66	0.60	0.00	0.76	0.00	0.93	0.76	0.00
3	1.43	0.70	0.00	0.00	0.00	0.93	0.76	0.00
4	1.05	0.95	0.00	0.11	0.00	0.93	0.87	0.00
5	1.01	0.99	0.00	0.00	0.00	0.93	0.87	0.00
6	0.86	1.16	0.00	0.00	0.00	0.93	0.87	0.00
7	0.77	1.29	0.00	0.00	0.00	0.93	0.87	0.00
8	0.72	1.39	0.00	0.00	0.00	0.93	0.87	0.00
9	0.60	1.67	0.00	0.00	0.00	0.93	0.87	0.01
10	0.59	1.70	0.00	0.02	0.00	0.93	0.90	0.01
11	0.52	1.92	0.00	0.02	0.00	0.93	0.92	0.01
12	0.51	1.96	0.00	0.00	0.00	0.93	0.92	0.01

For 75m span module, modal frequencies (mode 6,7,8 and 9) are close to predominant frequency of El-Centro earthquake (1.47 Hz). However, modal frequencies (mode 10,11 and 12) are also close to predominant frequency earthquake data found in Bangabandhu bridge (2.00 Hz). As first nine modal frequencies are closer to El-Centro earthquake than earthquake data from Bangabandhu bridge, displacements for El-Centro earthquake are far greater than earthquake data from Bangabandhu bridge.

Table 5.12: Modal Participating Mass Ratios (100 m)

Mode	Period	Frequency	UX	UY	UZ	Sum UX	Sum UY	Sum UZ
Unitless	Sec	Cyc/sec	Unitless	Unitless	Unitless	Unitless	Unitless	Unitless
1	1.99	0.50	0.96	0.00	0.00	0.96	0.00	0.00
2	1.72	0.58	0.00	0.78	0.00	0.96	0.78	0.00
3	1.61	0.62	0.00	0.00	0.00	0.96	0.78	0.00
4	1.34	0.75	0.00	0.10	0.00	0.96	0.88	0.00
5	1.25	0.80	0.00	0.00	0.00	0.96	0.88	0.00
6	1.06	0.94	0.00	0.00	0.00	0.96	0.88	0.00
7	1.03	0.97	0.00	0.00	0.00	0.96	0.88	0.00
8	0.88	1.14	0.00	0.00	0.00	0.96	0.88	0.00
9	0.79	1.26	0.00	0.04	0.00	0.96	0.92	0.00
10	0.73	1.37	0.00	0.00	0.00	0.96	0.92	0.00
11	0.63	1.59	0.00	0.00	0.00	0.96	0.92	0.00
12	0.62	1.62	0.00	0.00	0.00	0.96	0.92	0.01

For 100m span bridge, modal frequency for (mode 9 ,10,11 and 12) are close to predominant frequency of El-Centro earthquake (1.47 Hz). Thus, displacement due to El-Centro earthquake are far greater than earthquake data from Bangabandhu bridge.

Table 5.13: Modal Participating Mass Ratios (125 m)

Mode	Period	Frequency	UX	UY	UZ	Sum UX	Sum UY	Sum UZ
Unitless	Sec	Cyc/sec	Unitless	Unitless	Unitless	Unitless	Unitless	Unitless
1	2.29	0.44	0.96	0.00	0.00	0.96	0.00	0.00
2	2.02	0.49	0.00	0.79	0.00	0.96	0.79	0.00
3	1.93	0.52	0.00	0.00	0.00	0.96	0.79	0.00
4	1.71	0.58	0.00	0.09	0.00	0.96	0.88	0.00
5	1.40	0.71	0.00	0.00	0.00	0.96	0.88	0.00
6	1.40	0.72	0.00	0.00	0.00	0.96	0.88	0.00
7	1.18	0.84	0.00	0.00	0.00	0.96	0.88	0.00
8	1.10	0.91	0.00	0.04	0.00	0.96	0.92	0.00
9	0.97	1.03	0.00	0.00	0.00	0.96	0.92	0.00
10	0.87	1.15	0.00	0.00	0.00	0.96	0.92	0.00
11	0.80	1.25	0.00	0.00	0.00	0.96	0.92	0.01
12	0.71	1.41	0.00	0.02	0.00	0.96	0.94	0.01

For 125m span bridge, modal frequencies (mode 10,11 and 12) are close to predominant frequency of El-Centro earthquake (1.47 Hz). Thus, displacement due to El-Centro earthquake are far greater than earthquake data from Bangabandhu bridge.

5.4 Flexural and Stress Capacity Check for Extreme Event

According to AASHTO Load Combination for Extreme Event, all the bridges are checked for Flexural and stress. The combination for extreme event is as follows:

1.25 Dead Load+ 1.0 Live Load+ 1.0 Earthquake Load

In this earthquake Load case, asynchronous motion at 0.5s lag is being considered as vertical displacement governed due to this case.

In the case of 100 m span analysis model, which resembles the Bangabandhu bridge, flexural capacity check is shown in **Figure 5.28**.

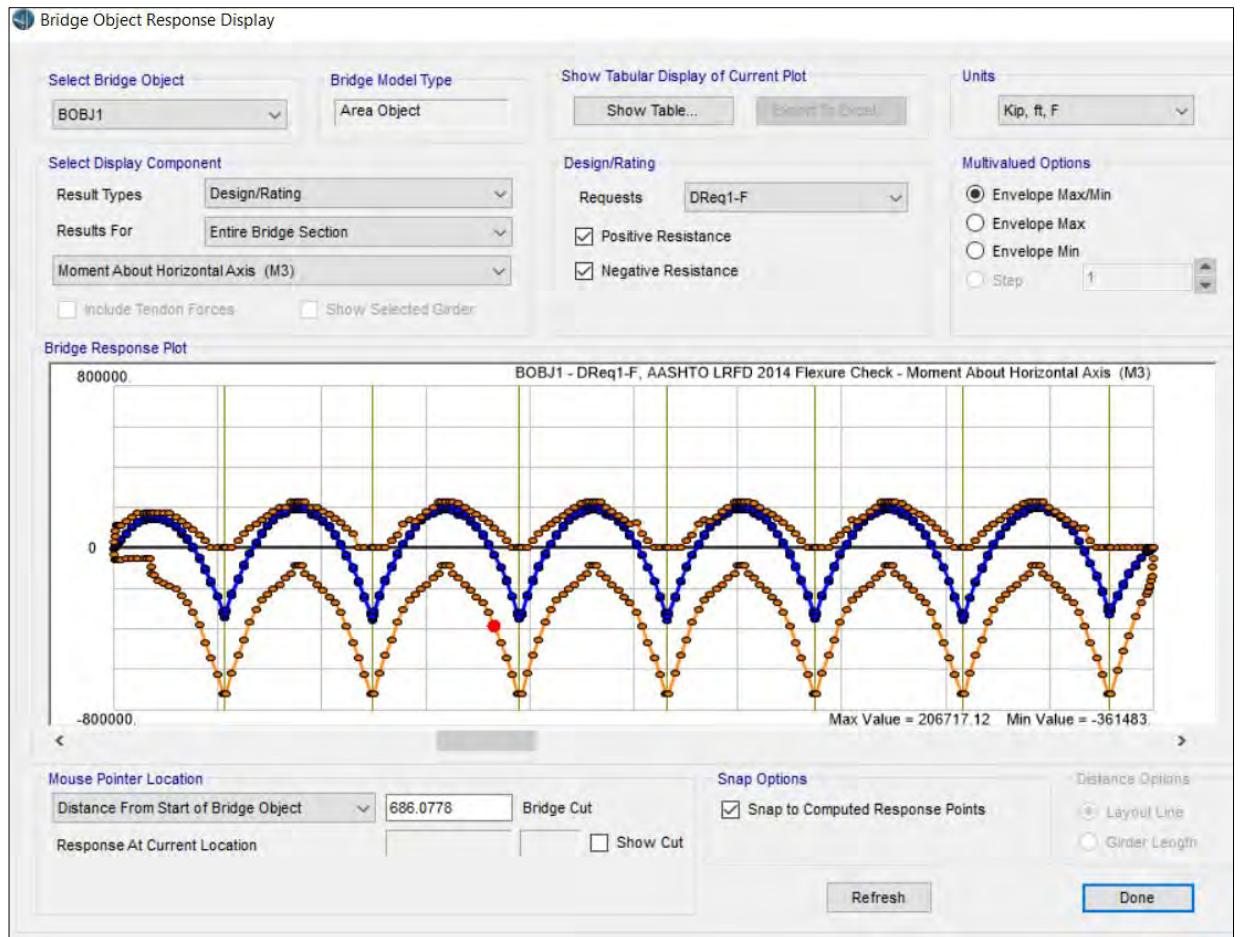


Figure 5.28: Flexural capacity check according AASHTO LRFD,2014 (100 m)

Maximum induced Positive Moment = 2,06,717 Kip-ft

Maximum Positive Moment Capacity = 2, 28,771 Kip-ft

Maximum induced Negative Moment = 3,61,483 Kip-ft

Maximum Negative Moment Capacity = 7, 21,387 Kip-ft

Stress capacity check is also important for design in extreme event I. Bottom and top stress check is shown in **Figure 5.29** and **Figure 5.30** respectively for 100m bridge.



Figure 5.29: Bottom longitudinal stress capacity check (100 m)

For Bottom,

$$\text{Tensile Stress Limit} = 0.5\sqrt{f'_c}(\text{MPa}) = 0.5\sqrt{44.83} \text{ MPa} = 3.34 \text{ MPa}$$

Maximum Tensile Stress = 0 MPa

$$\text{Compressive Stress Limit} = 0.45 f'_c (\text{MPa}) = 0.45 \times 44.83 \text{ MPa} = 20.16 \text{ MPa}$$

Maximum Compressive Stress = 13.66 MPa

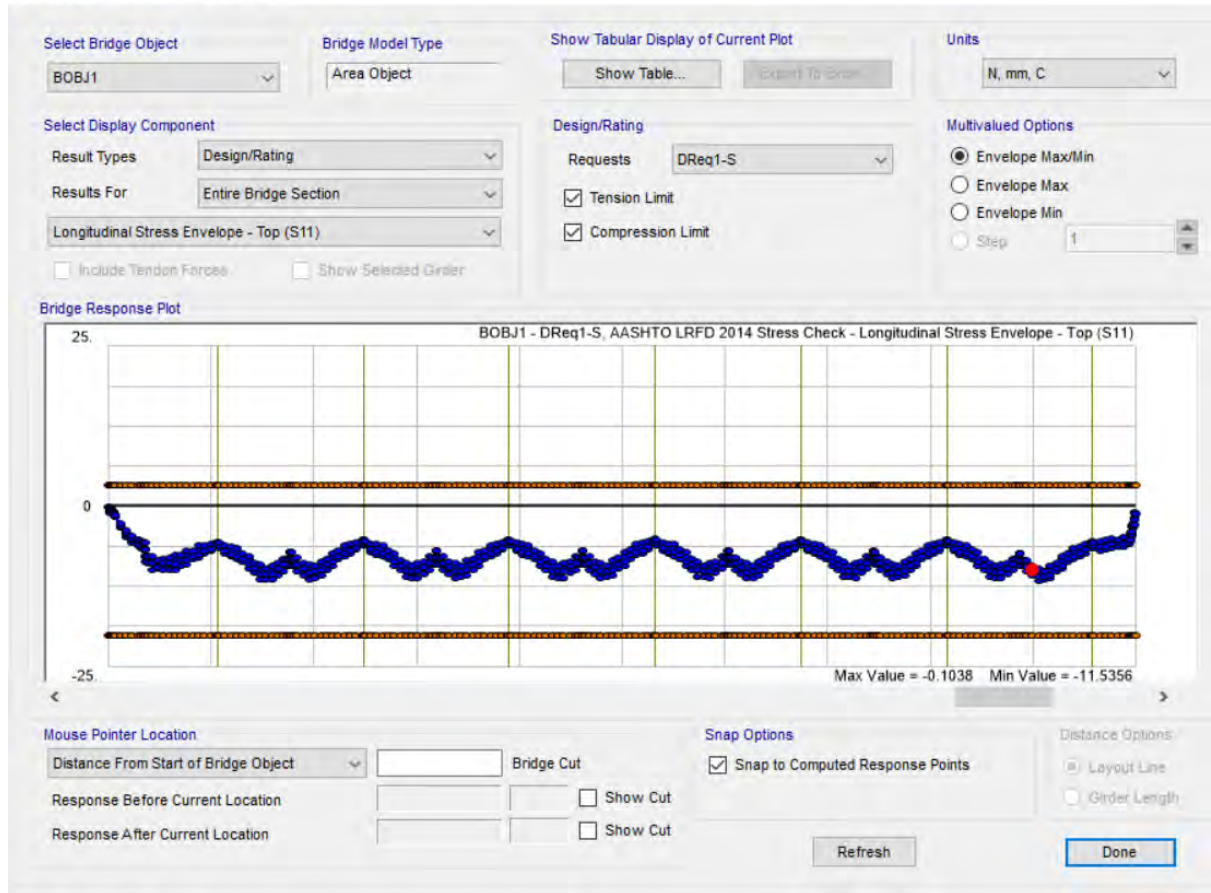


Figure 5.30: Top longitudinal stress capacity check (100 m)

For Top,

$$\text{Tensile Stress Limit} = 0.5\sqrt{f'_c}(\text{MPa}) = 0.5\sqrt{44.83} \text{ MPa} = 3.34 \text{ MPa}$$

$$\text{Maximum Tensile Stress} = 0 \text{ MPa}$$

$$\text{Compressive Stress Limit} = 0.45 f'_c (\text{MPa}) = 0.45 \times 44.83 \text{ MPa} = 20.16 \text{ MPa}$$

$$\text{Maximum Compressive Stress} = 11.54 \text{ MPa}$$

For 75 m Span, flexural capacity is done according to AASHTO LRFD (2014) provision as shown in **Figure 5.31**.

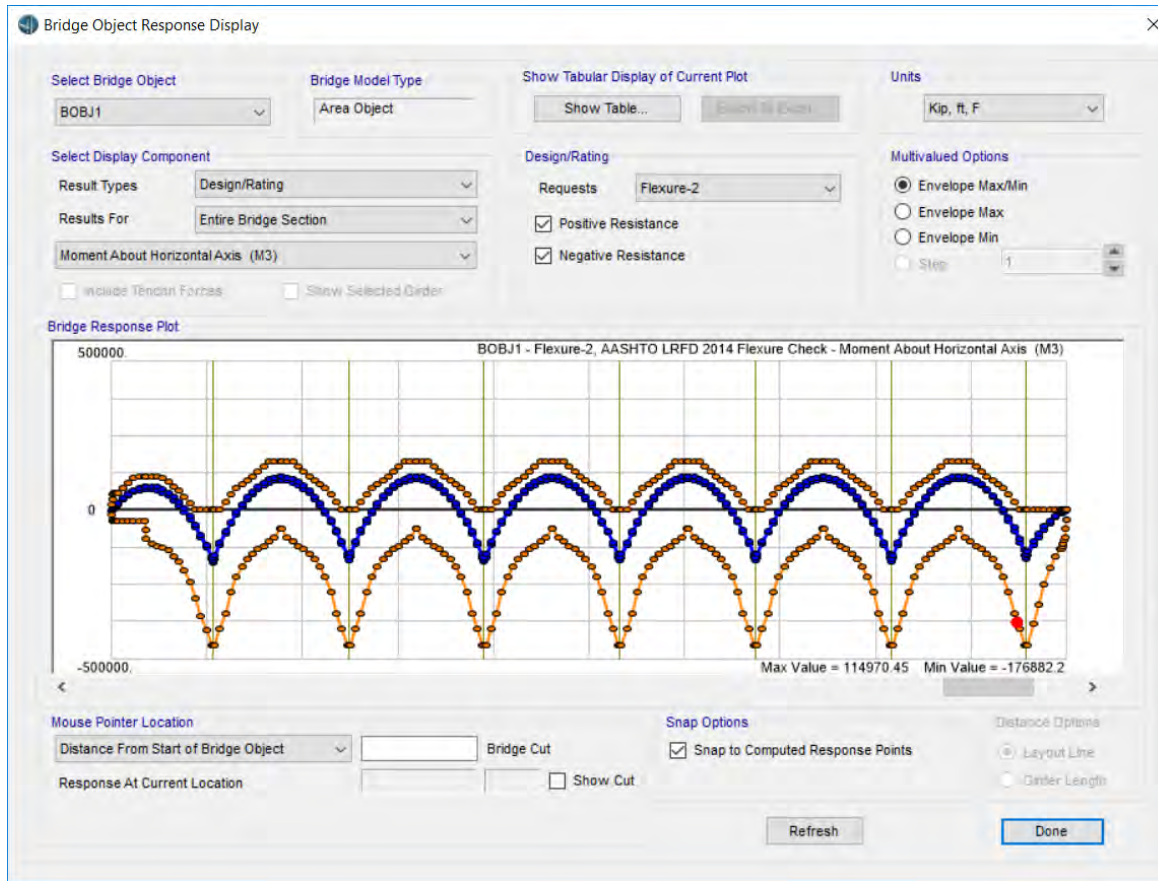


Figure 5.31: Flexural capacity check according AASHTO LRFD,2014 (75 m)

Maximum induced Positive Moment = 1,14,970.00 Kip-ft

Maximum Positive Moment Capacity = 1, 65,047.00 Kip-ft

Maximum induced Negative Moment = 1,76,882.00 Kip-ft

Maximum Negative Moment Capacity = 456567.00 Kip-ft

Stress capacity check is also important for design in extreme event I. Bottom and top stress check is shown in **Figure 5.32** and **Figure 5.33** respectively for 75m bridge.

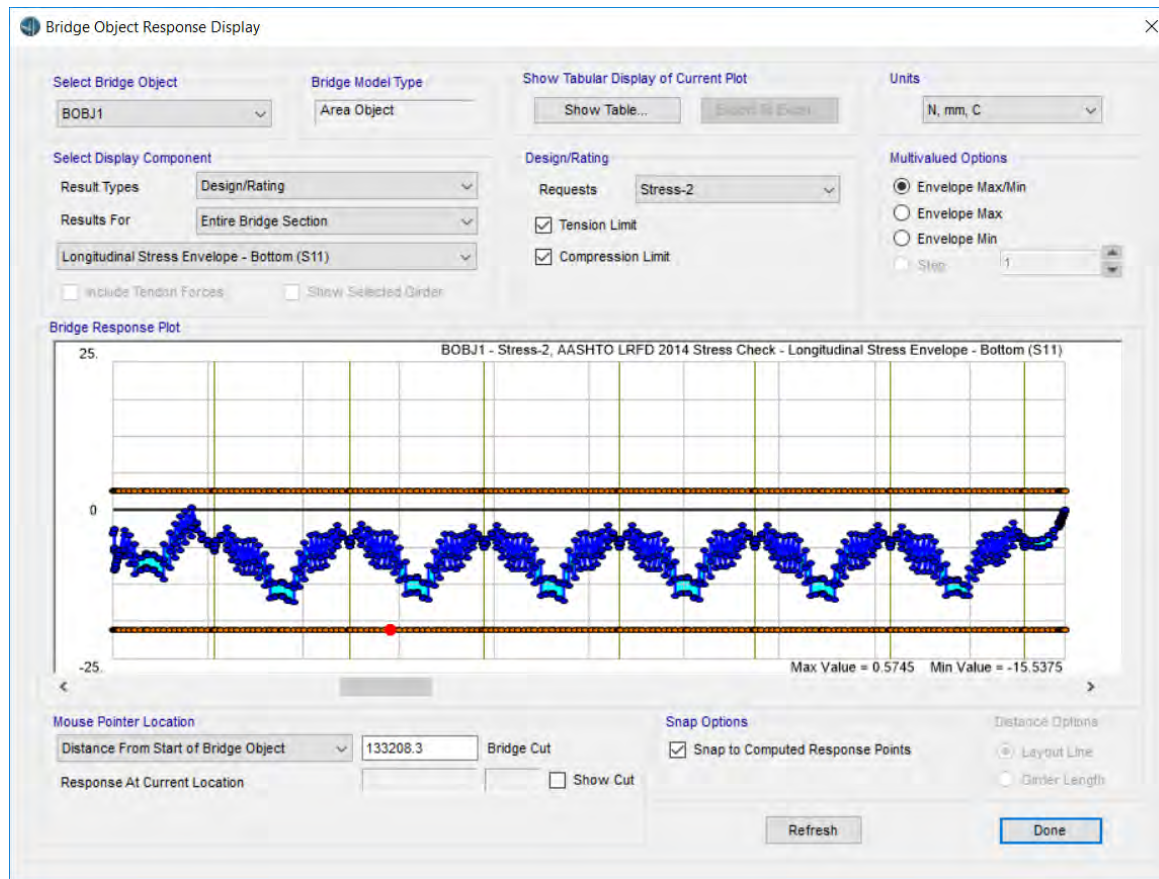


Figure 5.32: Bottom longitudinal stress capacity check (75 m)

Bottom Longitudinal Stress,

$$\text{Tensile Stress Limit} = 0.5\sqrt{f'_c}(\text{MPa}) = 0.5\sqrt{44.83} \text{ MPa} = 3.34 \text{ MPa}$$

$$\text{Maximum Tensile Stress} = 0 \text{ MPa}$$

$$\text{Compressive Stress Limit} = 0.45 f'_c (\text{MPa}) = 0.45 \times 44.83 \text{ MPa} = 20.16 \text{ MPa}$$

$$\text{Maximum Compressive Stress} = 15.54 \text{ MPa}$$

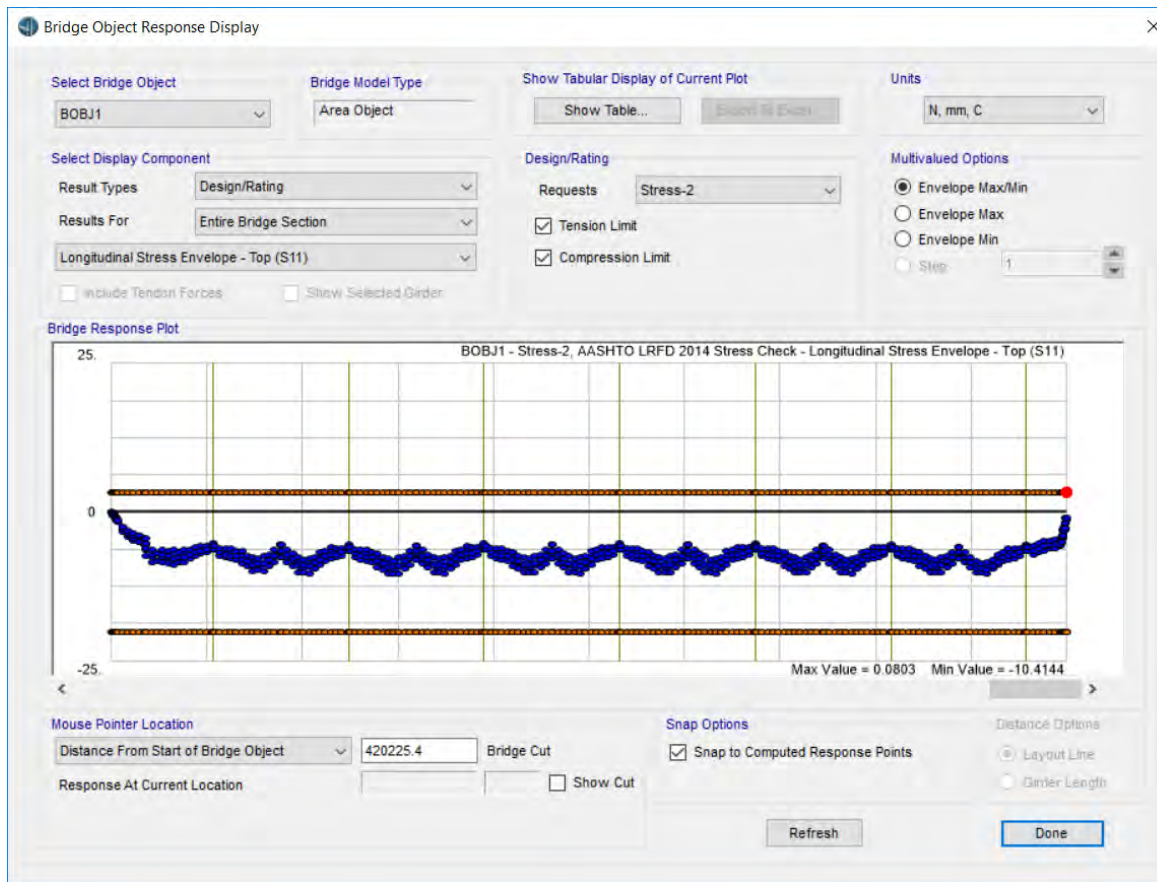


Figure 5.33: Top longitudinal Stress capacity check (75 m)

Top Longitudinal Stress,

$$\text{Tensile Stress Limit} = 0.5\sqrt{f'_c}(\text{MPa}) = 0.5\sqrt{44.83} \text{ MPa} = 3.34 \text{ MPa}$$

$$\text{Maximum Tensile Stress} = 0 \text{ MPa}$$

$$\text{Compressive Stress Limit} = 0.45 f'_c (\text{MPa}) = 0.45 \times 44.83 \text{ MPa} = 20.16 \text{ MPa}$$

$$\text{Maximum Compressive Stress} = 10.41 \text{ MPa}$$

For 125 m Span, flexural capacity is done according to AASHTO LRFD (2014) provision as shown in **Figure 5.34**.

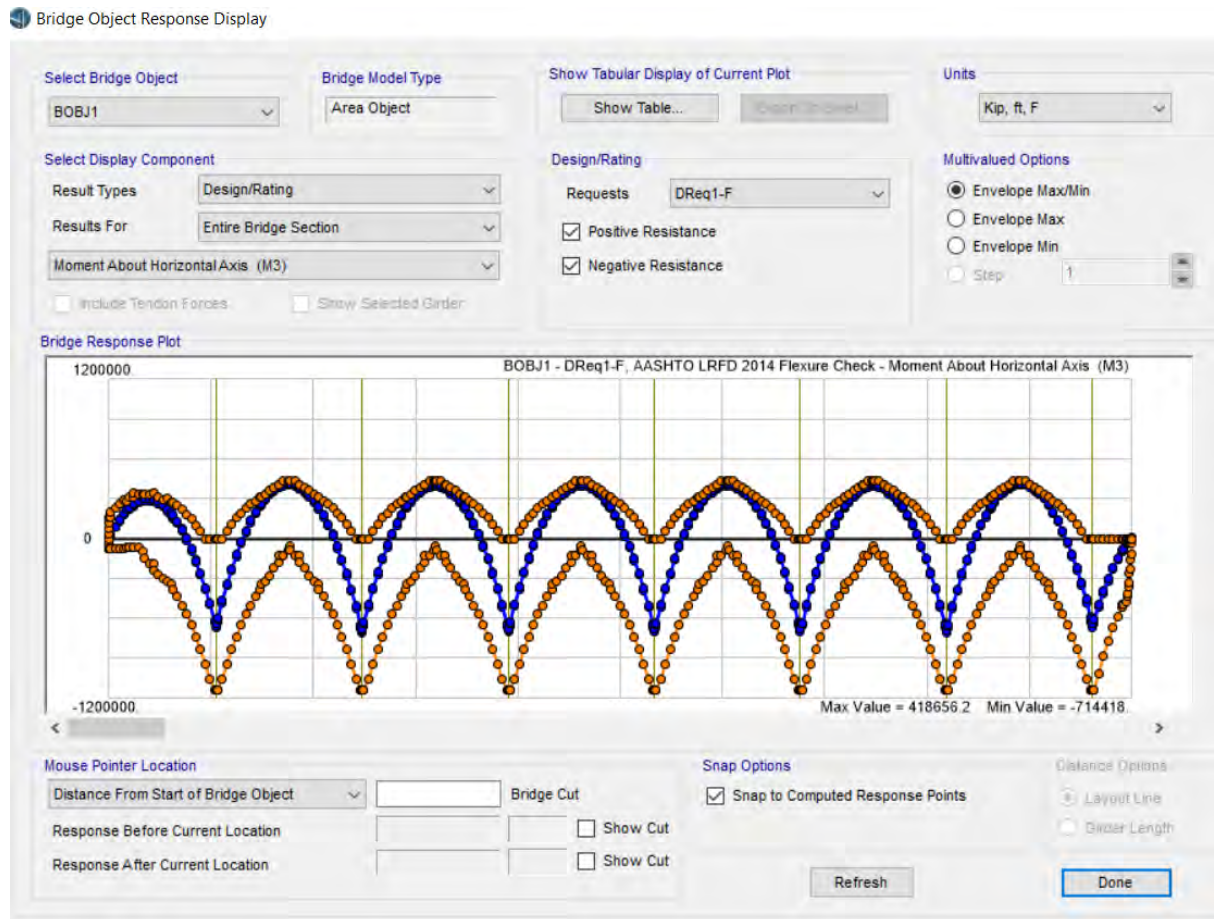


Figure 5.34: Flexural capacity check according AASHTO LRFD,2014 (125 m)

Maximum induced Positive Moment = 4, 18,656.00 Kip-ft

Maximum Positive Moment Capacity = 4,50,000.00 Kip-ft

Maximum induced Negative Moment = 7,14,418.00 Kip-ft

Maximum Negative Moment Capacity = 11,41,758.00 Kip-ft

Stress capacity check is also important for design in extreme event I. Bottom and top stress check is shown in **Figure 5.35** and **Figure 5.36** respectively for 75m bridge.

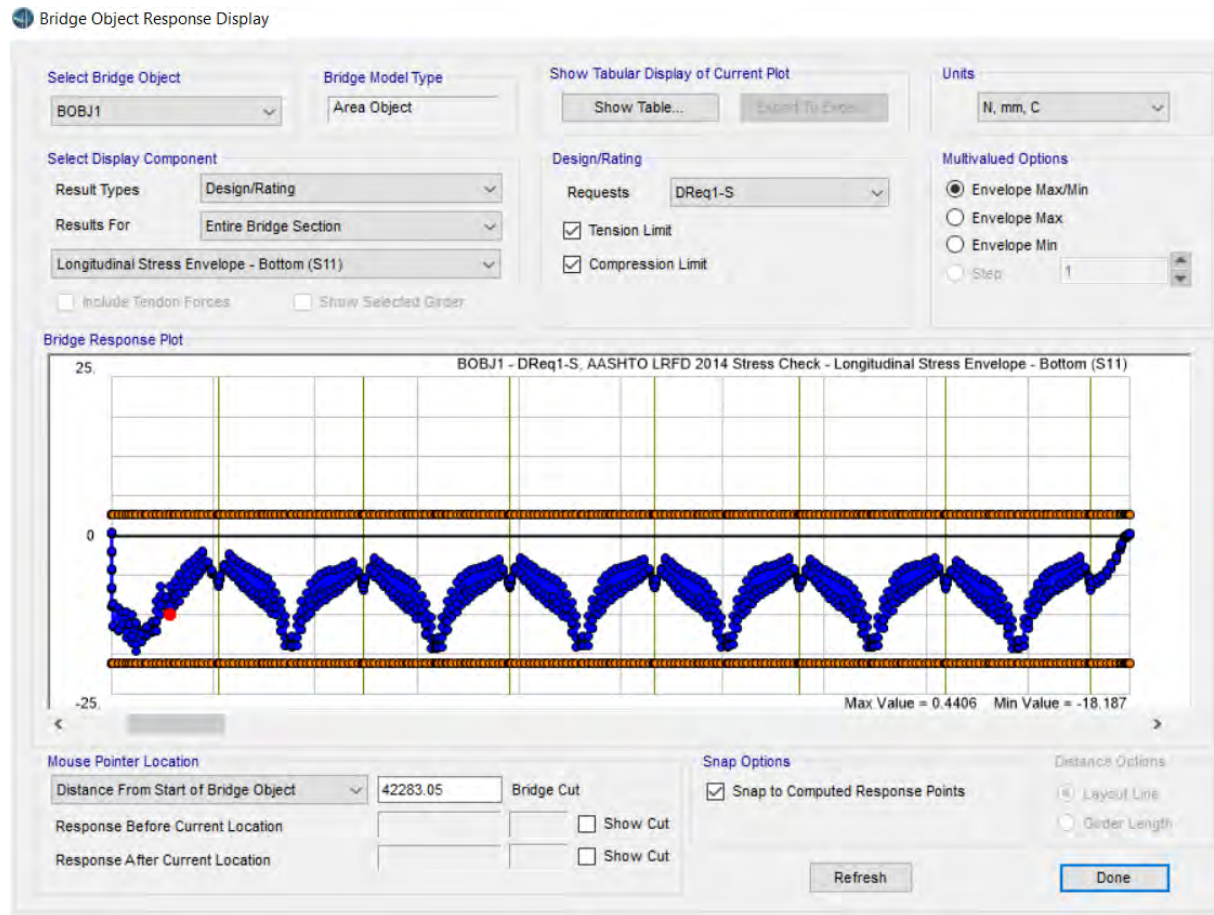


Figure 5.35: Bottom longitudinal stress capacity check (125 m)

Bottom Longitudinal Stress

$$\text{Tensile Stress Limit} = 0.5\sqrt{f'_c}(\text{MPa}) = 0.5\sqrt{44.83} \text{ MPa} = 3.34 \text{ MPa}$$

Maximum Tensile Stress = 0 MPa

$$\text{Compressive Stress Limit} = 0.45 f'_c (\text{MPa}) = 0.45 \times 44.83 \text{ MPa} = 20.16 \text{ MPa}$$

Maximum Compressive Stress = 18.19 MPa

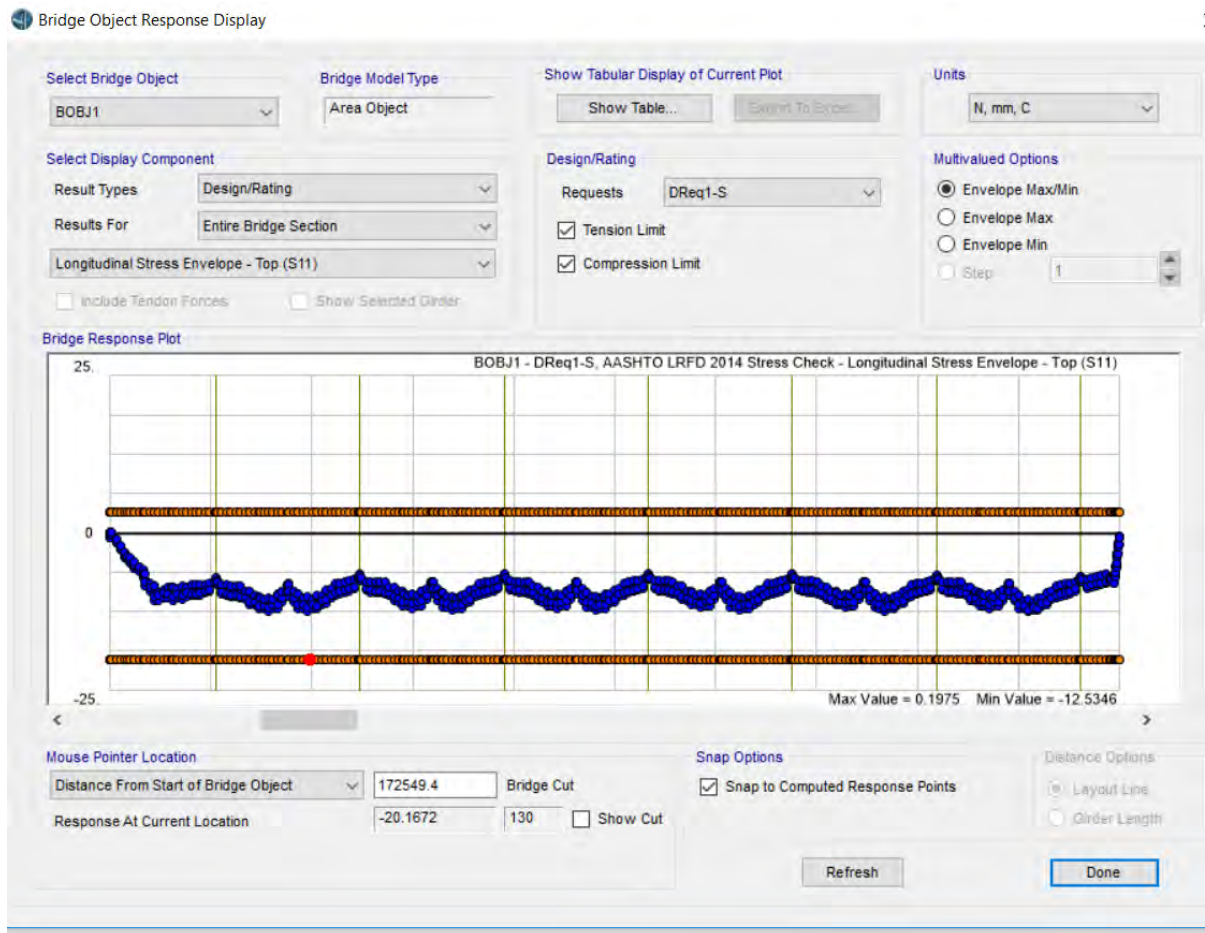


Figure 5.36: Top longitudinal stress capacity check (125 m)

Top Longitudinal Stress

$$\text{Tensile Stress Limit} = 0.5\sqrt{f'_c}(\text{MPa}) = 0.5\sqrt{44.83} \text{ MPa} = 3.34 \text{ MPa}$$

Maximum Tensile Stress = 0 MPa

$$\text{Compressive Stress Limit} = 0.45 f'_c (\text{MPa}) = 0.45 \times 44.83 \text{ MPa} = 20.16 \text{ MPa}$$

Maximum Compressive Stress = 12.53 MPa

Chapter 6

CONCLUSIONS AND RECOMMENDATIONS

The main objective of the present study is to observe the response of three box girder bridge model due synchronous and asynchronous motion.

6.1 Conclusions

Findings of the present study are summarized in the following:

- i. When data from Bangabandhu bridge is applied as seismic loading with scale factor, displacement in longitudinal, transverse and vertical direction are studied for all three bridge span modules. longitudinal displacement is same in magnitude throughout the bridge Which means full box girder system is longitudinally displaced with same magnitude. Synchronous motion governs in longitudinal displacement for all bridge modules. For transverse displacement, synchronous motion governs for all the load cases. However, asynchronous 0.2s motion is close to synchronous motion in all cases except load case 4. For vertical displacement, asynchronous 0.5s motion governs for all bridge modules. For 100m and 125m module asynchronous 0.5s motion is 7.5 times of synchronous motion. However, for 75m module asynchronous motion 13 times of synchronous motion. Displacement in all three directions are found to be insignificant for this seismic loading condition.
- ii. When El-Centro earthquake data is applied, asynchronous 0.01s motion governs in longitudinal displacement for 100m and 125 span modules. However, for 75m module, synchronous motion governs. In case of transverse displacement, asynchronous 0.1s motion governs for 100m module. However, for 75m and 125m module asynchronous 0.01s motion governs. For vertical displacement, asynchronous motion 1.0s governs in 100m and 125m modules. Asynchronous 1.0s motion is 3 and 2.4 times of synchronous motion for 100m and 125m module respectively. For However, for 75m module, asynchronous 0.5s motion governs. Asynchronous 0.5s motion is 5 times of synchronous motion. Displacement is found to be close to displacement capacity of seismic isolators (100m span module) for El-Centro Earthquake data input.
- iii. Both data from Bangabandhu bridge and El-Centro earthquake are scaled such way that peak ground acceleration for both cases are 0.47g (design PGA for seismic isolation system). Even though, Bangabandhu bridge data shows insignificant

displacement, El-Centro input shows magnified displacement. This is because predominant frequency of El-Centro earthquake is closer to modal frequency of three span modules compared to data from Bangabandhu bridge.

- iv. Considering asynchronous effect with damping properties of seismic devices, the design of bridge modules (75m, 100m and 125m span module) has been checked for Extreme Event I from data of Bangabandhu bridge. It is found that top and bottom stresses are within allowable limit. Flexural capacity is also within the limit.
- v. As 100m bridge is similar to that of a 7-span module of Jamuna multipurpose bridge, it can be seen that present bearings are essential for proper functioning of the bridge during seismic event. In case of seismic isolation malfunction, displacement due to asynchronous motion will significantly exceed allowable displacement. Thus, maintenance of the bearings is critical for the seismic performance of Jamuna Multipurpose bridge.

6.2 Recommendations

- i. In the study, the design is only for straight concrete box Girder Bridge. Curved Bridge can be used for future study.
- ii. Response can be also studied for bridge with different bearing properties.
- iii. Future studies can include span higher than 125m.
- iv. Correlation between various earthquake data and dynamic properties can be made for future study.
- v. As bearing properties play a major role in seismic response, Provision for conducting asynchronous analysis with bearing properties can be studied further.

REFERENCES

- Ali, M.H. and Choudhury, J.R. (1992) "Tectonics and earthquake Occurrence in Bangladesh", Paper presented at 36th Annual Convention of the Institution of Engineers, Dhaka.
- Ali, M.H. and Choudhury, J.R. (1994) "Seismic Zoning of Bangladesh" Paper presented at the International Seminar on Recent Developments in Earthquake disaster Mitigation, Institute of Engineers, Dhaka.
- American Association of state Highway and Transportation Officials (AASHTO) (2002) "Standard Specifications for Highway Bridges", 17th Edition, Washington, D.C.
- Ahsan. R, Hasan M. M. and Reza S. M. (2010), "Modal Analysis of The Jamuna Multi-Purpose Bridge Considering Soil-Structure Interaction" 3rd International Earthquake Symposium, Bangladesh, Dhaka, March.5-6 2010.
- Buckle I.G., (1996) "Overview of Seismic Design Methods for Bridges in Different Countries and Future Directions". Eleventh World Conference on Earthquake Engineering. ISBN: 008-0428223.
- Burdette N.J., Elnashai A.S. A Lupoi and Sextos A.G. (2008);" Effect of Asynchronous Earthquake Motion on Complex Bridges I: Methodology and Input Motion". Journal of Bridge Engineering, Vol. 13, No. 2, ISSN 1084-0702/2008/2-158–165.
- BBA, (2019), "Bangabandhu Bridge." <http://www.bba.gov.bd/site/page/e938dadf-914c-4635-8f4c-1aa2316f3d6b/Bangabandhu-Bridge>. Last Accessed 12 February, 2019.
- Carnevale L., Imperatore S., Lavorato D., Nuti, C. G. Leoni and Tropeano G., (2012), Assessment of Seismic Behavior of R.C. Bridges under Asynchronous Motion and Comparison with Simplified Approaches"; Proceedings of the fifteenth world conference of earthquake engineering, Lisbon, Portugal.
- Castellano, M.G., Cestarollo, A. (1999), "Seismic isolation of the Jamuna multipurpose bridge", Transactions on the Built Environment vol-38, WIT Press, ISSN 1743-3509.
- Chen W.F and Duan, L., (2000) "Bridge Engineering Handbook", (Florida: CRC Press), 266-267.

Crewe. J.A, Norman. J.A.P, "Experimental Modelling of Multiple Support Excitation of Long Span Bridges". 4th International Conference on Earthquake Engineering Taipei, Taiwan, pg-127.

Department of the Environment (Merrison Committee of Inquiry) (1973). Inquiry into the Basis of Design and Method of Erection of Steel Box Girder Bridges. London.

EERI. (1990). "Lorna Prieta Earthquake Reconnaissance Report. II Earthquake Spectra, Special Supplement to Vol. 6.

EERI. (1995). "Northridge Earthquake Reconnaissance Report." Earthquake Spectra, Special Supplement to Vol. 11.

EERI. (1991). "Costa Rica Earthquake Reconnaissance Report." Earthquake Spectra, Special Supplement to vol.7.

EXCA, (2019). "Stolmasundet Bridge." <https://www.exca.eu/light-projects/2302/>. Last Accessed 10 February, 2019.

Fam, A. R., and Turkstra, C. J., (1975). "A finite element scheme for box bridge analysis." Comput. Struct. J., 5, 179-186.

FIP, (2019). "Vasoflon bearings." <https://www.fipindustriale.it/index.php?area=106&menu=30&page=145&lingua=1>. Last Accessed 19 February, 2019.

Fung, G. G., et al. (1971). "Field Investigation of Bridge Damage in the San Fernando Earthquake. II Technical Report, Bridge Department, Division of Highways, California Department of Transportation, Sacramento, California.

Gazi., A., (2009), "Structural Performance of Some Existing Bridges of Bangladesh Under Earthquake Load", "M.Sc. Dissertation, Bangladesh University of Engineering and Technology.

Monti, G., Nuti, C., and Pinto, E.P., (1996), " Nonlinear response of bridges under multisupport excitation", Journal of Structural Vol-122, Engineering, Pg-1147.

Mutsuddy. R. (2009), "Response of Curved Flyover Bridges Under Seismic Loading", M.Sc Dissertation, Bangladesh University of Engineering and Technology.

Mwafy A M., Kwon O.S., Elnashai A. and Hashash Y M. A. (2010), "Wave Passage and Ground Motion Incoherency Effects on Seismic Response of an Extended Bridge". Journal of Bridge Engineering, Vol. 16, Issue 3.

Man-Chung Tang, T. Y. Lin International China (2010), “The New Shibampo Bridge, Chongqing, China”, Technical Report, Structural Engineering International.

National Oceanic and Atmospheric Administration (NOAA), (2019) “Geologic Hazards Photos Volume 1: Earthquake Damage to Transportation Systems”.
ftp://ftp.ngdc.noaa.gov/hazards/cdroms/geohazards_v1/document/647004.htm.

Priestley, M. J. N., and Park R. (1984). Strength and Ductility of Bridge Substructures.” Bulletin No. 71, Road Research Unit, National Roads Board, Wellington, New Zealand.

Priestley, M. J. N., F. Seible, and G. MacRae. (1995). "The Kobe Earthquake of January 17, 1995: Initial Impressions from a Quick Reconnaissance." Report SSRP-95103, University of California, San Diego.

Rafik I. and Xin L. (2003), Effect of Retrofitting Application on Reinforced Concrete Bridges, Research Paper, Department of Civil and Environmental Engineering, Washington State University, USA.

Rahai. A and Arezoumandi. M. “Effect of Vertical Motion of Earthquake on RC Bridge Pier.” 14th World Conference on Earthquake Engineering, Beijing, China.

Ramadan, O. And Novak. M. (1993). "Simulation of Spatially Incoherent Random Ground Motions." Journal of Engineering Mechanics, ASCE, Vol 119(No. 5), 997-1016.

Rodriguez. S, (2004), “Design of Long Span Concrete Box Girder Bridges: Challenges and Solutions.” Structures Congress 2004, Nashville, Tennessee, United States.

Sarıtaş F. (2013), “Dynamic Responses of Bridges under Effects of Asynchronous and Multiple Support Excitations”. 2nd International Balkans Conference on Challenges of Civil Engineering, BCCCE, Epoka University, Tirana, Albania.

Sextos, A.G., Pitilakis, K.D., and Kappos, A.J. (2018), “Inelastic Dynamic Analysis of RC Bridges Accounting for Spatial Variability of Ground Motion, Site Effects and Soil-Structure Interaction Phenomena. Part 1: Methodology and Analytical Tools”, J. Earthquake Eng. and Struct. Dyn, 32: 607-627.

Shinozuka, M., and Zhang. R. (1996). "Equivalence between Kriging and CPDF Method for Conditional Simulation." Journal of Engineering Mechanics, ASCE, Vol 122(No. 6), 530-538.

- Siddique, S. (2006), "Seismic Performance Evaluation of Framed Buildings Designed as per Bangladesh National Building Code", M.Sc. Thesis, Department of Civil Engineering, BUET, Dhaka.
- Sisodiya, R. G., Cheung, Y. K., and Ghali, A. (1970). "Finite-element analysis of skew, curved box girder bridges." *Int. Assoc. Bridges Struct. Eng., (IABSE)*, 30(11), 191-199.
- Smith, D.A. and Hendy, C. R. (2002), "Strengthening of Irwell Valley Bridge, UK". *Bridge Engineering*. Institute of Civil Engineers. Page 33-41.
- Spanos, P. D., and M. P. Mignolet. (1990). "Simulation of Stationary Random Processes: Two-Stage MA to ARMA approach." *Journal of Engineering Mechanics, ASCE*, Vol.116 (No. 3), 620~641.
- Stanton, J.F., Roeder, C. W. and Campbell, T. I., (1993), " High Load Multi-Rotational Bridge Bearings", NCHRP Report 10-20A, Transportation Research Board, National Research Council, Washington, D.C.
- Taly, N., (2015), "Highway Bridge Superstructure Engineering: LRFD Approaches to Design and Analysis", New York: CRC Press.
- Tiliouine B. and Ouanani., M., (2012) "3-D Nonlinear Earthquake Response of R.C. Box Girder Bridges with Expansion Joints and Bearing Devices"; Proceedings of the fifteenth world conference of earthquake engineering Lisbon, Portugal.
- Tzanetos, N., Elnashai, A.S., Hamdan, F.H. and Antoniou S., (2000)," Inelastic Dynamic Response of RC Bridges subjected to Spatial Non-Synchronous Earthquake Motion", *Advances in Structural Engineering* Vol. 3, Pg-191.
- Wald, D. J., Burdich L. J. and Somerville. P. G. (1988), "Simulation of Acceleration Time Histories Close to Large Earthquakes". II Proc., *Earthquake Engineering and Soil Dynamics II-Recent Advances in Ground Motion Evaluation*, J. L. V. Thun, ed., ASCE, New York.
- Wang J., (2003) "Analysis of the Seismic Response of Highway Bridges to Multiple Support Excitation," Ph.D. Dissertation. University of Canterbury.

Vehicular Loads

Load Length Type	Minimum Distance	Maximum Distance	Uniform Load	Uniform Width Type	Uniform Width	Axle Load	Axle Width Type	Axle Width
Leading Load	Infinite		0.	Fixed Width	1.	0.4	Two Points	6.
Leading Load	Infinite		0.	Fixed Width	1.	0.4	Two Points	6.
Fixed Length	14.	30.	0.	Fixed Width	1.	1.6	Two Points	6.
Variable Length	14.	30.	0.	Fixed Width	1.	1.6	Two Points	6.

Floating Axle Loads

	Value	Width Type	Axle Width
For Lane Moments	0	One Point	0.0033
For Other Responses	0	One Point	0.0033

Floating Axle Load Scale Factor: 1

Double the Lane Moment Load when Calculating Negative Span Moments

Ignore Vertical Loads if Horizontal Centrifugal or Braking Loads are Defined

Superelevation Effects

Adjust Vertical Loads for Superelevation

Axle Load Factor: _____

Uniform Load Factor: _____

Figure. A.1: HSn-44 loading

Lane Loading

The screenshot shows a dialog box titled "Bridge Line Load Distribution Definition Data". It contains the following fields and settings:

- Load Name:** Lane1
- Units:** lb, ft, F
- Load Direction:**
 - Load Type: Force
 - Coordinate System: GLOBAL
 - Direction: Gravity
- Load Value:** Value: 640.
- Load Transverse Location:**
 - Reference Location: Left Edge of Deck
 - Load Distance from Reference Location: 13.8615
- Load Vertical Location:** Top Slab is Loaded at Midheight of its Thinnest Portion

Buttons: OK, Cancel

Figure. A.2: Lane loading for typical lane

Dead Load

Railing

The screenshot shows a dialog box titled "Bridge Line Load Distribution Definition Data". It contains the following fields and settings:

- Load Name:** Railing-C
- Units:** lb, ft, F
- Load Direction:**
 - Load Type: Force
 - Coordinate System: GLOBAL
 - Direction: Gravity
- Load Value:** Value: 300.
- Load Transverse Location:**
 - Reference Location: Left Edge of Deck
 - Load Distance from Reference Location: 30.3478
- Load Vertical Location:** Top Slab is Loaded at Midheight of its Thinnest Portion

Buttons: OK, Cancel

Figure. A.3: Typical load for railing

Wearing Course

Bridge Area Load Distribution Definition Data

Load Name: WC Units: lb, ft, F

Load Direction: Load Type: Force, Coordinate System: GLOBAL, Direction: Gravity

Load Value: Left Edge Value: 30., Right Edge Value: 30.

Load Transverse Location: Left Reference Location: Left Edge of Deck, Left Load Distance from Left Ref. Location: 7.874, Right Reference Location: Right Edge of Deck, Right Load Distance from Right Ref. Location: 7.874

Load Vertical Location: Top Slab is Loaded at Midheight of its Thinnest Portion

OK Cancel

Figure. A.4: Loading for wearing course

Appendix B 75 m Span Bridge Details

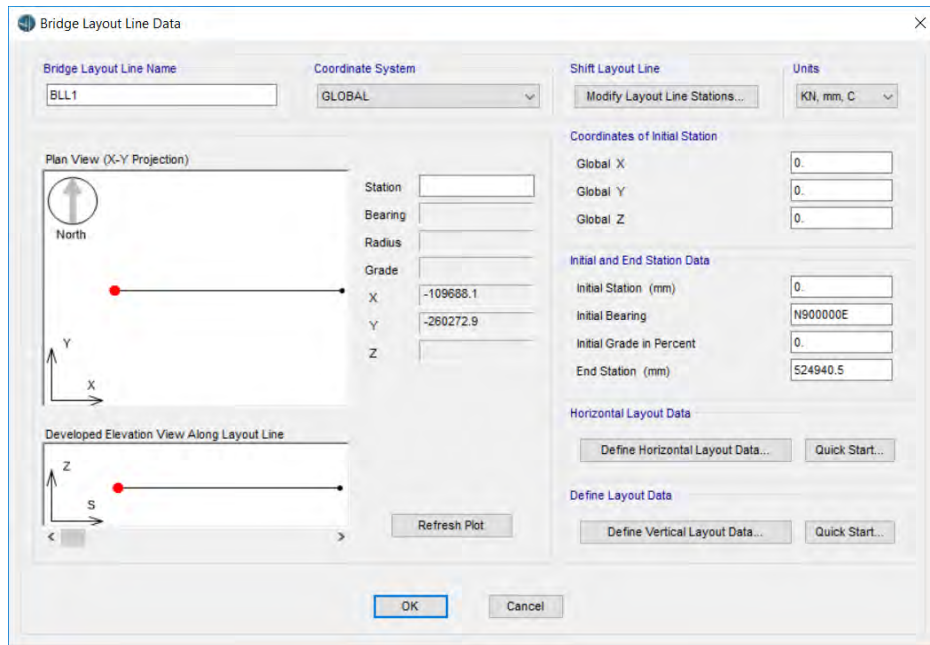


Figure. B.1: Bridge layout line

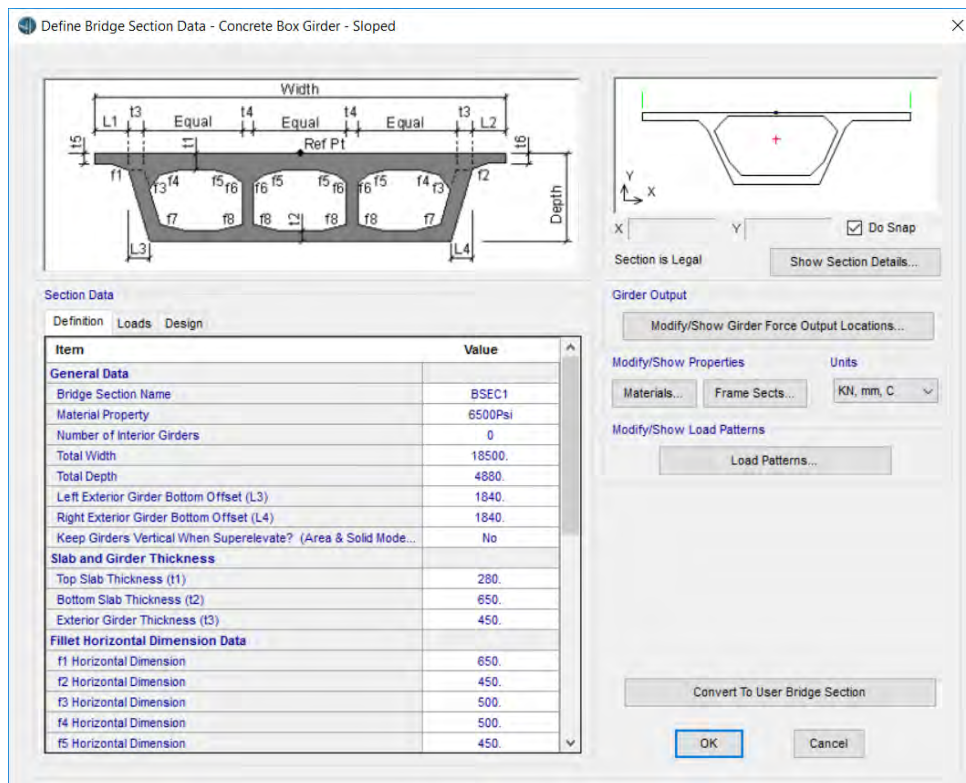


Figure. B.2: Girder section

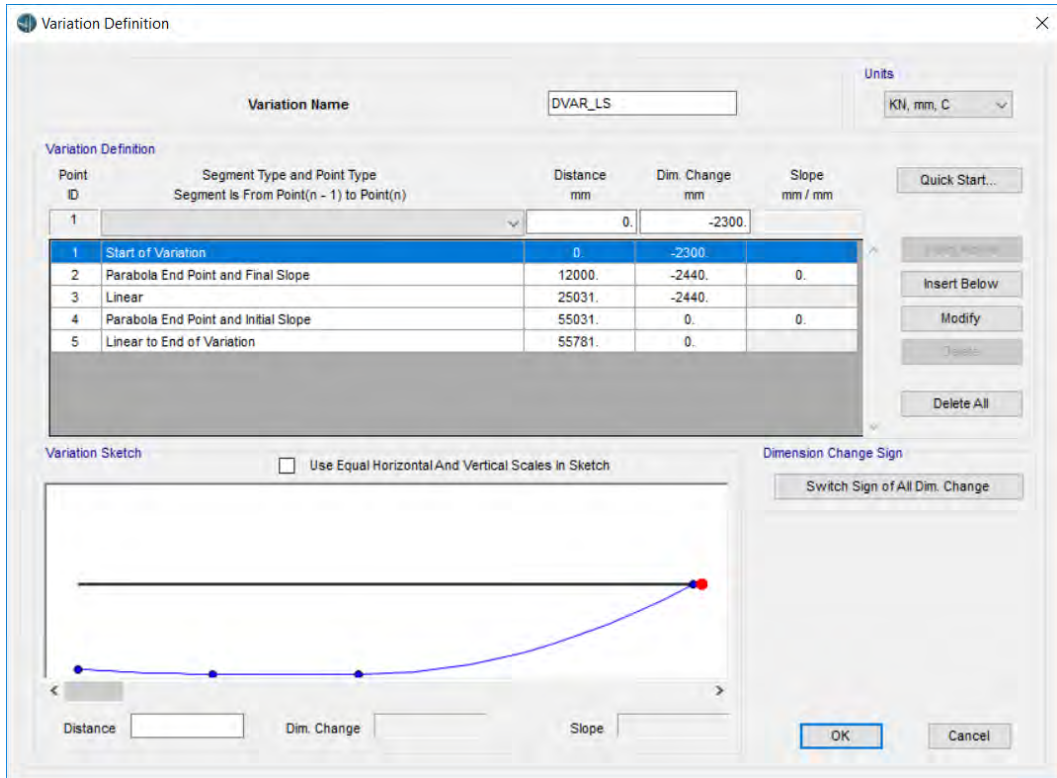


Figure. B.3: Depth variation of left segment

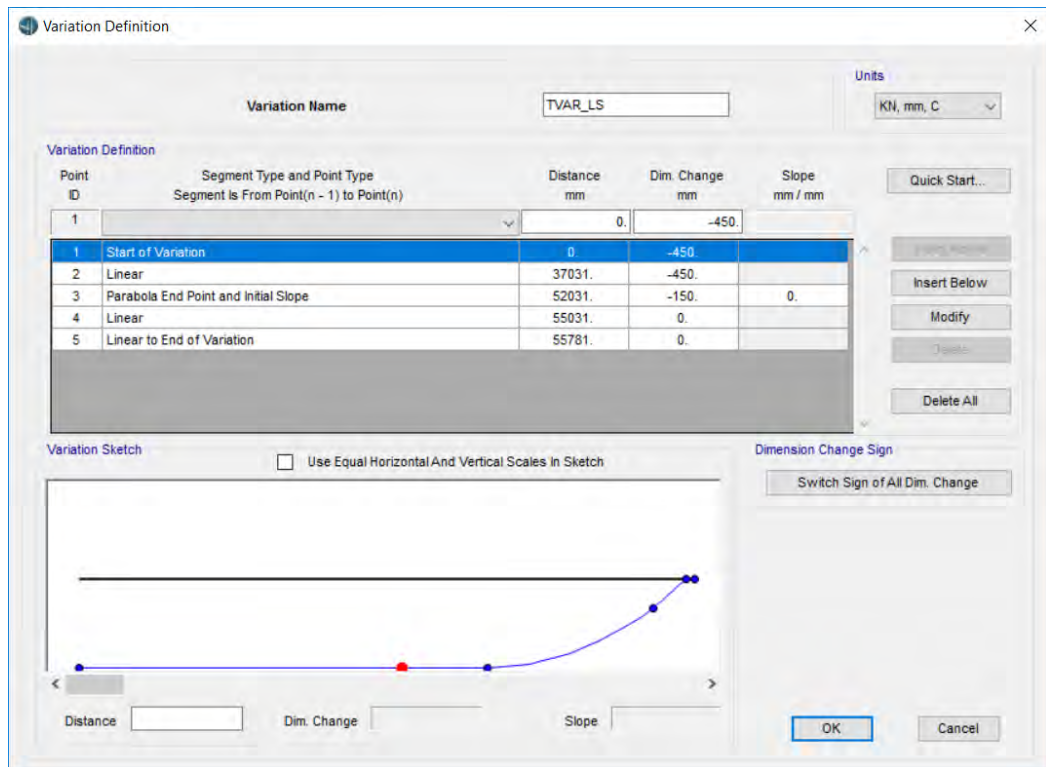


Figure. B.4: Bottom slab thickness variation at left segment

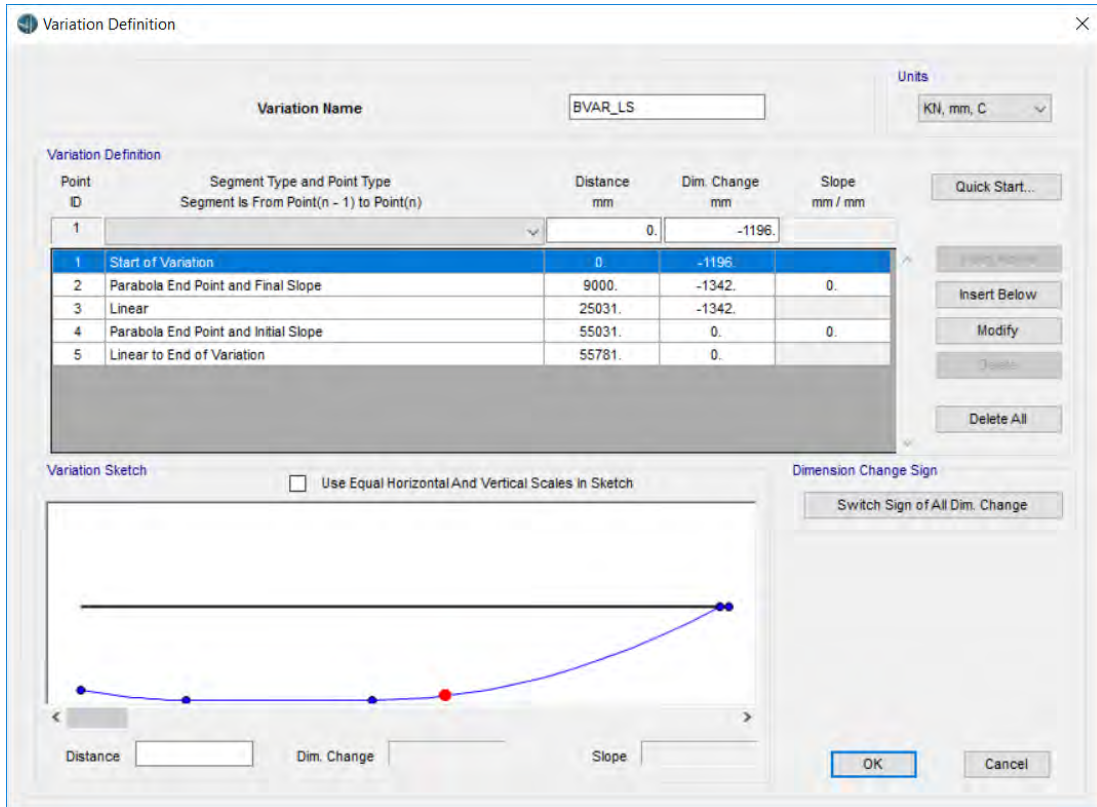


Figure. B.5: Cross section variation of left segment

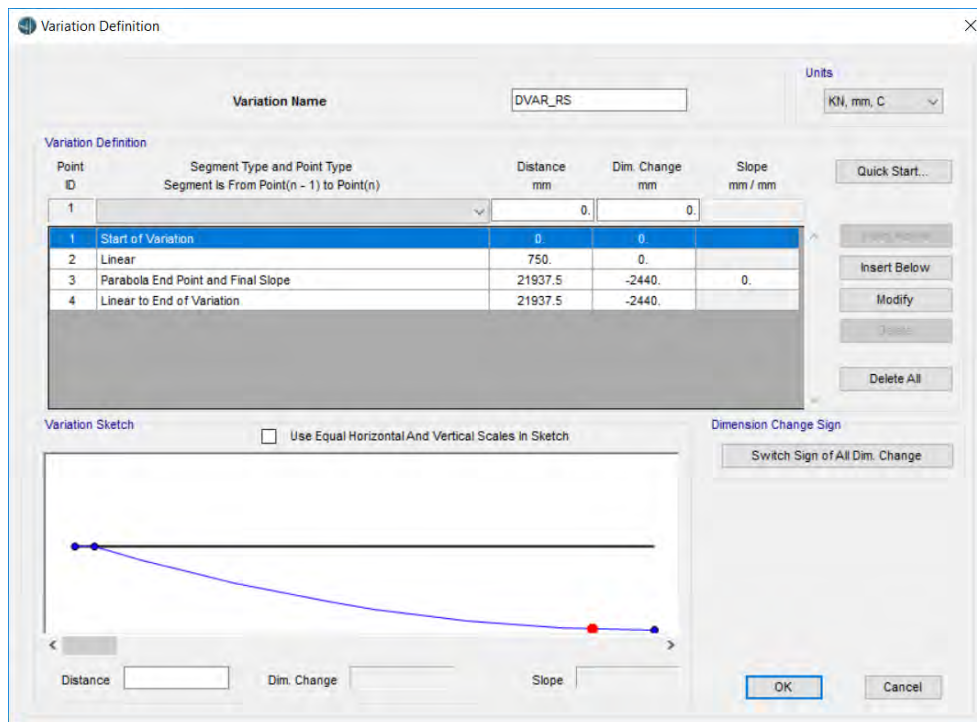


Figure. B.6: Section depth variation of right segment

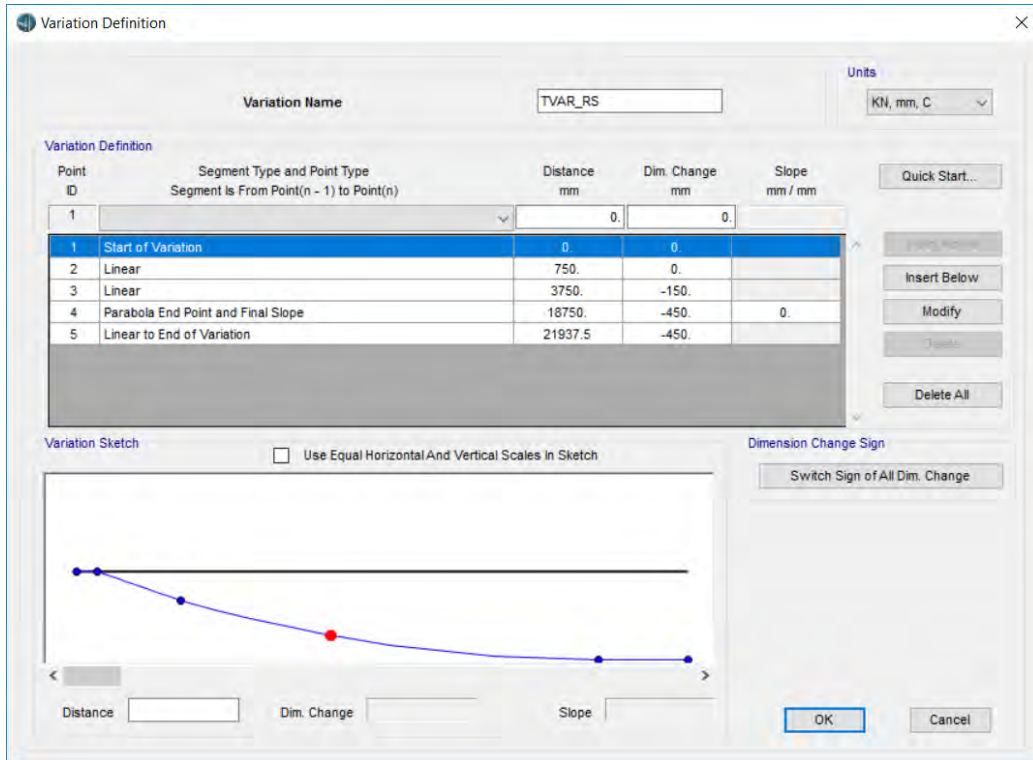


Figure. B.7: Bottom slab thickness variation of right segment

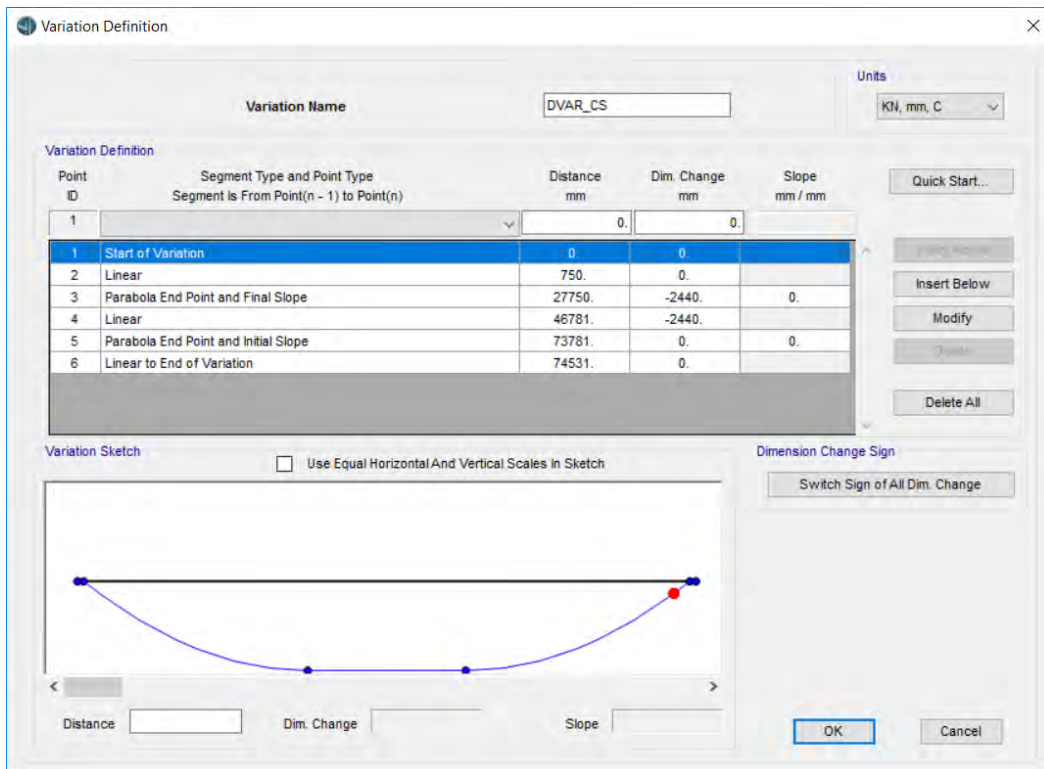


Figure. B.8: Section depth variation of typical segment

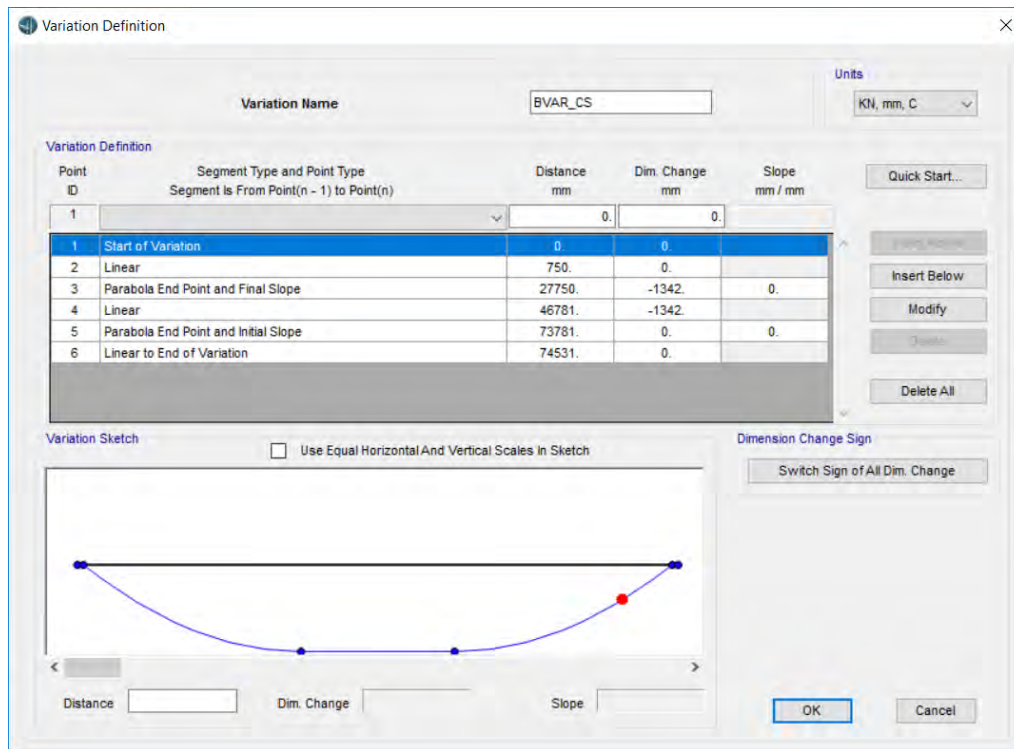


Figure. B.9: Girder width variation of typical segment

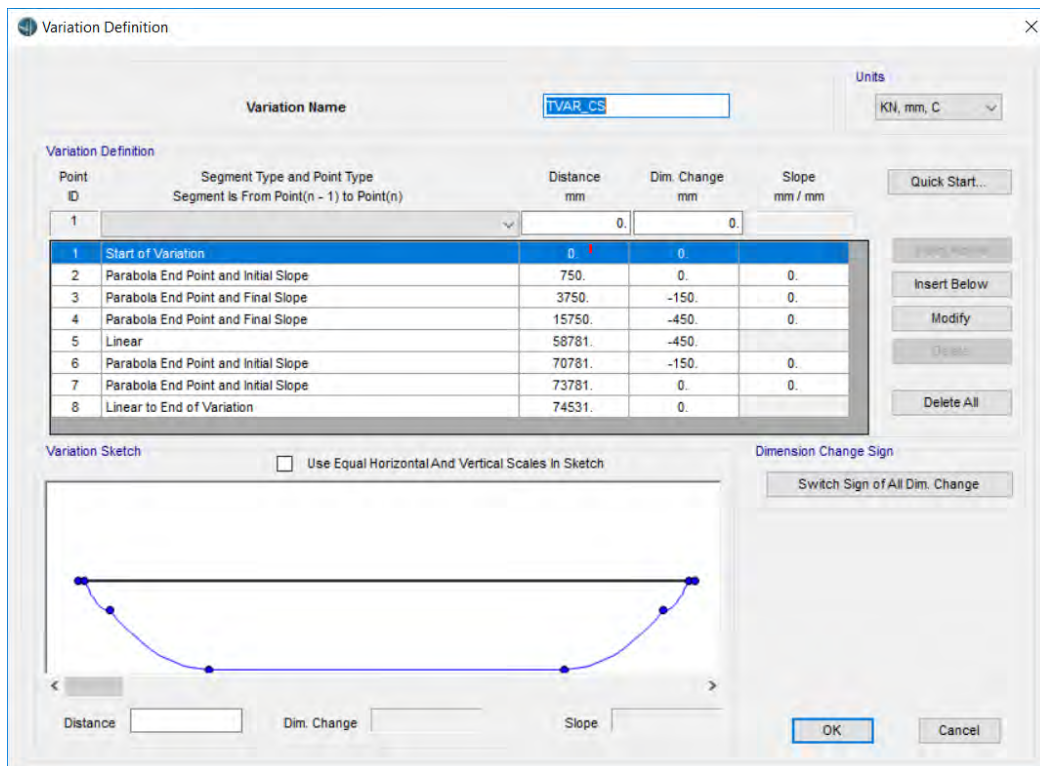


Figure. B.10: Bottom slab thickness variation of typical segment

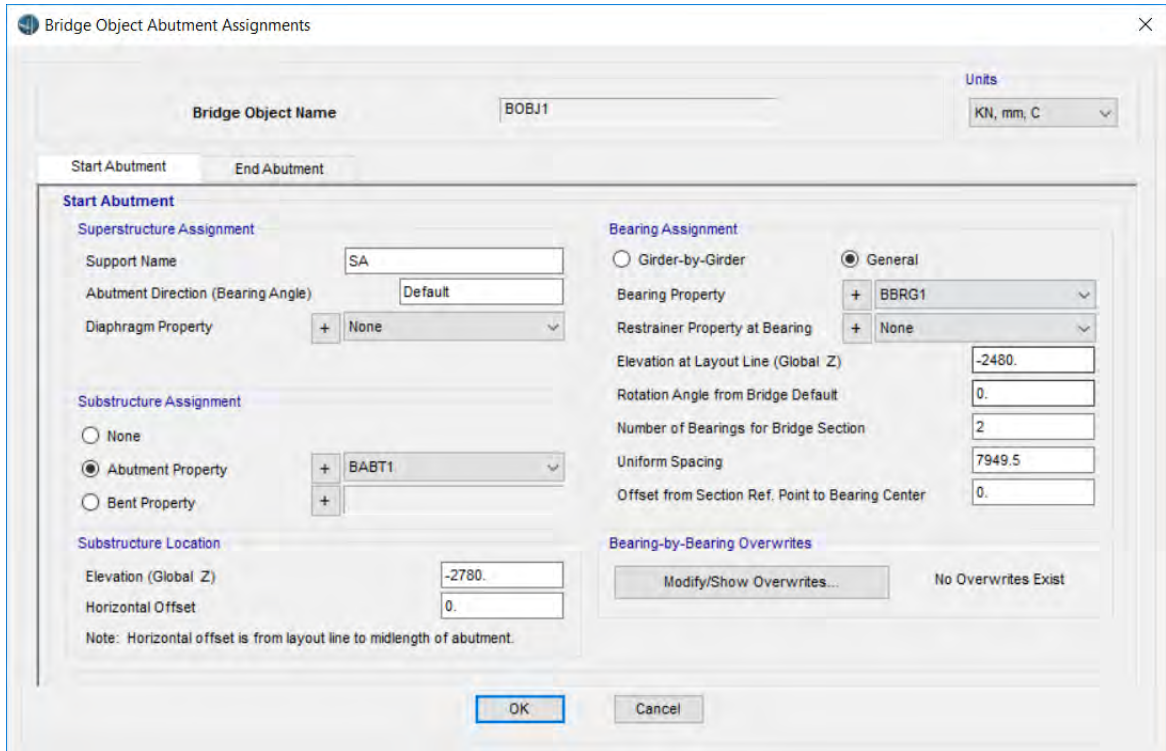


Figure. B.11: Start abutment

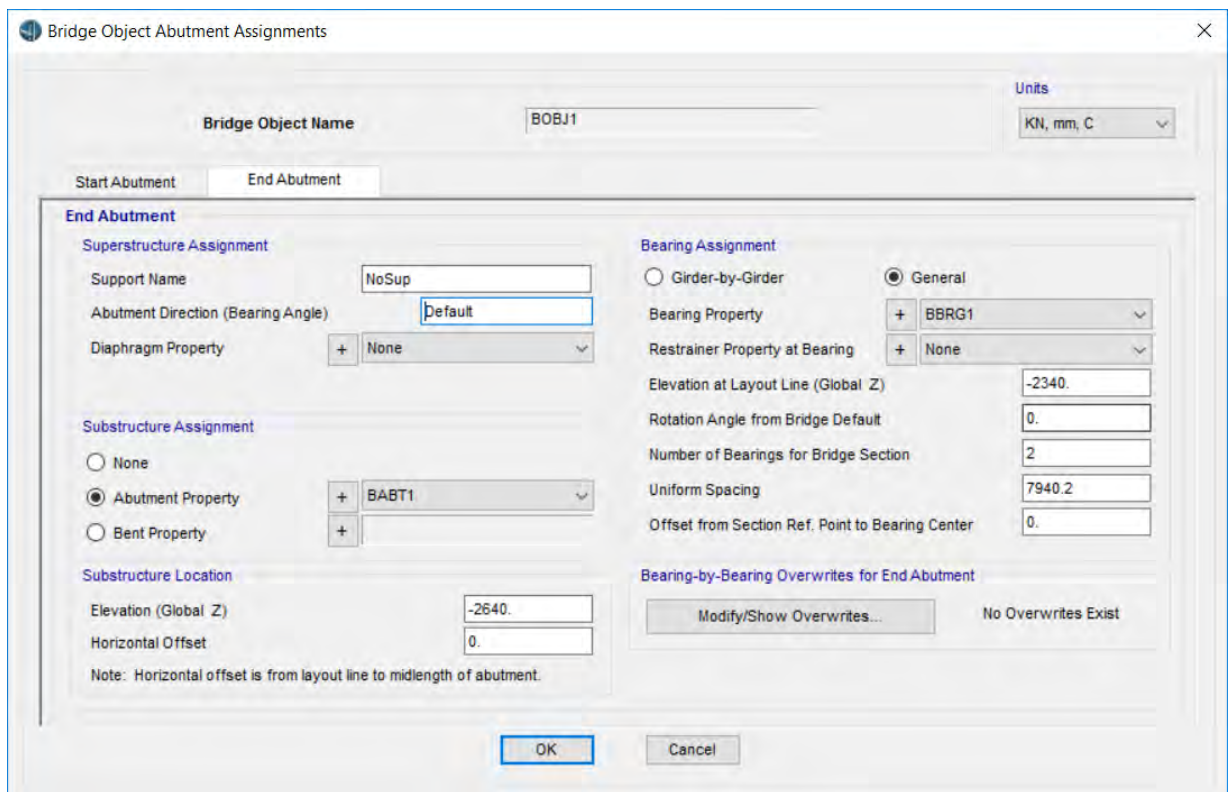


Figure. B.12: Start abutment

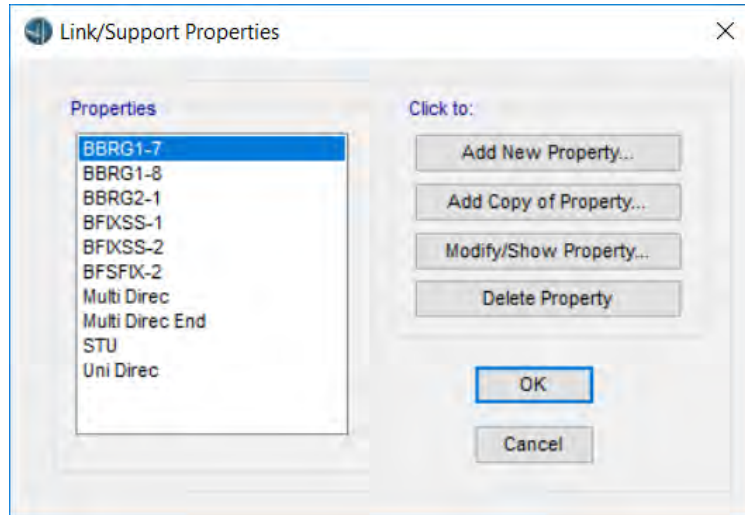


Figure. B.13: List of assigned seismic isolation

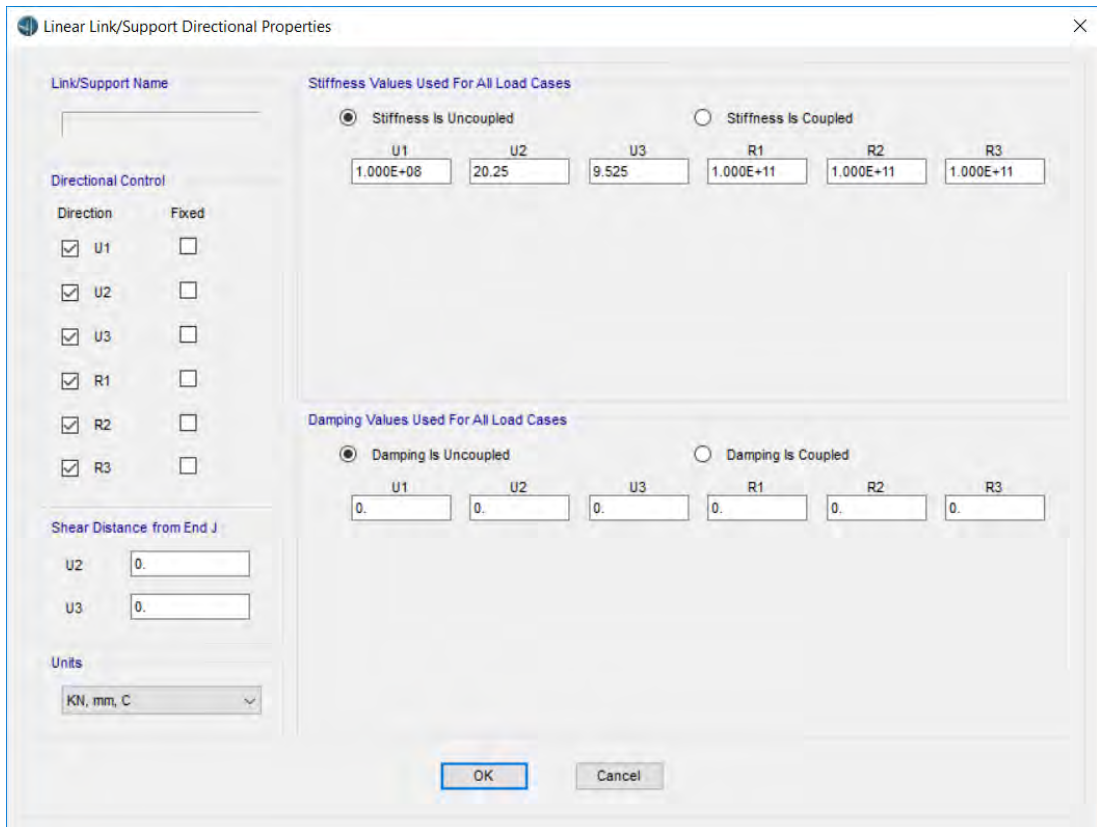


Figure. B.14: Typical multidirectional bearing

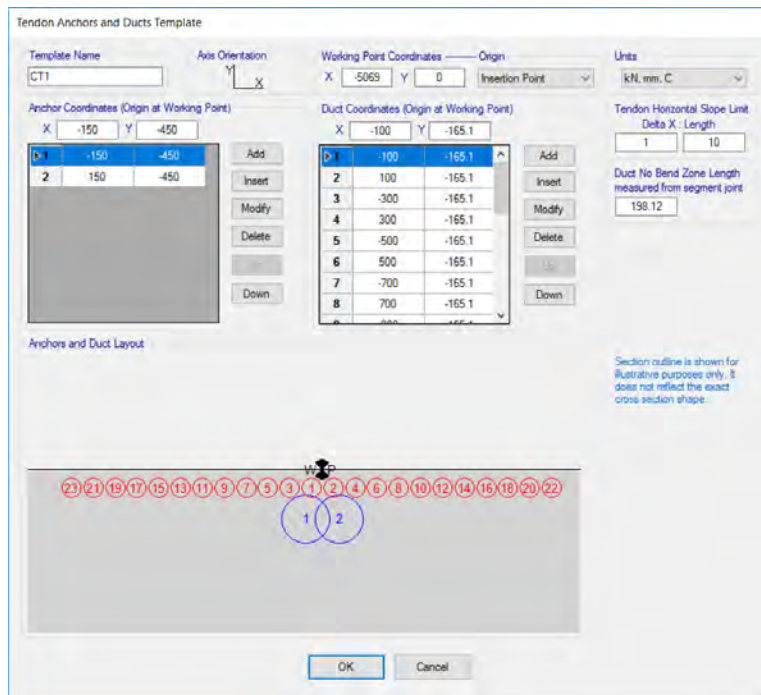


Figure. B.15: Cantilever tendon duct template layout

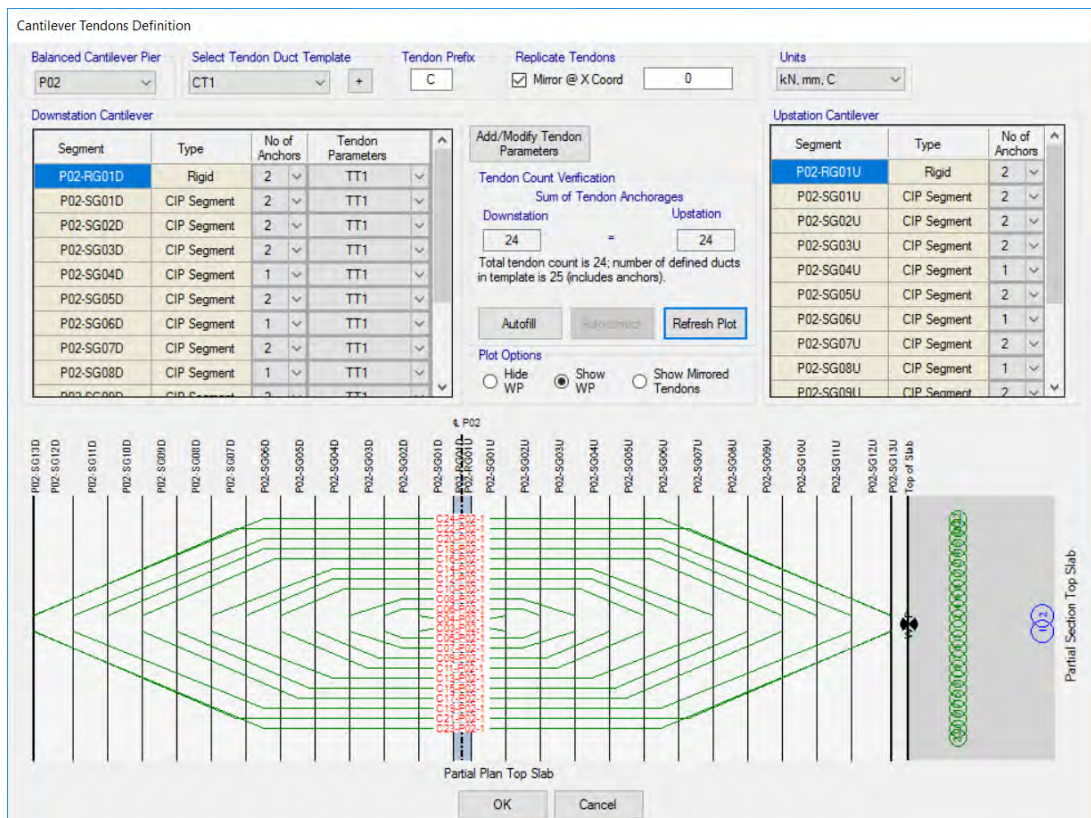


Figure. B.16: Cantilever tendon layout template

Tendon Parameters

Tendon Parameter Name: TT1 Units: kN, mm, C Tendon Load Pattern: + Prestress-T

Tendon Parameters

Prestress Type: Post Tension

Jack From: Start

Material Property: + A416Gr270

Tendon Area: + 3360

Based on Tendon Size: 1 Tnd(s) 0.6"-24

Max Discretization Length: 1000

Design Parameters

Bonding Type: Bonded

Duct Diameter: 100.1

Min Duct Bend Radius: 9144

Tendon Modeling Options

Model As Loads

Model As Elements

Load Type Tendon Load

Force Force (kN) Stress (kN/mm²)

Stress 3100 0.004788

Loss Parameters

Curvature Coefficient (Unitless): 0.15

Wobble Coefficient (1/mm): 6.5617E-07

Anchorage Set Slip (mm): 6.349

Other Loss Parameters

Elastic Shortening Stress (kN/mm²): 0.02068

Creep Stress (kN/mm²): 0.03447

Shrinkage Stress (kN/mm²): 0.04826


Steel Relaxation Stress (kN/mm²): 0.03447

When tendons are modeled as elements, the Other Loss Parameters (elastic, creep, shrinkage, and relaxation losses) apply in addition to the losses computed by analysis.

OK Cancel

Figure. B.17: Top cantilever tendon parameter (TT1)

Tendon Anchors and Ducts Template

Template Name: B2 Axis Orientation:  Working Point Origin: Bottom Left Corner Units: kN, mm, C

Anchor Coordinates (Origin at Working Point)

X	Y
400	350

Duct Coordinates (Origin at Working Point)

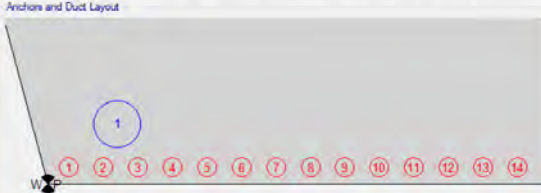
D	X	Y
1	120	99.06
2	320	99.06
3	520	99.06
4	720	99.06
5	920	99.06
6	1120	99.06
7	1320	99.06
8	1520	99.06

Tendon Horizontal Slope Limit

Delta X	Length
1	10

Duct No Bend Zone Length measured from segment joint: 198.12

Anchors and Duct Layout



Section outline is shown for illustrative purposes only. It does not reflect the exact cross section shape.

OK Cancel

Figure. B.18: Typical bottom tendon duct template layout

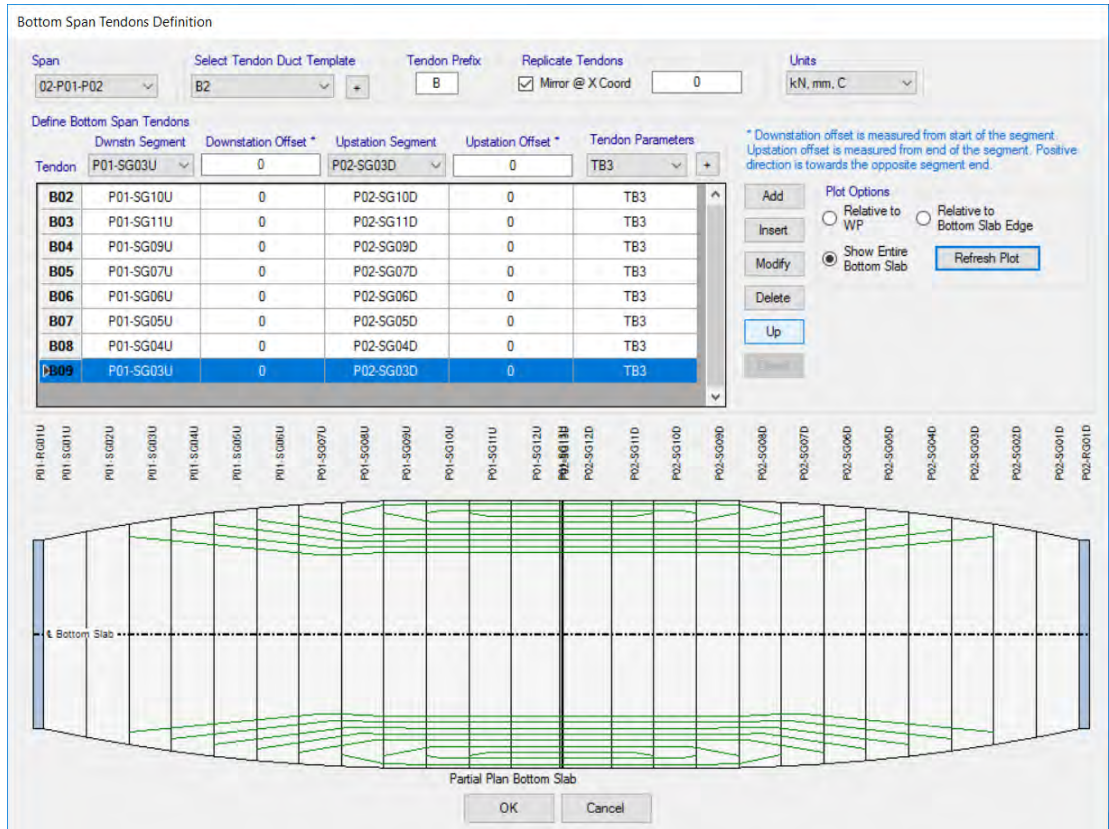


Figure. B.19: Typical bottom tendon layout template

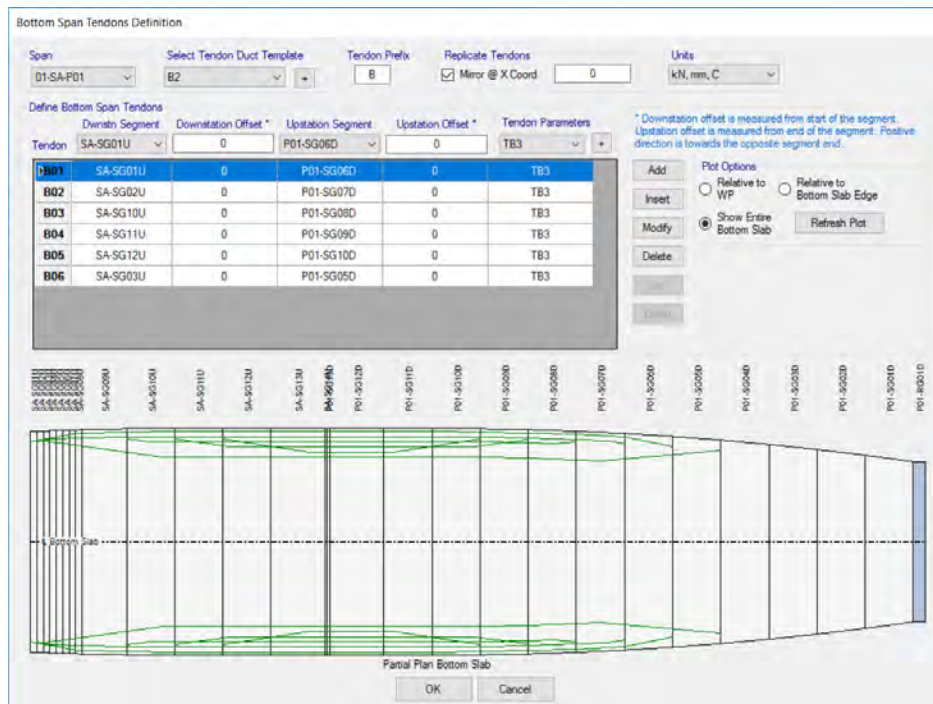


Figure. B.20: Left segment bottom tendon layout

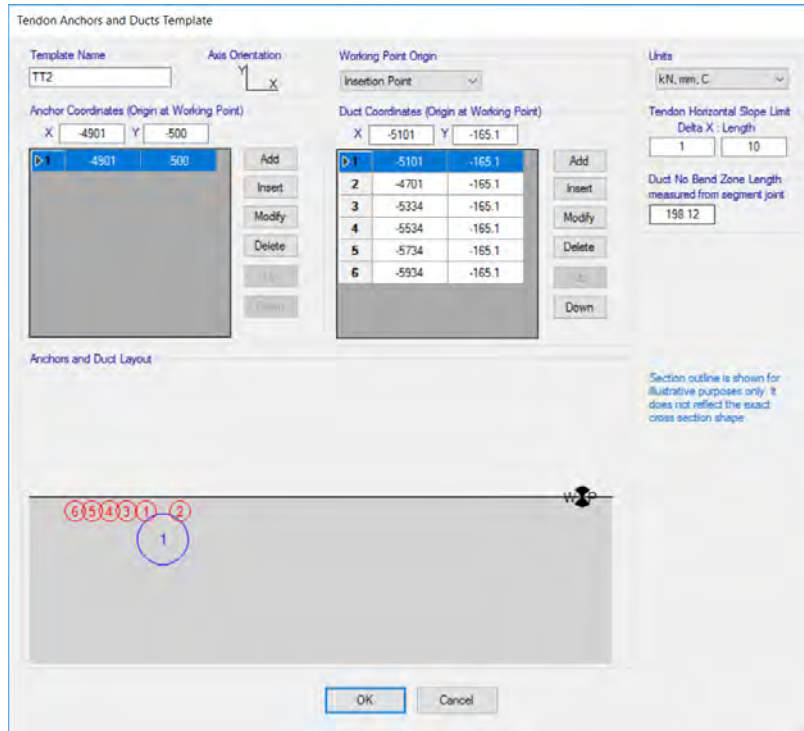


Figure. B.21: Left segment top tendon duct template layout

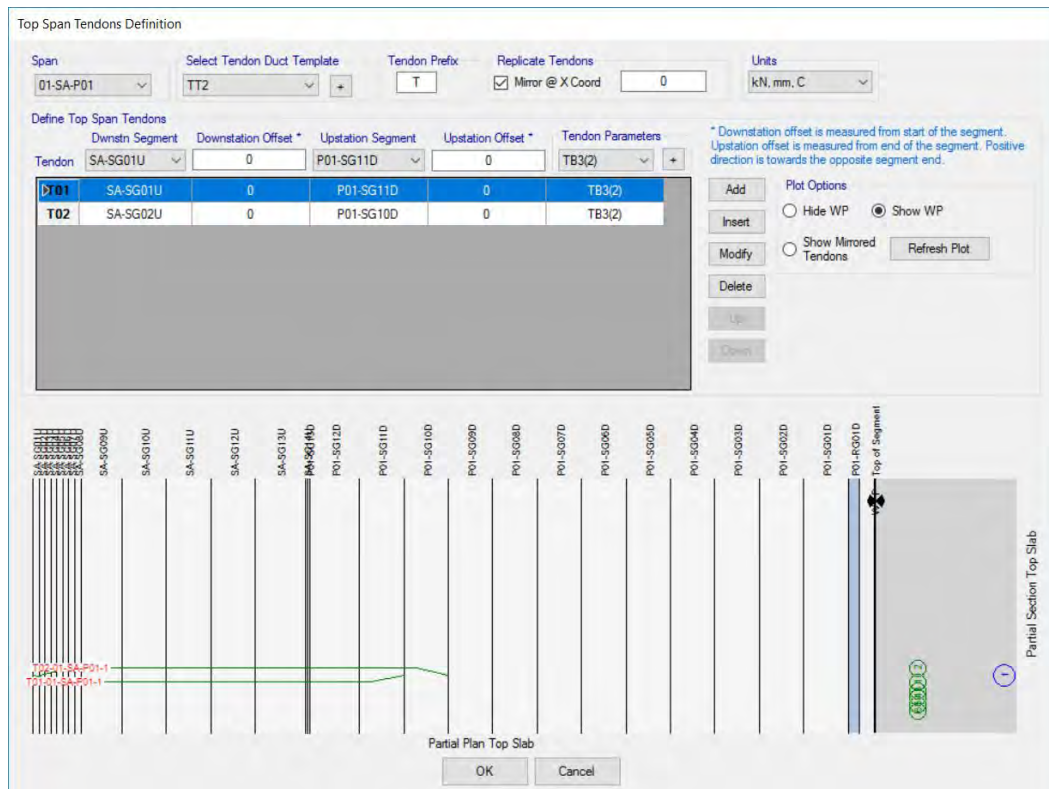


Figure. B.22: Left segment top tendon layout

Tendon Parameters

Tendon Parameter Name	Units	Tendon Load Pattern
TB3	kN, mm, C	+ Prestress-B

Tendon Parameters		Tendon Modeling Options	
Prestress Type	Post Tension	<input type="radio"/> Model As Loads	
Jack From	Start	<input checked="" type="radio"/> Model As Elements	
Material Property	+ A416Gr270	Load Type	Tendon Load
Tendon Area	+ 3360	<input checked="" type="radio"/> Force	Force (kN)
Based on Tendon Size:	1 Tnd(s) 0.6"-24	<input type="radio"/> Stress	6600
Max Discretization Length	1000		Stress (kN/mm2)
			0.004788
Design Parameters		Loss Parameters	
Bonding Type	Bonded	Curvature Coefficient (Unitless)	0.15
Duct Diameter	100.1	Wobble Coefficient (1/mm)	6.5617E-07
Min Duct Bend Radius	9144	Anchorage Set Slip (mm)	6.349
		Other Loss Parameters	
		Elastic Shortening Stress [kN/mm2]	0.02068
		Creep Stress [kN/mm2]	0.03447
		Shrinkage Stress [kN/mm2]	0.04826
		Steel Relaxation Stress [kN/mm2]	0.03447

When tendons are modeled as elements, the Other Loss Parameters (elastic, creep, shrinkage, and relaxation losses) apply in addition to the losses computed by analysis.

OK Cancel

Figure. B.23: Bottom tendon parameter (TB3)

Tendon Parameters

Tendon Parameter Name	Units	Tendon Load Pattern
TB3(2)	kN, mm, C	+ Prestress-B

Tendon Parameters		Tendon Modeling Options	
Prestress Type	Post Tension	<input type="radio"/> Model As Loads	
Jack From	Start	<input checked="" type="radio"/> Model As Elements	
Material Property	+ A416Gr270	Load Type	Tendon Load
Tendon Area	+ 3360	<input checked="" type="radio"/> Force	Force (kN)
Based on Tendon Size:	1 Tnd(s) 0.6"-24	<input type="radio"/> Stress	3300
Max Discretization Length	1000		Stress (kN/mm2)
			0.004788
Design Parameters		Loss Parameters	
Bonding Type	Bonded	Curvature Coefficient (Unitless)	0.15
Duct Diameter	100.1	Wobble Coefficient (1/mm)	6.5617E-07
Min Duct Bend Radius	9144	Anchorage Set Slip (mm)	6.349
		Other Loss Parameters	
		Elastic Shortening Stress [kN/mm2]	0.02068
		Creep Stress [kN/mm2]	0.03447
		Shrinkage Stress [kN/mm2]	0.04826
		Steel Relaxation Stress [kN/mm2]	0.03447

When tendons are modeled as elements, the Other Loss Parameters (elastic, creep, shrinkage, and relaxation losses) apply in addition to the losses computed by analysis.

OK Cancel

Figure. B.24: Left segment top tendon parameter (TB3(2))

Appendix C 125 m Span Bridge Details

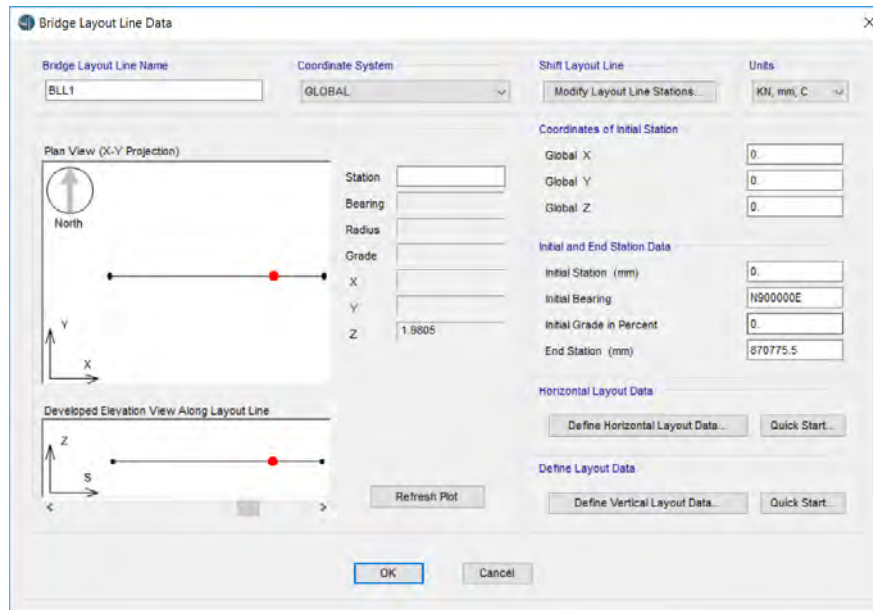


Figure. C.1: Bridge layout line

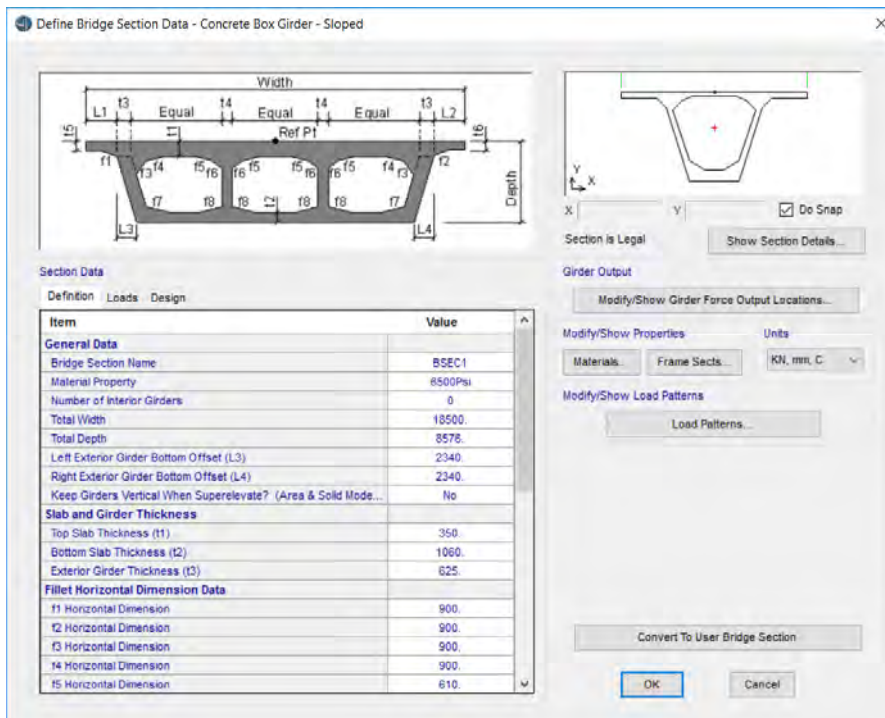


Figure. C.2: Girder section

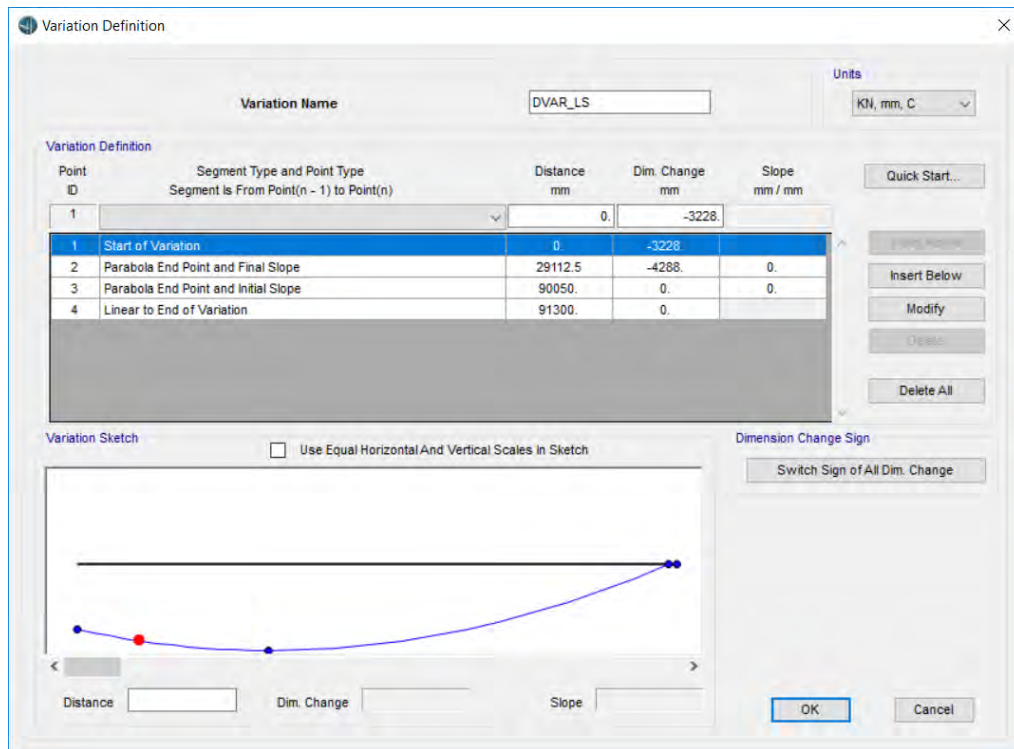


Figure. C.3: Depth variation of left segment

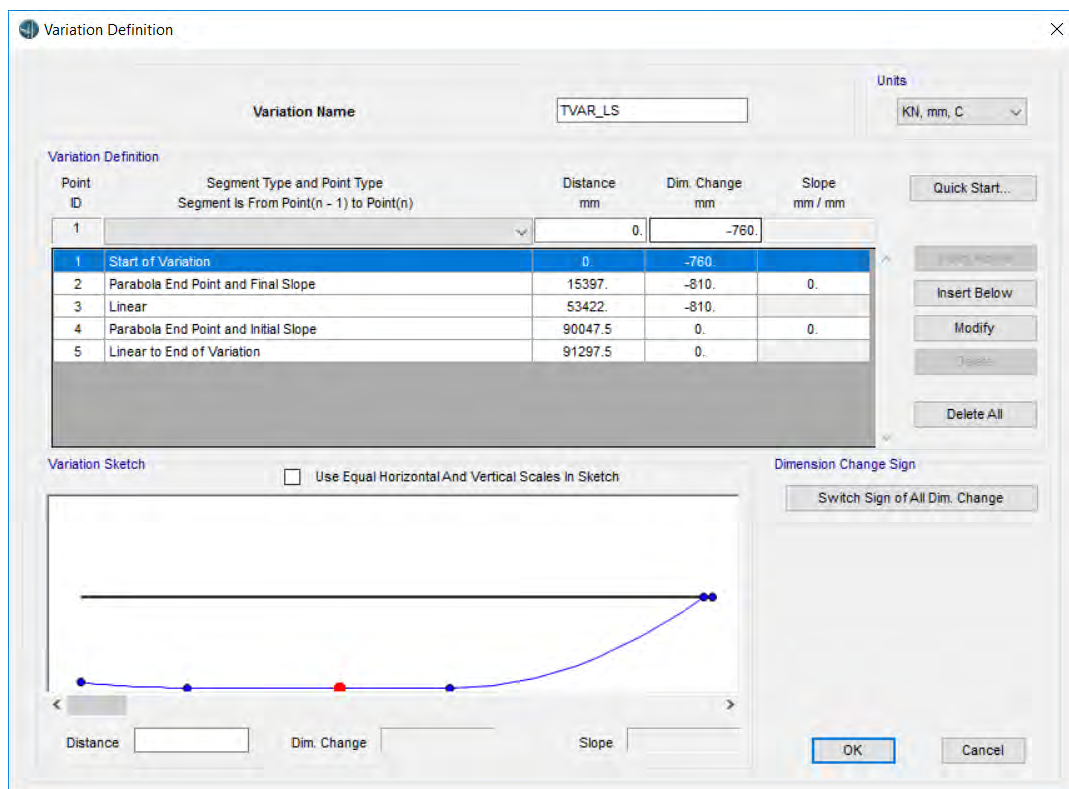


Figure. C.4: Bottom slab thickness variation at left segment

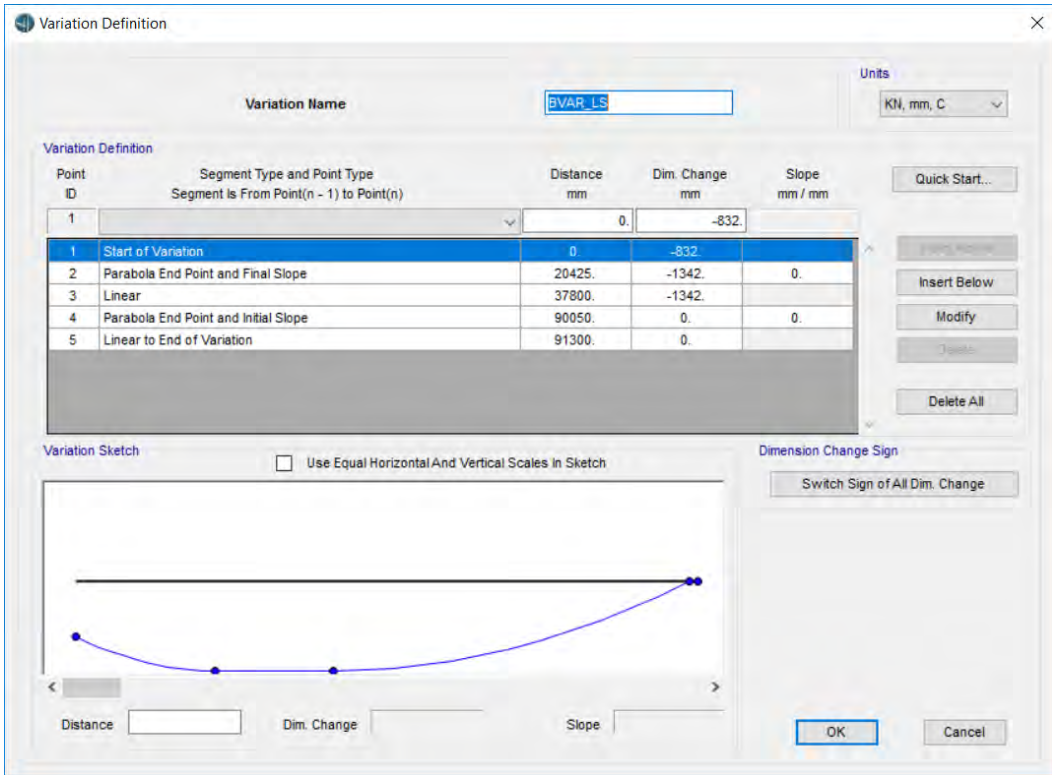


Figure. C.5: Cross section variation of left segment

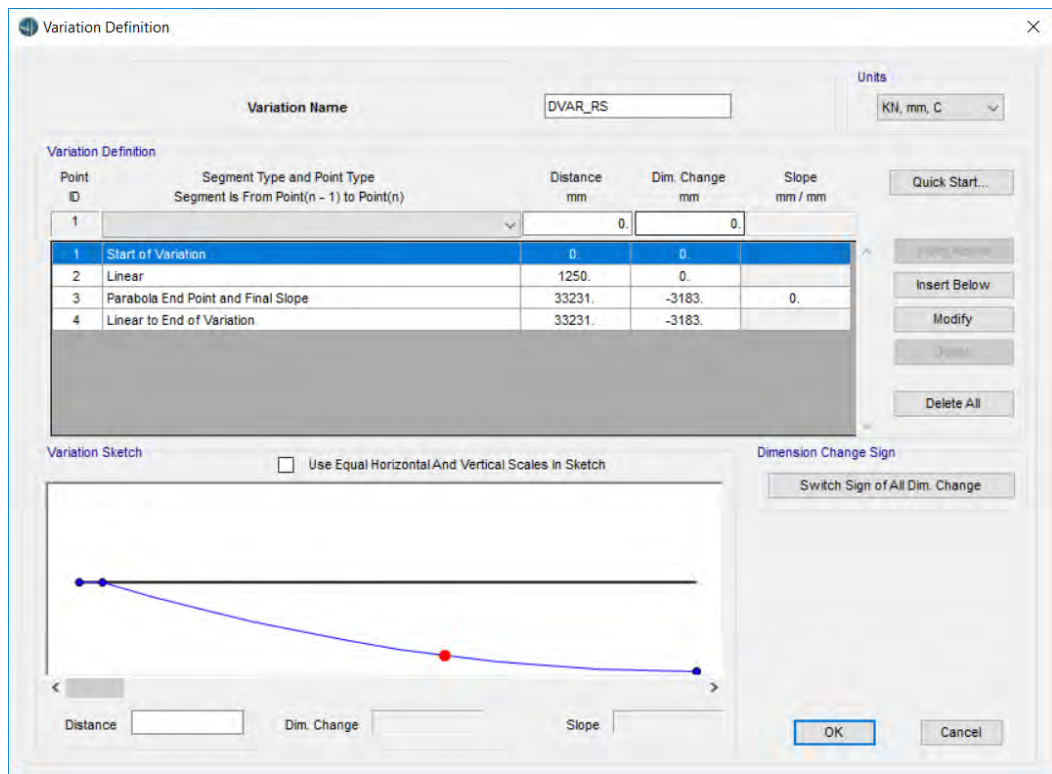


Figure. C.6: Section depth variation of right segment

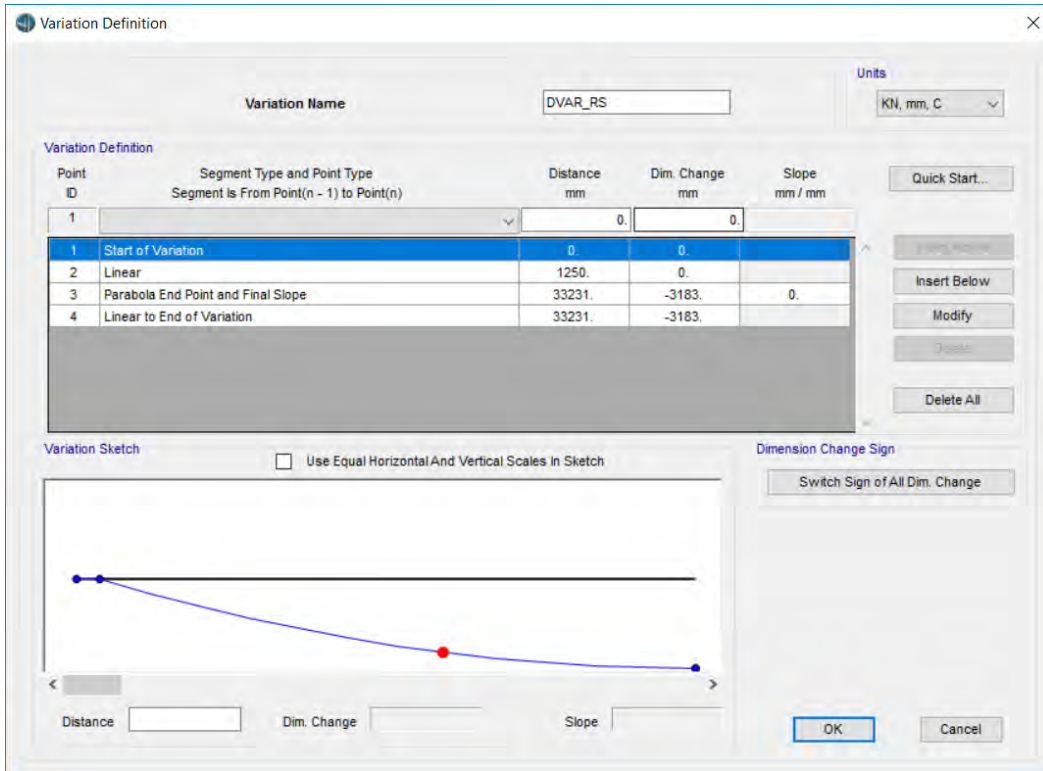


Figure. C.7: Bottom slab thickness variation of right segment

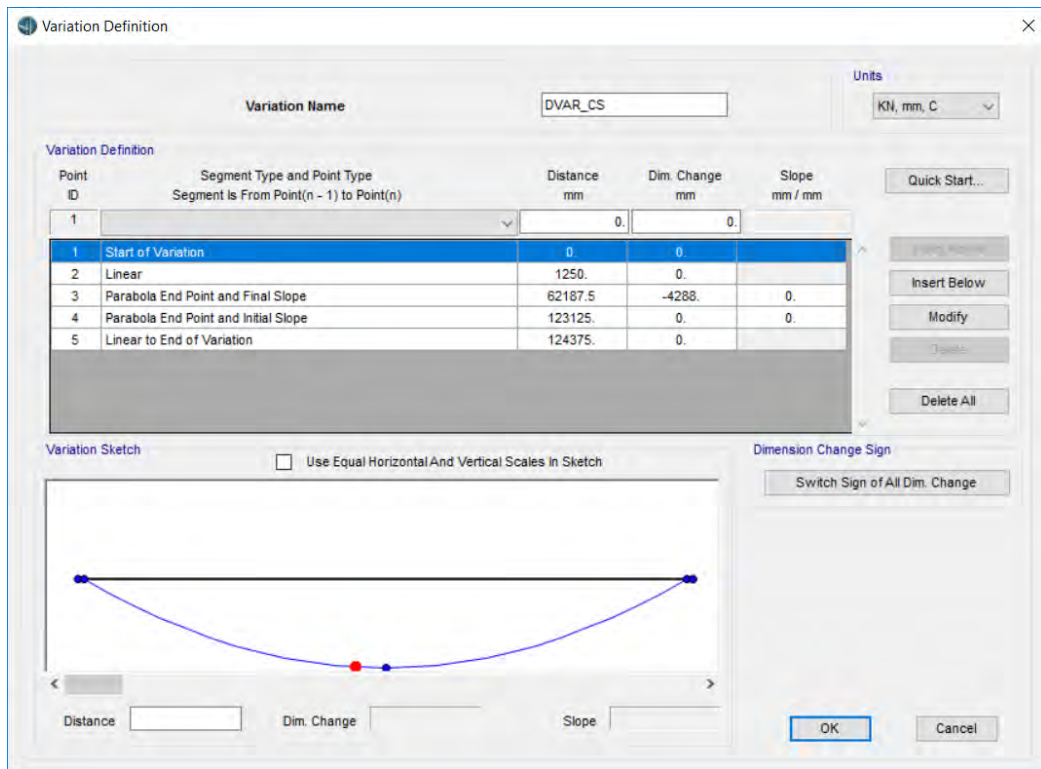


Figure. C.8: Section depth variation of typical segment

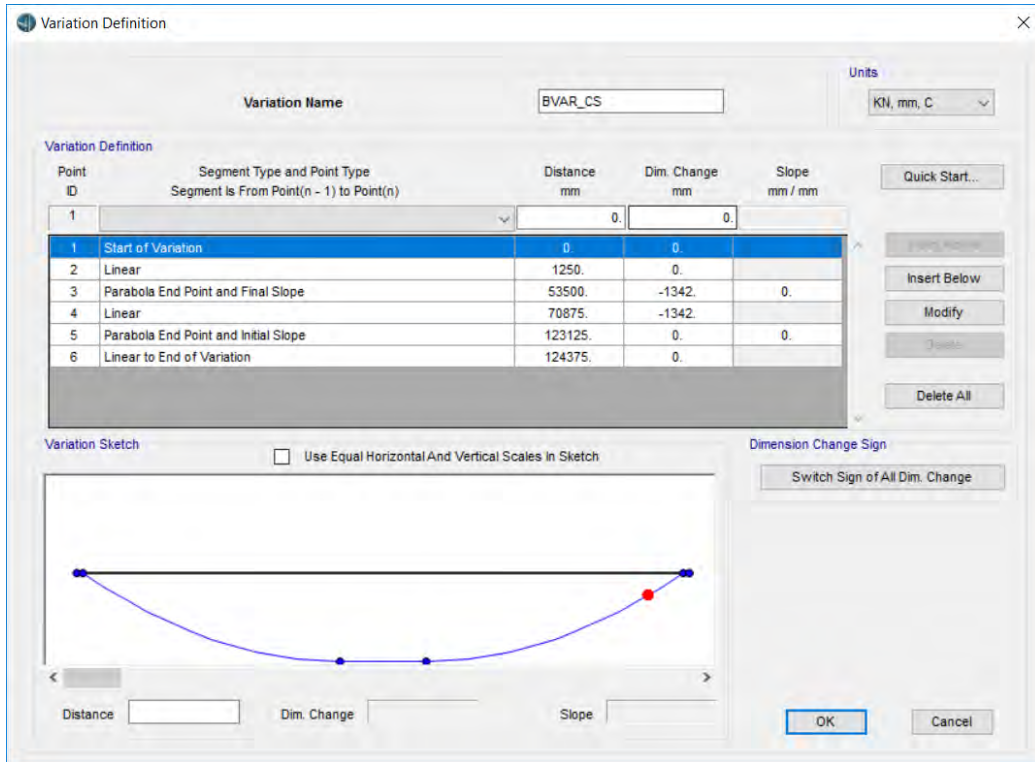


Figure. C.9: Girder width variation of typical segment

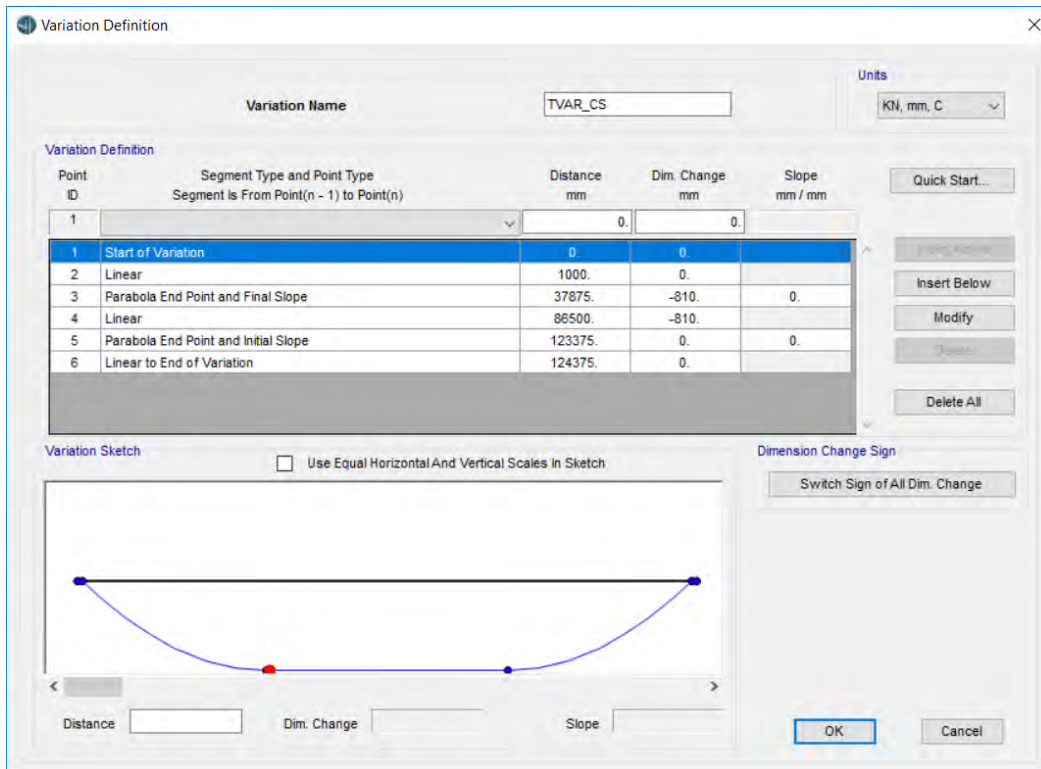


Figure. C.10: Bottom slab thickness variation of typical segment

Bridge Object Abutment Assignments

Bridge Object Name: BOBJ1

Units: KN, mm, C

Start Abutment | End Abutment

Start Abutment

Superstructure Assignment

Support Name: SA

Abutment Direction (Bearing Angle): Default

Diaphragm Property: + None

Substructure Assignment

None

Abutment Property: + BABT1

Bent Property: +

Substructure Location

Elevation (Global Z): -5498.

Horizontal Offset: 0.

Note: Horizontal offset is from layout line to midlength of abutment.

Bearing Assignment

Girder-by-Girder

General

Bearing Property: + BBRG1

Restrainer Property at Bearing: + None

Elevation at Layout Line (Global Z): -5198.

Rotation Angle from Bridge Default: 0.

Number of Bearings for Bridge Section: 2

Uniform Spacing: 6075.

Offset from Section Ref. Point to Bearing Center: 0.

Bearing-by-Bearing Overwrites

Modify/Show Overwrites... No Overwrites Exist

OK Cancel

Figure. C.11: Start abutment

Bridge Object Abutment Assignments

Bridge Object Name: BOBJ1

Units: KN, mm, C

Start Abutment | End Abutment

End Abutment

Superstructure Assignment

Support Name: EA

Abutment Direction (Bearing Angle): Default

Diaphragm Property: + None

Substructure Assignment

None

Abutment Property: + BABT1

Bent Property: +

Substructure Location

Elevation (Global Z): -5488.

Horizontal Offset: 0.

Note: Horizontal offset is from layout line to midlength of abutment.

Bearing Assignment

Girder-by-Girder

General

Bearing Property: + BBRG1

Restrainer Property at Bearing: + None

Elevation at Layout Line (Global Z): -5188.

Rotation Angle from Bridge Default: 0.

Number of Bearings for Bridge Section: 2

Uniform Spacing: 6699.8

Offset from Section Ref. Point to Bearing Center: 0.

Bearing-by-Bearing Overwrites for End Abutment

Modify/Show Overwrites... No Overwrites Exist

OK Cancel

Figure. C.12: End abutment

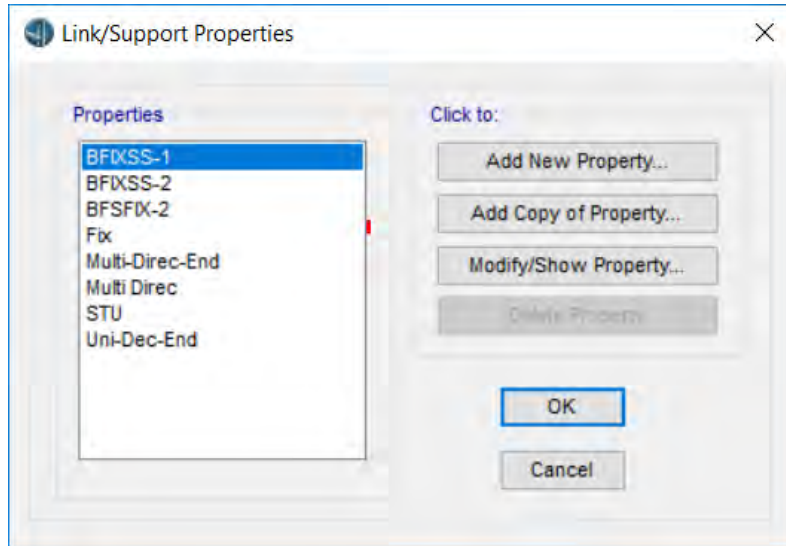


Figure. C.13: List of assigned seismic isolation

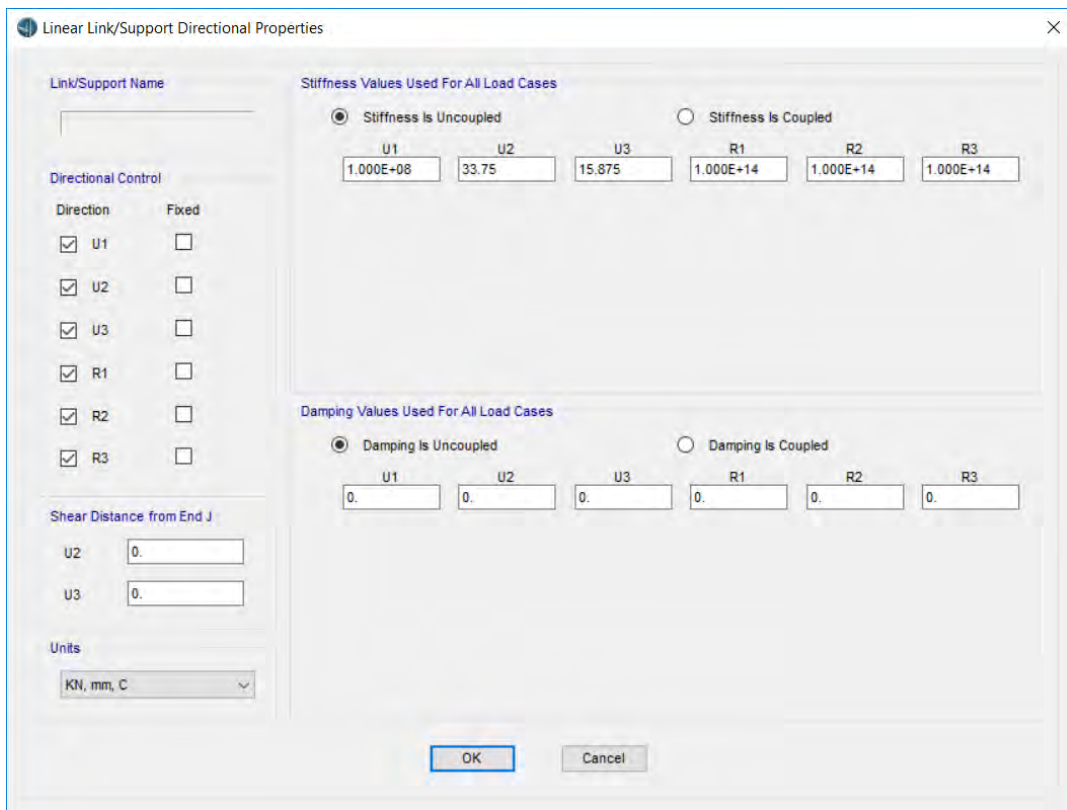


Figure. C.14: Typical multidirectional bearing (2)

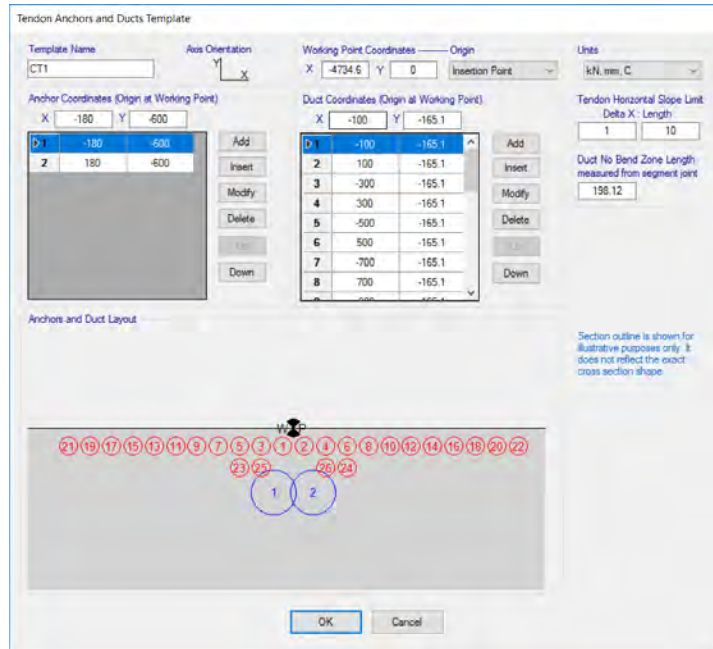


Figure. C.15: Cantilever tendon duct template layout

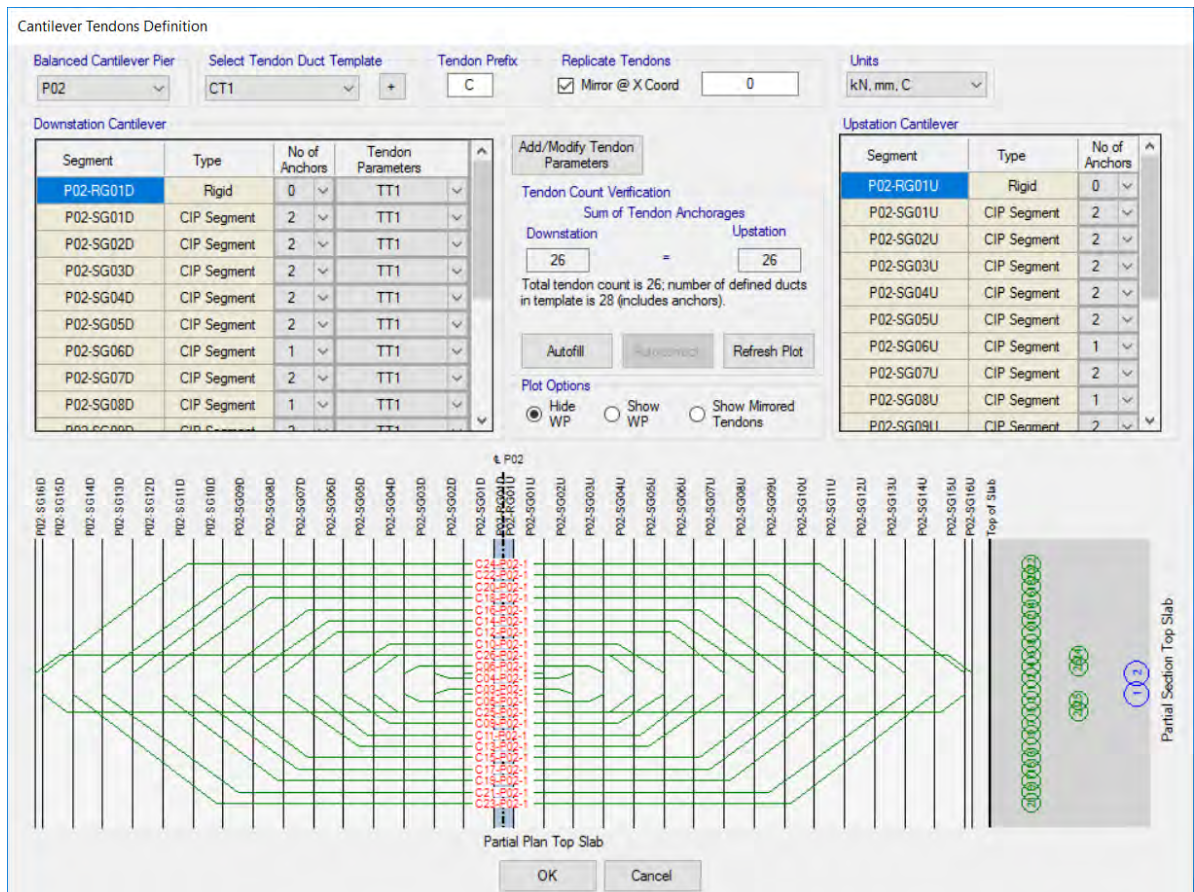


Figure. C.16: Cantilever tendon layout template

Tendon Parameters

Tendon Parameter Name: TT1 Units: kN, mm, C Tendon Load Pattern: Prestress-T

Tendon Parameters

Prestress Type: Post Tension

Jack From: Start

Material Property: A416Gr270

Tendon Area: 3360

Based on Tendon Size: 1 Tnd(s) 0.6"-24

Max Discretization Length: 1000

Design Parameters

Bonding Type: Bonded

Duct Diameter: 100.1

Min Duct Bend Radius: 9144

When tendons are modeled as elements, the Other Loss Parameters (elastic, creep, shrinkage, and relaxation losses) apply in addition to the losses computed by analysis.

Tendon Modeling Options

Model As Loads

Model As Elements

Load Type Tendon Load

Force Force (kN) Stress (kN/mm²)

Stress 4824 0.004788

Loss Parameters

Curvature Coefficient (Unitless): 0.15

Wobble Coefficient (1/mm): 6.5617E-07

Anchorage Set Slip (mm): 6.349

Other Loss Parameters

Elastic Shortening Stress (kN/mm²): 0.02068

Creep Stress (kN/mm²): 0.03447

Shrinkage Stress (kN/mm²): 0.04826

Steel Relaxation Stress (kN/mm²): 0.03447

OK Cancel

Figure. C.17: Cantilever tendon layout template

Tendon Anchors and Ducts Template

Template Name: B2 Axis Orientation: Y, X Working Point Origin: Bottom Left Corner Units: kN, mm, C

Anchor Coordinates (Origin at Working Point)

X	520	Y	500
---	-----	---	-----

Duct Coordinates (Origin at Working Point)

X	120	Y	99.06
2	320	99.06	
3	520	99.06	
4	720	99.06	
5	920	99.06	
6	1120	99.06	
7	1320	99.06	
8	1520	99.06	

Tendon Horizontal Slope Limit: Delta X: Length: 1: 10

Duct No Bend Zone Length measured from segment joint: 198.12

Anchors and Duct Layout

Section outline is shown for illustrative purposes only. It does not reflect the exact cross section shape.

OK Cancel

Figure. C.18: Typical bottom tendon duct template layout

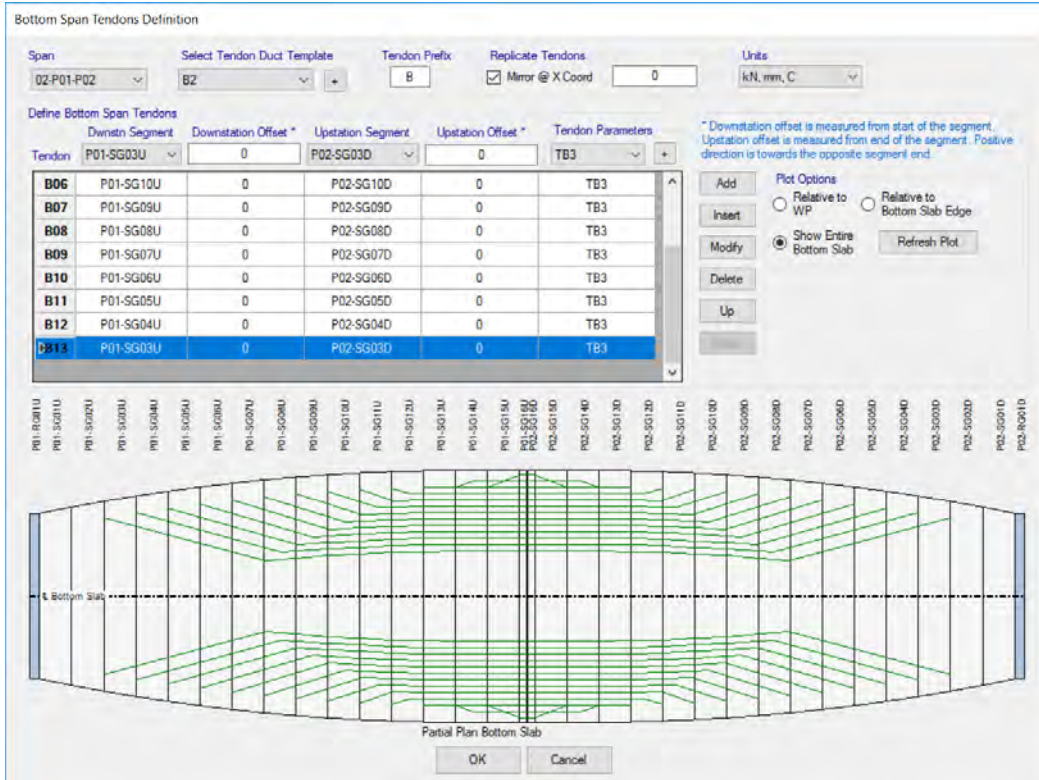


Figure. C.19: Typical bottom tendon layout template

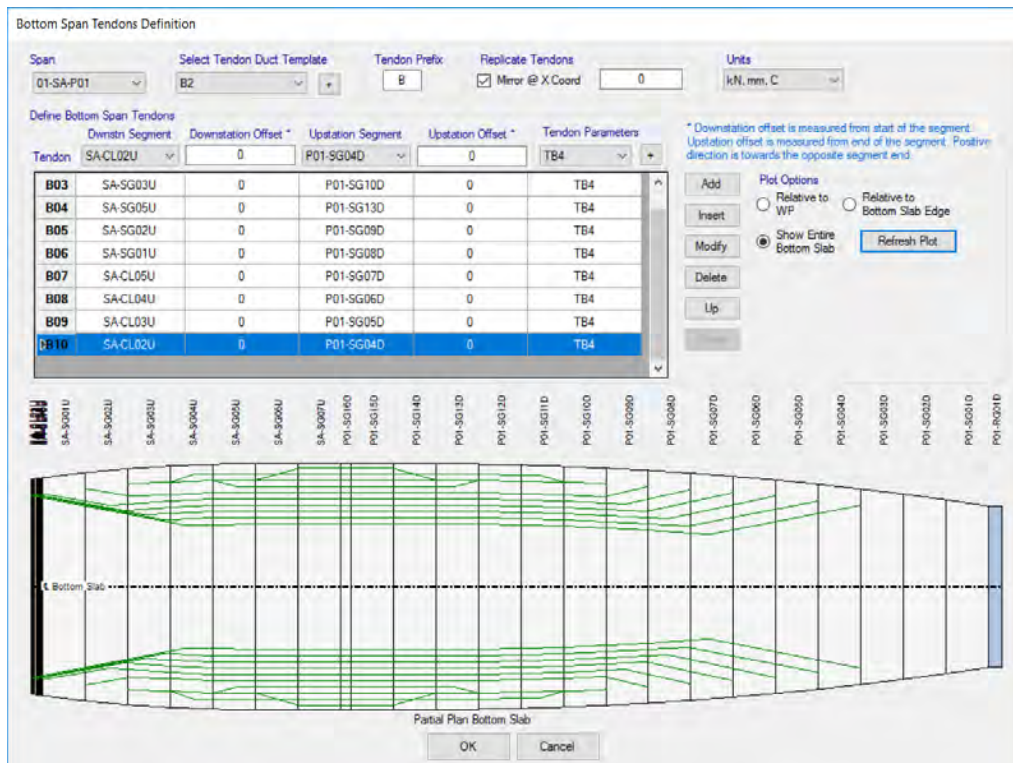


Figure. C.20: Left segment bottom tendon layout

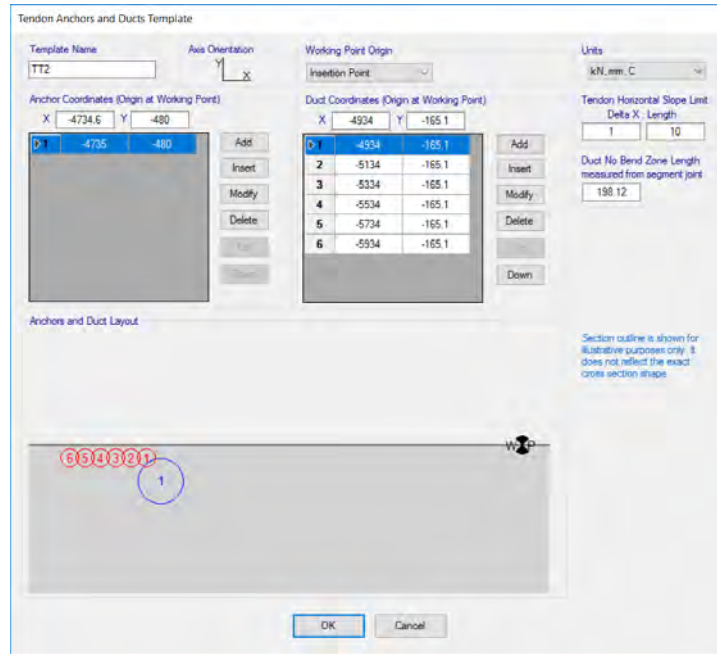


Figure. C.21: Left segment top tendon duct template layout

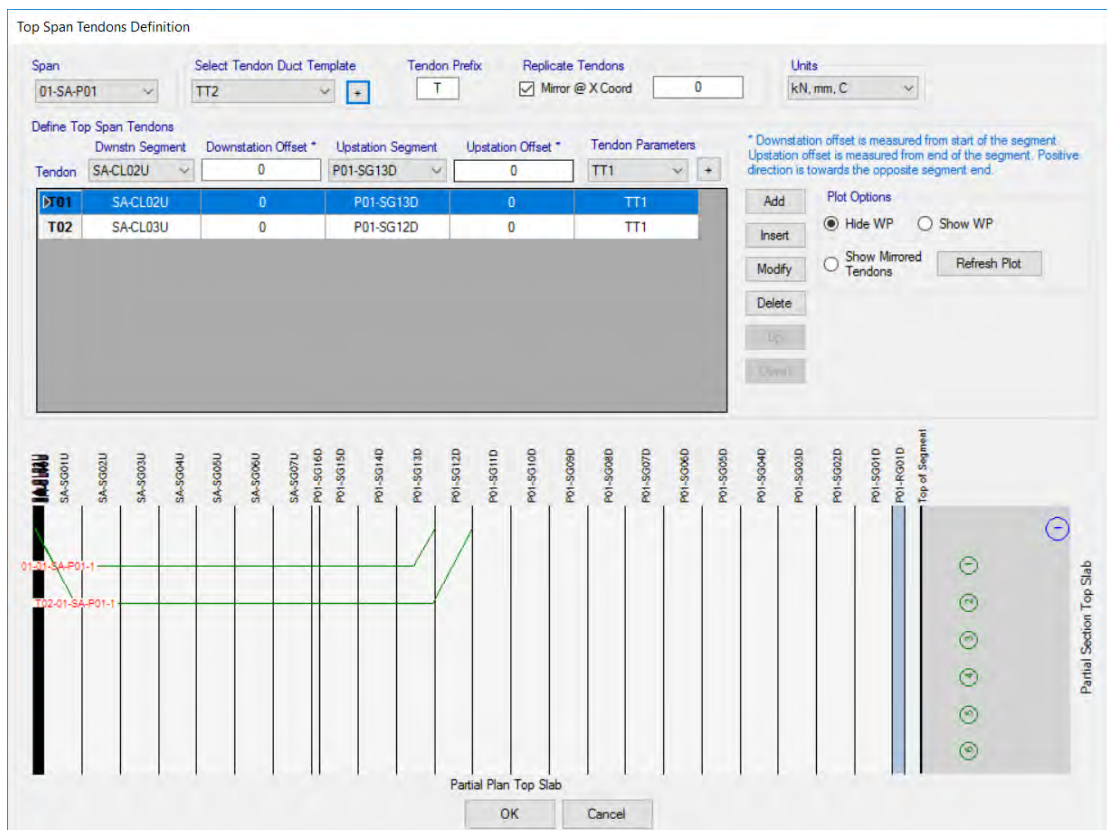


Figure. C.22: Left segment top tendon layout

Tendon Parameters

Tendon Parameter Name	Units	Tendon Load Pattern
TB3	kN, mm, C	+ Prestress-B

Tendon Parameters

Prestress Type: Post Tension

Jack From: Start

Material Property: + A416Gr270

Tendon Area: + 3360

Based on Tendon Size: 1 Tnd(s) 0.6"-24

Max Discretization Length: 1000

Design Parameters

Bonding Type: Bonded

Duct Diameter: 100.1

Min Duct Bend Radius: 9144

When tendons are modeled as elements, the Other Loss Parameters (elastic, creep, shrinkage, and relaxation losses) apply in addition to the losses computed by analysis.

Tendon Modeling Options

Model As Loads

Model As Elements

Load Type	Tendon Load Force (kN)	Stress (kN/mm ²)
<input checked="" type="radio"/> Force	9504	0.004788
<input type="radio"/> Stress		

Loss Parameters

Curvature Coefficient (Unitless)	0.15
Wobble Coefficient (1/mm)	6.5617E-07
Anchorage Set Slip (mm)	6.349

Other Loss Parameters

Elastic Shortening Stress [kN/mm ²]	0.02068
Creep Stress [kN/mm ²]	0.03447
Shrinkage Stress [kN/mm ²]	0.04826
Steel Relaxation Stress [kN/mm ²]	0.03447

OK Cancel

Figure. C.23: Bottom tendon parameter (TB3)

Tendon Parameters

Tendon Parameter Name	Units	Tendon Load Pattern
TB4	kN, mm, C	+ Prestress-B

Tendon Parameters

Prestress Type: Post Tension

Jack From: Start

Material Property: + A416Gr270

Tendon Area: + 3360

Based on Tendon Size: 1 Tnd(s) 0.6"-24

Max Discretization Length: 1000

Design Parameters

Bonding Type: Bonded

Duct Diameter: 100.1

Min Duct Bend Radius: 9144

When tendons are modeled as elements, the Other Loss Parameters (elastic, creep, shrinkage, and relaxation losses) apply in addition to the losses computed by analysis.

Tendon Modeling Options

Model As Loads

Model As Elements

Load Type	Tendon Load Force (kN)	Stress (kN/mm ²)
<input checked="" type="radio"/> Force	9266	0.004788
<input type="radio"/> Stress		

Loss Parameters

Curvature Coefficient (Unitless)	0.15
Wobble Coefficient (1/mm)	6.5617E-07
Anchorage Set Slip (mm)	6.349

Other Loss Parameters

Elastic Shortening Stress [kN/mm ²]	0.02068
Creep Stress [kN/mm ²]	0.03447
Shrinkage Stress [kN/mm ²]	0.04826
Steel Relaxation Stress [kN/mm ²]	0.03447

OK Cancel

Figure. C.24: Left segment top tendon parameter (TB4)